LBL-107
c.1

RECEIVED
LAWRENCE
RADIATION LABORATORY

LIBRARY AND
DOCUMENTS SECTION

STUDIES OF GAS-SURFACE INTERACTIONS AT THE (100) CRYSTAL FACE OF PLATINUM BY MOLECULAR BEAM SCATTERING, LOW ENERGY ELECTRON DIFFRACTION, AND AUGER ELECTRON SPECTROSCOPY

Lloyd Albert West
(Ph. D. Thesis)

November 1971

AEC Contract No. W-7405-eng-48

For Reference

Not to be taken from this room

LBL-107
c.1

DISCLAIMER

This document was prepared as an account of work sponsored by the United States Government. While this document is believed to contain correct information, neither the United States Government nor any agency thereof, nor the Regents of the University of California, nor any of their employees, makes any warranty, express or implied, or assumes any legal responsibility for the accuracy, completeness, or usefulness of any information, apparatus, product, or process disclosed, or represents that its use would not infringe privately owned rights. Reference herein to any specific commercial product, process, or service by its trade name, trademark, manufacturer, or otherwise, does not necessarily constitute or imply its endorsement, recommendation, or favoring by the United States Government or any agency thereof, or the Regents of the University of California. The views and opinions of authors expressed herein do not necessarily state or reflect those of the United States Government or any agency thereof or the Regents of the University of California.

0 0 0 0 3 6 0 0 4 5 8

for my family and former teachers

0 0 0 0 3 6 0 3 4 5 9

PREFACE

This thesis contains a portion of the results garnered during four years from 1967 to 1971 in the Department of Chemistry at the University of California and at the Inorganic Materials Research Division of what was then called Lawrence Radiation Laboratory but is now called Lawrence Berkeley Laboratory.

It cannot convey the elation of detecting the scattered beam for the first time, or the frustration of equipment failures, or the pain I experienced after running my fingers through a belt sander. Hopefully, however, the information contained in this volume will serve as a guide for others who will continue the study of the interactions of gases with solid surfaces. For that reason, some parts of Chapter II have been written as a manual to instruct future operators because, better than anyone else, I understand how the system operates for I guided its construction and know every nut, bolt, and valve.

This work was commenced at the end of an era when money was free and anything seemed possible. Since that time, man has set foot upon the face of the moon and the social climate has undergone a change. Science is no longer the darling of Industry and Government, and the idea of an ivory tower wherein knowledge for knowledge's sake may be pursued has given way to a social awareness.

Good experiments can still be performed, but more effort is required to find the necessary funds. Much of the credit for this

work must go to Professor Gabor A. Somorjai who demonstrated an unfailing faith in the project and an utterly amazing ability to secure the finances required to implement it in an atmosphere of ever tightening budgets.

Now, as I submit this thesis, I can look back on four fruitful years of labor. As has been so aptly put: "The hill has been kind to her guests, serving up lavish feasts for the eye and mind, providing an unequalled environment for creative and satisfying work."*

---

* The Magnet, 15, #6, June 1971.

Table of Contents

Abstract viii

I. Introduction 1

A. History of Molecular Beam Studies 4

B. Problems of Surface Contamination 5

C. Surface Characterization 7

1. Low Energy Electron Diffraction (LEED) 8

2. Auger Electron Spectroscopy (AES). 20

D. Atomic and Molecular Beam Scattering 27

1. Diffraction 32

2. Reactive Scattering 35

3. Scattering Theories 36

E. Clean Surfaces 41

II. Experimental 45

A. Sample Preparation 45

B. Apparatus 49

1. Design Considerations 49

2. Signal-to-Noise Considerations 57

3. Scattering Chamber 63

a. Pumping 66

b. Detector and Ionizer 71

c. Lock-in Amplifier 83

d. LEED Optics 87

e. Auger Spectrometer 88

f. Pump-down and Bakeout Procedures 92

4. Selector Chamber 93

5. Source Chamber 94

a. Beam Source 95

b. Gas Handling System 100

6. Interlocks and Pump-down Procedure 102

7. Experimental Procedure 105

III. Selected Properties of the Pt(100) Substrate 112

A. Surface Structure 112

B. Surface Contamination and Gas Adsorption 115

IV. Scattering of Monatomic Gases 119

A. Introduction 119

B. Effect of Surface Order and Disorder on Helium Atomic Beam Scattering 120

C. Effect of Adsorbed Gases on Helium Atomic Beam Scattering 134

D. Effect of Surface Temperature on Scattered Helium Intensity 138

E. Scattering of Other Monatomic Gases 142

F. Discussion 144

V. Scattering of Polyatomic Gases 150

A. Introduction 150

B. Non-Reactive Scattering Studies 163

1. Nitrogen and its Oxides 163

2. Hydrocarbons, Carbon Dioxide, and Carbon Monoxide . 171

3. Oxygen and Ammonia 177

4. Hydrogen and Deuterium 182

5. Discussion 186

0 0 0 0 3 6 0 3 4 6 0

C. Verification of a Classical Model for Gas-Solid Scattering 192

D. Reactive Scattering Studies 199

1. Ammonia Oxidation 200

2. Deuterium Oxidation and Hydrogen-Deuterium Exchange on (100) Platinum 203

a. Oxidation of Deuterium 203

b. Exchange of Hydrogen with Deuterium 206

3. Thermal Dissociation of Hydrocarbons on (100) Platinum 208

4. Dissociation of Nitrous Oxide on (100) Platinum . . 210

a. Results 217

b. Discussion 224

VI. Conclusions and Recommendations 226

VII. APPENDIX 231

A. Computer Programs 231

B. Etchants and Cleaning Solutions 253

C. Photographic Data and Slide Preparation 254

D. New Ionizer 255

Symbols 261

References 264

Acknowledgments 275

0 0 0 0 3 6 0 5 4 6 1

STUDIES OF GAS-SURFACE INTERACTIONS AT THE (100) CRYSTAL FACE OF PLATINUM BY MOLECULAR BEAM SCATTERING, LOW ENERGY ELECTRON DIFFRACTION, AND AUGER ELECTRON SPECTROSCOPY

Lloyd Albert West

Inorganic Materials Research Division, Lawrence Berkeley Laboratory
and Department of Chemistry, University of California,
Berkeley, California

ABSTRACT

An apparatus has been constructed to investigate energy transfer and chemical reactions at the gas-surface interface and the mechanisms of gas-solid interactions. Low energy electron diffraction and Auger electron spectroscopy were employed to characterize the surface structure and the chemical composition of the solid and the adsorbed layer. A thermal molecular beam provided gaseous species at a predetermined angle of incidence with respect to the surface normal and a quadrupole mass spectrometer detected the angular distributions of the incident and scattered beams. Ultra high vacuum conditions ($< 10^{-8}$ torr) were maintained in the scattering chamber throughout the experiments. Helium beam scattering studies were conducted from the ordered and disordered Pt(100) crystal face to assess the role of surface structures in the scattering process. The intensity of the beam scattered at the specular angle was observed to increase by nearly an order of magnitude upon atomic ordering of the metal surface. Ordered domains of graphitic carbon also yielded high intensity peaks in the specular direction. Other experiments with polyatomic molecular beams were used to probe the nature of surface chemical reactions. The dissociation of nitrous

oxide on the clean and carbon covered platinum surface was investigated in the temperature range T_s = 900°K to 1500°K. The clean surface dissociated N_2O only poorly at the surface temperatures employed in this work, but the dissociation product NO was fully accommodated on the surface before reemission as indicated by the cosine angular distribution of the scattered species. On the carbon covered surface, the scattering process appeared to be different due to the strongly exothermic interaction of the N_2O with the carbon and evidence for a fast "direct" reactive scattering mechanism was detected. At higher surface temperatures, the incident N_2O beam removed the carbon layer by oxidation. The exchange of hydrogen with deuterium and the oxidation of ammonia were attempted without success. This lack of reactivity has been ascribed to the low density of atomic steps on the Pt(100) surface when compared to stepped single crystal surfaces, evaporated films, or polycrystalline foils of platinum.

0 0 0 0 3 6 0 3 4 6 2

I. INTRODUCTION

Solid surfaces are known to affect the rates of a great many liquid and gas phase chemical reactions and to be important in the formation of desirable chemical products. For this reason, a large research effort has historically been directed toward the search for suitable surfaces to catalyze specific reactions. Unfortunately, most of the experiments were not conducted in a manner conducive to the elucidation of the fundamental surface chemical processes involved.

This thesis contains the description of a system constructed to investigate, on a molecular scale, the detailed mechanisms of and the nature of energy transfer during gas-solid interactions. It also reports the results of experiments that investigated the interaction of atomic and molecular beams with the surface of platinum.

As is the case in the study of other chemical reactions, one would like to characterize the gas-surface system of interest by a collection of experimental parameters that can be varied independently in order to determine the effect of each one on the total process. For a study of the interaction of gases with solid surfaces, the most likely parameters are a) the strength of the gas-solid potential, b) the crystalline orientation and order of the surface, c) the surface temperature, d) the energy (both translational and internal) of the incident gas particles, e) the angle at which the gas strikes the surface, and of course f) the chemical composition of the gaseous and solid species.

Reduced to these terms, it readily becomes apparent that one wishes to study the collision of an atomic or molecular beam with a well-characterized surface. Such an experiment is conceptually very simple as shown in Fig. I-1. One simply generates a beam of particles having a well-defined speed and impinges it at a predetermined incident angle on a solid with a known surface temperature. The energy and angular distribution of the scattered species (both reacted and unreacted) are then determined with an appropriate detector. From the incident and scattering angles, the known mass of the particles, and from the velocities of the incident and scattered beams, one can obtain the momentum and energy changes occurring during the scattering process if a model for the interaction is postulated.

In this thesis we report on studies of molecular beam scattering from the (100) face of platinum single crystals. A quadrupole mass spectrometer was employed to ascertain the angular distributions of the incident and scattered beams while the structure of the scattering surface was monitored by low energy electron diffraction. The composition of the surface was probed by Auger electron spectroscopy. Experiments were carried out under ultra high vacuum conditions ($< 10^{-8}$ torr) to maintain a surface free of gases adsorbed from the ambient during the collision process. The incident and scattered angles, the surface temperature, and the incident gas velocity could all be determined in these investigations-only the velocity of the scattered beam could not be measured independently in the present system.

0 0 0 0 3 6 0 3 4 6 3

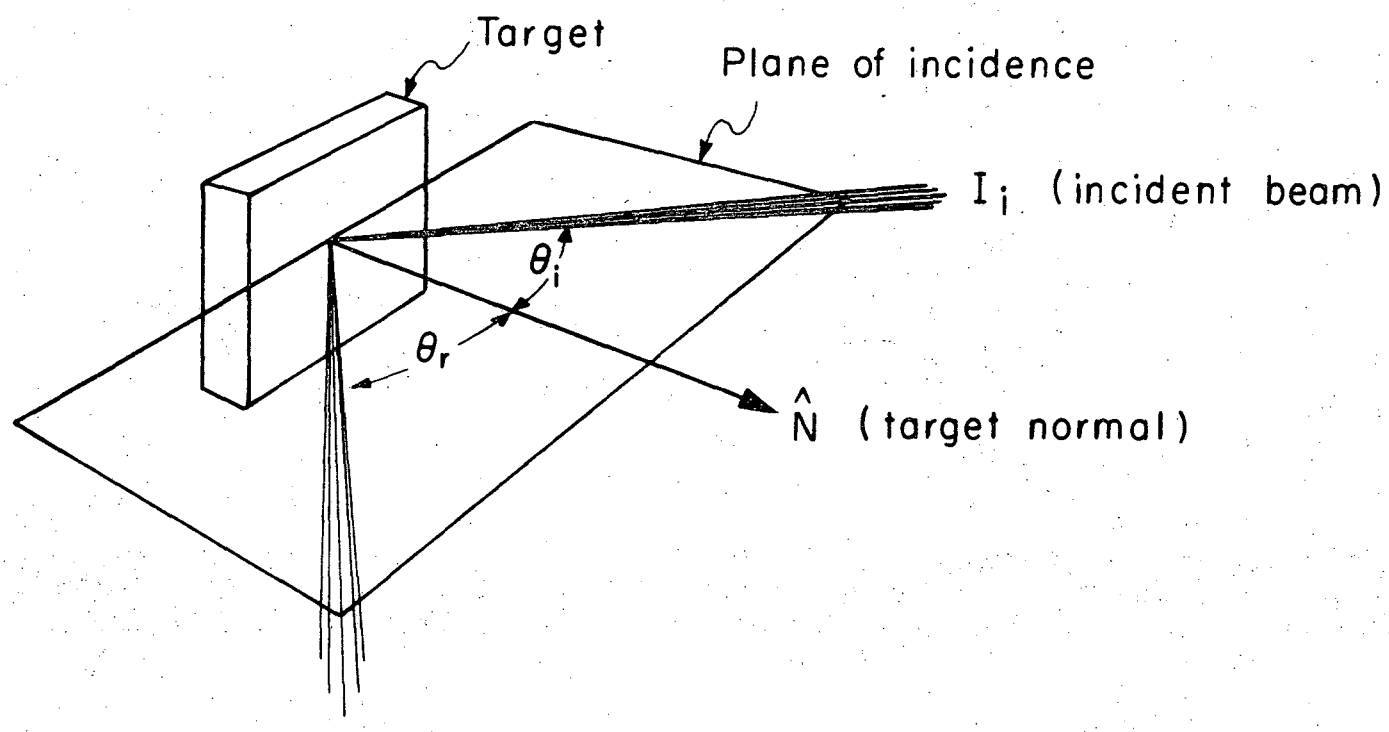

XBL 708-1973

Fig. I-1. Schematic representation of the gas-solid scattering experiment.

A. History of Molecular Beam Studies

Since the pioneering experiments of Dunoyer in 1911,[1] molecular beam techniques have evolved into a powerful tool for the study of the fundamental properties of atoms, molecules, and nuclei. One need hardly remind the reader of the direct observations of spatial quantization, or the compilation of nuclear spin, magnetic moment, and quadrupole moment data, or the discovery of the Lamb shift to substantiate this claim in the field of physics (see Ref. 2). Of more interest to the field of chemistry has been the elucidation of elementary reaction steps, the investigation of collision complexes, and the calculation of interaction potentials from experiments with crossed molecular beams.[3-5]

Beam technology was first applied to the study of gas-solid interactions during the late nineteen-twenties and early thirties by Otto Stern and his co-workers at the University of Hamburg. Their observation of helium atom diffraction from a cleaved LiF surface[2,6] provided additional proof of the de Broglie postulate on wave particle duality. Several groups continued the investigation of beam-surface interactions throughout the decade of the thirties[2,7] and found angular scattering distributions which could not be attributed to diffraction, yet deviated from Knudsen scattering. [Knudsen[8] pointed out that molecules restituted from a surface, even in the absence of equilibrium, should be distributed in space as the cosine of the scattering angle measured from the surface normal.] From the late thirties

until the early fifties, little more work was done until Hurlbut began his examination of the scatting of aerodynamic gases from engineering surfaces.[9,10] The current period in the study of gas-solid interactions began in 1960 when Hollister, Brackman, and Fite pointed out the advantages of using modulated beams and a.c. detection techniques.[11]

B. Problems of Surface Contamination

A comparison of the literature cited above shows that, while certain trends are indeed discernible,[7] inconsistencies are also present in the data. The interpretation of the early experimental results obtained in surface scattering studies is currently clouded by the unknown properties, irreproducible contamination, and polycrystalline nature of many of the target surfaces employed. Only the cleaved LiF surface seems immune to such problems, and it has been experimentally demonstrated[12] that the scattering properties of this surface are remarkably unaffected by contamination. This is definitely not the case for other surfaces (see Chapters IV and V).

Due to the seemingly uncontrollable difficulties of surface contamination, early investigators attempted to concentrate on gas scattering studies that were perturbed as little as possible by surface impurities. Consequently many experiments were performed using polycrystalline metal surfaces at high temperatures to reduce unwanted contamination and rare gas beams to minimize the probability of troublesome chemical reactions with the substrate.

Recognition of the role played by the surface in determining the observed scattering distribution has led recent experimenters to choose single crystal targets[13-16] and to devise methods to ensure their cleanliness during the course of the scattering experiment. The most widely used of these methods are: (1) high surface temperatures so that the rate of desorption of the gases in the ambient is higher than their rate of adsorption,[17] and (2) continuous deposition of the scattering surface at a rate in excess of the maximum possible arrival rate of contaminants.[13] The first of these methods is restricted to the thermally stable faces of a few refractory metals and does not permit one to examine the temperature dependence of a phenomenon with complete freedom of choice of target surfaces and incident gases. Method (2) also suffers from severely limited temperature variability, because the epitaxial growth on a given substrate of a smooth, oriented single crystal film takes place in a narrow temperature range. The second approach is also restricted to those crystal faces that can be deposited in a dominant orientation, thus effectively ruling out the investigation of high index faces or stepped surfaces.

A more satisfactory, although experimentally more complicated and costly, approach to this problem of keeping the surface clean is to use ultra high vacuum technology (i.e., ambient pressures below 10^{-8} torr). An order of magnitude calculation shows that for a typical solid with a surface density of 10^{15} atoms/cm^2, approximately one thousand seconds are required to produce a monolayer of adsorbed

gas atoms at a gas pressure of 10^{-9} torr, assuming that every atom striking the surface condenses.

C. Surface Characterization

Despite the recent use of single crystal targets for studies of gas-solid interactions, too little emphasis has been placed upon the attainment of well defined surface conditions. Detailed information on the exact crystallographic nature of the surface structure is necessary if one hopes to provide a sound experimental basis for a theoretical explanation of the observed scattering patterns.

Unfortunately, most experimentalists are faced with the problem of not being able to characterize their surface during an experiment. Rather, they must rely upon a subsequent examination of the target by x-ray and optical or electron microscope techniques. It has been well established that certain solids undergo surface reconstruction under vacuum conditions.[18] Such surface phase transformations may markedly affect a scattering distribution, but due to the nature of the transition, may be undetectable by the usual x-ray and optical microscope measurements under atmospheric conditions.

Of course, in a system designed to study gas-solid interactions by molecular beam techniques, one probe of the surface conditions is the helium atomic beam itself.[16] Like all tools, however, it has its limitations and the ideal approach is to combine several complimentary methods for characterizing the surface. Ellipsometry, low energy

electron diffraction (LEED), ion neutralization spectroscopy (INS), photo-electron spectroscopy (ESCA), work function measurements, flash desorption analysis, and Auger electron spectroscopy (AES) are just a few of the many techniques available today.

One advantage of a clean ultra high vacuum (UHV) system over a conventional diffusion pumped vacuum system is that it permits the use of sensitive in situ probes of the nature of the scattering surface. The two techniques that have been used in this work to characterize the surface employ scattered electrons. Low energy electron diffraction or, more commonly, LEED analyzes electrons elastically scattered from the crystal surface, while electrons emitted by the surfaces as the result of secondary processes are analyzed by a technique called Auger electron spectroscopy, after the French scientist who first discovered the effect.[19]

1. Low Energy Electron Diffraction (LEED).

This thesis is not the proper place for a detailed explanation of the theory and practice of LEED, but for completeness a brief synopsis will be given. For more detail, the reader is referred to the literature.[18]

In 1927, as the result of a laboratory accident, Davisson and Germer[20,21] discovered that electrons could be diffracted in a manner analogous to x-rays. They found that the positions of the most intense electron beams could be predicted by assuming that rows of surface atoms acted like the lines in a two-dimensional diffraction grating

(see Fig. I-2) and that the wavelength associated with the electrons was given by the de Broglie relationship

$$\lambda = \frac{h}{P} = \frac{h}{\sqrt{2mE}} = \frac{h}{\sqrt{2meV}} \qquad \text{(I-1)}$$

where h is Planck's constant, P is the particle momentum, m is the mass of the electron, E is the energy of the electron and e is the electronic charge. Substituting numerical values into the above equation, we obtain

$$\lambda = \sqrt{\frac{150.4}{V(\text{volts})}} \quad [\text{Å}] \qquad \text{(I-2)}$$

where V is the accelerating potential (in volts) that the electrons experience before striking the crystal.

Unlike comparable wave length x-rays that penetrate deeply into the bulk of the solid, slow electrons (i.e., those having wavelengths roughly equivalent to lattice spacings) are scattered primarily from the first few atomic layers as shown schematically in Fig. I-3. For this reason, electrons are an extremely valuable probe of the surface region. Unfortunately, the kinematic, or single scattering theory which works so well for predicting scattered x-ray intensities usually fails in LEED due to inelastic processes and the multiple scattering indicated in Fig. I-3. This does not mean, however, that LEED is not a useful tool for the study of surface features, for one can learn

Fig. I-2. Two dimensional diffraction representation. In this figure, α_i is the angle of incidence measured from some (arbitrarily chosen) azimuth lying in the surface plane and ψ is the scattering angle transverse to the incident plane.

0 0 0 0 3 6 0 3 4 6 7

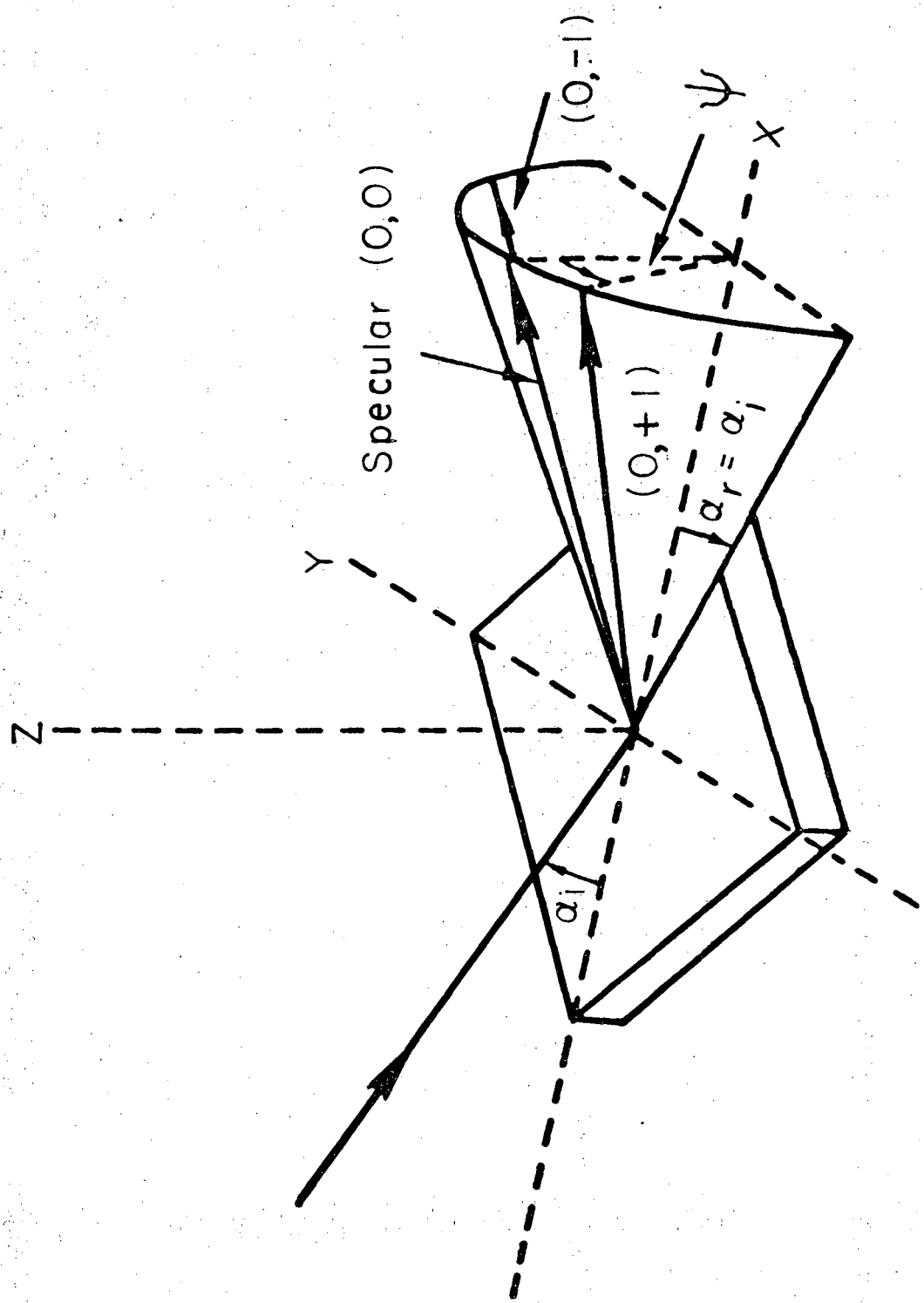

XBL708-3774

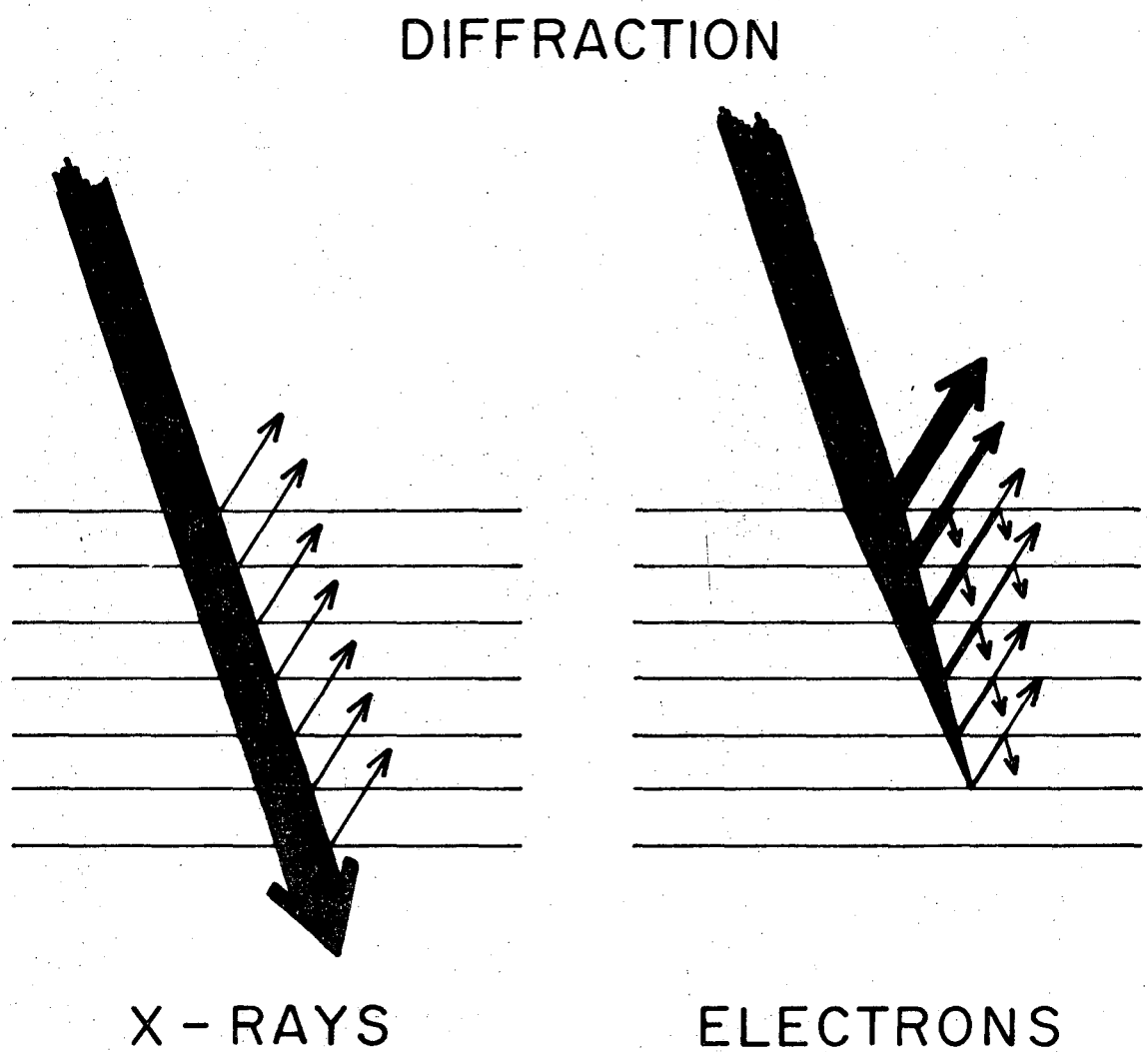

XBL 7012-7436

Fig. I-3. Schematic illustration of the scattering of x-rays and low energy electrons by the atomic planes of a crystal. The breadth of the arrows shows relative intensities.

a good deal of surface information from studies of the temperature dependence of the scattered intensities, and from changes in the diffraction pattern itself (although one cannot at present deduce unambiguously the location of surface atoms from the pattern alone).

The technique of low energy electron diffraction as applied in this work is shown in Fig. I-4. Electrons emitted from a hot filament in the electron gun are formed into a monochromatic beam having an area approximately 1 mm^2 and are permitted to strike the surface of a single crystal specimen at a near normal angle of incidence. Back scattered electrons are energy analyzed by a series of grids and those that have lost energy are discarded. The elastically reflected portion is then post accelerated into a phosphor screen maintained at + 6 KV where the diffraction spots are easily seen or photographed. Such a visual display system has its main value in that it allows the experimenter to monitor continuously the entire diffraction pattern as a function of electron voltage or changing surface conditions.

Several surface phenomena have been discovered via LEED techniques.[18] It has been found that solid surfaces can undergo structural rearrangements or changes in chemical composition independent of the bulk, that the structure of the surface (atomic arrangement) can differ from that of the bulk unit cell, that certain atoms and molecules chemisorbed on the surfaces form ordered arrays, and that surface atoms undergo larger mean displacements than do bulk atoms.

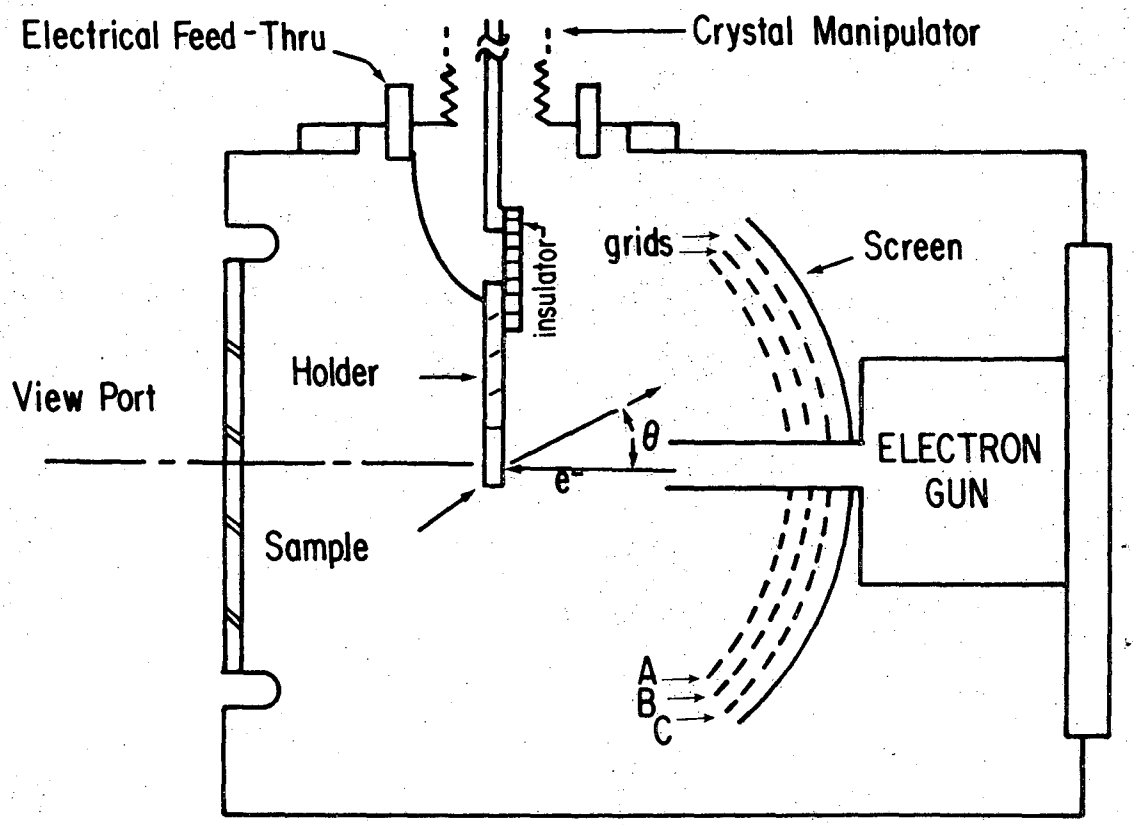

XBL 703-556

Fig. I-4. Low energy electron diffraction apparatus of the post acceleration type used in this work.

LEED nomenclature is based upon a surface unit cell containing a single atom. The structure obtained by projecting the primitive unit cell of the substrate to the surface is called a (1×1) array and any additional diffraction features are then indexed with respect to this cell. For instance, a surface structure having the crystal lattice spacing in one dimension and twice the spacing in the other dimension would be called a (1×2) surface net, while a structure with twice the lattice spacing in both dimensions would be called a (2×2) array. Because the diffraction pattern is a picture of reciprocal space, the actual spot spacings are inversely related to the real space grating separation. Thus the (1×2) has extra diffraction spots at $(\frac{1}{2}\ 0)$ and multiples thereof, while the (2×2) structure has additional spots in the $(\frac{1}{2}\ 0)$, $(0\ \frac{1}{2})$ and $(\frac{1}{2}\ \frac{1}{2})$ positions. These structures are demonstrated schematically in Fig. I-5 with the f.c.c. (110) surface which has a rectangular unit cell so that the two axes can be differentiated. Note that the only difference between the (2×2) diffraction pattern and that due to coexisting (1×2) and (2×1) domains is the spot in the $(\frac{1}{2}\ \frac{1}{2})$ position. For a more complete treatment of nomenclature, the interested reader is referred to the literature.[22]

Figure I-6 shows the diffraction pattern indicative of a clean (100) platinum surface. The extra features along the x and y axes are the result of a surface phase transformation in which the outermost atomic layer has undergone a rearrangement into a hexagonally symmetric array that is coincident with the underlying bulk structure every

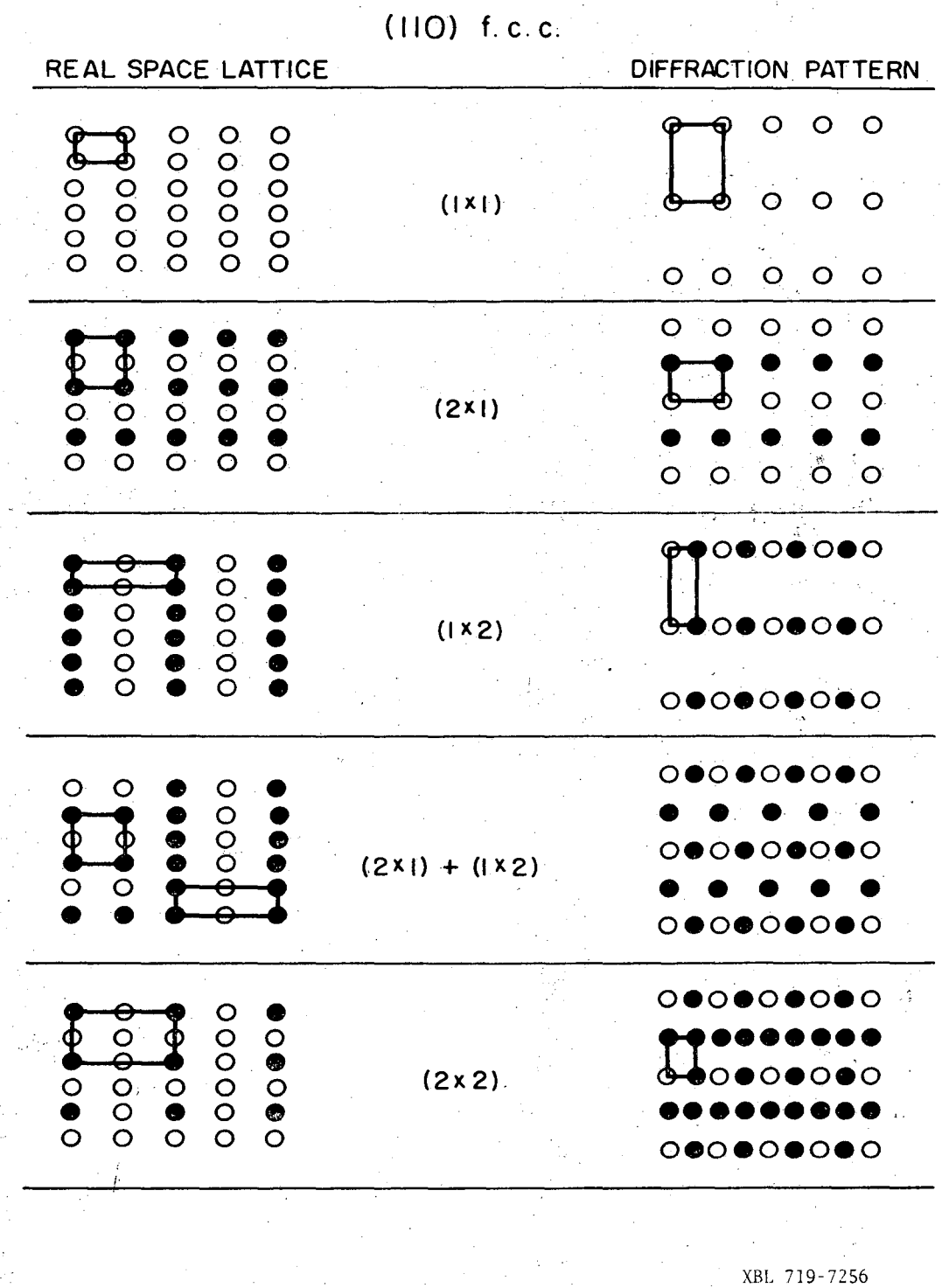

Fig. I-5. Surface structures and corresponding diffraction patterns for the (110) f.c.c. crystal plane.

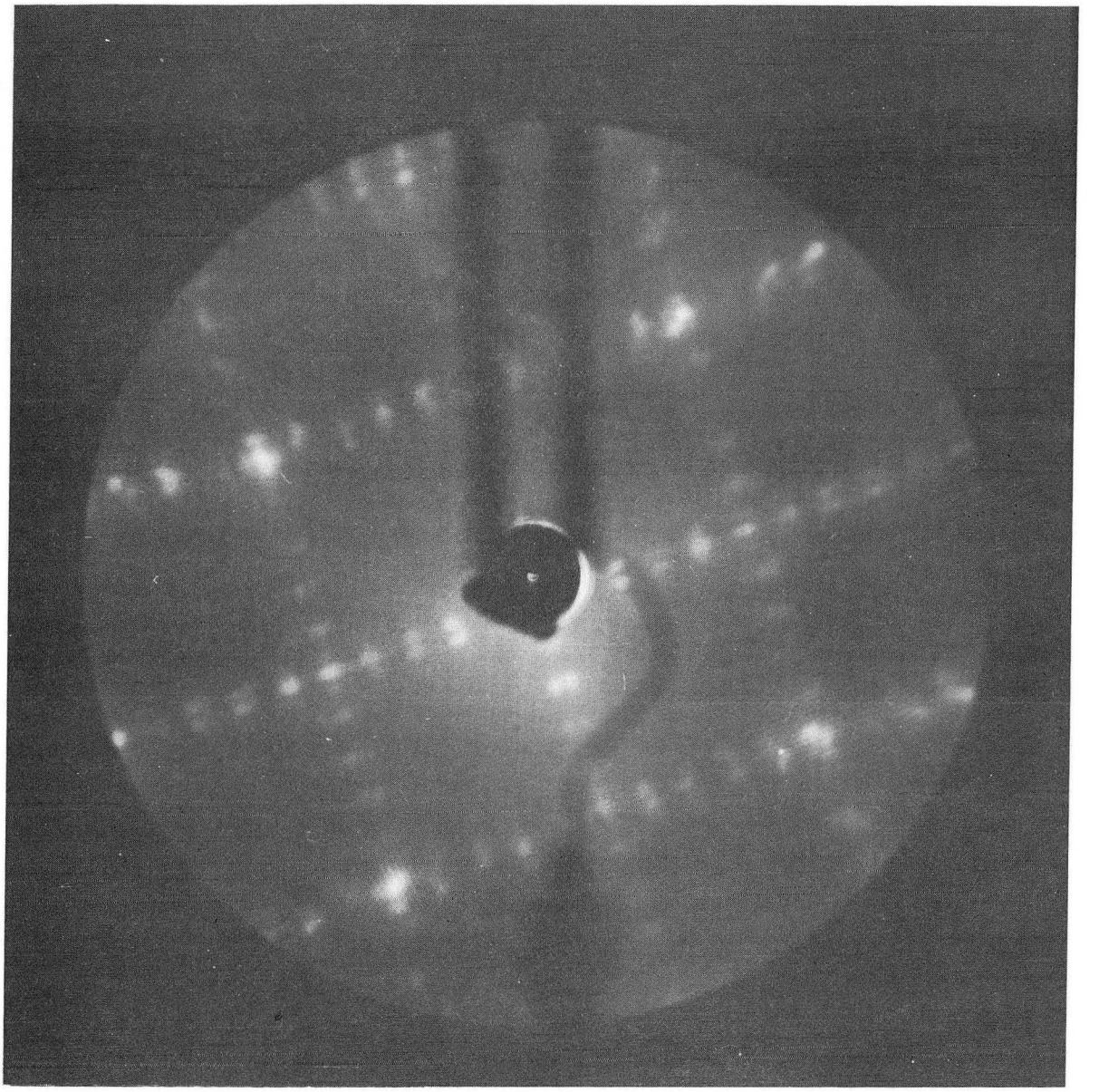

XBB 684-1737

Fig. I-6. Pt(100) - (5×1) diffraction pattern at V = 124 volts.

fifth atomic row. A compression of roughly 5% is necessary to match the hexagonal array to the square bulk structure, and as a result there is presumably a slight out-of-plane buckling so that this surface probably has a slightly undulatory appearance. This pattern is called the (5×1) mesh and will be referred to frequently in the following pages. We must infer the physical structure of this surface because the theoretical complexity of the multiple scattering process has to date hampered intensity analyses. It is hoped that the next few years will see the resolution of this problem as a wealth of structural information awaits the surface chemist.

The theory of LEED attempts to predict both the shape of the observed intensity profiles and the positions of diffraction maxima. A typical plot of spot intensity of the specularly reflected beam versus electron energy is presented in Fig. I-7. For relatively high electron energies (typically above 150 volts), the location of the major peaks can usually be adequately predicted by the Bragg Law: $n\lambda = d \sin\theta$ although there are often additional "fractional order" peaks and other structure present as seen in the figure. A full kinematic treatment,[23] while yielding overall qualitative agreement, still cannot account for all of the observed peaks and intensity ratios because the very aspect of low energy electrons that makes them extremely useful as a surface probe (i.e., the large elastic collision cross sections which limit penetration) also enhances the likelihood of multiple scattering processes, thus invalidating the

0 0 0 0 3 6 0 5 4 7 0

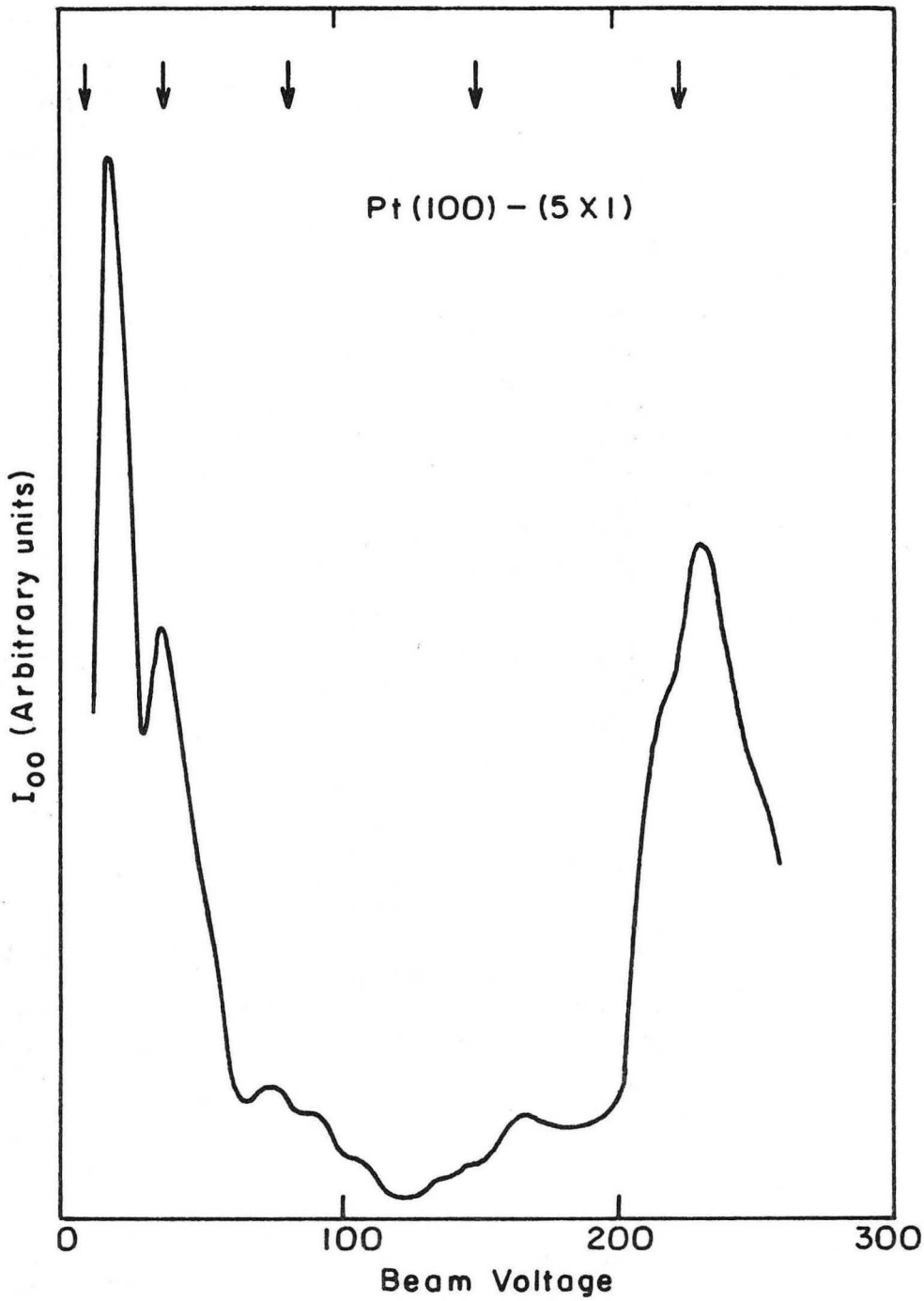

XBL 719-7328

Fig. I-7. Intensity distribution of the (00) or specularly reflected electron beam for a Pt(100)-(5×1) surface structure at an incident angle of 4° from the surface normal. The arrows indicate the location of Bragg peaks.

single scattering approach. Fine structure in the intensity-voltage plot can result from plasma losses and from electron-phonon interactions.

Several dynamical theories for the calculation of LEED intensities have been advanced. These theories attempt to solve the Schrödinger equation in either its differential equation or integral equation representation to arrive at the diffracted intensities. Typical of the former calculation is the wave function matching approach of Boudreau and Heine,[24] while the latter technique is exemplified by the self consistent multiple scattering approach of McRae,[25-27] or the S matrix formulation based on the work of Beeby.[28] Duke and Tucker[29] have also evolved a single electron propagator formalism that takes cognizance of inelastic processes.

2. Auger Electron Spectroscopy (AES)

It was stated in the previous section that only the elastically back scattered electrons contain diffraction information. That these electrons represent only a few percent of the incident monochromatic beam is graphically demonstrated in Fig. I-8 where we plot the electron distribution as a function of energy. Except for the small number of electrons at the primary beam voltage, E_p, the vast majority are scattered inelastically and thus lose energy through interactions with the bulk and/or surface plasmons (i.e., electron gases), interband and intraband transitions, true secondary emission, or Auger processes.

Clearly if one had a method for extracting information from even a small portion of this large number of inelastic electrons, he would

0 0 0 0 3 6 0 5 4 7 1

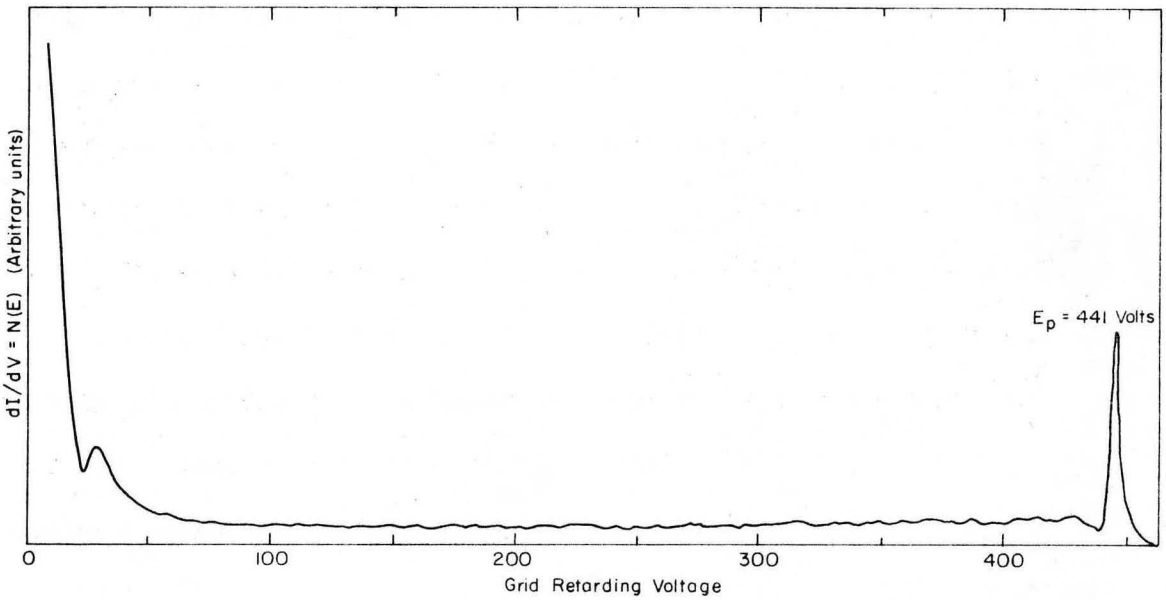

XBL 719-7325

Fig. I-8. Energy distribution of electrons scattered from a surface. The peak height is proportional to the number of electrons with a given energy, showing that most electrons have lost the major fraction of their energy to the solid.

have a valuable tool for surface analysis. Lander[30] first suggested that the use of Auger electrons would provide qualitative and quantitative information on the nature of atoms near the surface. Unfortunately, the Auger peaks are barely discernable on a plot such as that in Fig. I-8 because the transition intensities are so weak that the peaks are sometimes obscured by the rapidly changing background at low voltages. Electronic differentiation of this curve, however, renders even the smallest peaks readily detectable, yet this technique was only applied to the problem in 1968,[31] although it has long been used in all types of resonance spectroscopy. Figure I-9 shows the effect of differentiation on the peak shape. With this single advance, AES figuratively exploded into use among surface scientists.

At this juncture in time, three distinct types of apparatus are available: (1) the cylindrical mirror analyzer, (2) the 127° electrostatic analyzer, and (3) the retarding grid analyzer. This latter mode is the one adopted for this work because it is easily adaptable to a set of LEED optics. The typical experimental arrangement for combined LEED-AES studies is shown schematically in Fig. I-10, except that a normal incidence gun was employed rather than the glancing incidence gun portrayed. In the Auger mode, the entire reflected electron current is modulated at some frequency ω and collected by the positively charged fluorescent screen. A lock-in amplifier serves to differentiate electronically the signal by detecting the

0 0 0 0 3 6 0 0 4 7 2

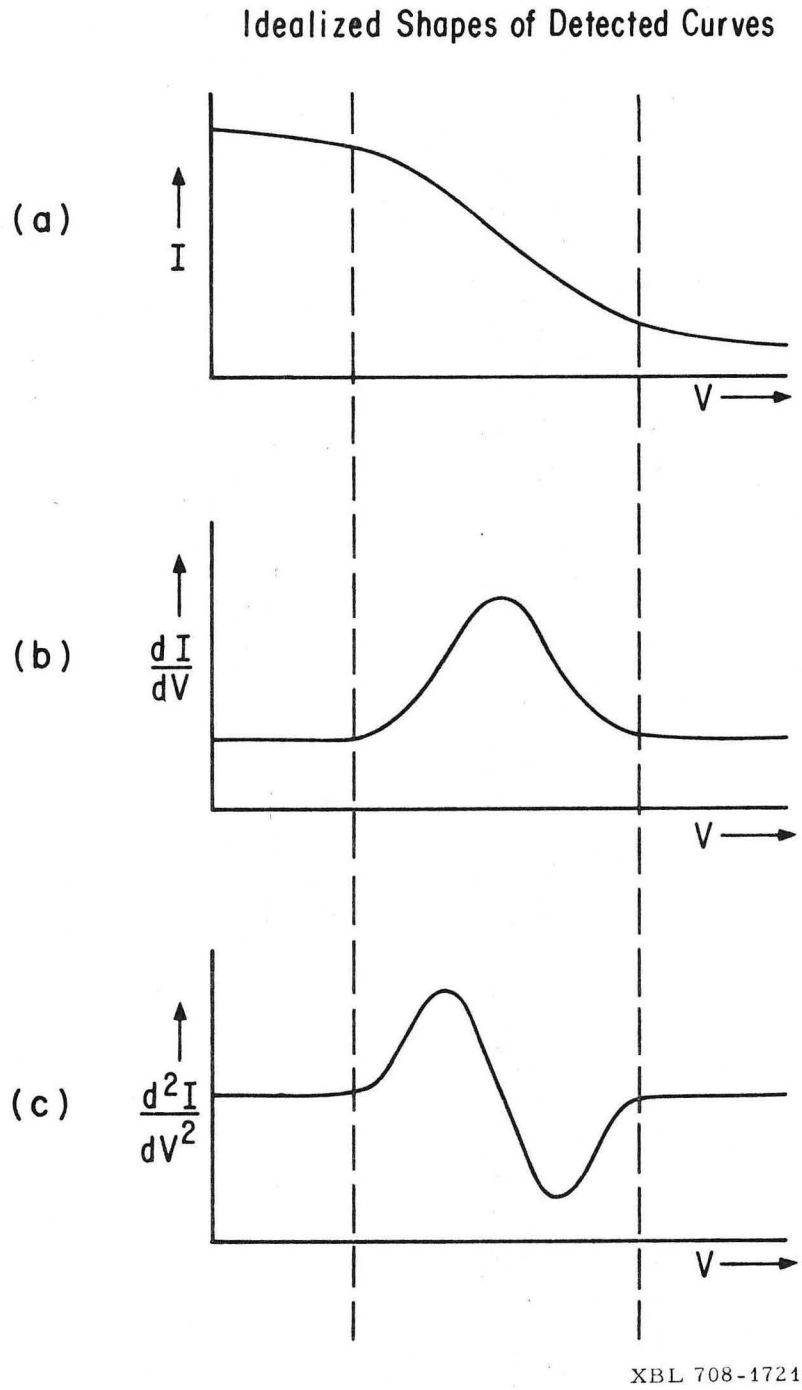

Fig. I-9. Plots of the collected current I and its first and second derivatives as a function of the applied retarding voltage V.

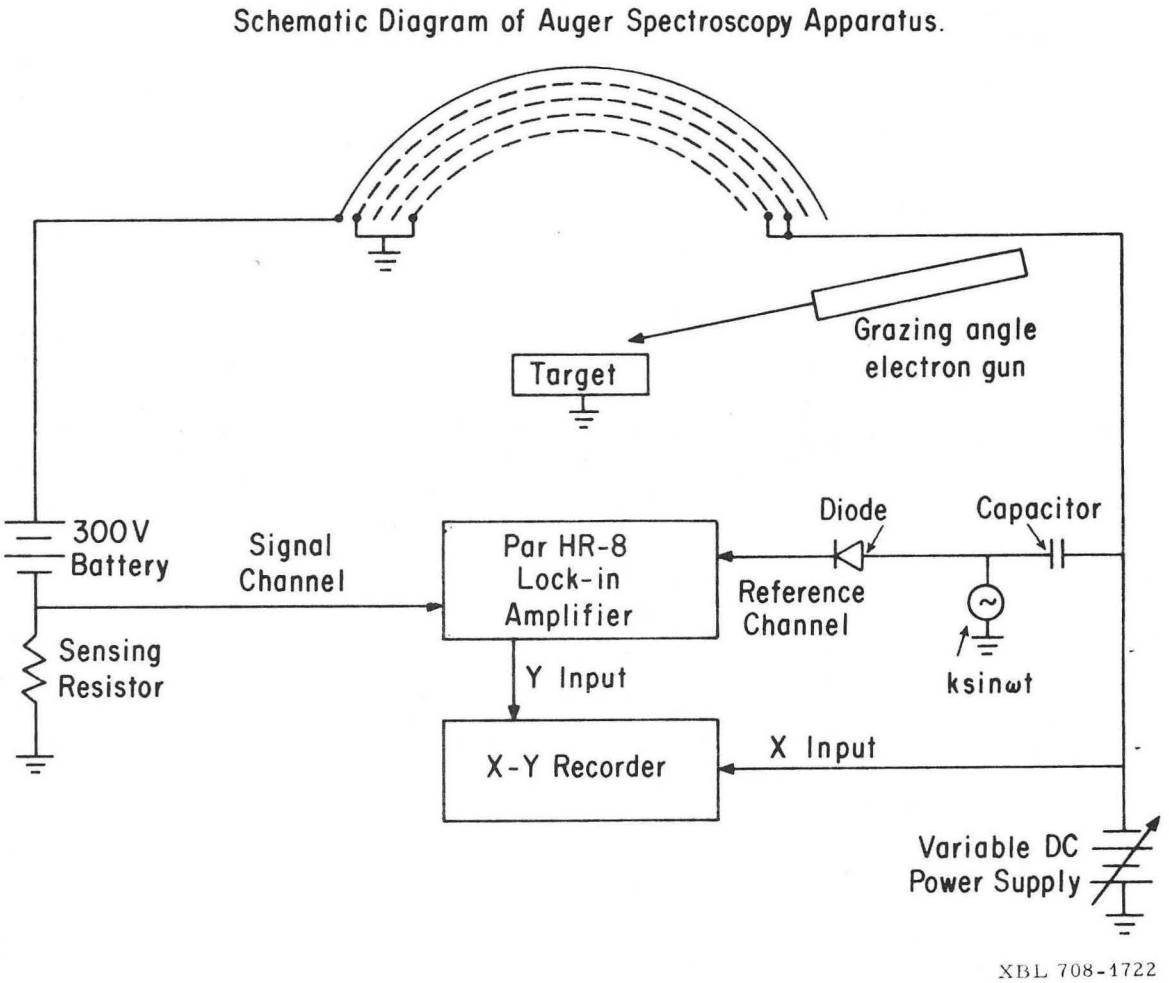

Fig. I-10. Block diagram of the retarding field apparatus used in this work for Auger Electron Spectroscopy.

0 0 0 0 3 6 0 5 4 7 3

second harmonic 2ω in order to obtain the spectrum shown in Fig. I-11 in which the transitions are clearly visible.

The Auger process is a radiationless transition that may occur whenever a highly excited, singly ionized ion is created. Such a species can be prepared by expelling an electron from an inner atomic orbital if the target is bombarded with a moderately energetic (1-5 KeV) beam of electrons or x-rays. The excited ion relaxes by dropping an electron from a higher energy state into the vacancy, simultaneously releasing any excess energy through an electrostatic interaction to a second electron that is then expelled from the ion. This Auger electron has an energy that is characteristic of the parent atom and is independent of the nature and energy of the exciting source employed. For a complete account of the theory of the Auger transition, the interested reader is referred to a book by Burhop.[32]

Quantitative as well as qualitative information should be available from AES. Using the atomic energy levels obtained from x-ray data, it is possible to calculate the expected Auger transition energies for any element in the periodic table (except hydrogen and helium which have less than three electrons). In the present state of development of AES, however, the assignment of an observed transition to a specific set of energy levels in a given atom is still tentative. It is thus incumbent upon each experimenter to adequately characterize his own substrate and then to calibrate his system for those substances of particular interest to him. While quantitative

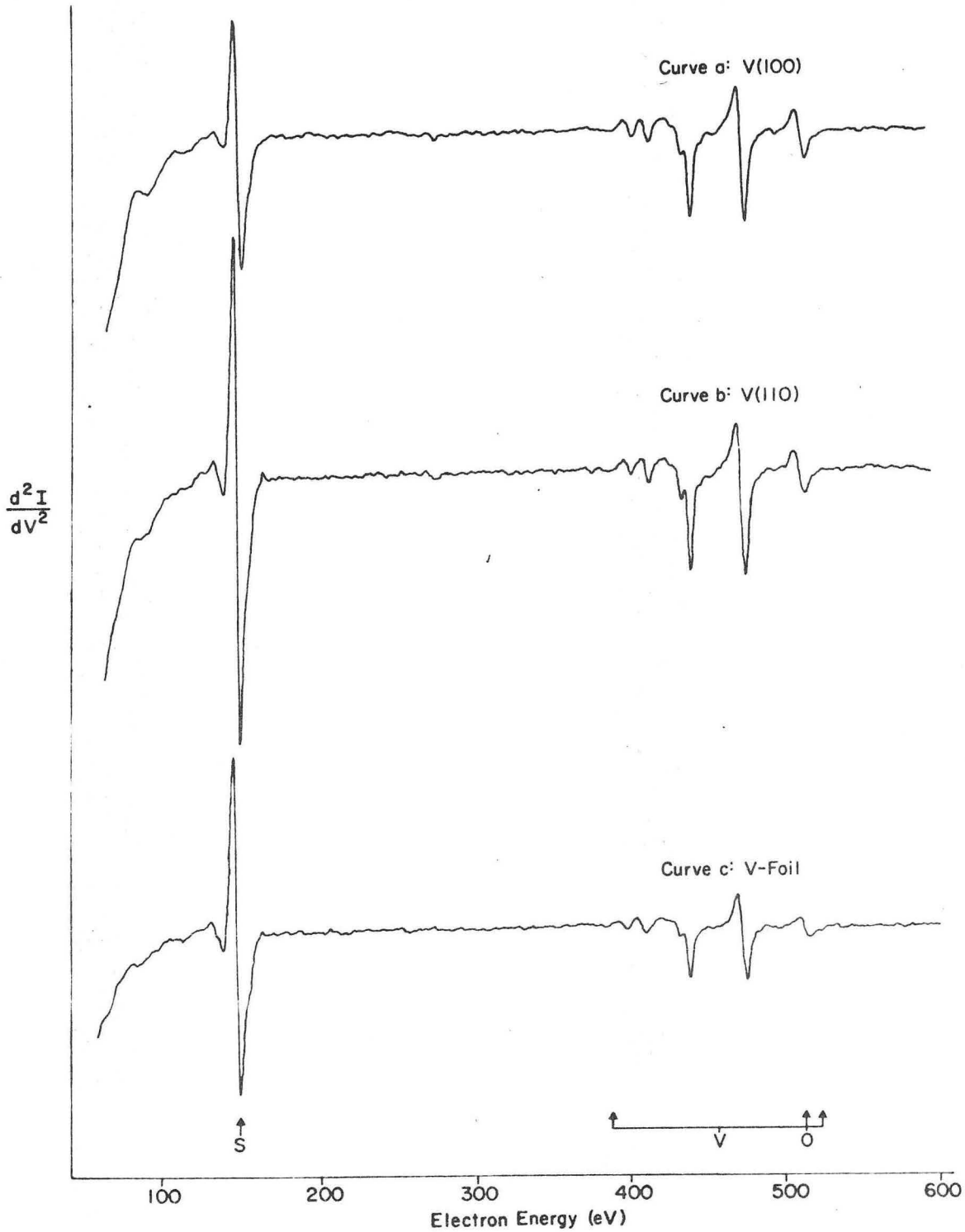

XBL 7012-7402

Fig. I-11. Auger emission spectra from various vanadium surfaces indicating the readily discernible peaks using E_p = 2500 volts.

information is theoretically attainable[33] it has not yet become generally available. However, Weber and Johnson[34] have demonstrated that the peak to peak height of an adsorbed potassium impurity on a germanium (111) substrate varies directly as the coverage, thus indicating that at least for some systems, an exact quantitative analysis is on the horizon.

In our work with platinum surfaces, the impurity spectra of most interest are those of carbon, nitrogen and oxygen, and although no quantitative calibration was attempted, changes in peak intensities were readily followed. Some of these points will be discussed more thoroughly in the following sections. Figure I-12 presents the Auger spectrum of platinum both in a clean state and in the presence of carbon and carbon monoxide. The impurity transitions are easily distinguishable from the noise level.

D. Atomic and Molecular Beam Scattering

We have already pointed out that while scattering experiments with crossed molecular beams have long been used to probe the dynamics of gas-phase chemical reactions, the application of atomic and molecular beams to the study of gas-solid interactions is a relatively recent phenomenon. The reasons for this lag can be traced to the complexity of the particle-surface interaction and to the inherent experimental difficulties. With the advent of ultra high vacuum technology, sophisticated electronic detection equipment, high purity

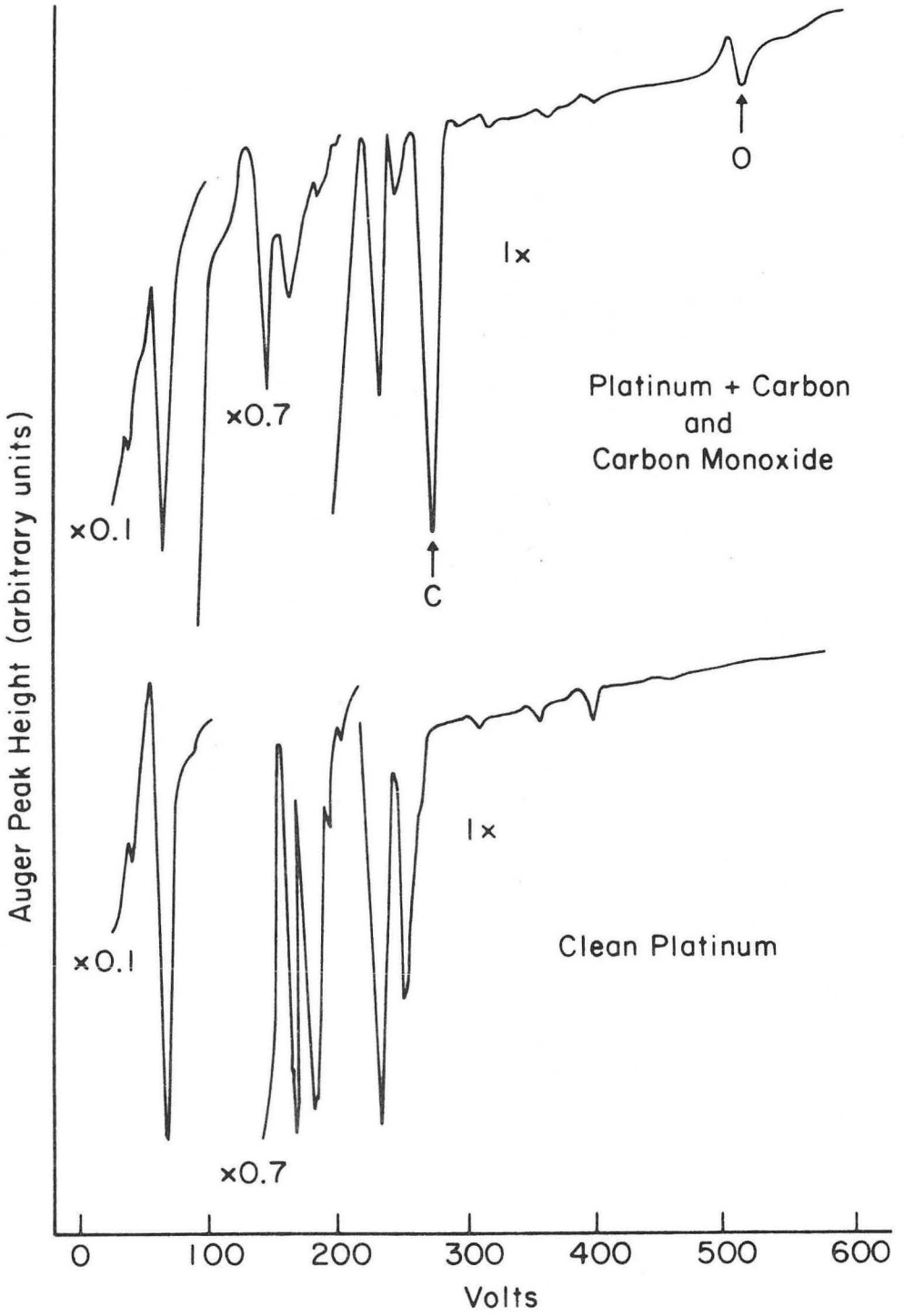

XBL 719-7306

Fig. I-12. Auger emission spectra for clean and contaminated platinum surfaces using E_p = 2000 volts. Note the changes in the spectrum induced by the presence of carbon.

0 0 0 0 3 6 0 3 4 7 5

single crystals and associated metallurgical techniques for their preparation, sensitive tools for surface analysis, and improved molecular beam sources, many of these problems became tractable.

Several types of surface chemical reactions can be visualized: (1) the gas molecule may dissociate or undergo rearrangement during its collision with the solid;[17,35] (2) the incident molecule may undergo reaction with the surface yielding a surface atom among the volatile reaction products;[14,36-39] (3) the gas molecule may react with a gas previously adsorbed on the surface;[40,41] and (4) adsorbed atoms may associate on the surface to form gaseous molecular reaction products.[42,43] Molecular beam techniques provide an ideal way to study the elementary steps of reactions such as those above. One can easily vary the energy and approach angle of the incident beam. The angular distribution and identity of the particles scattered from the surface may be ascertained using a mass spectrometer. The energy accommodation between an incident gas and an inert solid may be studied as well as the manner in which reaction exothermicity is partitioned between the thermal energy of the surface and the kinetic energy of a volatile reaction product. Controlled changes in the state of the surface (specifically changes in surface order, crystallographic orientation, surface impurities, etc.) permit their roles in a reaction to be investigated.

Recent reviews by Smith and Saltsburg[44] and Stickney[7] discuss rare gas scattering from several surfaces. Hurlbut[45] concentrates on the study of gas-solid collision dynamics through 1962. A more current paper by Merrill[46] pays particular attention to reactive

scattering. Unfortunately, while more and more emphasis is being placed on studying surface chemical reactions, there is still far too little information available in the literature.

When a beam of atoms or molecules strikes a surface it may undergo elastic scattering or it may exchange energy with the solid. In the case of an elastic collision, one would expect to observe diffraction for the light elements because their de Broglie wavelengths are comparable to atomic distances.* Heavier species might not show diffraction due to stronger surface interactions arising from higher polarizabilities and heats of adsorption causing inelastic collisions, but still might show scattering in the specular direction. We will reserve the term specular scattering to imply that the width of the scattered beam is the same as the incident beam and that the angles of incidence θ_i and reflection θ_r (both measured with respect to the surface normal) are equal. In the case of energy exchange, the particles may gain or lose only a portion of their initial energy, or they may reach complete thermal equilibrium with the solid. In this latter case, the angular distribution of the restituted particles would be in agreement with the well known cosine law pictured in Fig. I-13. Here we have plotted the data in the familiar polar coordinate system as well as in the rectilinear representation used more frequently in the literature. Notice however that in either plot, the maximum

---

* For a helium atom with a velocity of 10^5 cm/sec, $\lambda = h/mv$ yields a wavelength of 1 Å.

0 0 0 0 3 6 0 5 4 7 6

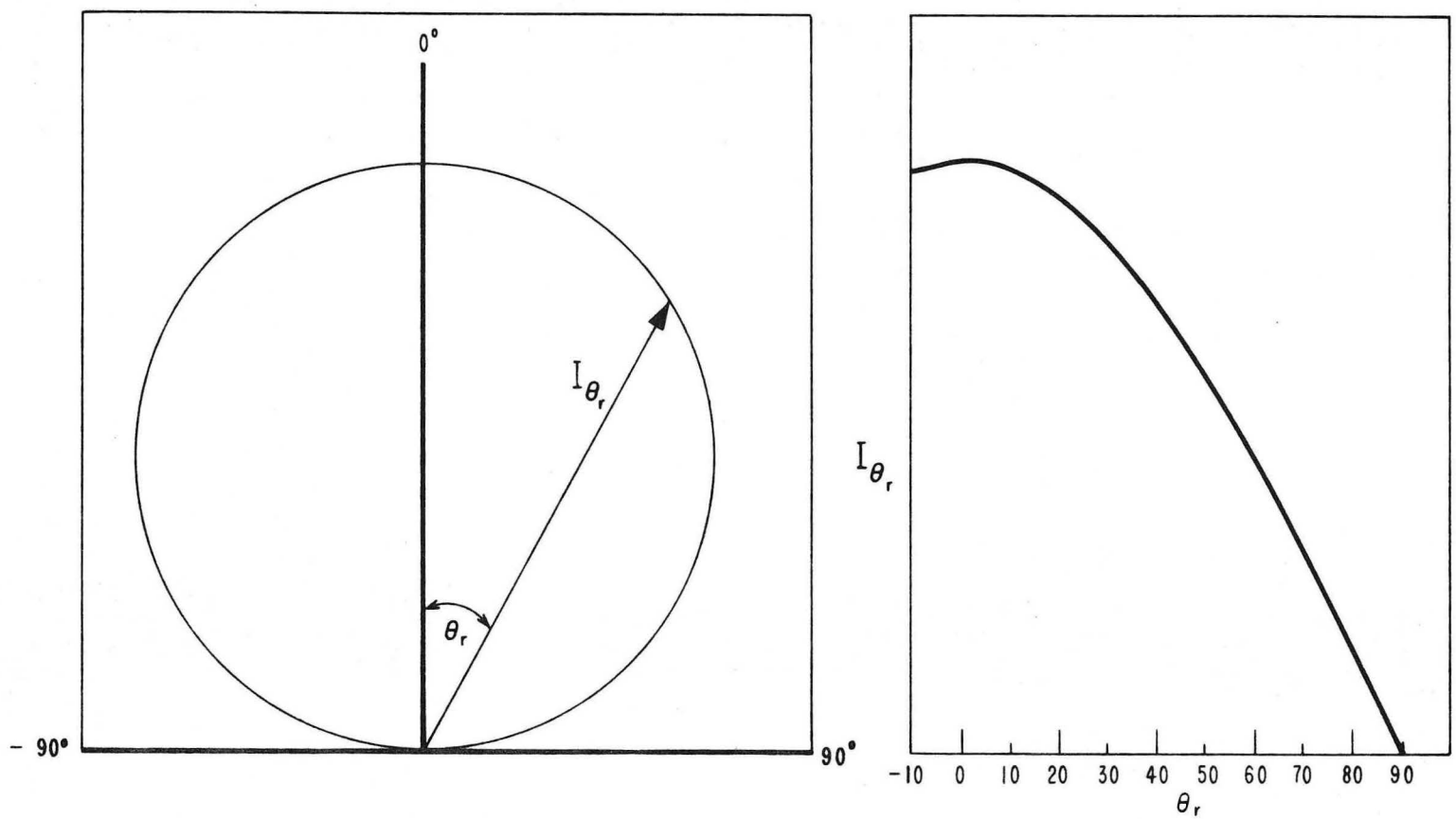

XBL708-3572

Fig. I-13. Cosine angular distribution plotted in polar coordinates (left) and in rectilinear coordinates (right).

intensity occurs at the surface normal, $\theta_r = 0°$. For less than complete accommodation, one observes what is termed directed scattering as shown in Fig. I-14. Here the maximum scattered intensity no longer occurs at the surface normal but at some other angle which may or may not coincide with the specular direction (indicated by the small arrow on the figure). Because the intensity maximum in Fig. I-14 is displaced toward the surface normal and in the direction of the incident beam with respect to the specular ray, such a lobe would be referred to as backscattered. Similarly, a distribution displaced toward the surface tangent would be termed forward scattered because it is rotated away from the direction of the incident beam relative to the specular position. Backward and forward scattering are sometimes referred to as subspecular and supraspectular scattering, respectively, but these terms should be avoided as they may confuse an unwary reader.

1. Diffraction

Diffraction has indeed been observed with He, H, H_2, and D_2 from the cleaved (100) surface of LiF.[2,6,12,44] However, with the clean low index faces of single crystal gold, silver, platinum, nickel and tungsten, diffraction features have not yet been seen although specular scattering is intense. This lack of diffraction may be due to the fact that the incoming gas atoms experience a relatively smooth surface potential arising from the highly mobile electron gas in the metal. To test this hypothesis one might study the scattering of helium from a semiconductor surface in which the

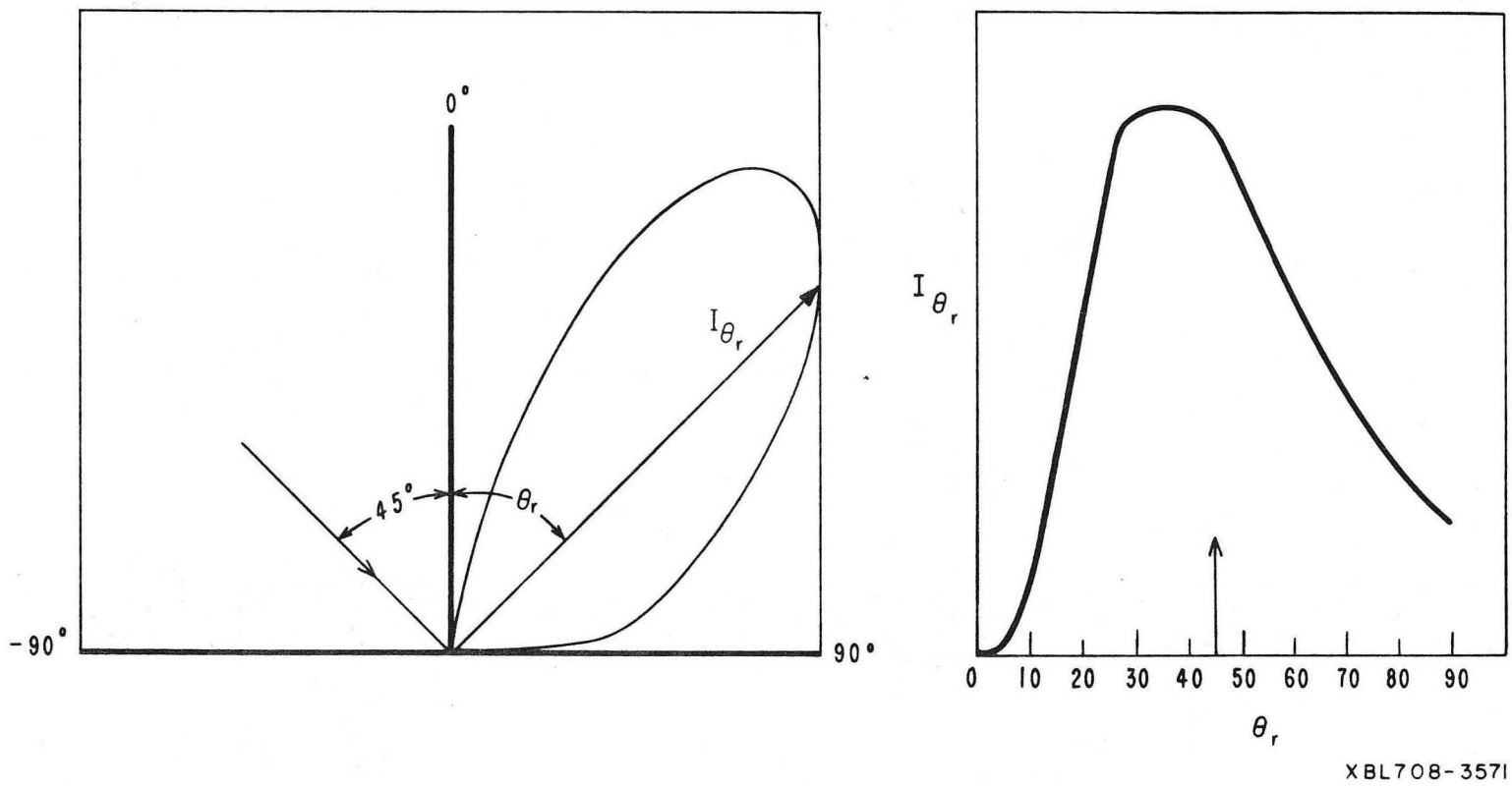

Fig. I-14. Directed scattering plotted in polar coordinates (left) and rectilinear coordinates (right).

0 0 0 3 6 0 3 4 7 7

number of conduction electrons could easily be reduced by lowering the surface temperature to 77°K. Weinberg and Merrill[47] have reported strong diffraction beams in the presence of a carbide overlayer on a (110) tungsten surface and recently Stickney and Tendulkar[48] have observed diffraction features from the (112) tungsten plane. This latter instance is the first indication that clean metals exhibit atom diffraction and it suggests that atomically rough high index crystallographic faces are more likely to yield diffraction than atomically smooth low index faces.

In general, studies of rare gas scattering have shown that helium scatters strongly at the specular angle provided the surface is clean and single crystalline while the heavier noble gases tend to produce broader scattering patterns that may be displaced toward the surface normal (i.e., backscattered). Such behavior may be accounted for on the basis of energy exchange between collision partners of nearly equal mass, increased van der Waals attraction due to the higher polarizability of the heavier gases,[49,50] and trapping.

While helium scatters specularly from clean well-ordered surfaces, several workers including this author have found that the helium scattering from polycrystalline and contaminated surfaces is much broader and less intense. In fact, Smith and Saltsburg[13] found that polycrystalline gold films scattered helium diffusely. These two authors[51,52] have also observed the degradation of the scattered signal due to surface adsorption of background contaminants. Similar findings have also been reported by others.[53-56] In all, the helium

beam appears to be a sensitive probe of surface structure.

2. Reactive Scattering

The number of reported investigations of surface chemical reactions by molecular beams is severely limited. Smith and Fite[35] reported studying the nickel-chlorine system through its volatile chlorides, NiCl and $NiCl_2$. Smith and Fite[35] have also examined the thermal dissociation of hydrogen on tungsten at elevated temperatures (2500°K) and they found that while the reflected molecular hydrogen was lobular, the angular distribution of the product atomic hydrogen was diffuse. Another study of the Ni/Cl_2 system, as well as the Ni/Br_2 system, was conducted by McKinley.[38,39] He reported the first order dependence of the $NiCl_2$ product on the incident Cl_2 beam strength. Krakowski and Olander[17] probed the dissociation of hydrogen at the tantalum surface and observed a first order mechanism consistent with a hydrogen/metal bond strength of 65 kcal/mole.

More recently, Madix and Schwarz[36] have studied the Ge/Cl_2 reaction and extracted rate parameters. Madix, Parks, Susu, and Schwarz[37] also reacted atomic and molecular oxygen with the surface of germanium in a similar experiment. The low pressure hydrogen/deuterium exchange on a nickel surface has been investigated by Palmer, et al.[40] and this work has lately been extended to the platinum system.[41] In both instances the authors observed that the hydrogen-deuteride product was strongly peaked about the surface normal, conforming to a $\cos^3 \theta_r$ dependence. This behavior is believed

to be consistent with a surface reaction between adsorbed mobile H and D atoms. The latter report also presents evidence that the oxidation of deuterium proceeds by interaction of adsorbed deuterium atoms and oxygen molecules, and yields deuterium oxide with a diffuse angular distribution. Muschlitz and his coworkers[57,58] have studied the thermal dissociation of nitrous oxide, N_2O, at the surface of a hot tungsten ribbon and have observed the formation of both N_2 and NO. Finally, van Willigen[59] has investigated the surface recombination of hydrogen atoms to form molecular hydrogen. To date no theories are available to describe reactive scattering.

3. Scattering Theories

Rare gas scattering from surfaces has been reviewed in the literature[7,44-46] and several theories have been advanced to explain the observed results. One complication in the development of these theories, however, is that the explicit functional form of the gas-solid potential is not well known, which is in contrast to the case for gas-gas interactions. Cabrera, Celli, Goodman and Manson[60,61] have developed a quantum mechanical model to describe elastic scattering (diffraction) and briefly discuss its extension to inelastic processes (phonon exchange). Formalisms based upon numerical integration of the classical equations of motion for a gas atom and the surface have been reported by Goodman,[62-70] Oman,[71-75] McClure,[76-78] Raff,[79-81] and Busby.[82] These calculations have generally produced results in qualitative and sometimes quantitative agreement with experimental measurements.

0 0 0 0 3 6 0 3 4 7 9

Goodman's theory in its three dimensional form treats the gas and solid as hard spheres with the addition of an adjustable Morse potential. Although the surface is initially assumed at rest (0°K), quantitative fits to experimentally determined accommodation coefficients have been achieved. Calculations of angular distributions using a two dimensional solid have been less successful, however.[67] One interesting aspect of Goodman's research is that he finds a molecule can be trapped in the potential well for several vibrations and then escape, still retaining some memory of its initial energy and direction. This same "hopping" phenomenon has been observed by Busby, et al.[82] and was used by Lennard-Jones and Devonshire[83] to explain some of Stern's original work. Goodman's calculations also suggest that the gas-solid collision is essentially languid and that most of the energy exchange occurs during the repulsive part of the collision, the attractive portion of potential having relatively little effect on the interaction.

The scattering theory of Oman assumes that the interaction between the gas atoms (assumed to be point masses) and the lattice atoms is expressable as a pairwise additive Lennard-Jones 6-12 potential. Both independent and coupled harmonic oscillators have been used to simulate the lattice dynamics. Because of the complexity of the calculations, statistical methods must be used to smooth the data. The agreement between the theory and the scattering results for thermal energy beams (.01 - .05 eV) is only qualitative, but much better fits are observed with epithermal beams (1-2 eV).[75] This is not too

surprising because the independent oscillator assumption requires that the collision be rapid rather than languid as is the case for thermal beams.

McClure has achieved quantitative agreement between his results and the experimental measurements of Smith, et al.[84] for the scattering from LiF. He employs the so called finite range interaction (FRI) model between the gas atom and a solid that consists of an array of two dimensional anisotropic, independent harmonic oscillators plus fixed centers of potential force. His calculations have pointed out the effect of structure scattering (i.e., scattering resulting from the structure of the solid) and have led to the prediction of "surface rainbows." These rainbows are analogous to those observed in cross beam scattering[3-5] and arise whenever $\frac{\partial(\theta_r - \theta_i)}{\partial B} = 0$ if B is the impact parameter parallel to the line of surface atoms. The net result of the rainbow is to preferentially scatter large numbers of atoms in specific directions as has been observed with LiF.[85,86]

The finite range interaction model was also used by Raff and his associates[79-81] to describe the gas-solid interaction. Their formulation employs a Morse function for the potential between the gas atom and the lattice sites. The solid is represented by independent harmonic oscillators with nine movable lattice sites harmonically coupled to fixed centers that may represent either the (100) or (111) crystal planes. Again the solution to the differential equations of motion is time consuming so that small ensembles must be employed, but

structure scattering seems to be observable.

An additional theory has been put forth by Busby, Haygood, and Link.[82] The interaction is modeled as the collision of hard spheres. Both a finite surface temperature and an attractive surface field energy are employed. Quantitative agreement between calculations and the scattering of high energy (.3 - .5 eV) argon beams from solid argon could be attained. The most surprising facet of the experimental and theoretical observations was that the angle of maximum scattered intensity was fixed with respect to the surface normal, independent of the incident angle.

While the above theoretical models have relied upon numerical calculations to determine the angular distribution of scattered particles, a closed form analytic solution that yields surprisingly good agreement between theory and observation for rare gas scattering has been evolved. This is the so called "hard cube" theory originally formulated by Logan and Stickney.[87] In this model the gas and surface atoms are assumed to be rigid elastic particles subject only to an impulsive collision. The surface is assumed to be perfectly smooth so that tangetial momentum is conserved in the collision. The lattice atoms are represented by cubes that have a one dimensional Maxwell-Boltzmann velocity distribution and are constrained by square well potentials to move only normal to the surface. In constrast to some of the more sophisticated lattice theories, this model permits the use of a finite surface temperature. Qualitative agreement with several trends in the experimental data were found: 1) as the energy

of the beam increases, the angle of maximum scattering intensity θ_m increases; 2) as the solid temperature increases, θ_m decreases; 3) θ_m increases as θ_i increases; and 4) as the mass of the incident gas atom increases, the width of the scattering distribution increases. In more physical terms, the first two trends indicate that when the gas is more energetic than the solid, it has a high probability of losing energy to the surface, whereas when the surface is hot, it has a high probability of transferring energy to a cooler gas.

The original work was extended by Logan, Keck, and Stickney[88] and then modified by Logan and Keck[89] to produce the "soft cube" formulation which substituted harmonic oscillators for the surface atoms and included a potential with attractive and repulsive regions. Only by using a monoenergetic beam could a closed form solution be achieved. Agreement between the calculated and observed data was still only qualitative, and the calculated patterns were always narrower than the experimental ones.

Summarizing these theories, we must state that for rare gas scattering, the theoretical treatments are relatively good in that they qualitatively predict the observed dependence upon incident angle, gas temperature, and surface temperature. For its simplicity, one must commend the hard cube model and the insights it yields, but the finite range interaction model of McClure would seem at present to provide the most realistic calculational results. Scattering theories for reactive surface collisions have yet to be developed.

0 0 0 0 3 6 0 0 4 8 1

E. Clean Surfaces

We mentioned the need for clean and characterized surfaces in sections B and C of this chapter. In all likelihood, a prime contributor to the lack of consistent scattering results from one laboratory to another [viz. the work of Hinchen and Foley[54] compared to the work of Smith and Merrill[90] or West and Somorjai[55]] is the unknown state of surface cleanliness. Thus, contamination of the sample crystal surface is a key factor in all molecular beam-surface studies, just as it is in all surface research.

One source of contamination is the ambient gases in the scattering chamber. Figure I-15 shows a typical mass spectrum of the residual gases found in the ultra high vacuum (UHV) system used in this work. The most prevalent gases are hydrogen, carbon monoxide, and water. From the kinetic theory of gases, one can easily show that at a gas pressure of 10^{-6} torr, each surface atom is struck by a gas molecule on the average of once every second. Pressures considerably below this limit are necessary if one wishes to maintain a surface free of adsorbed gases for any length of time. Alternatively, the approaches suggested in section B may be used.

In addition to possible contamination of the surface by background gases, contamination can occur through sample preparation (cutting, polishing, etching), via contact with crystal supports and thermocouples, or by out-diffusion of bulk impurities. This latter source can be extremely insidious because a bulk impurity

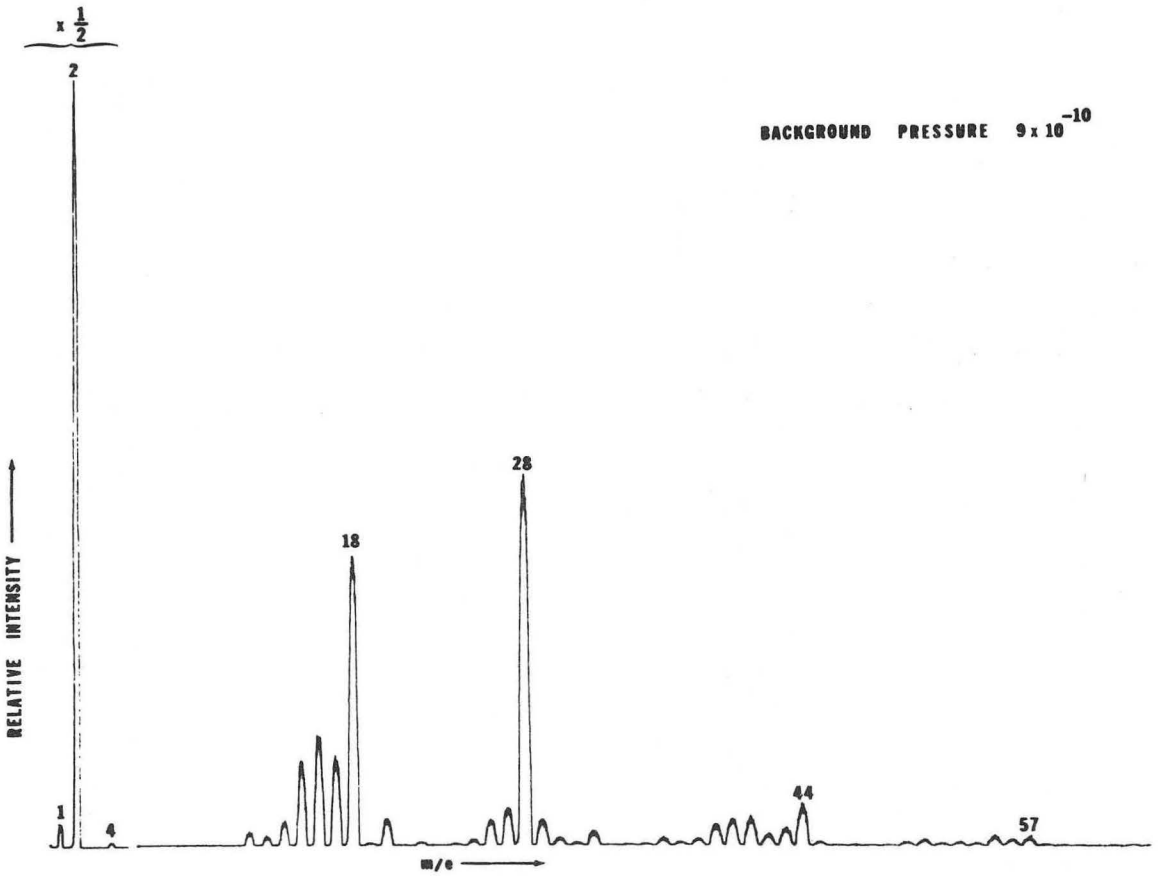

XBL 702-355

Fig. I-15. Typical mass spectrum of the residual gases in the UHV scattering chamber at a pressure of 9×10^{-10} torr.

0 0 0 0 3 6 0 5 4 8 2

concentration exceeding 0.01 parts per million could supply enough impurity atoms to produce more than a tenth of a monolayer coverage if every impurity precipitated out on the surface. Ion bombardment can be used to removed the outermost atomic layers, however. Measurements of sputtering yields have shown that the surface removal rate corresponds roughly to one substrate atom per ion under the conditions characteristic of a LEED system.[91] Thus, repeated cycles of heating (to induce diffusion of surface segregating components) followed by ion bombardment can be used to remove impurities resulting from sample preparation and bulk diffusion. Unfortunately, elevated temperatures can also lead to the surface migration of contaminants from the sample holders and thermocouples to the crystal surface. For this reason, the specimen should be mounted if possible on high purity holders of the same material. So far we have confined our attention to the preparation of a "clean" surface. Exactly what do we mean by this word?

No existing experimental technique is capable of specifying with any certainty that all the exposed atoms of the solid surface are identical. In practice the identification of a clean surface can be made only within the limits of sensitivity of a given technique. Thus, a clean surface will henceforth be defined as a surface upon which there are no detectable impurities. Clearly this is a working definition and we must now discuss detection limits of the equipment used in this work.

Jona[92] has shown that even one-tenth of a monolayer of disordered silicon atoms deposited uniformly upon a Si(111) substrate yields a

measurable decrease in the heights of specularly reflected LEED intensity maxima. Similarly, Goodman[93] has observed perceptible changes in the Ni(111)-(1×1) LEED diffraction pattern as the result of exposure to ambient gases for 10^{-7} torr-sec. (This corresponds to 0.1 monolayer at unity striking probability.) If the impurity forms an ordered array on the surface, then electron diffraction should be sensitive to coverages below one-tenth of a monolayer.

It has already been pointed out in section C-2 that Auger spectroscopy (AES) is sensitive to coverages below the monolayer level. The theoretical detection limit of this tool, set by signal to noise considerations, is approximately 10^{12} to 10^{13} atoms/cm^2 or ~ 0.01 monolayer and has apparently been approached for the case of oxygen on silicon.[33]

Thus, by combined LEED-Auger measurements on a crystal, a report of a clean surface means in a practical sense that any contaminants are probably below one percent of a monolayer, except for hydrogen which cannot be detected.

0 0 0 0 3 6 0 5 4 8 3

II. EXPERIMENTAL

Before proceeding to describe the equipment and materials used in this research, a few comments on some of the general principles and pitfalls involved in the study of gas-solid interactions should be made. Neutral particles, unlike ions, electrons, and photons, are comparatively difficult to focus and to detect. In order to form a directed beam of neutral molecules, one must rely upon the inherently low efficiency process of collimation. Detection too presents difficulties as it is usually necessary to ionize the molecules before they can be observed. This is again an inefficient process except in the case of alkali metal compounds. Coupled to these intensity problems is the fact that residual gas molecules in the scattering region, particularly those of the beam species, significantly reduce the signal-to-noise ratio. Consequently, a large part of the experimental effort expended in the study of gas-solid interactions goes toward the construction of a system having a large enough signal-to-noise ratio to permit reliable measurements of the phenomenon to be examined. This chapter discusses the techniques and equipment evolved for that purpose.

A. Sample Preparation

The single crystal rod of platinum from which specimens were cut for this work was obtained from the Materials Research Corporation and had a specified purity of 99.999%, or an impurity concentration of below 10 ppm. Back-reflection Laue x-ray techniques were used to

orient the rod within 1° of the (100) crystal plane, and then a disk shaped sample 7 mm in diameter and 1 mm thick was removed by spark cutting. This crystal was next etched in 375°K 50% aqua regia until it yielded a Laue pattern. After reorienting, it was transferred, still on the goniometer, to an abrasive wheel which was used to grind the front surface parallel to the (100) plane. Successively finer grades of polishing cloth were used, concluding with a treatment on one micron diamond paste. A final polish on 0.05μ alumina for thirty to sixty minutes was employed to remove the diamond scratches. At this point the crystal was removed from the goniometer and the opposite side was ground parallel to the polished face and then prepared in an identical manner. Scanning electron microscopy showed that the crystal surface was smooth at the micron level except for isolated scratches.

High purity (99.9%) platinum support tabs 0.5 mm thick were spot welded to the edges of the sample so that it could be attached to a Varian multipurpose electromechanical feedthrough (crystal manipulator). A Pt-Pt-10% Rh thermocouple was attached to the upper edge of the back face so that the crystal temperature could be monitored. This completed assembly was etched in hot 50% aqua regia for fifteen minutes to remove the mechanical damage introduced during the final polishing and then thoroughly rinsed in distilled water and reagent grade methanol. Following this treatment, the unit was mounted on the crystal manipulator. One can see a typical example of the large flat bottomed etch pits that are formed in the SEM photograph shown in Fig. II-1. To enchance the picture contrast the surface of

0 0 0 0 3 6 0 5 4 8 4

XBB 7010-4914

Fig. II-1. Scanning electron microscope (SEM) photograph of an etched Pt(100) surface tilted at 45° to the incident electron beam to enhance the picture contrast.

Fig. II-2a. Photograph of the apparatus, denoted MBA-Echo, built for the study of gas-solid interactions. To provide a scale, the flange containing the window on the left-most chember is 8 inches (21 cm) in diameter.

0 0 0 0 3 6 0 3 4 8 6

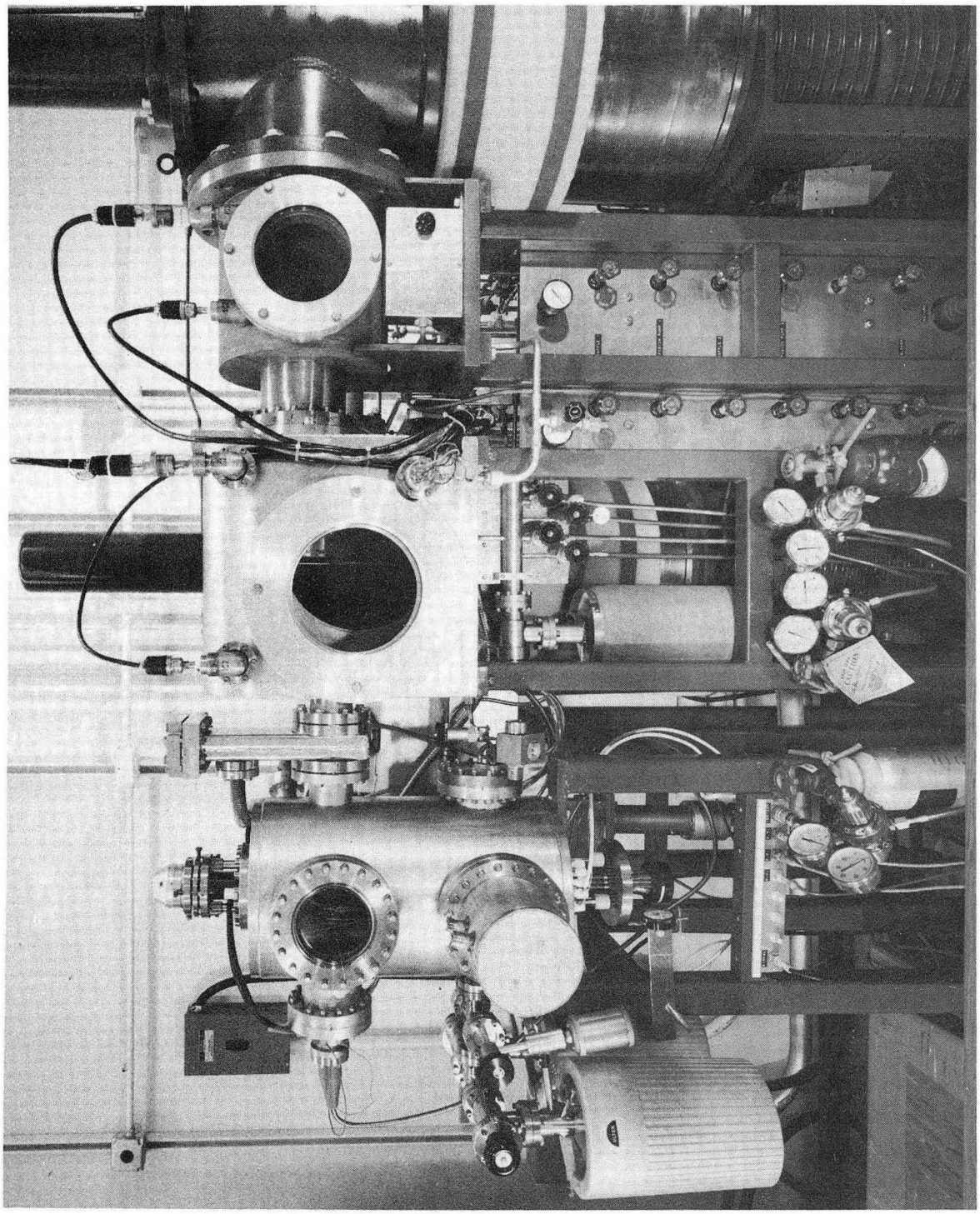

XBB 702-875

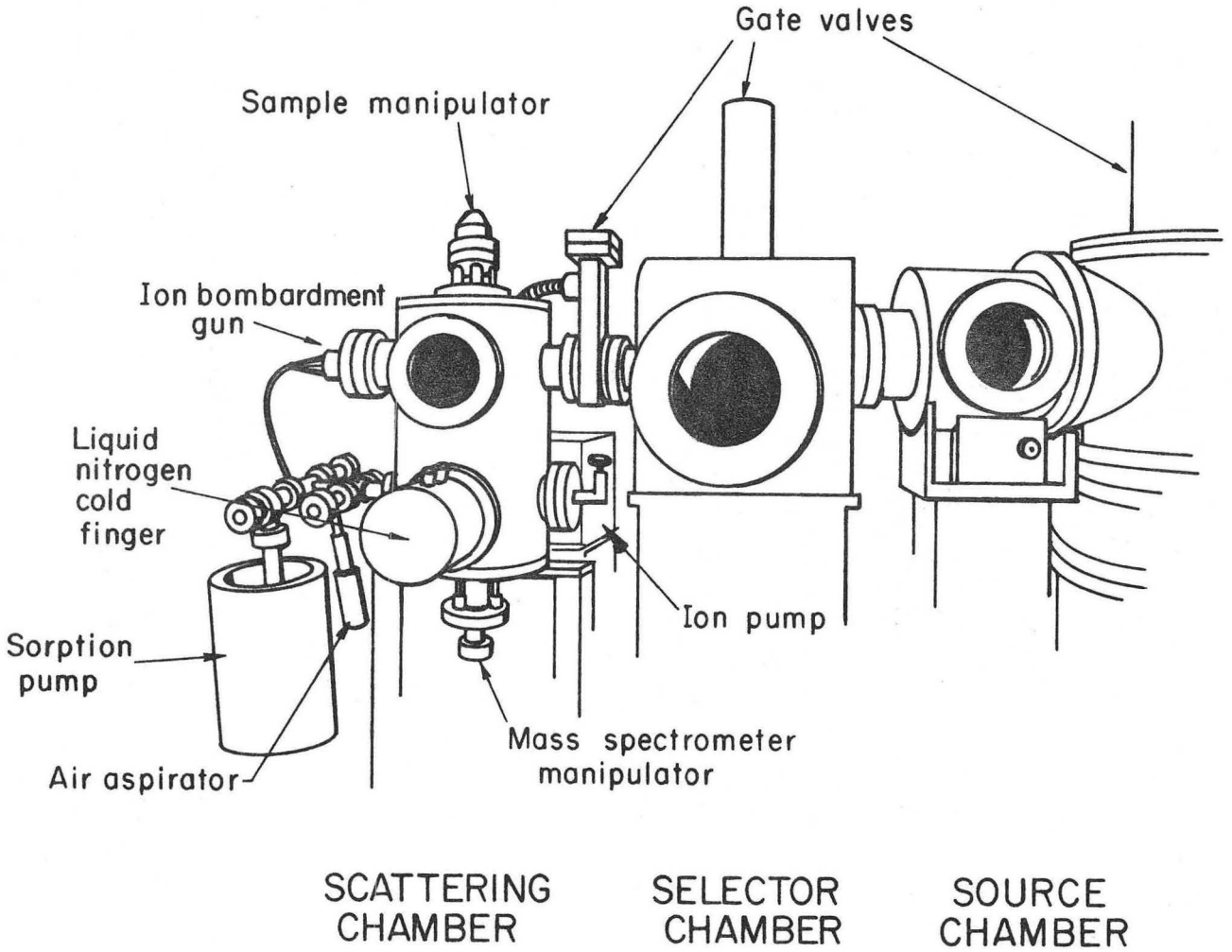

XBL704-2670

Fig. II-2b. Identification of the major components of MBA-Echo and their location.

0 0 0 0 6 0 9 4 8 7

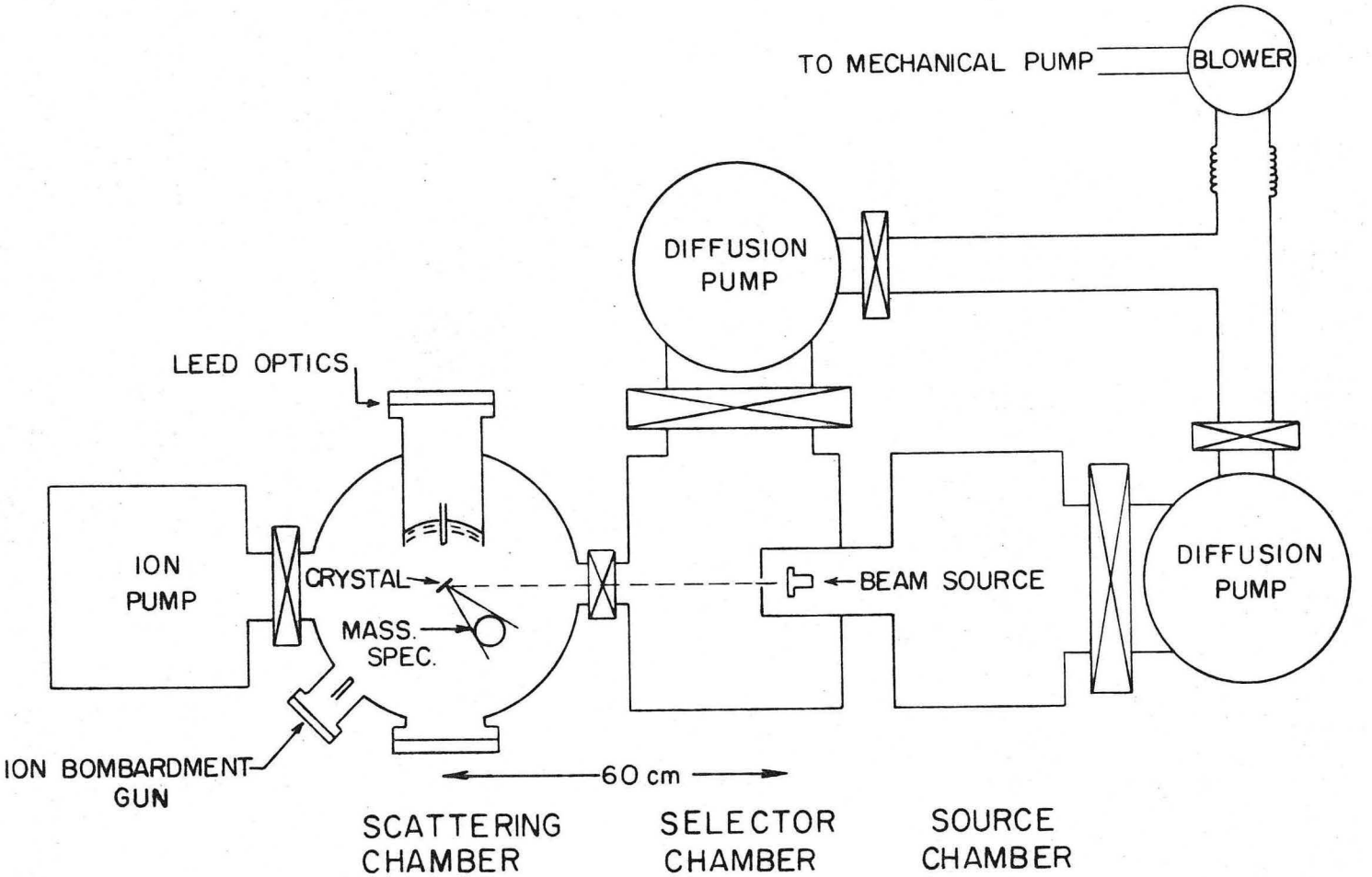

XBL 702-279

Fig. II-3. Schematic diagram of the molecular beam scattering apparatus showing differential pumping network.

I or number of molecules per second reaching a detector located some distance L downstream on the axis of the source is given by

$$I = Q \left[\frac{A_d}{4\pi (L/2)^2} \right] = \frac{QA_d}{\pi L^2} \qquad \text{(II-1)}$$

In this equation, Q represents the total effusive flow from an orifice of area A_s separating a gas with an average velocity $\bar{v}$ and number density n from a vacuum. The kinetic theory of gases may be used to show that

$$Q_s = \frac{1}{4} n \bar{v} A_s = 3.51 \times 10^{22} \frac{pA_s}{\sqrt{MT}} \left[\frac{\text{atoms}}{\text{sec}} \right] \qquad \text{(II-2)}$$

provided the pressure is expressed in torr, the area in cm^2, and the gas mass in grams per moles. For an orifice of area 0.015 cm^2 emitting hydrogen at a temperature of 300°K with a driving pressure of 0.1 torr, $Q_s = 2.15 \times 10^{18}$ atoms/sec. The bracketed term in Eq. (II-1) is the ratio of the detector area A_d to the surface area of the spherical effusion pattern at a distance L from the source. Substituting numerical values into Eq. (II-1) and replacing the pressure by the pressure gradient across the orifice (because the "vacuum" pressure may not be negligible) produces

$$I = \frac{1.12 \times 10^{22}}{\sqrt{MT}} (p_{oven} - p_o) \frac{A_s A_d}{L^2} \left[\text{atoms/sec} \right] \qquad \text{(II-3)}$$

where the distance L is in cm and the area A_d in cm^2.

In the typical molecular beam experiment employing a non-condensible gas, the source is located in a chamber that is isolated from the scattering region by a small collimating orifice whose dual functions are (1) to form a molecular beam by selecting a small portion of the effusive flow from the oven and (2) to permit differential pumping of the second chamber so that low pressures can be attained. The fraction of molecules entering the second chamber from the beam source is usually quite small, and for an ideal effusion source located 30 mm from a collimating orifice 2 mm in diameter is less than 0.5% of the total molecular flow. For this reason, the speed of the pump on the source chamber should be large, or the accumulation of unpumped gases will attenuate the beam according to the Beer-Lambert Law:

$$I = I_o \exp\left[-\ell/\lambda(p)\right] \qquad \text{(II-4)}$$

Here $\lambda(p)$ represents the pressure dependent mean free path and is given by

$$\lambda(p) = \frac{1}{\sqrt{2}\pi\sigma^2 n} = \frac{2.33 \times 10^{-4} T}{p\sigma^2(\text{Å})} \text{ [cm]} \qquad \text{(II-5)}$$

where σ is the collision diameter of the molecule in angstrom units.

During the early planning stages of the apparatus, it was decided that eventually experiments probing the energy dependence of surface reactions would be undertaken. Provisions therefore had to be

made for the use of a rotating disk velocity selector. A minimum length selector may be 8 cm long so that the overall source to collimator distance might be 10 cm. To ensure only a 1% attenuation in the beam requires

$$\lambda > \frac{-\ell}{\ln(0.99)} = 100.6\ell \qquad \text{(II-6)}$$

Thus if ℓ = 10 cm, the pressure in the source chamber must be roughly 1×10^{-5} torr according to Eq. (II-5). To maintain such a pressure under the load from a standard effusion source requires an excessive pumping speed as will now be shown.

Pump speeds are conventionally reported in liters per second. At a specified temperature and pressure, this number can be converted to the number of molecules removed per second by multiplying by N_o/RT. Thus

$$S[\text{liters/sec}] = SN_o/RT = 3.21 \times 10^{19}\ S[\text{atoms/torr sec}] \qquad \text{(II-7)}$$

at 300°K. Clearly the minimum source pressure attainable is given by

$$p_1 = \frac{Q_s}{3.21 \times 10^{19}\ S_1}\ [\text{torr}] \qquad \text{(II-8)}$$

where Q_s is the source leak rate. Thus we see that

$$S_1 = \frac{Q_s}{3.21 \times 10^{19}\ p_1}\ [\text{liters/sec}] \qquad \text{(II-9)}$$

is the required pumping speed. Using the previously arrived at values of $p_1 = 1 \times 10^{-5}$ torr and $Q_s = 2.15 \times 10^{18}$ atoms/sec yields $S \sim 6700$ liters/sec. In the vicinity of the source, the actual pumping speed of a well trapped diffusion pump that can be isolated by a gate valve may be only 30% of its rated value due to conductance limitations. Thus a pump with a speed of 20,00 liters/sec would probably be required to evacuate the source chamber and such a pump is prohibitively large.

The way to avoid this difficulty is to tolerate a higher pressure in the source chamber and then to interpose an intermediate chamber containing the selector between it and the scattering chamber. A 1500 ℓ/sec pump attached to the source chamber would maintain a pressure of 1×10^{-4} torr under the conditions stated previously. If the source to collimator distance were reduced to 3.0 cm, the beam attenuation would be roughly 10% in the source chamber, but a pressure in the 10^{-7} torr range could easily be achieved in the selector chamber so that losses there would be negligible. This is the approach that was taken as has already been illustrated in Fig. II-3.

2. <u>Signal-to-Noise Considerations</u>

At the beginning of this chapter we stated that the signal-to-noise limitation rather than the magnitude of the signal itself was a major difficulty in the study of gas-solid interactions. The discussion in this section is devoted to an evaluation of this ratio at the target for a d.c. molecular beam in a system such as that shown in Fig. II-3.

Although there are many sources of noise in a molecular beam experiment, by far the greatest contribution comes from the background pressure of the beam species in the scattering chamber. This component may be the largest contributor to the ambient atmosphere if a non-condensible gas beam is employed. For most cases the signal-to-noise ratio can be considered to be the intensity of the beam at the target surface divided by the intensity of the impinging background gases. A relatively simple way to obtain this value is to divide the equivalent pressure of the incident beam by the background pressure in the scattering chamber. The equivalent beam pressure is defined as the pressure of a gas, contained under equilibrium conditions at the beam temperature,* necessary to produce the same collision rate with a surface as the intensity of the beam. Thus

$$I = \frac{1}{4} n \bar{v} = \xi \, p/\sqrt{MT} \quad [\text{atoms/sec cm}^2] \qquad \text{(II-10)}$$

---

* The temperature of a molecular beam is only a meaningful quantity if the velocity distribution of the beam is represented by some well-defined function of the source temperature. For low pressure effusion from a Knudsen cell, $T_B = T_{source}$. However, for high pressure flow from a Knudsen cell, multichannel array, or nozzle source, the beam's velocity distribution is no longer of the simple Maxwell-Boltzmann type and one must <u>define</u> a beam temperature through a functional relationship with a measured beam velocity.

where $\xi = 3.51 \times 10^{22}$ atom $gm^{1/2}$ $deg^{1/2}$/torr cm^2 sec in Eq. (II-2) so that the pressure is given by

$$p = \frac{1}{\xi} I\sqrt{MT} \quad [\text{torr}] \tag{II-11}$$

Substituting from Eq. (II-1) which applies for ideal source aperture yields

$$p_B = \frac{Q_s}{\xi \pi L^2} \sqrt{MT_B} \quad [\text{torr}] \tag{II-12}$$

The leak rate Q_3 into the scattering chamber has three components: (1) the contribution from the molecular beam source itself, (2) the contribution from a beam formed by molecules effusing from the scattering chamber orifice and collimated by the selector chamber orifice, and (3) the contribution from background gas effusion through the selector chamber orifice. These terms may be written as

$$Q_3 = \frac{A_2}{\pi(a+b)^2} Q_s + \left(\frac{1}{4} n_1 \bar{v}_1 A_1\right) \frac{A_2}{\pi b^2} + \frac{1}{4} n_2 \bar{v}_2 A_2 \tag{II-13}$$

where subscripts 1 and 2 refer to the source and collimator chambers, respectively. A_i, $\bar{v}_i$, and n_i represent the collimator area, the average velocity of a particle in equilibrium with the chamber walls, and the number density in the given chamber. Q_s is the source leak rate, a is the source to source collimator distance, and b is the source collimator to selector collimator distance. Substituting from

Eq. (II-10) produces

$$Q_3 = \frac{A_2}{\pi(a+b)^2} Q_s + \frac{A_1 A_2}{\pi b^2} \frac{\xi}{\sqrt{MT_1}} p_1 + A_2 \frac{\xi}{\sqrt{MT_2}} p_2 \qquad \text{(II-14)}$$

Using $p = Q/KS$ where $K = 3.21 \times 10^{19}$ atoms/torr-liter to eliminate p_1 and p_2 above in terms of pumping speeds, and obtaining p_3 from the same relation gives

$$p_3 = \frac{1}{KS_3}\left[\frac{A_2}{\pi(a+b)^2} Q_s + \frac{A_1 A_2}{\pi b^2} \frac{\xi}{\sqrt{MT_1}} \frac{Q_s}{KS_1} + A_2 \frac{\xi}{\sqrt{MT_2}} \frac{Q_2}{KS_2}\right]$$

$$= \frac{1}{KS_3}\left[\frac{A_2}{\pi(a+b)^2} Q_s + \frac{A_1 A_2}{\pi b^2} \frac{\xi}{\sqrt{MT_1}} \frac{Q_s}{KS_1} + A_2 \frac{\xi}{\sqrt{MT_2}} \frac{1}{KS_2}\left(\frac{A_1}{\pi a^2} Q_s + \frac{\xi}{\sqrt{MT_1}} A_1 p_1\right)\right]$$

$$= \frac{1}{KS_3}\left[\frac{A_2}{\pi(a+b)^2} Q_s + \frac{A_1 A_2}{\pi b^2} \frac{\xi}{\sqrt{MT_1}} \frac{Q_s}{KS_1} + \frac{\xi}{\sqrt{MT_2}} \frac{A_2}{KS_2}\left(\frac{A_1}{\pi a^2} Q_s + \frac{\xi}{\sqrt{MT_1}} A_1 \frac{Q_s}{KS_1}\right)\right]$$

$$= \frac{Q_s}{KS_3}\left[\frac{A_2}{\pi(a+b)^2} + \frac{\xi A_1 A_2}{KS_2\sqrt{MT}}\left\{\frac{1}{\pi a^2} + \frac{1}{\pi b^2}\frac{S_2}{S_1} + \frac{\xi}{\sqrt{MT}}\frac{1}{KS_1}\right\}\right] \qquad \text{(II-15)}$$

In the last line of Eq. (II-15) we have set $T_1 = T_2 = T$ because the chamber walls should all be at the same temperature.

Utilizing the preceeding equations to calculate the signal-to-noise ratio, we find that

$$\frac{S}{N} \sim \frac{p_B}{p_3} = \frac{K}{\xi}\frac{\sqrt{MT_B}}{\pi L^2} \frac{S_3}{\left[\frac{A_2}{\pi(a+b)^2} + \frac{\xi A_1 A_2}{KS_2\sqrt{MT}}\left\{\frac{1}{\pi a^2} + \frac{1}{\pi b^2}\frac{S_2}{S_1} + \frac{\xi}{KS_1\sqrt{MT}}\right\}\right]} \qquad \text{(II-16)}$$

Substituting numerical values typical of the system used in this work results in S/N ~ 20 which is the signal to noise ratio at the crystal. From this calculation it is apparent that 95% of the gas striking the crystal comes from the molecular beam and that the unscattered d.c. signal should be readily observable both upstream and downstream from the crystal position on the beam line. This is indeed the case and measurements of the incident beam profile can easily be made in the d.c. mode as shown in Fig. II-4 where a signal-to-noise ratio of 10 is observable.

The difficulty arises when the beam is scattered by the crystal because this disperses the incident intensity over the 2π steradians exposed to the crystal surface in some unknown manner. In Eq. (II-16) this process has the effect of reducing the numerator still further. If we assume that the angular distribution of the scattered gas follows the cosine law, which is the worst possible case, then the reduction in the scattered pressure and hence the signal-to-noise ratio goes as the detector area divided by the surface area of the spherical emission pattern. For the detector area and distance used in this work

$$\frac{S}{N} \sim 20 \frac{\pi(.12)^2}{4\pi(2.1/2)^2} \sim 0.07 \qquad \text{(II-17)}$$

which should be a lower limit for the true S/N ratio. Clearly beam signals of this magnitude cannot be discriminated readily from the background signals. Two things can be done to improve this state of

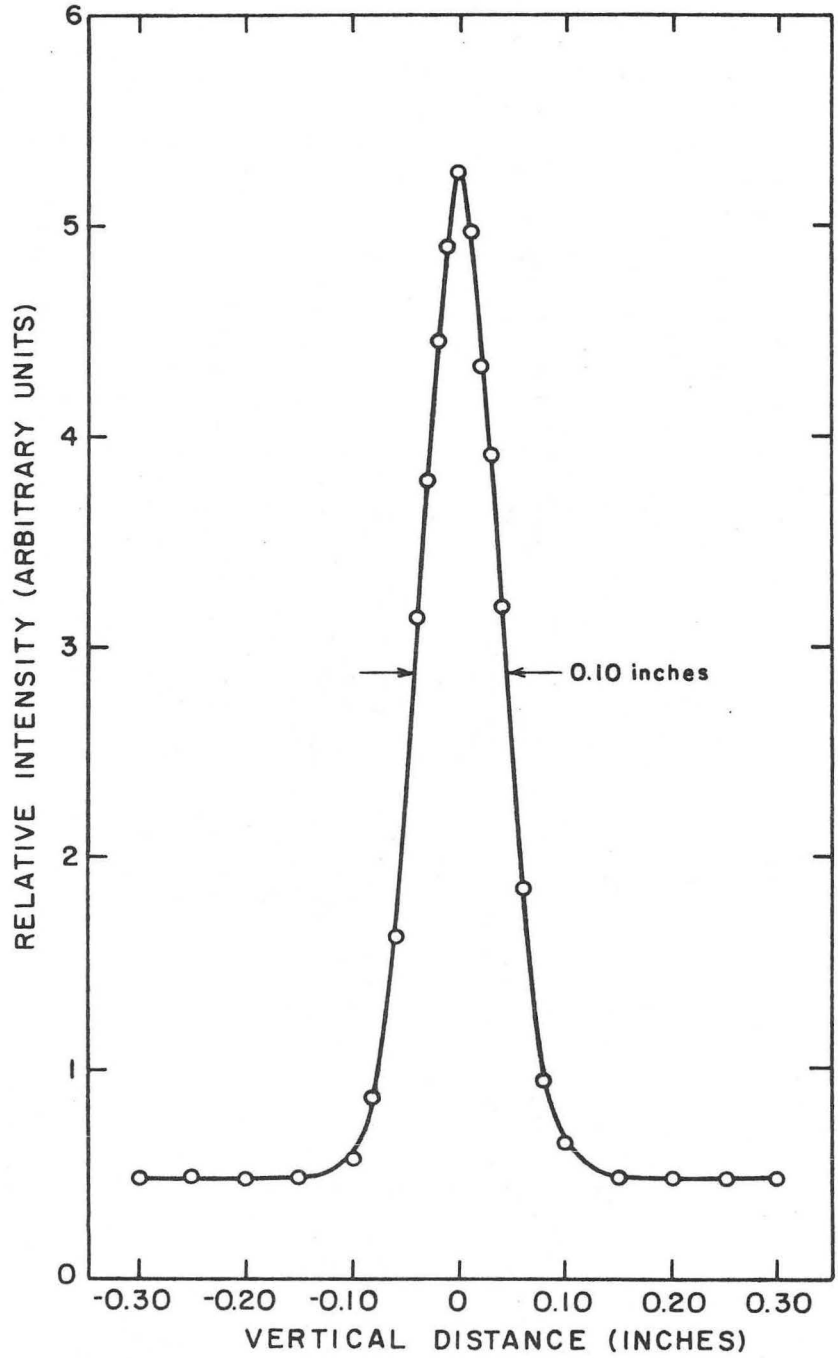

XBL 702-280

Fig. II-4. Xenon vertical beam profile in the d.c. mode demonstrating a S/N ratio of 10.

affairs. First, the incident beam can be periodically interrupted by a mechanical chopping device. This permits a.c. signal recovery techniques (i.e., lock-in detection) to be employed. Second, the effusion source can be replaced by a nozzle source[94] or by a multichannel array.[17,57,58] The latter course was followed in this work because the pumping requirements were less stringent. The net effect of the multichannel array is to increase the centerline beam intensity over that of an effusion source at the same total flow rate because the angular emission is sharply peaked along the beam axis.[95-100]

3. Scattering Chamber

Figure II-5 shows a cut-away drawing of the bakeable (475°K) ultra high vacuum scattering chamber indicating the placement of the quadrupole mass spectrometer used to detect the beam and the electron optics used to monitor the surface structure via LEED and Auger electron spectroscopy (AES). The chamber itself consists of a 0.48 cm thick sheet of 304 series stainless steel welded into a cylinder 30 cm in diameter and 50 cm in height and enclosing a volume of approximately 35 liters. Thick plates (2.54 cm) are welded to the ends of this cylinder to insure that the structure will not deform under the strain caused by the external and internal pressure differences. As seen in the figure, various sized copper-sealed access ports are situated in convenient locations about the cylinder's circumference, as well as in its top and bottom. During pump-down a Hastings DV 3-M thermocouple gauge is used to monitor the pressure in the system, while under

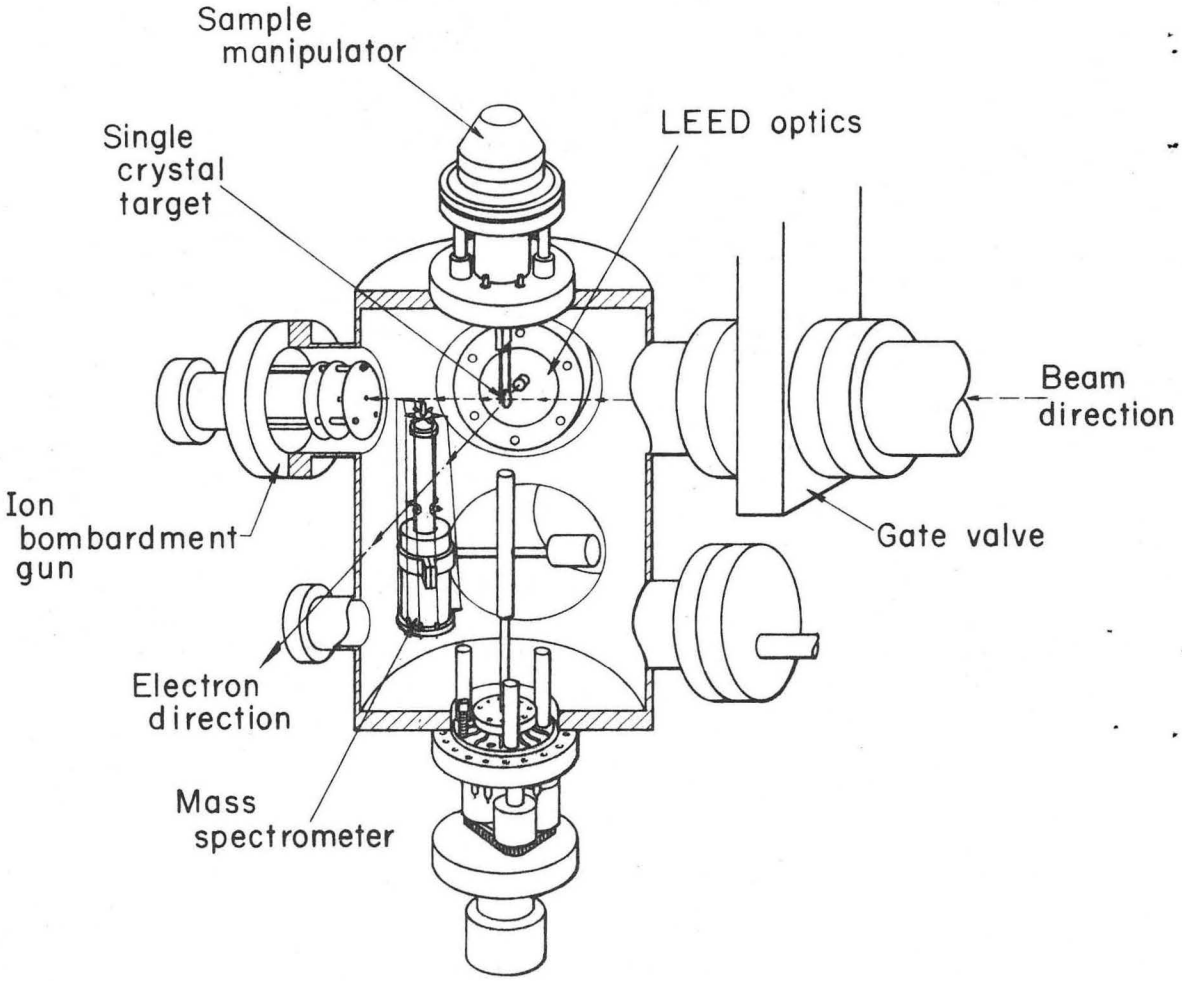

SCATTERING CHAMBER

XBL704-2668

Fig. II-5. Detailed view of the scattering chamber. The ion pump (not shown) is located on the port below the LEED optics.

0 0 0 0 3 6 0 5 4 9 3

operating conditions a nude Varian ionization gauge mounted directly in the chamber is used to measure total pressures. In the absence of a molecular beam, the gate valve between the scattering and selector chambers is kept closed, thus allowing the UHV chamber to be used independently for LEED, AES, or flash desorption experiments. Gases may be introduced directly into the chamber background via a precision leak valve (Granville-Phillips Company) mounted immediately below the gate valve.

The molecular beam enters the scattering chamber along a fixed line intersecting the axis of the cylindrical chamber by traversing a bakeable gate valve (Whittaker model SVS-3) which has been fitted with a (changeable) collimating orifice* 1.5 mm in diameter. As previously stated in section A of this chapter, the target is an oriented single crystal disk of platinum suspended from a Varian crystal manipulator at the point where the LEED, ion bombardment, and molecular beams intersect the axis of the scattering chamber.** This mounting allows the crystal

---

* For future reference, the removable portion of the collimator is a stainless steel plate 1.625 inches in diameter and 0.125 inches thick containing six equally spaced #40 holes on a 1.3125 ± .002 inch diameter bolt circle. The mating side of this plate (i.e., the side nearest the selector chamber) has been microfinished on 1μ diamond paste.

** Actually, the LEED optics have been found to be slightly out of alignment with the axis of the scattering chamber so that the electron beam must be magnetically bent to strike the crystal when it is on its normal rotational axis.

to be rotated about an axis that bisects its scattering surface and is also perpendicular to the plane of incidence (defined by the surface normal and the direction of the incident beam). In this way the incident angle θ_i may be varied for the scattering experiments and the crystal may be positioned with respect to the ion and electron beams. Sample temperatures above room temperature are attained through resistive heating while low temperatures may be reached by the use of a special liquid nitrogen cooled holder.[101,102]

a. Pumping. In order to study molecular beam scattering from a surface in an ultra high vacuum environment, differential pumping techniques must be used to avoid flooding the scattering chamber with background gas molecules effusing through the collimating orifice from the selector chamber. Even so, a high pumping rate must be employed to maintain the ambient as gas free as possible. This point has already been raised in the discussion of the signal-to-noise ratio. Ideally the pump should be located directly opposite the beam source so that the beam molecules pass directly into the pump unless scattered by the target surface.

For this work a 400-liter/sec vacuum ionization pump (Varian Noble Vac Ion) was chosen. The high speed is desirable because, even for such "noble gas" pumps, the pumping speed falls to roughly 30% of the maximum rate observed for N_2 when one pumps He or Ar. A manually operated bakeable gate valve connects the pump to UHV scattering chamber. This permits the pump to be isolated and left in operation

0 0 0 0 3 6 0 5 4 9 4

when the main chamber is opened, thus facilitating later pump-down.

After the pump was installed, it was discovered that its magnetic field influenced the performance of the LEED optics. In order to ameliorate the situation, the pump was enclosed in a Varian field shield equipped with heater strips for bakeout, but this was still found to be unsatisfactory. Consequently, more shielding in the form of soft iron pannels 0.125 inch (3.2 mm) thick was placed between the pump and the chamber to act as a flux conducting path. Additionally the LEED optics were surrounded by a mu-metal can to further protect them and mu-metal sheets were located along the pumping port to extend the shielding. In this configuration the LEED optics perform satisfactorily although completely balancing the fields for intensity work is a time consuming trial and error process.

Because carbon monoxide, one of the principal residual gases in the stainless steel scattering chamber, interacts strongly with the platinum surface, it was desirable to reduce its partial pressure to as low a value as possible. This was done by adding a titanium sublimation pump to the scattering chamber. The pump, with a (calculated) pumping speed of ~ 400 ℓ/sec for CO in its conductance limited mode, was constructed around a commercially available titanium filament holder (Ultek Corporation) and mounted as shown in Fig. II-6. To prevent any sublimed titanium not intercepted by the shilding from reaching the scattering chamber, the pump was attached to the system at right angles by means of a stainless steel "Tee". Current to heat

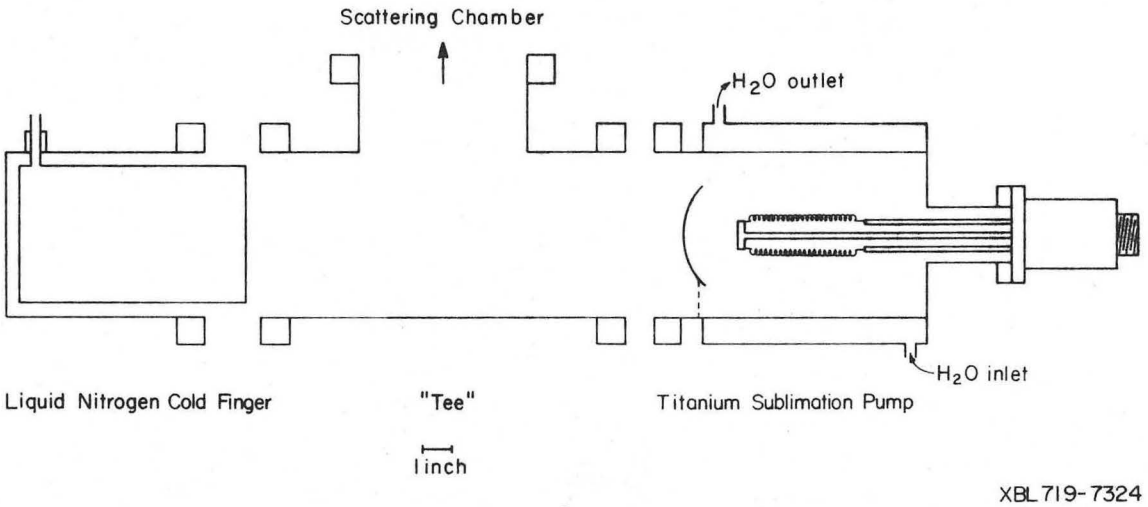

Fig. II-6. Cut away drawing of the titanium sublimation pump and liquid nitrogen cold finger mounting assembly. The "Tee" is attached to the port below the scattering chamber window shown in Fig. II-2a and 2b.

0 0 0 0 3 6 0 5 4 9 5

the filament was supplied by the d.c. crystal heater (normal conditions 50 amps for 60 seconds). While a fresh layer of titanium was usually deposited prior to an experimental run, periodic sublimation (i.e., once a day) was generally found sufficient to maintain a low ambient pressure in the UHV chamber. This approach also conserves titanium as it allows the fresh film to reach some degree of saturation before a new layer is evaporated. Figure II-7 shows the effect of the sublimation pump on the ambient CO concentration. The pressure burst is due to gas released by the filament when it is heated, but if one follows the CO pressure for twenty minutes, it shows a factor of two improvement over the time zero reading and the CO level is still decreasing. Another benefit of the sublimation pump is that it can be used during ion bombardment to remove chemically active gases such as H_2, N_2, O_2, CO, CO_2 and H_2O from the ambient because its pumping speed for noble gases is practically nil.

Evacuation of the scattering chamber is initiated by an air aspirator (Varian GASP Roughing Pump) to a pressure of roughly 200 torr followed by the serial application of two sorption pumps (Ultek Model 50-135) to a pressure of 10^{-3} torr or lower. At this point, the gate valve to the ion pump can be opened. Pressures below 10^{-7} torr are regularly achieved within two hours. Use of the aspirator considerably shortens the pumpdown time as it removes ~ 80% of the gas molecules in the chamber. (One sorption pump was usually sufficient to reduce the system pressure below 1μ after the use of the aspirator.)

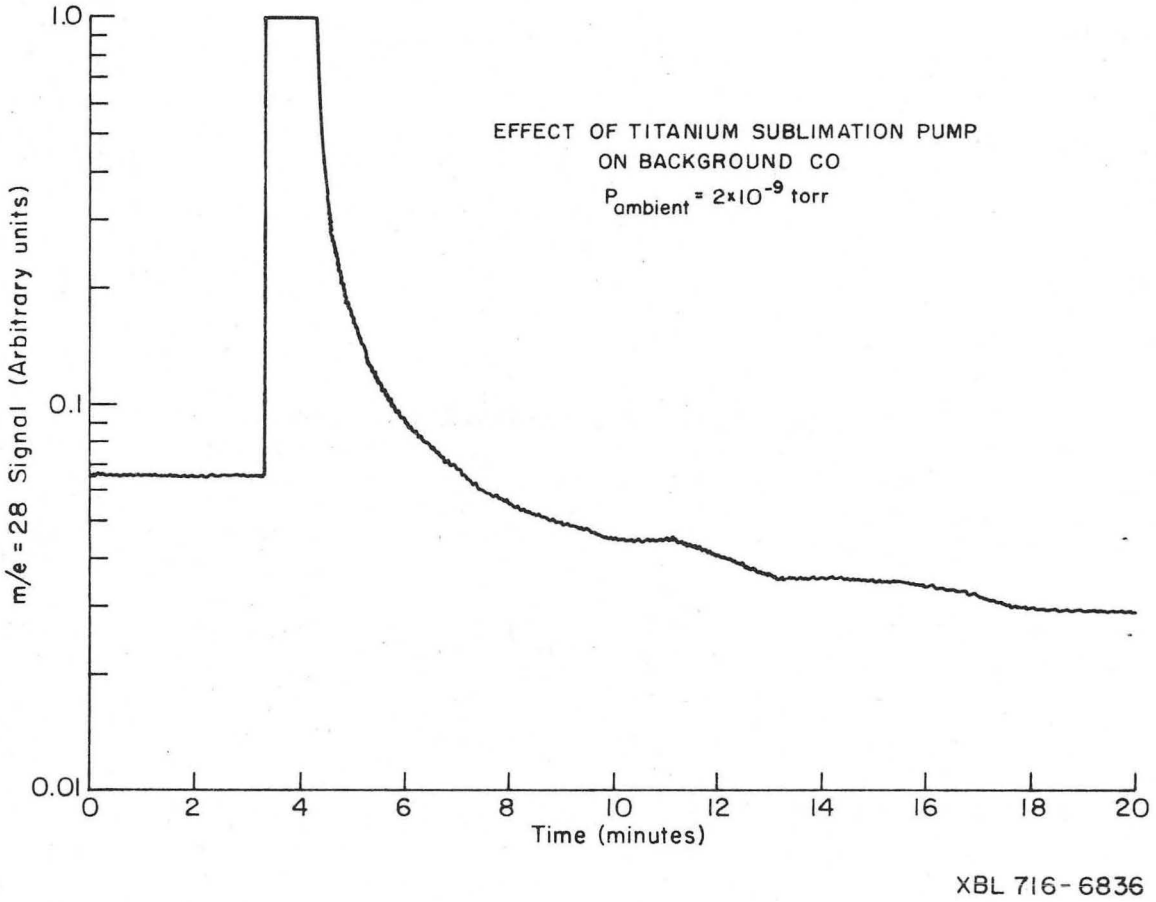

Fig. II-7. Effect of sublimed titanium on the ambient CO concentration.

0 0 0 0 3 6 0 5 4 9 6

Opposite the sublimation pump on the "Tee" was placed a liquid nitrogen cold finger to remove condensible gases (mainly water) from the UHV chamber. The ultimate system pressure attained under the influence of the ion and sublimation pumps was 5×10^{-10} torr.

b. Detector and Ionizer. In order to detect the angular distribution of the scattered parent beam or the scattered products of a surface reaction, a quadrupole mass spectrometer (Electronic Associates, Inc., model 250-A) is used. Its versatile mounting, pictured in Fig. II-8, is built from a commercial rotary motion feedthrough (Huntington Mechanical Labs) that has had the standard length 9.5 mm diameter shaft replaced by one extending 30 cm beyond the flange face. This feedthrough is attached to a specially built linear motion drive containing the electrical connections necessary for the operation of the quadrupole. Alignment of the rotating shaft is maintained by a Thompson Ball-Bushing located on the axis of the scattering chamber. One advantage of this mounting system is that the mass spectrometer may be readily inserted or removed from the scattering chamber with all its internal connections intact. The mounting allows study of the scattered beam both in and transverse to the plane of incidence and rotation about the crystal's rotary axis from -10° to +190° with respect to the parent beam line. Zero degrees in the laboratory frame of reference is conventionally taken as the location of the incident beam maximum on the downstream side of the crystal. Figure II-9 illustrates the in-plane and out-of-plane angles which can be monitored. Due to uncertainties in out-of-plane ionization

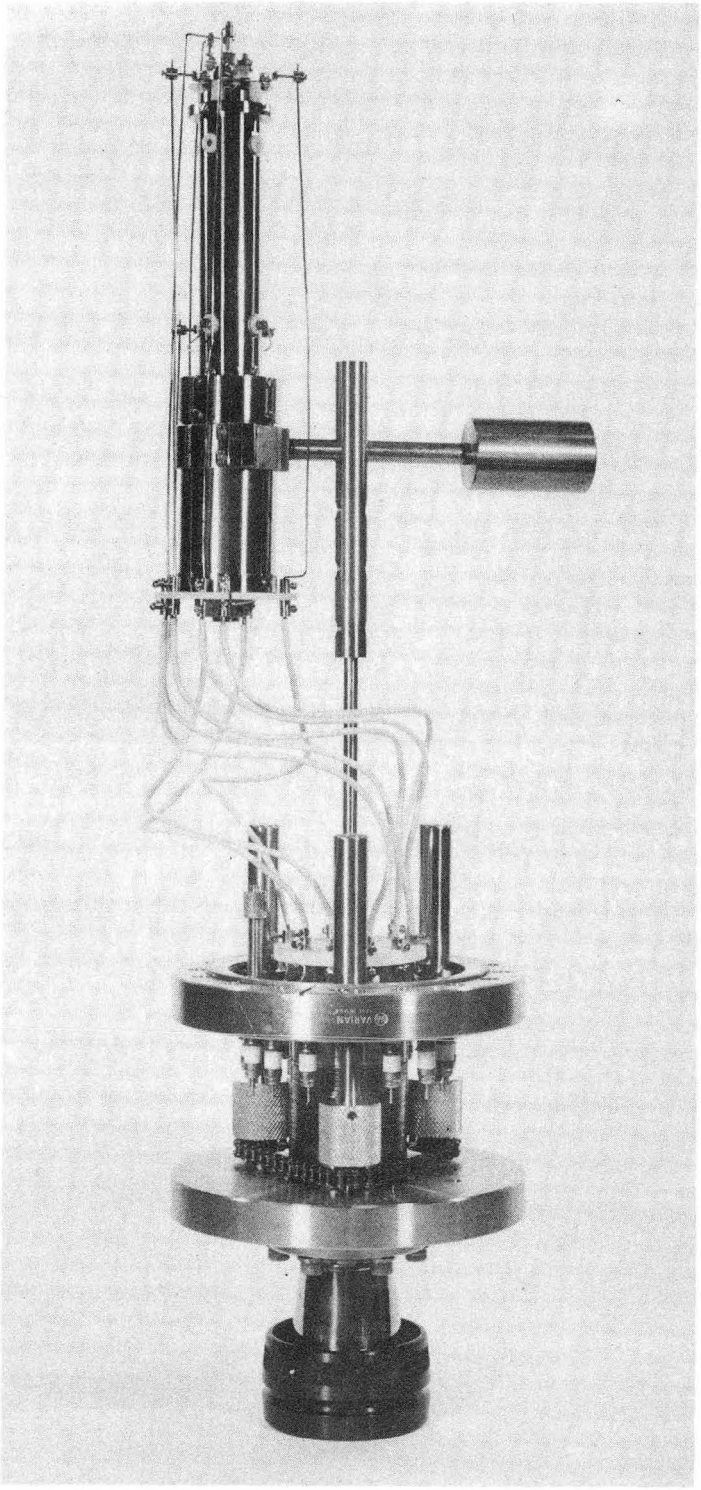

XBB 691-480

Fig. II-8. Quadrupole mass spectrometer and linear-rotary motion feedthrough.

0 0 0 0 3 6 0 3 4 9 7

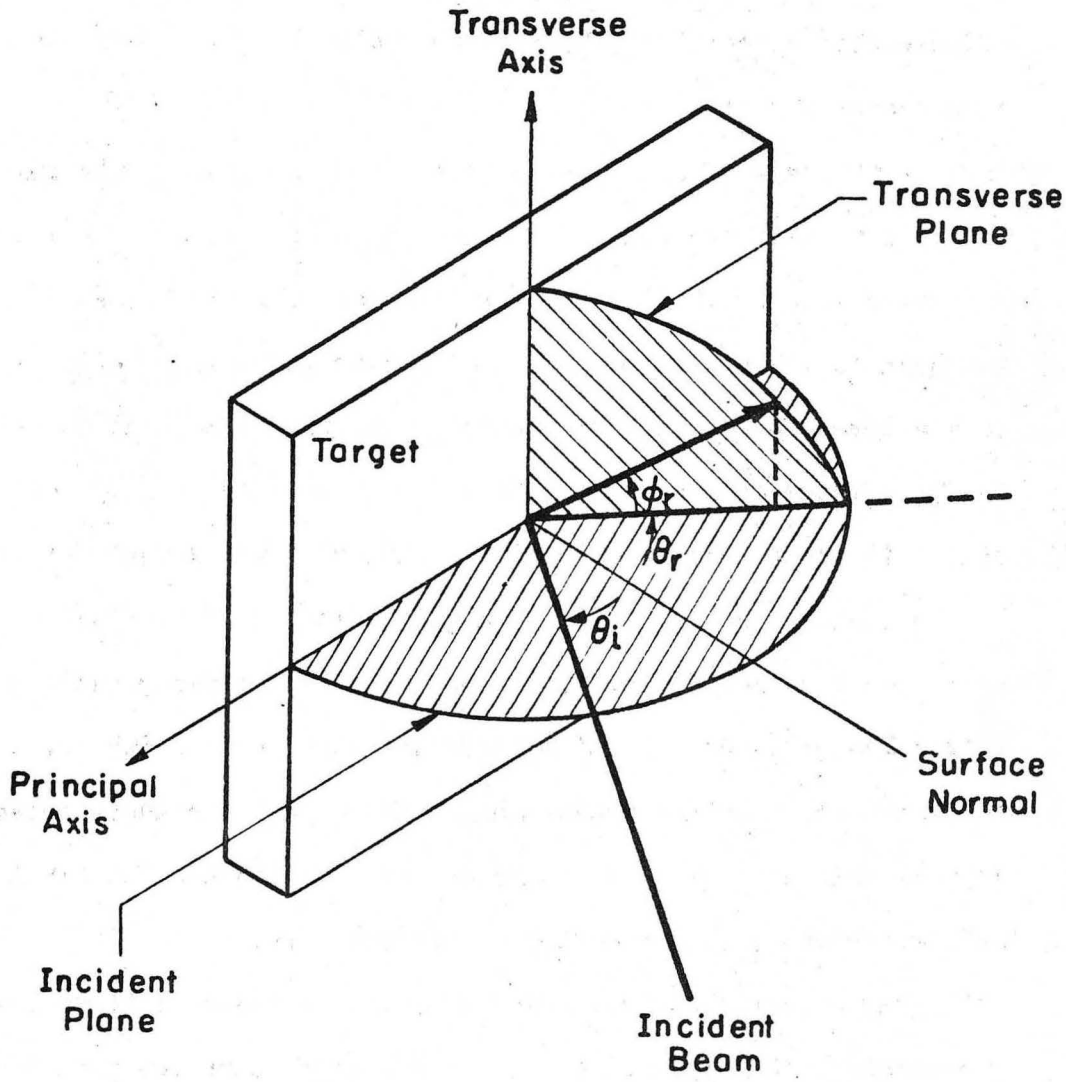

XBL 7110-7352

Fig. II-9. A representation of the in-plane and out-of-plane scattering angles that can be monitored. In this work ϕ_r was restricted to zero degrees so that only scattering in the incident plane was measured.

efficiencies compared to the in-plane values, ϕ_r was restricted to zero degrees.

With respect to a point source located at the scattering center (i.e., crystal), the angular resolution of the detector is 7°, whereas the divergence of the beam across the chamber is less than 1°. These two quantities are independent. (The divergence is merely a measure of the spreading of the beam, not its physical size, and is negligible in this system as can be ascertained by comparing the physical diameter of the incident beam measured in the upstream and downstream locations. Figure II-10 presents a typical angular profile of the incident beam which has a half-width of 7.5° (full-width at half-maximum). Presumably this value is detector limited and the actual beam width may be somewhat less than the measurement. The actual distances between the surface and the ionizer aperture and the surface and the final beam collimator are 2.1 cm and 21.5 cm respectively.

The angular resolution was achieved by adding collimation apertures to the standard Pierce type ionizer supplied with the quadrupole (see Fig. II-11). While this addition served its purpose, it also introduced an unexpected bias factor into the viewing angle because of the finite width of the incident beam as indicated in Fig. II-12. Although the exact magnitude of this effect was never experimentally ascertained, an approximate calculation will now be made. Qualitatively, the overall effect would be to increase the magnitude of the small angle scattering with respect to that near the surface tangent.

0 0 0 0 3 6 0 3 4 9 8

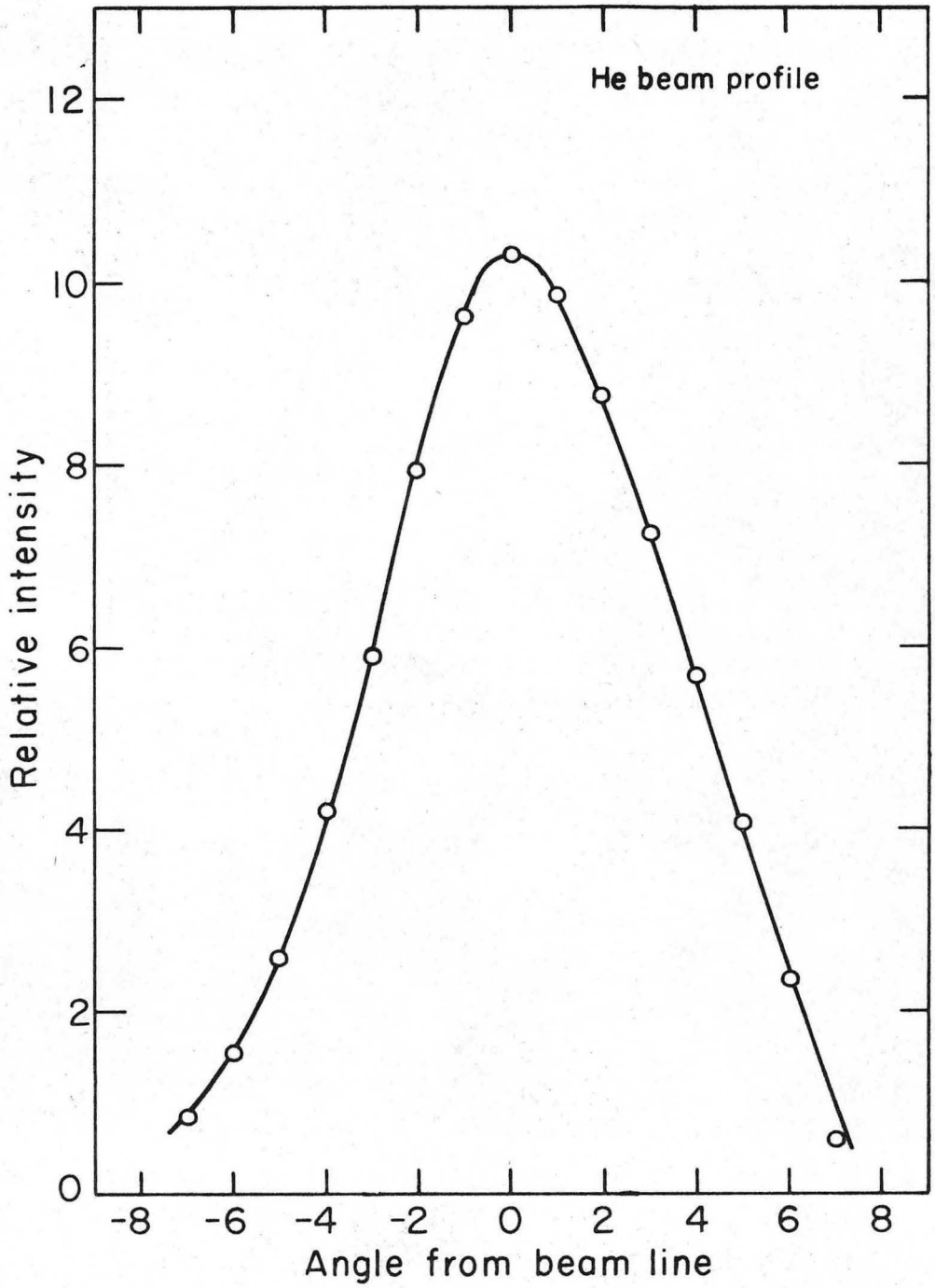

XBL 709-6677

Fig. II-10. Angular profile of the unscattered incident beam.

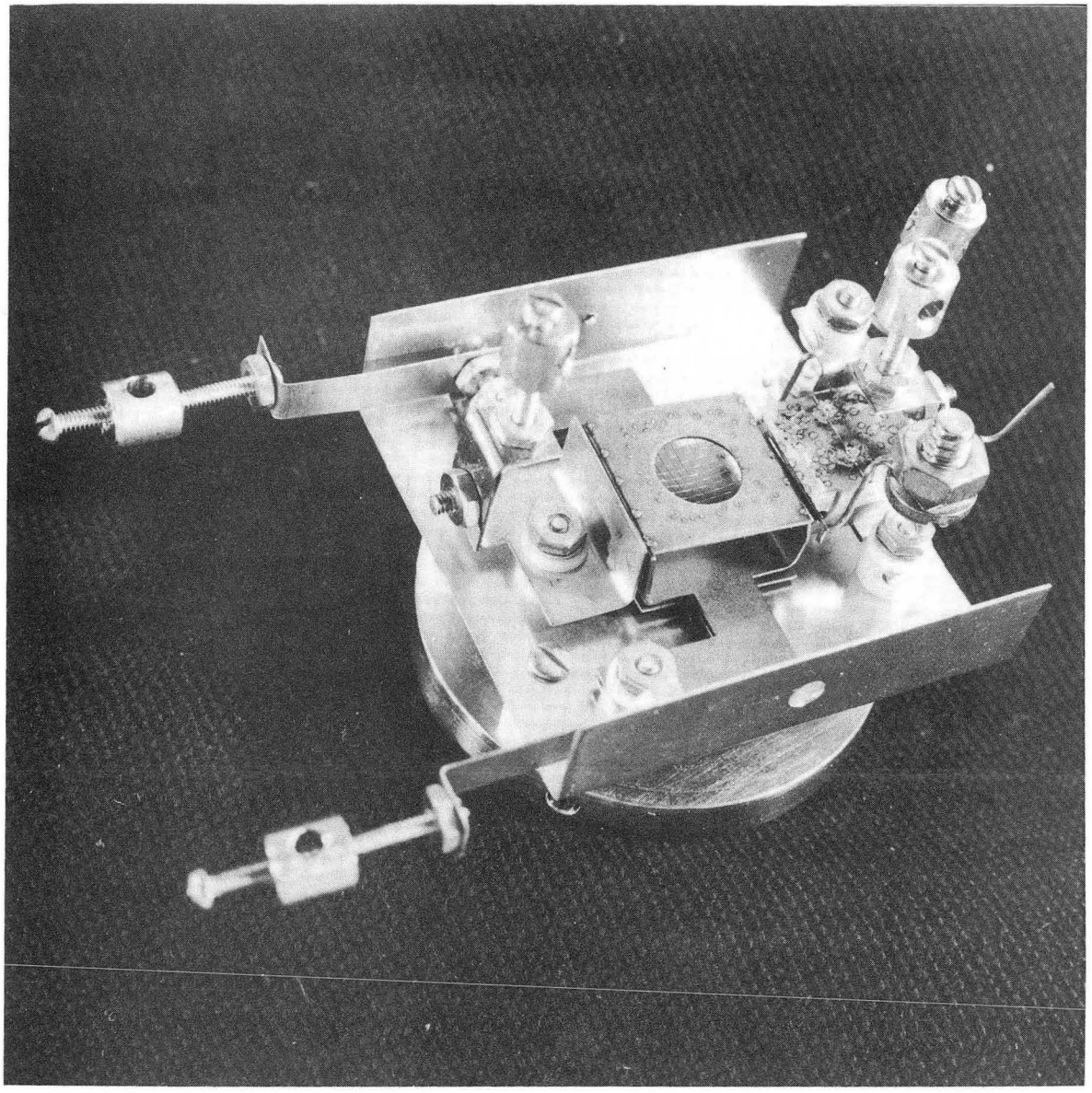

XBB 704-1944

Fig. II-11. Modified EAI ionizer showing the resolution defining beam collimation aperture.

0 0 0 0 3 6 0 5 4 9 9

From the geometry shown in Fig. II-12 it is apparent that

$$z = w/\cos\theta_i \tag{II-18}$$

$$y = z\cos\theta_r = w\cos\theta_r/\cos\theta_i \tag{II-19}$$

$$x = z\sin\theta_r = w\sin\theta_r/\cos\theta_i \tag{II-20}$$

The ratio of the length of the sides of similar triangles yields

$$\frac{\ell_1 + y}{R + r - x} = \frac{D + y}{r - x} \tag{II-21}$$

or solving for ℓ_1 we obtain:

$$\ell_1 = D + \frac{R(D+y)}{r-x} \tag{II-22}$$

In a similar manner one uses point 2 and the opposite edge of the ionizer collimator to obtain

$$\ell_2 = D + \frac{R(D+y)}{r+x} \tag{II-23}$$

Thus we see that the total width of the beam at the center of the ionizer is

$$\ell_1 + \ell_2 = 2D + \frac{2rR(D+y)}{r^2 - x^2} \tag{II-24}$$

VIEWING ANGLE BIAS

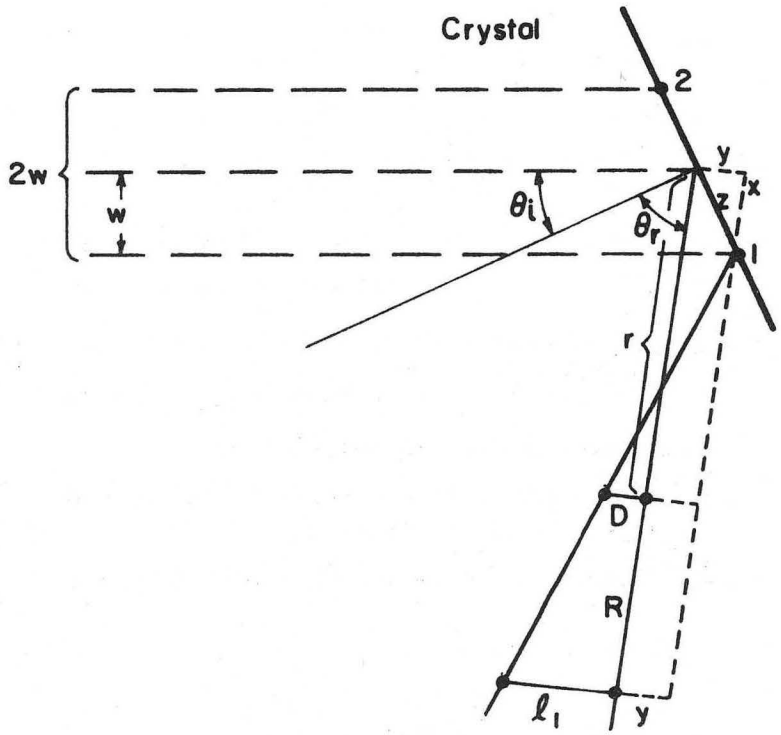

θ_i Incident Angle

θ_r Reflected Angle

2w 0.100" = Width of Incident Beam

2D 0.102" = Width of Collimator Slit

r 0.811" = Distance from Crystal to Collimator

R 0.720" = Distance from Collimator to Center of Extractor Aperture

$\ell_1+\ell_2$ = Width of Detected Beam at Center of Ionizer

XBL719 - 7312

Fig. II-12. Origin of potential viewing angle bias due to ionizer aperture. For clarity, ℓ_2 was omitted from the drawing although it can be obtained by extending a line from point 2 through the right most edge of the collimator (not shown).

where x and y are defined above. The variation of ℓ_1, ℓ_2, and their sum with changes in the reflected angle at a fixed angle of incidence is shown in Fig. II-13. Even at $\theta_r = 90°$, the width of the beam is nearly twice the collimator diameter for $\theta_i = 45°$. From Eq. (II-24) it is also apparent that merely increasing r (the separation between the crystal and detector) has only a small effect on the relative error unless R can be made comparable to D. If D = R, the relative error goes as D/r and this can be minimized. Clearly the viewing angle bias is a definite problem for such a flowthrough ionizer. A potential solution to this problem is discussed in Appendix VII-D.

An approximate correction factor can be arrived at if one arbitrarily assumes that the ionizer lenses extract equally efficiently from the volume of a cylinder having a diameter equal to $\ell_1 + \ell_2$ at $\theta_r = 90°$ (θ_i fixed) and with zero efficiency elsewhere. Since increasing the diameter of the beam for a fixed number of particles lowers its density, a multiplicative correction factor can be calculated by dividing the cylinder volume at θ_r by that at $\theta_r = 90°$. The result of such a calculation is presented in Fig. II-14 where the reciprocal correction factor is displayed for three angles of incidence. In fact, it is not known with any certainty how the ion extraction efficiency varies with distance from the extractor aperture. If the extraction region were smaller than that assumed, there would be no effect on the calculation, but if the extraction region were somewhat larger than that assumed, the small angle scattering would be closer to

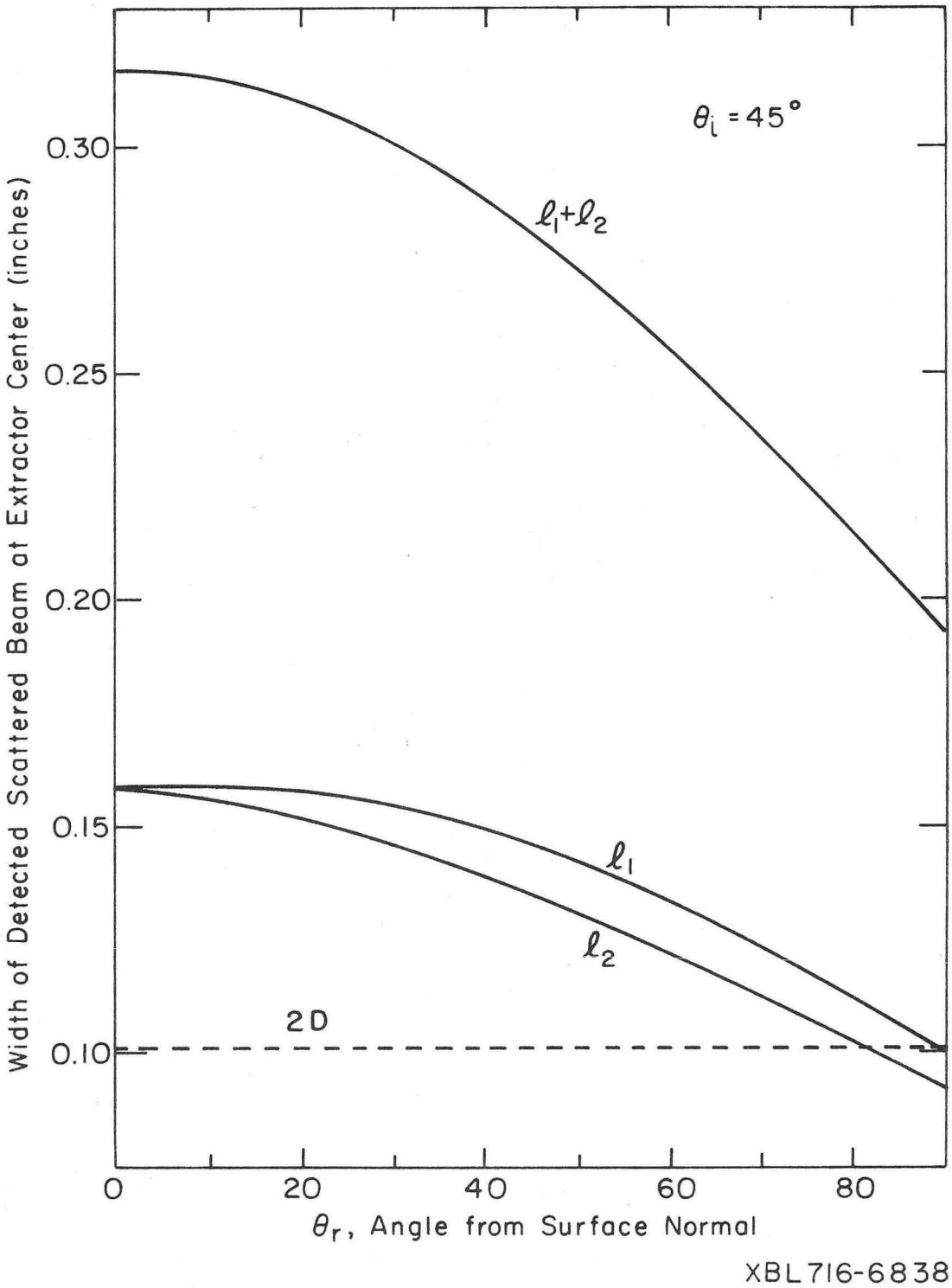

Fig. II-13. Calculated beam width $\ell_1 + \ell_2$ as a function of scattering angle θ_r for an incident angle of 45°. Note that 2D represents the width of the collimation aperture.

0 0 0 0 3 6 0 3 3 0 1

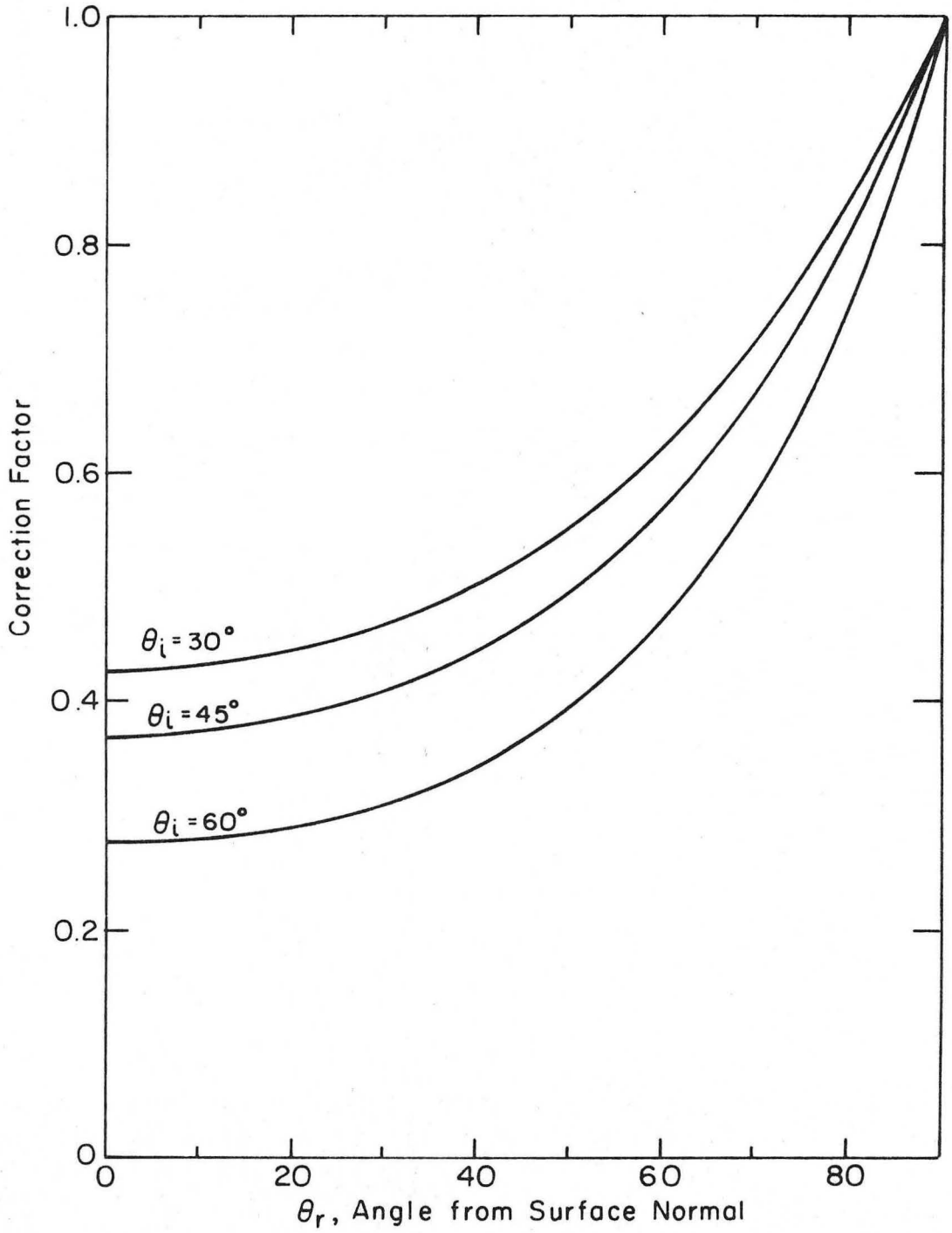

XBL 716-6837

the true signal than indicated by Fig. II-14. Then again, extraction of an ion with equal probability from anywhere in the ionizer would mean that the entire calculation could be disregarded. For these reasons, no viewing factor corrections have been applied to any of the measured intensity distributions. This neglect is probably justified by the fact that most measurements are in an angular range where the correction factor is fairly constant. Of course, one could experimentally determine this factor by comparing an observed angular distribution for a gas that scatters diffusely with the expected cos θ_r dependence.

When the mass spectrometer was placed in the scattering chamber, the ionizer was aligned by passing a laser beam along the molecular beam flight path through the ionizer collimating slits. Because the laser beam was somewhat smaller than the aperture size, the two collimation slits were mistakenly aligned so that the flight path connecting them was not quite parallel to the beam line. Ideally the beam maxima should occur at 0° with the quadrupole in the downstream position and 180° with the quadrupole in the upstream position whereas experimentally the maxima are at 0° and 173°, respectively. Using the law of sines and the law of cosines on the figure below, one can eventually deduce that the quadrupole should be rotated about <u>its</u> axis of symmetry by $\delta = 5.8°$. This twist has no effect on the operation of the quadrupole, however, as the collimator that observes the beam at 0° also observes the scattered beam.

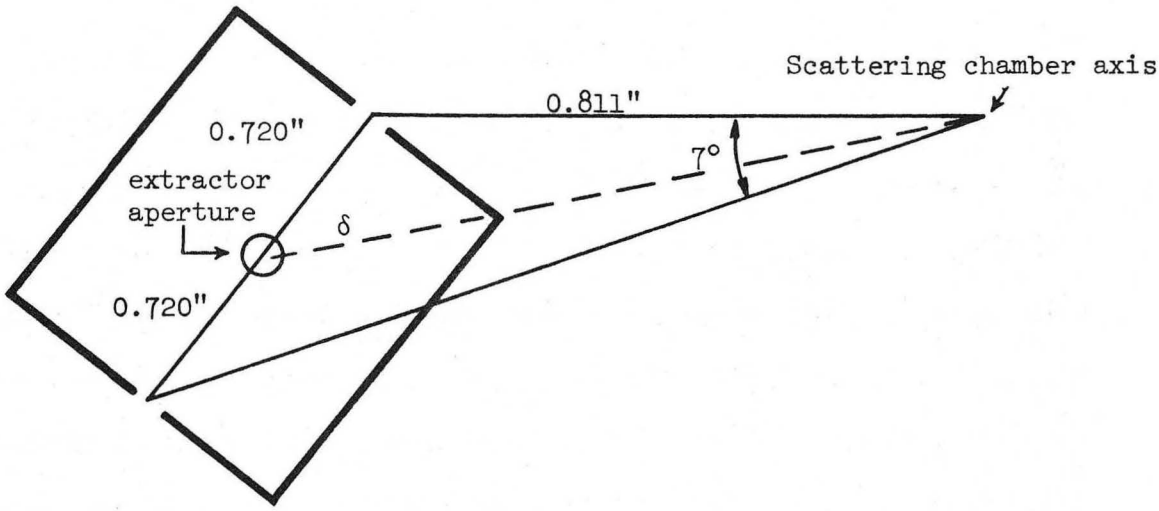

c. Lock-in Amplifier. As has already been indicated several times, the incident molecular beam is modulated (150 hertz) to take advantage of the great power of a.c. signal recovery techniques so that the scattered signal may be discerned from the background noise. Figure II-15 shows an oscilloscope trace of the modulated incident beam. Because essentially all of the scattered signal information occurs at one frequency, a very narrow bandwidth can be used in an effort to improve the signal-to-noise ratio. In this work, the narrow band amplification and phase sensitive detection were supplied by a Princeton Applied Research Model HR-8 Lock-in Amplifier.

The current output from the electron multiplier of the mass spectrometer is grounded through a 1 MΩ resistor connected in parallel with the input of a PAR Type A plug-in preamplifier. The lock-in thus sees a weak a.c. signal including noise that is first amplified and then passed through a signal tuned amplifier to discard sidebands

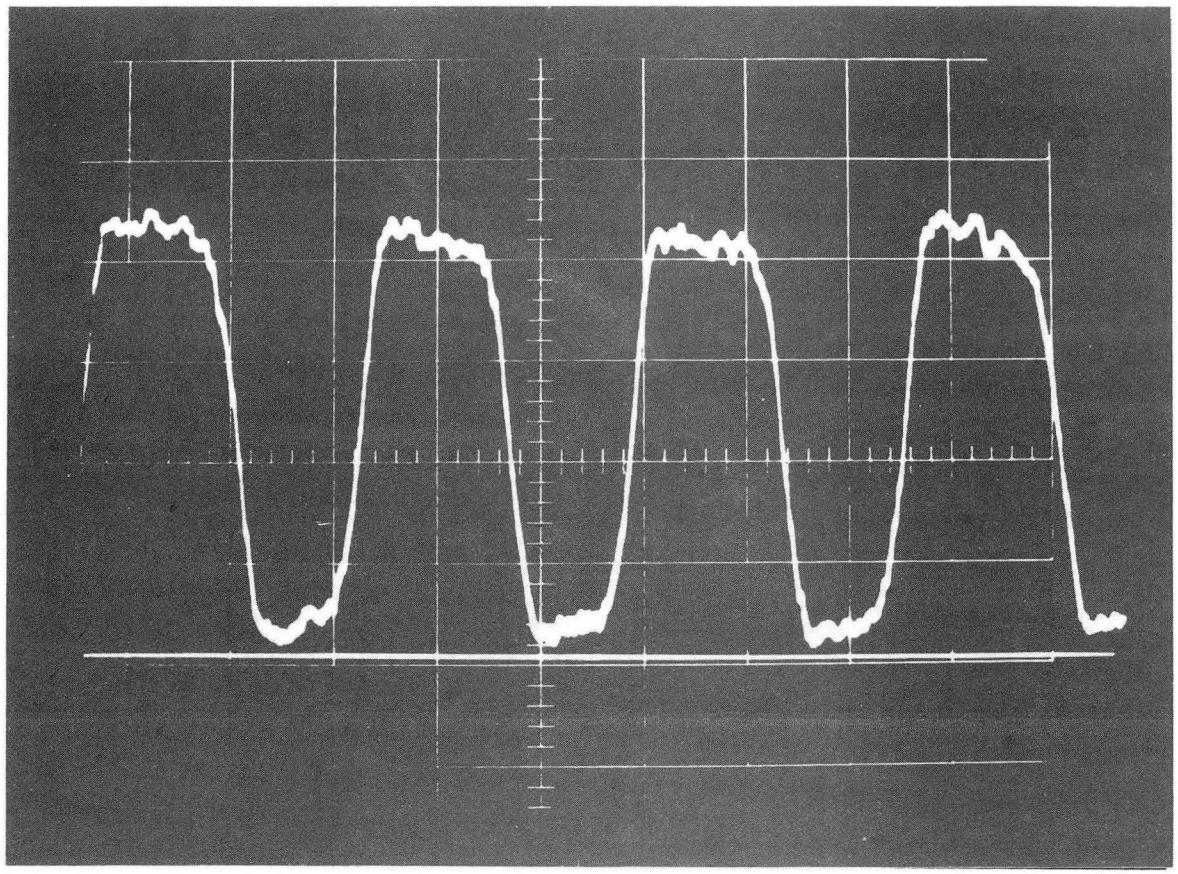

XBB 7110-4691

Fig. II-15. Oscilloscope trace of the modulated incident molecular beam. Each large division of the horizontal scale represents 2.5 milliseconds.

while further amplifying the signal at the desired frequency. This result is then beat against an a.c. signal derived from the modulation device (a vibrating tuning fork supplied by American Time Products) to produce, after filtration, a d.c. signal that is fed to a Leeds and Northrup stripchart recorder. Most of this work used either a 3 or 10 second time constant and a roll-off of 12 db/oct.

If the input signal to the lock-in is represented by $y(t) = S_o \sin(\omega t+\phi)$ and the reference signal is $F(t)$, then the output signal is given by

$$\mathcal{E} = \frac{1}{\tau} \int_{-\frac{\tau}{2}}^{\frac{\tau}{2}} y(t)\, F(t)\, dt \qquad \text{(II-25)}$$

where $\omega = \frac{2\pi}{\tau}$ is the modulation frequency. A reference signal that can be used is one that reverses the sign of $y(t)$ every half period and the Fourier expansion of such a function is

$$F(t) = \frac{4}{\pi} \sum_{n=0}^{\infty} \frac{\sin(2n+1)\omega t}{(2n+1)} \qquad \text{(II-26)}$$

Thus we have

$$\mathcal{E} = \frac{1}{\tau} \int_{-\frac{\tau}{2}}^{\frac{\tau}{2}} S_o \sin(\omega t+\phi) \frac{4}{\pi} \sum_{n=0}^{\infty} \frac{\sin(2n+1)\omega t}{(2n+1)} \, dt$$

$$= \frac{4}{\pi} S_o \sum_{n=0}^{\infty} \left\{ \frac{\cos\phi}{\tau} \int \frac{\sin\omega t \, \sin(2n+1)\omega t}{(2n+1)} \, dt \right.$$

$$\left. + \frac{\sin\phi}{\tau} \int \frac{\cos\omega t \, \sin(2n+1)\omega t}{(2n+1)} \, dt \right\}$$

$$= \frac{2}{\pi} S_o \cos\phi \qquad \text{(II-27)}$$

where S_o is the amplitude of the input signal and ϕ is the phase angle between the signal and reference frequencies. Obviously the d.c. output is a linear function of S_o for all values of S_o.

In practice, ϕ was adjusted to produce a maximum output signal when the quadrupole was located at 0° (i.e., downstream from the crystal position) and then locked at that value for the experimental run. Thus it was implicitly assumed that the scattered particles had the same phase as the incident particles after traveling the same distance.

While it was not possible to make exact phase measurements because the reference signal is derived electronically rather than from a photocell at the chopper, it was possible to measure phase

differences due to molecular transit times when the detector was located on opposite sides of the scattering center. From this information one can calculate the most probable gas velocity because

$$v_{m.p.} \sim \frac{2(r+R)}{(\Delta\phi\tau/360^\circ)} = \frac{42.0 \times 10^4}{\Delta\phi} \text{ cm/sec} \qquad \text{(II-28)}$$

Two experiments yielded $\Delta\phi = 3.3 \pm 1.0^\circ$ for He and $8.7 \pm 0.5^\circ$ for N_2O which translates into 1.27×10^5 cm/sec and 4.83×10^4 cm/sec respectively. For a gas effusing from a Knudsen cell, the most probable velocity is given by

$$v_{m.p.} = \sqrt{\frac{3RT}{M}} \qquad \text{(II-29)}$$

In the cases of He and N_2O this equation yields 1.37×10^5 cm/sec and 4.12×10^4 cm/sec respectively. The helium result is obviously fortuitous, but the nitrous oxide value is reasonable because one expects a gas effusing from a multichannel array driven at high pressures (several torr) to have a slightly greater average velocity than a gas from an effusion cell.[99,100]

d. LEED Optics. The electron optics used in this work are of the post acceleration three-grid construction commercially available from Varian and a schematic diagram has already been shown in Fig. I-4. The power supplies used to control the filament, filament can, cathode anodes, and screen are similar to those used by Varian, but all were

built at Lawrence Berkeley Laboratory. A d.c. rather than an a.c. power supply is used to heat the filament in order to reduce noise in the Auger mode. During all experiments the inner and outer grids were grounded, and the middle grid was operated at the cathode potential.

e. Auger Spectrometer. In order to more fully characterize the nature of the scattering surface, it was decided to use the LEED optics as a retarding field energy analyzer to perform Auger electron spectroscopy experiments. The grid system in the LEED mode is employed as above to impede the inelastic component and to transmit the elastic component of the back-reflected electrons while the fluorescent screen displays the diffraction pattern. The same grid system in the Auger mode functions as a high pass filter to analyze the energy distribution of the inelastically scattered electrons while the screen serves as the electron collector. AES is necessary to obtain a detailed chemical analysis of the surface region and to provide information complimentary to the structural data available from concurrent LEED studies.

Minimal modifications in the optics were required. The Varian high voltage coupling to the screen was replaced in the Auger mode by a double shielded cable (RG 63B/U)* that conducted the modulated signal to the detection electronics. Double shielding with the inner guard

---

* This 125Ω cable (LBL Stock Catalogue No. 6145-24158) consists of a RG63B center core surrounded by an additional braided shield over the jacket with this shield covered by an outer vinyl coating.

driven by the capacitance neutralizer was found necessary to reduce the noise pick-up.

Figure II-16 gives the circuit diagram of the power supply built for the Auger experiments. It consists basically of four components: (1) a capacitance neutralizer similar to that employed by Varian, (2) a 0 to -3 kV programmable power supply (Model UPMD-530N-M4 available from Power Designs, Inc.), (3) a variable rate sweep generator, and (4) a frequency doubler (Burr Brown 4094/15C Multiplier/Divider). Once the internal components were properly shielded from a.c. pick-up, the performance of the unit was in all ways equal to that of the instrument purchased from Varian and modified for high resolution chemical shift work. The sweep generator used for most experiments was borrowed from a Vacuum Generators Auger system. Because the availability of this device depended upon the status of an independent experiment, a new ramp generator was designed and built, but to date its performance has been inadequate. The UHV chamber had no port to admit a glancing incidence electron gun so the AES studies reported in this thesis were made using the normal incidence LEED gun operated at voltages up to 1500 volts by a Power Designs Model HV-1565 high voltage supply. At this voltage, however, the emission was very unstable and so the voltage was normally maintained at 1000 volts which was adequate for most work. The modulated signals were processed by the same Princeton Applied Research HR-8 used in the molecular beam work.

Fig. II-16. Circuit diagram of the AES power supply built for this work, LBL drawing number 8S9053A.

AUGER POWER SUPPLY

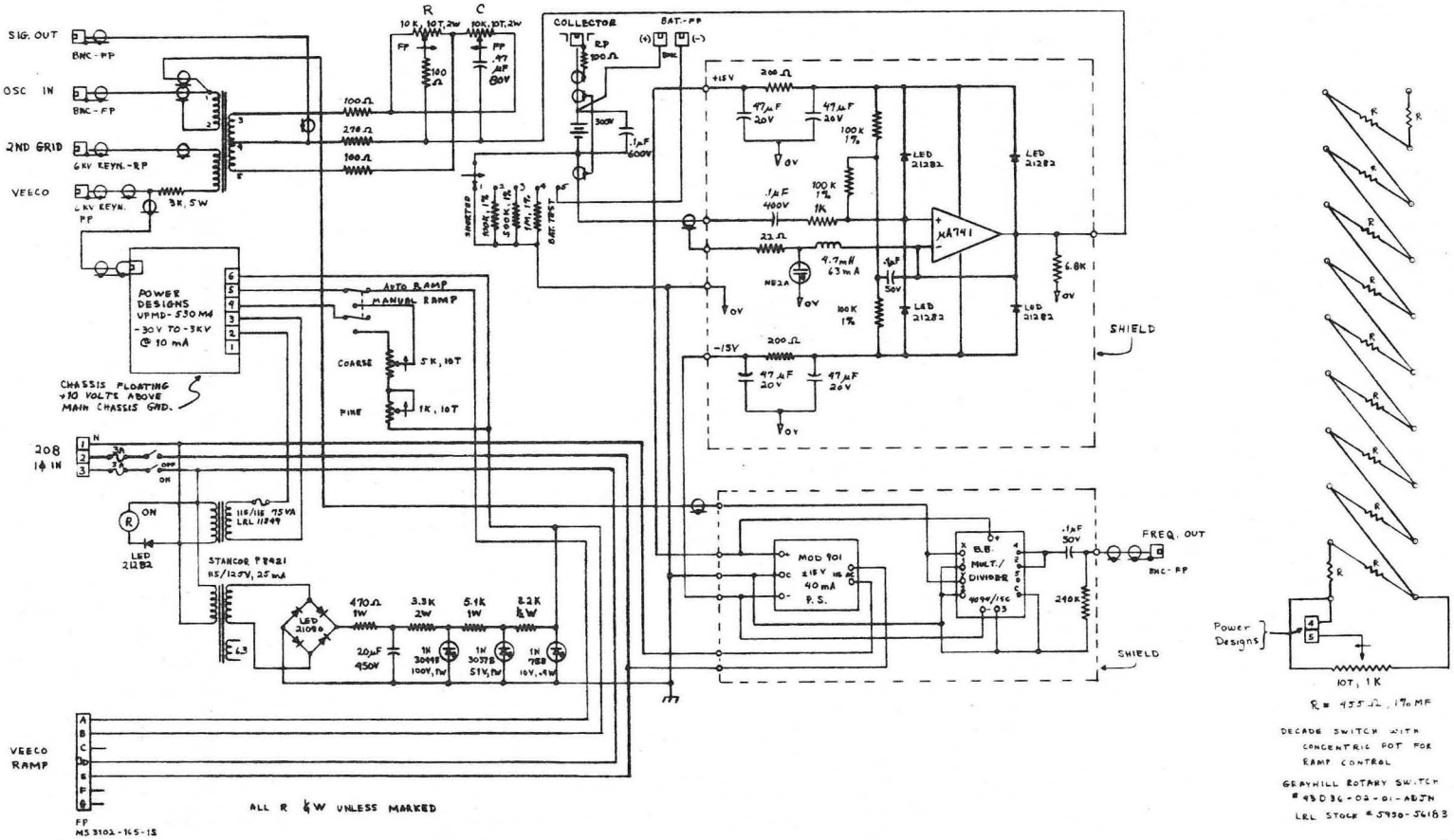

XBL 719-7323

f. Pump-down and Bakeout Procedures. Assume that the UHV chamber has been brought to atmospheric pressure with dry nitrogen for a change of sample or modifications to the mass spectrometer. Approximately thirty minutes before initiating pump-down, the two sorption pumps (S P) should be cooled with liquid nitrogen. Once all the flanges have been tightened in place, the system is ready for evacuation and the air aspirator is activated by admitting ~ 70 psig of dry nitrogen to its inlet. At this point the suction valve is opened and the aspirator permitted to operate for roughly five minutes, after which the valve is closed and S P II opened. The nitrogen flow may now be turned off. Within 10 to 15 minutes the pressure on the thermocouple gauge should read in the low micron range and S P I may be substituted for S P II. Once the system pressure ceases to decline, S P I can be closed and the gate valve to the ion pump opened (if the pump had been left in operation) or the pump may be started according to its instruction manual. At this point the liquid nitrogen containers may be removed from the sorption pumps so that they may warm up to room temperature.

Situated on the metal support frame of the scattering chamber are three 10 amp electrical outlets containing four plug receptacles each. These outlets are controlled by the bakeout electronics in Rack #05 and are powerless except during heating cycles. Before proceeding with the bakeout procedure, the driver mechanism should be removed from the precision leak valve according to the Granville-Phillips instructions and the thermal sensing switch should be attached

to the manipulator flange and then to the yellow cord near the leak-valve. Bakeout is accomplished by wrapping the UHV system with heating tapes. Experience has shown that full power should be applied to the tapes near the bottom of the chamber and on the pumping "Tee," but that half power via series connection of two similar units should be used on the tapes around the ion pump gate valve, Whittaker valve, and near the top of the system. After the chamber has been thus prepared, it should be wrapped in several layers of aluminum foil to retain as much heat as possible. Asbestos sheet and glass wool were also tried as wrapping material but discarded as unsatisfactory.

To initiate the bakeout, the pressure sensitive relay to the ion pump must be turned on and warmed up for half an hour. Following this, the two timers on the master control can each be set for 24 hours and the heating sequence begun. The ion pump may also be baked out at this time. A 48 hour bakeout at a temperature of 425-475°K (150-200°C) has been found adequate to attain pressures in the 10^{-10} torr range.

4. Selector Chamber

This chamber, again constructed entirely of 304 series stainless steel, acts primarily as a buffer between the source chamber containing the oven which generates the beam and the scattering chamber. During an experiment using an oven pressure of several torr, the pressure in the selector chamber is 3×10^{-7} torr. A tuning fork beam modulator (American Time Products, type L-40 light chopper) with a frequency of 150 Hz is currently used to generate an a.c. molecular beam.

Alternatively a rotating disk velocity selector[103] is placed in the chamber to prepare monochromatic beams for use in scattering and surface chemical reaction studies. The chamber is also large enough to permit the use of other state selecting devices such as inhomogeneous magnetic fields, electron beam excitation, or flash photolysis cells which may be useful in future studies.

A nominal 10-inch (25.4 cm) oil diffusion pump (MCF-1400 with Dow Corning-704 fluid) trapped by a liquid nitrogen baffle and protected by an air operated gate valve (Temescal Metallurgical Corp.) is mounted to one side of this chamber. Low pressures are measured with a VG-1B ion gauge and higher pressures with a Hastings model DV 3-M thermocouple gauge.

5. Source Chamber

Like the rest of the system, the source chamber is fabricated of stainless steel. It is pumped by a diffusion pump identical to that used to evacuate the selector chamber. To handle the large gas load during operation of the beam, both pumps are backed by a rotary blower (Rootes model RS-120), but unfortunately its operation causes excessive vibration of the system and so its use is limited to initial pump-down until it can be isolated by a bellows.

In order to insure that the crystal, gate valve collimator, and the source chamber collimator were all collinear, a laser beam was used to align the last slit (source collimator) with the first two positions. The main body of the chamber was then welded in place to

the tube in which the oven resides. The collimator slit between the source and selector chambers has the same dimensions as the beam (0.8 × 4.8 mm).

a. Beam Source. A glass multichannel plate (Bendix Mosaic Fabrication) consisting of a 0.8 by 4.8 mm rectangular array of tubes (diameter 5μ, length-to-diameter ratio 100) is used to generate a thermal molecular beam of some noncondensible gas. Figure II-17 shows a photograph of the plate detail. The capillary array is held between gold O-rings to provide a leak-tight seal. Belville spring washers* apply a constant load against the plate so that the stress relieved stainless steel oven in which it is housed can be heated to 600°K or cooled to 77°K without shattering the array which is made of borosilicate glass.

In Fig. II-18 is shown an exploded view of the oven. The liquid nitrogen coils were silver soldered to the oven body and then covered by a threaded alumina insulator wrapped with 3.2 m (10.5 feet) of 0.25 mm (0.010 inch) Ta wire for heating purposes. Glass capillary arrays similar to the one used in this work have also been used by other authors[57,58] for molecular beam studies, and their characteristics have been fully investigated.[95-100] The change in beam intensity at the crystal with driving pressure in the oven is shown in Fig. II-19. One can see that pressures above 10 torr produce little gain in intensity.

---

* The author wishes to thank Don Hunt for this mounting suggestion.

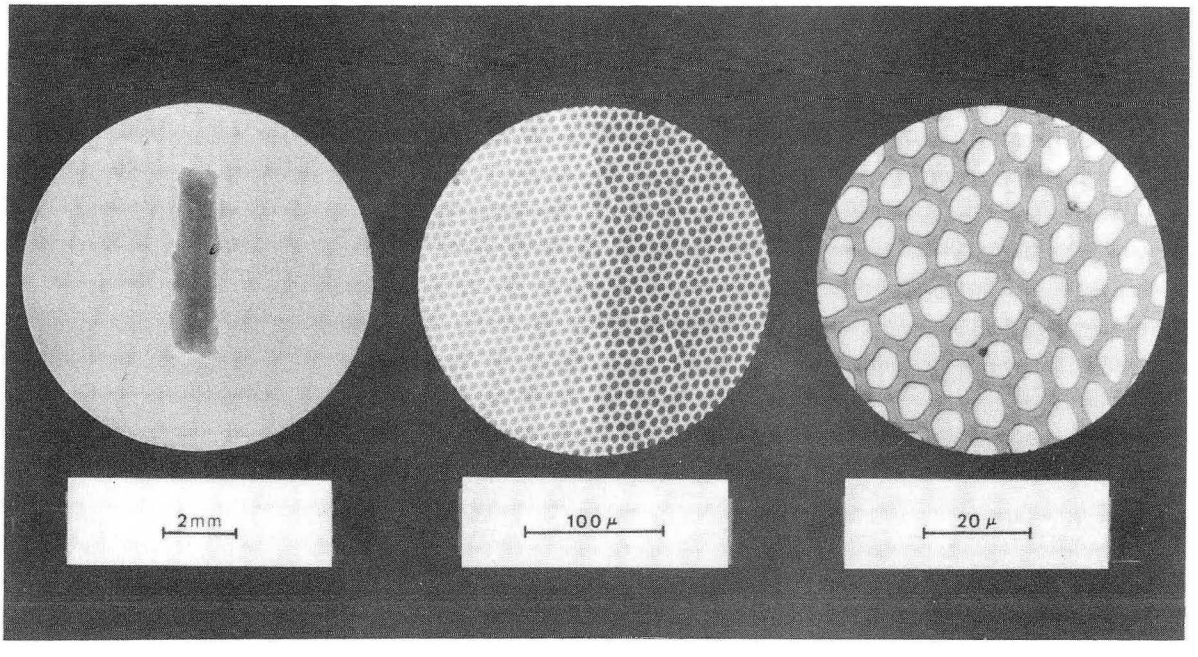

XBB 707-3371

Fig. II-17. Detailed view of the multichannel capillary array used in the molecular beam source.

0 0 0 0 3 6 0 3 3 0 8

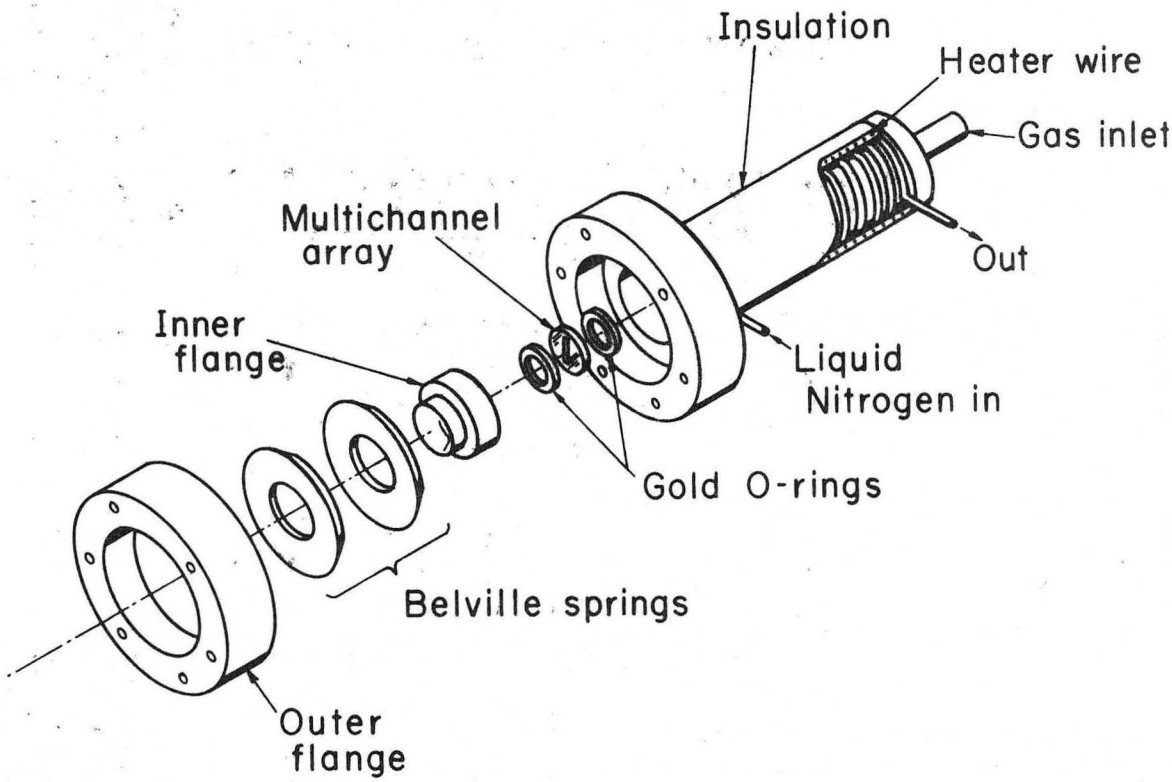

XBL 704-2669

Fig. II-18. Exploded view of the molecular beam source demonstrating how the glass capillary array is held in place.

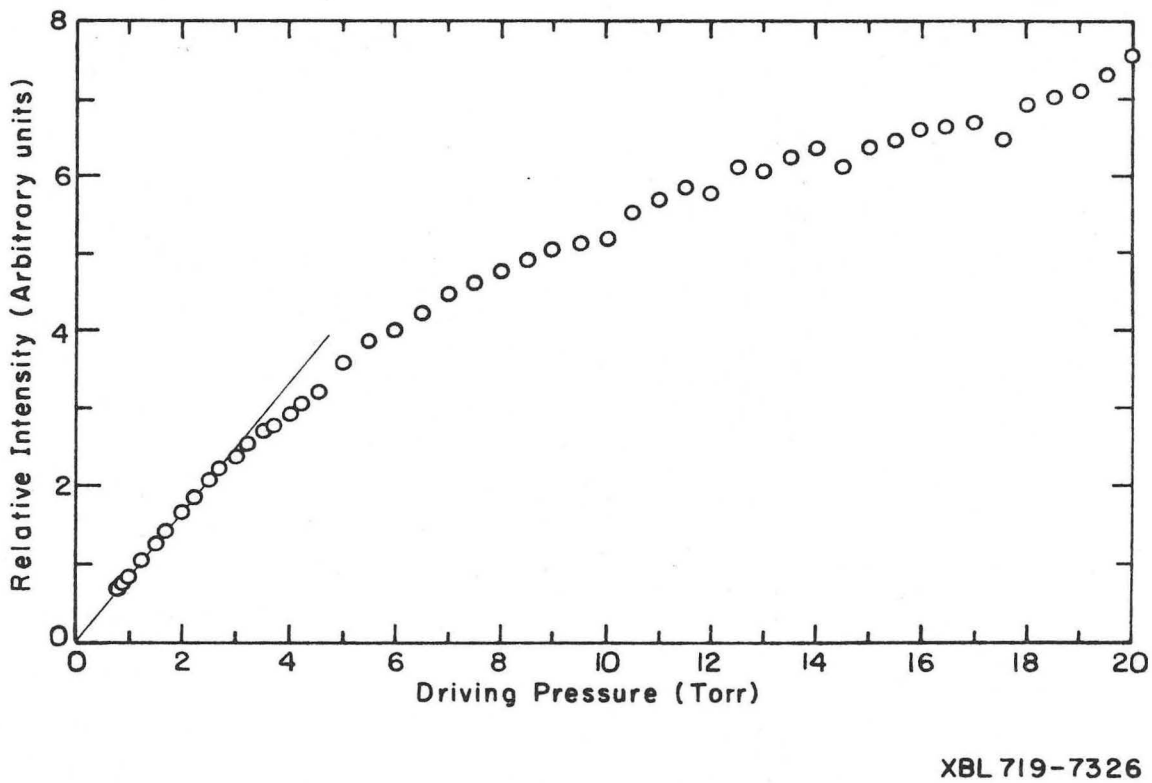

Fig. II-19a. Pressure-intensity relationship for a helium beam at $T_B = 300°K$.

0 0 0 0 3 6 0 5 5 0 9

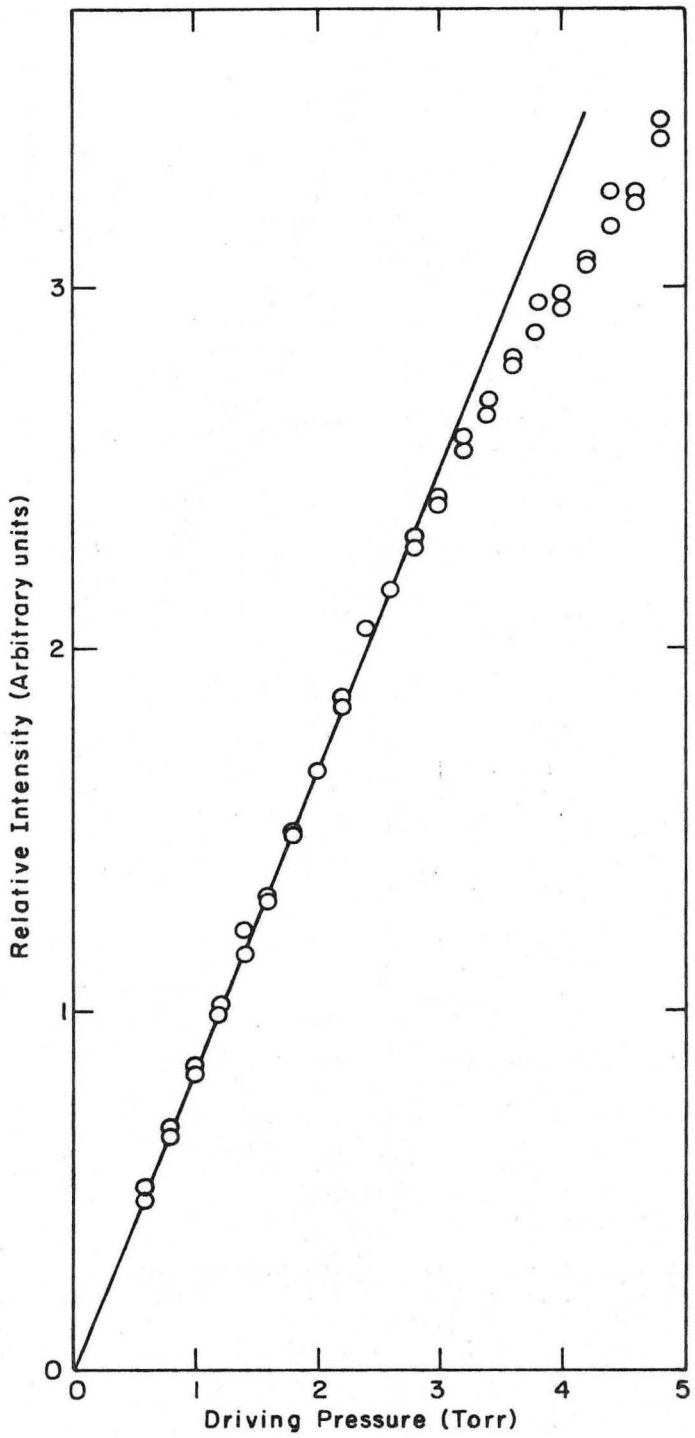

XBL 719-7327

Fig. II-19b. Enlargement of low pressure range from Fig. II-19a showing that the beam intensity is directly proportional to the driving pressure.

In the ultra high vacuum chamber, the total background pressure increases linearly with the pressure in the oven, having an incremental change of approximately 2.3×10^{-11} torr per torr of driving pressure up to a value of 4 torr.

b. Gas Handling System. The gas handling system for the oven is shown in Fig. II-20. It consists of a glass vacuum line evacuated by a 10 ℓ/sec oil diffusion pump connected to the large rough pump and a ~ 1 ℓ/sec Kinney KC-2 forepump connected directly to the molecular seive trap. Coupling the sieve trap to the system pump as shown in the drawing led to difficulties if the glass system was pumped when the ten inch diffusion pumps were in operation (usually the case!) because the resultant gas flow actuated the over-pressure alarms. Thus the change to an independent pump was made. Also the sorption pump shown on the LEED manifold was removed because the interconnection to the glass system provides all the needed pumping capacity. Precise flow conditions from the high pressure inlet manifold or the pressurized five liter flask to the oven are maintained by a variable sapphire leak valve (Varian). The one liter flask acts as a ballast reservoir to damp out any rapid pressure fluctuations on the beam side of the leak valve. Final beam driving pressures are monitored with a Wallace and Tiernan absolute pressure gauge (range 0.1 to 20 torr). To minimize contamination of either the beam gases or the sapphire leak by stopcock grease, single O-ring sealed Teflon needle valves (Fisher and Porter Co.) have been used in place of high-vacuum stopcocks in this system.

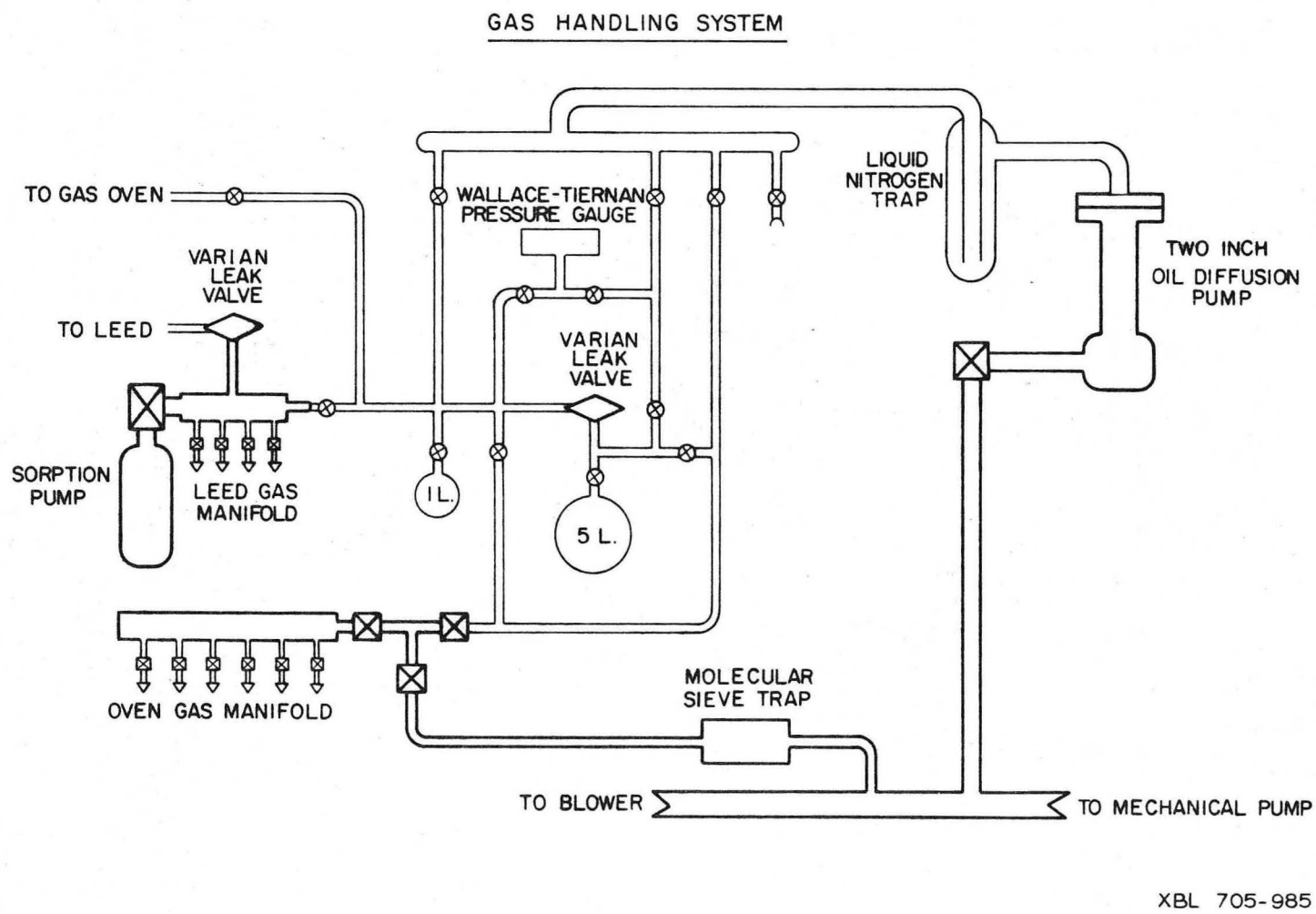

Fig. II-20. Schematic layout of the gas inlet system used to prepare gases for beam studies and LEED-AES experiments.

These are indicated by circled crosses in the drawing while metal valves are indicated by a cross in a square. The beam species can consist of either gases or vapor from a high vapor pressure (> 5 torr) liquid.

6. Interlocks and Pump-down Procedure

With an apparatus of this size and complexity, any electrical or vacuum failure can result in serious damage to parts of the system, especially components of the ultra high vacuum chamber. Consequently a system of "fail-safe" safety devices was designed to isolate the damaged part from the rest of the system.

Power input to the diffusion pump heating elements is controlled by water flow, water temperature, and fore-vacuum pressure sensors. All valves, except those on the scattering chamber, are air operated and wired such that they are normally closed. Thus, a sudden loss of electrical power causes all air operated valves to close and remain in that position if any condition not favorable to their opening still exists when the electric power returns. Additionally the valves are interlocked to one another so that they can only be operated in a set sequence, and the valves connecting the diffusion pumps to the source and selector chambers are connected to pressure sensors that close them whenever the pressure in either chamber exceeds a preset value. Finally the mechanical pump is interlocked to the system vent valve so that the pump cannot be started if the vent is open. Table II.1 gives a list of the interlocks and Fig. II-21 identifies the valve location on the system vacuum map.

Table II.1. Vacuum Interlocks for MBA-Echo

Device	Interlocks
MP 1	V-8 closed
Blower	H_2O flow on, MP 1 on
DP 1	TC-4 vacuum OK, liquid nitrogen level OK, V-4 open
DP 2	TC-4 vacuum OK, liquid nitrogen level OK, V-5 open
V-1	none
V-2*	V-6 closed, V-7 closed
V-3*	V-6 closed, V-7 closed
V-4	none
V-5	none
V-6*	V-5 open, TC-4 vacuum OK, liquid nitrogen level OK, TC-3 vacuum OK
V-7*	V-4 open, TC-4 vacuum OK, liquid nitrogen level OK, TC-2 vacuum OK
V-8	none

* Note: Attempting to open V-2 or V-3 when V-6 and V-7 are already open results in the latter two valves closing and either V2 or V3 opening. A similar effect occurs if the valve roles are interchanged.

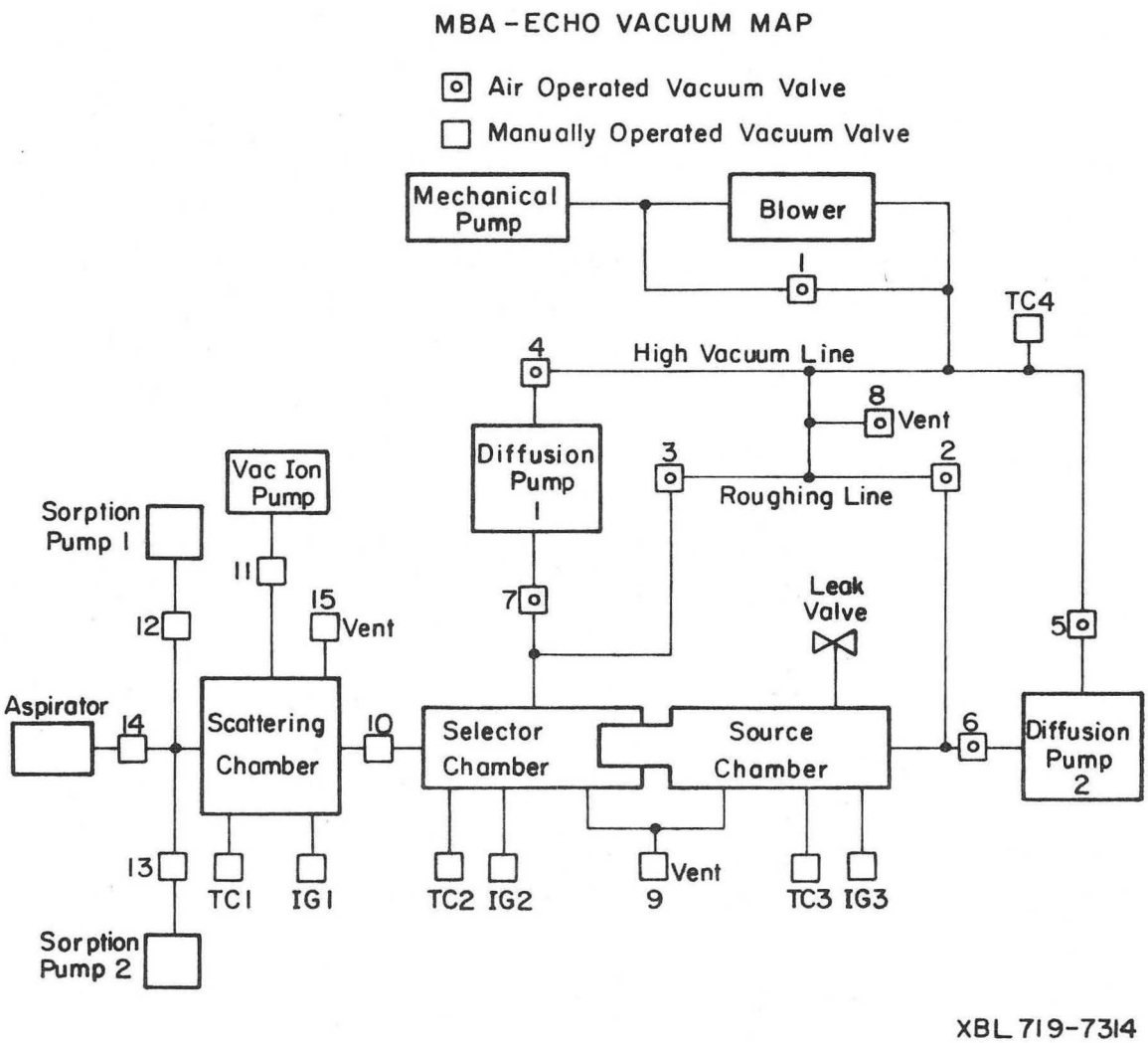

Fig. II-21. MBA-Echo vacuum map identifying the valves referred to in the text.

3 5 5 0 3 6 0 3 5 1 2

Both the mass spectrometer and the LEED power supplies are interlocked to line voltage through a relay that requires manual resetting after a power failure. In this way current surges through the spectrometer ionizer and the LEED electron gun filaments can be averted. The ion pump on the scattering chamber is self protected. Automatic shutdown results from the excessive ion currents due to high pressure. Because the Whittaker gate valve is kept closed except during a beam experiment, a vacuum failure in the beam system will usually not effect the UHV chamber. However, should system alarms go off during a run (and it has happened!), the best course of action is to close the Whittaker valve and then seek out the cause of the problem.

The set of instructions presented in Table II.2 has been prepared as an aid to operating the beam system vacuum components. While following the list, an operator is urged to carefully consider the consequences of pushing or not pushing a given button, just in case something has been accidentally omitted from the instructions. Once the main diffusion pumps are running the system can be left in operation for long periods of time providing the 160 liter liquid nitrogen storage tank is filled periodically.

7. Experimental Procedure

Prior to the commencement of an experimental run, the surface of the crystal must be prepared. In the case of clean platinum, the ion pump gate valve must be throttled with the gate valve and then

Table II.2. Vacuum Operating Instructions for MBA-Echo

A: To let the entire system up to air from vacuum:

1. Make sure diffusion pumps are cool
2. Make sure V-10, V-6, V-7 are all closed. (V-4, V-5 may be open or closed as desired)
3. Make sure V-2, V-3 are open
4. Turn off MP1
5. Open system vent V-8 on vacuum map

B: To pump the system down from air to operating status:

1. Close V-8 on vacuum map
2. Make sure V-6, V-7 are closed
3. Make sure V-1 (blower bypass) is open as well as V-2, V-3
4. Make sure V-4, V-5 are open if diffusions pumps are not under vacuum
5. Turn on MP1
6. When TC-4 reads 1000μ, turn on the Blower and then close V-1
7. Fill liquid nitrogen traps (requires ~ 15 minutes)
8. Make sure V-4, V-5 are now open
9. Turn on DP1, DP2 when traps are cold and allow to warm up 30-60 minutes
10. Turn on IG-2, IG-3
11. Close V-2, V-3
12. Open V-6, V-7

Table II.2., continued

13. Open V-1 and turn off Blower if this has not already been done

14. System is ready to admit a beam when IG-2, IG-3 read below 1×10^{-6} torr

C: To let source and selector chambers up to air while the rest of the system is under vacuum:

1. Make sure diffusion pumps are cool
2. Make sure V-10, V-6, V-7 are all closed
3. Make sure V-2, V-3 are closed
4. Open vent marked V-9 on vacuum map (manually controlled)

D: To pump out source and selector chambers after step C

1. Close vent V-9
2. Make sure diffusion pumps are cool
3. Close V-4, V-5
4. Open V-2, V-3 <u>simultaneously</u>
5. Proceed with procedure B above starting at step 6

2×10^{-5} torr of O_2 allowed to flow through the system via the Granville-Phillips leak valve. The crystal is heated in this atmosphere at 1175°K for half an hour. To prepare the carbon covered platinum surface, the crystal is heated in ~ 10^{-7} torr of acetylene as above. During this time the beam gas can be admitted to the high pressure side (~ 2 psig) of the oven leak valve and the leak rate adjusted to provide a constant pressure as indicated by the Wallace and Tiernan gauge. It is usually desirable to start at about 1 to 2 torr and then work up to higher source pressures unless one knows exactly what pressure he wishes to maintain.

Following the crystal preparation, the UHV chamber is pumped out and then a fresh layer of titanium is deposited in the sublimation pump. The LEED optics are turned on and the surface of the crystal checked by LEED and/or AES. At this point the sample is raised above the beam line and brought to temperature if a high temperature run is desire.

The beam species may now be admitted to the scattering chamber by opening the Whittaker gate valve. After placing the quadrupole in the beam at its 0° maximum, one can tune the mass spectrometer to the peak or peaks of interest and, by adjusting the resolution and beam driving pressure, arrive at the desired incident beam strength. The peak selector panel allows several ions to be monitored with the flick of a switch when the RF-DC generator is operated in the Program mode, but the Sweep Width control <u>must</u> be set to zero--a significant difference from the Manual mode of operation. Once the quadrupole is

0 0 0 0 3 6 0 5 5 1 4

focused, the beam chopper can be turned on and the lock-in amplifier adjusted to the proper frequency and phase for a signal maximum. The incident signal is now recorded on the Leeds and Northrup strip chart recorder in the mass spectrometer console (Rack #00). A similar recording is next made with the quadrupole located at 180° in the laboratory reference frame, except that now two intensities are monitored with one at 90° from the maximum phase ϕ_o. From the two traces, the true peak intensity, the phase lead, and the intensity ratio between the two positions can be calculated. These measurements are each repeated twice more and then the crystal is lowered into place and the angle of incidence adjusted using the scale previously calibrated during the helium scattering experiments. During the run, the main beam signal at 180° is measured between every two experimental points so that the scattered intensities can be corrected for slow fluctuations in the incident intensity. A sample chart recording is shown in Fig. II-22.

Due to the physical size of the detector ionizer, instrument angles closer than about 50° to the beam line interfere with the incident beam, thus lab angles below 173° - 50° = 123° are inaccessible with the apparatus as it is currently assembled. For $\theta_i = 45°$, this means that angles less than 12° from the surface normal cannot be observed, and with 7 mm diameter crystals, angles much below 45° mean that part of the incident beam may strike the crystal supports rather than the crystal itself. Of course, better angular resolution and measurement angles closer to the surface normal cound be achieved with a

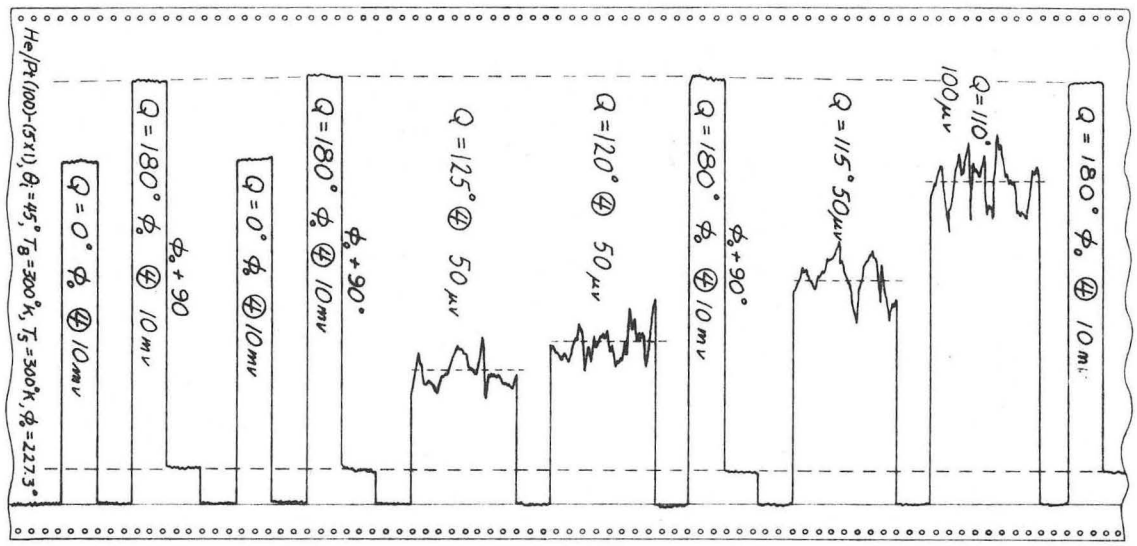

XBL 719-7313

Fig. II-22. Typical recorder trace of a molecular beam scattering experiment with helium. The chart notations refer to the phase of the lock-in amplifier relative to the phase ϕ_o of the incident beam, the sensitivity of the lock-in, the mass number of the monitored peak, and the position of the quadrupole Q in the laboratory reference frame.

0 0 0 0 3 6 0 5 5 1 5

corresponding drop in signal level if the detector were moved farther away from the scattering center.

After the run, the measured peak heights at each angle are processed by a computer program (see Appendix VII-A) that calculates the scattered intensity normalized to the strength of the incident beam at the 0° location. In this way a quantitative comparison of the scattering efficiency of various surfaces may be made. Scattered beam half-widths may also be compared to one another or to the half-width of the incident beam because all are expressed in terms of degrees of detector rotation.

III. SELECTED PROPERTIES OF THE Pt(100) SUBSTRATE

In any well controlled gas-solid scattering experiment, detailed information concerning the structural and chemical characteristics of the single crystal surface to be utilized should be available. The surface properties of platinum have been widely investigated[18,104] because this transition metal acts as an excellent catalyst for many chemical reactions involving gaseous reactants. For this reason and because of previous experience in this laboratory, platinum was chosen for further study in molecular beam scattering experiments.

A. Surface Structure

Platinum has a face-centered cubic crystal structure with a bulk lattice parameter of 3.916 Å and an inter-atomic distance of 2.77 Å. The high heat of sublimation of the solid (135 kcal/gram atom), permits a crystal to be heated quite close to its 2050°K melting point without excessive substrate loss from evaporation. Projection from the bulk unit cell to the surface suggests that the (100) face of platinum should possess a square unit cell of side 2.77 Å. Previous low energy electron diffraction studies[105,106] have revealed however that the clean Pt(100) surface is characterized by a large rectangular surface net of approximate dimension (5×1) with respect to the underlying bulk structure. (See Fig. I-6 and IV-4a for the diffraction pattern.) Similar anomalous structures have also been reported for the (100) faces of gold[107-109] and iridium,[110] elements adjacent to platinum in the periodic table.

Since these studies were conducted prior to the widespread use of Auger electron spectroscopy, it was inevitable that questions be raised concerning the cleanliness of these surfaces.[111] Through the epitaxial growth of gold on a (100) silver crystal, however, Palmberg and Rhodin[109] were able to convincingly demonstrate that a LEED pattern assumed the (5×1) structure after only three monolayers of gold had been deposited. Subsequently, Palmberg[112] employed AES to show the cleanliness of the Pt(100)-(5×1) surface. Similar evidence for the cleanliness of the (5×1) structure has been accummulated in this laboratory and will be presented in the following chapter. Grant and Haas[111] have suggested that the (1×1) diffraction pattern is indicative of the clean (100) surface and that the (5×1) array is stabilized by the presence of oxygen. This conclusion is not in agreement with Auger spectra that clearly show the presence of carbon on the surfaces yielding the (1×1) structure.

The appearance of the (5×1) surface has been interpreted by Fedak and Gjostein[107,108] as indicating the presence of a hexagonal overlayer forming a (5×20) coincidence lattice with the square (100) substrate. This analysis assumes the structure possesses both two-fold rotational and mirror symmetry. Palmberg,[112] on the other hand, suggests that the unit cell does not possess mirror symmetry, but is characterized by a parallelogram, with dimensions similar to those proposed above, rotated slightly with respect to the principal underlying (100) axes. In his thesis, Lyon[113] proposed that the (5×1)

surface unit cell might be due to ordered vacancies at the platinum-vacuum interface although this hypothesis now seems less likely than the hexagonal overlayer. Burton and Jura,[114] using an analogy with the surface energy of argon, postulated that a range of anomalous structures might arise due to displacements of rows of atoms. This argument is tenable for a simple (5×1) array, but it cannot account for the complexity (i.e., spot splitting) of the observed (5×1) diffraction pattern.

To date, based upon evidence compiled via LEED studies, the best explanation of the (5×1) surface structure is that it arises due to a phase transformation distorting the surface atoms from a four-fold into a six-fold rotational symmetry. Either small out-of-plane displacements or a slight compression (~ 5%) of the surface layer is necessary to achieve the observed fifth order coincidence if the hexagonal layer corresponds to the (111) face of platinum. This correspondence, however, is somewhat unlikely in view of the helium beam scattering results to be presented in the following chapter. The driving force for such a rearrangement is probably a small decrease in the surface free energy resulting from closer packing. Additionally, Rhodin, Palmberg, and Plummer[115] have presented strong arguments explaining the reconstruction of gold and platinum surfaces in terms of enhanced surface valency.

0 0 0 0 3 6 0 5 5 1 7

B. Surface Contamination and Gas Adsorption

In Chapter I, section D we pointed out the several possible sources of sample contamination with which one has to contend. While the amount of metallic impurities in an electron beam zone refined platinum crystal is typically on the order of 100 ppm or less, the concentration of any particular metal is so far below its solubility limit that there is no driving force to cause diffusion toward the surface. Thus even at elevated temperatures the distribution of these impurities is uniform and their effect on the surface is undetectable.

Non-metallic impurities, however, are somewhat more of a problem. Potential contaminants of this type include carbon, oxygen, sulfur, silicon, and chlorine. The Auger peak due to chlorine has not been observed on a platinum surface, presumably because it becomes volatile after diffusing to the surface. Silicon has been reported to segregate to the platinum surface at high temperatures but to disappear upon cooling.[112] Similarly, reversible segregation has been reported for sulfur at the surfaces of vanadium[116] and copper[117] although this impurity does not seem to be present in the case of platinum. During this work, no Auger electrons due to silicon were observed, but the crystals used were extensively heated in oxygen and it is known that such treatment irreversibly removes the silicon contaminant.[112] Oxygen does not easily adsorb on the low index faces of platinum and since the oxides of platinum are thermodynamically unstable at elevated

temperatures,[113] any oxygen diffusing to the surface from the bulk readily desorbs.

By far the most persistent platinum surface contaminant is carbon.[106,112,118] Trace amounts of this element stabilize the (1×1) surface structure. Siller, Oates, and McLellan[119] have studied the solubility of carbon in platinum and report values up to two (atomic) percent at 1520°K. Very rapid rates for carbon diffusion and a much lower solubility level have been found by Selman, Ellison, and Darling.[120] This rapid diffusion rate is in qualitative agreement with the observation that heating a surface coated with amorphous carbon above 1075°K for several minutes causes the carbon to aggregate into islands of graphite, all with their basal plane parallel to the platinum surface. The diffraction pattern of the resultant surface (Fig. IV-7a) consists of narrow rings or segmented rings concentric about the (00) reflection and indicates the presence of graphitic domains of random orientation. In order to remove the layer of surface carbon resulting from the original sample preparation, the crystal must be heated 30-60 minutes at 1175°K in ~ 10^{-5} torr of oxygen. Slightly milder cleaning conditions can be used once the bulk has been purged of carbon.

Another persistent contaminant of the platinum (100) surface is adsorbed carbon monoxide. Since CO is (a) one of the major constituents of the residual gases in a stainless steel UHV system, and (b) has a sticking probability on clean platinum near unity,[121,122] it posed a serious impediment to the studies reported in this thesis. Further, as revealed by flash desorption experiments,[106] there are at least

0 0 0 0 3 6 0 5 5 1 8

three binding states for CO on the (100) platinum substrate. The adsorbed molecules may be removed by heating the crystal to approximately 400, 450 and 880°K respectively. By flashing the crystal to temperatures approaching 1000°K it was possible to remove all the CO from the surface for times long enough to permit the study of atomic and molecular beam scattering from clean platinum. The crystal, however, must be flashed frequently if a clean surface is desired due to the gradual readsorption of carbon monoxide. CO also forms ordered surface structures of several types on the Pt(100) surface,[106,123] but their effect on beam scattering has not yet been fully investigated.

Two other gases used in this study form ordered surface structures on the Pt(100) surface. These gases are acetylene and hydrogen. When acetylene is adsorbed on the clean Pt(100)-(5×1) surface at room temperature, the fifth order diffraction spots disappear rapidly and continued adsorption results in the formation of a c(2×2) structure (see Fig. IV-9a). The pattern, in addition to the normal substrate spots, has extra spots at the center of each reciprocal unit mesh. These extra features with half-integral indices are less intense and more diffuse than the (1×1) diffraction spots. Removal of the acetylene to obtain the (5×1) surface was achieved by heating the crystal to ~ 425°K, but repeated adsorption-desorption cycles invariably led to the formation of ring-like diffraction patterns as the result of cracking the hydrocarbon.

Flash desorption and work function measurements showed that hydrogen did not appear to adsorb on the (100) face of platinum at gas pressures between 10^{-9} and 10^{-7} torr and at temperatures up to 1275°K. However, increasing the hydrogen pressure to greater than 3×10^{-5} torr for surface temperatures in the 775° to 1275°K range resulted in the formation of a (2×2) structure coupled with the disappearance of the fifth order features.[106] While the extra spots were as well defined as the (1×1) spots, they were somewhat less intense. The (2×2) surface structure proved to be very stable and could only be removed by heating the crystal in vacuum for a few minutes to 1475°K. An alternate route to regenerating the (5×1) structure was to heat the (2×2) structure in 2×10^{-8} torr of oxygen at 775°K. Due to the extreme conditions necessary to produce the (2×2) surface structure, it was not utilized for any scattering experiments.

0 0 0 0 3 6 0 5 5 1 9

IV. SCATTERING OF MONATOMIC GASES

A. Introduction

Of the different gases used in gas-solid scattering experiments, helium atomic beams appear to undergo the weakest interaction with the surface. The fraction of the incident beam scattered specularly (i.e., the incident and scattering angles are equal) has been reported to be a large as 25% in the case of (111) platinum[90] and 50% in the case of tungsten carbide.[47] This is at least an order of magnitude greater than the specularly directed component observed with other atomic beams. Such a weak interaction is not at all surprising in view of the small size, small mass, small polarizability, and low heat of adsorption on most solid surfaces of the helium atom. Despite its weak interaction with the surface, however, the helium beam was found to be very sensitive to surface contamination. Whether ordered or disordered, adsorbed impurities present to the incoming helium atoms a scattering surface having physical characteristics (i.e., atomic weight, dimensions, and force constants) quite different from those of the clean surface.

By the incorporation of LEED and AES into the ultra high vacuum scattering chamber, the atomic structure of the target surface could be monitored before, during, or after the scattering experiment. This ability to observe the surface *in situ* led to some interesting correlations between the observed helium scattering distributions and well-characterized surface conditions.

B. Effect of Surface Order and Disorder on Helium Atomic Beam Scattering

To investigate the effect of surface roughness on atomic beam scattering, experimental studies of helium scattering from freshly etched platinum surfaces were carried out. These surfaces did not exhibit diffraction at low electron beam voltages, but did yield weak (1×1) LEED patterns with large background intensities at high beam voltages (above 250 volts) where the contribution from bulk diffraction beams becomes important. From this information, we infer that the surface was quite disordered on an atomic scale and that the size of any ordered surface domains must have been less than 500 Å in diameter.[93] A SEM photograph of a freshly etched Pt(100) surface has already been shown in Fig. II-1. Figure IV-1 shows the density distribution in the plane of incidence as a function of the scattering angle θ_r for a helium beam scattered from an etched surface shortly after it was placed in the UHV chamber. In this case the angle of incidence θ_i was 45°. The scattered intensity has been normalized to the strength of the incident beam as described in the last section of chapter II so that the ordinate represents directly the percent of the incident helium atoms scattered into the detector at a given scattering angle θ_r measured from the surface normal. It can be seen from Fig. IV-1 that the angular distribution has a small but distinct peak near the specular angle although there is a pronounced cosine contribution as indicated by the scattered intensity component at $\theta_r = 0°$. The scattering curve expected for a cosine angular distribu-

0 0 0 0 3 6 0 5 5 2 0

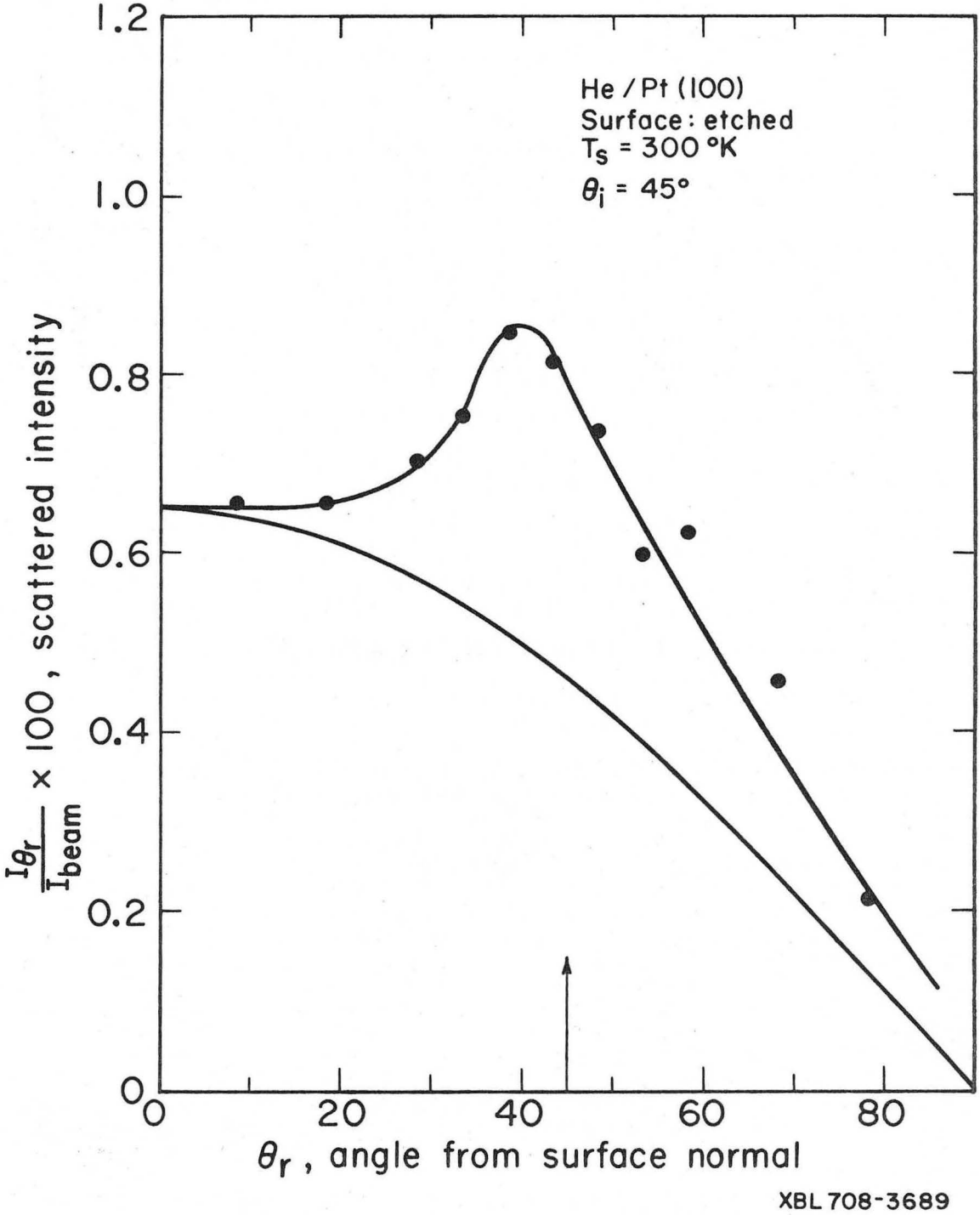

Fig. IV-1. Helium beam scattering profile from an etched Pt(100) surface. I_{beam} = incident beam intensity.

is indicated by the solid line in the same figure for reference. Note that the fraction scattered at the specular angle represents only 0.8% of the incident beam.

The scattering distribution obtained from a crystal surface after it had been ion bombarded for one hour with 300 volt argon ions is shown in Fig. IV-2. In many respects it is similar to the curve shown in Fig. IV-1 except that the dispersion of the specularly directed peak is greater and its maximum intensity lower. The intensity decrease may be due to increaed surface roughness resulting in more out-of-plane scatter or to the presence of adsorbed argon atoms as the crystal had not been flashed or annealed when the data were recorded. In this case, the crystal yielded no LEED pattern at any voltage, thus indicating that there is considerable disorder in the bulk as well as on the surface due to extended ion bombardment. Ion bombardment followed by subsequent annealing to remove surface damage is used most frequently to clean and order single crystal surfaces.

Several ion bombardment and annealing cycles followed by heating the crystal in oxygen to remove any residual surface carbon results in the characteristic (5×1) diffraction pattern (Fig. IV-3a) indicative of a clean, well-ordered (100) platinum substrate. Figure IV-3b presents the helium scattering curve taken from a surface in this state. In order to keep the surface free of adsorbed gases during the run (principally CO), it was found necessary to flash the sample to 1000°K between data points. The scattered intensity at the specular angle

0 0 0 0 3 6 0 5 5 2 1

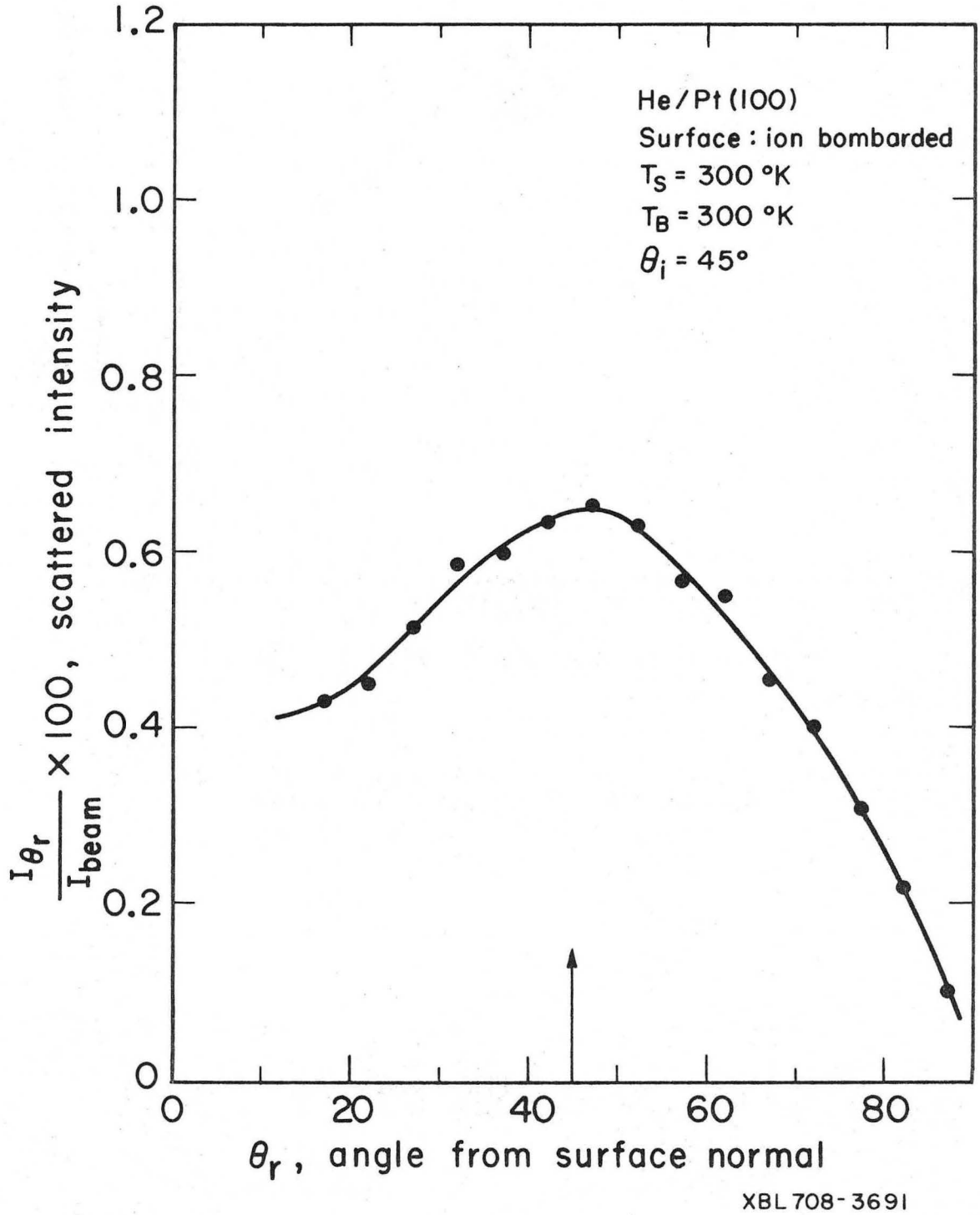

Fig. IV-2. Angular distribution of a helium beam scattered from an ion bombarded Pt(100) surface. I_{beam} = incident beam intensity.

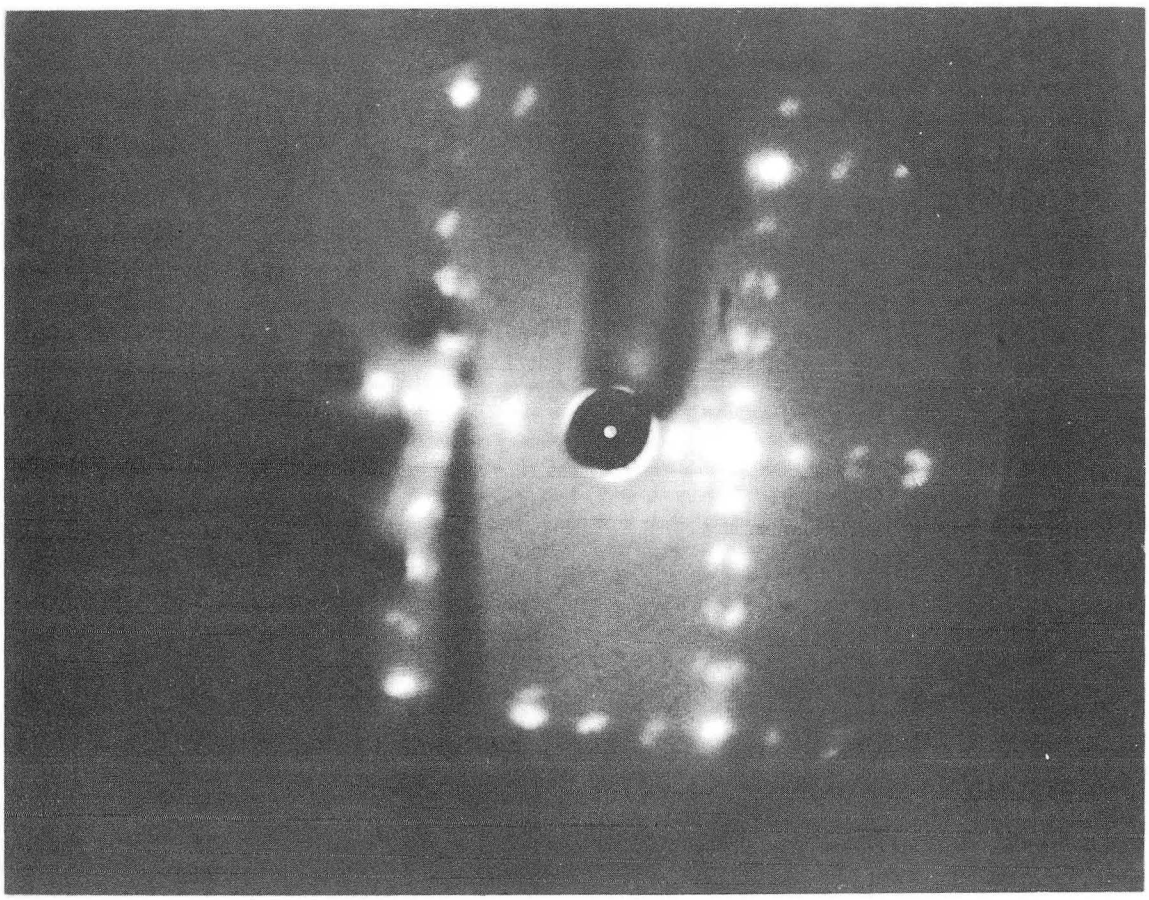

XBB 708-3757

Fig. IV-3a. Diffraction pattern at V = 63 volts of a clean Pt(100) surface showing the (5×1) surface structure. Fractional order spots along both the x and y axes are due to surface domains rotated 90° to one another.

0 0 0 0 3 6 0 5 5 2 2

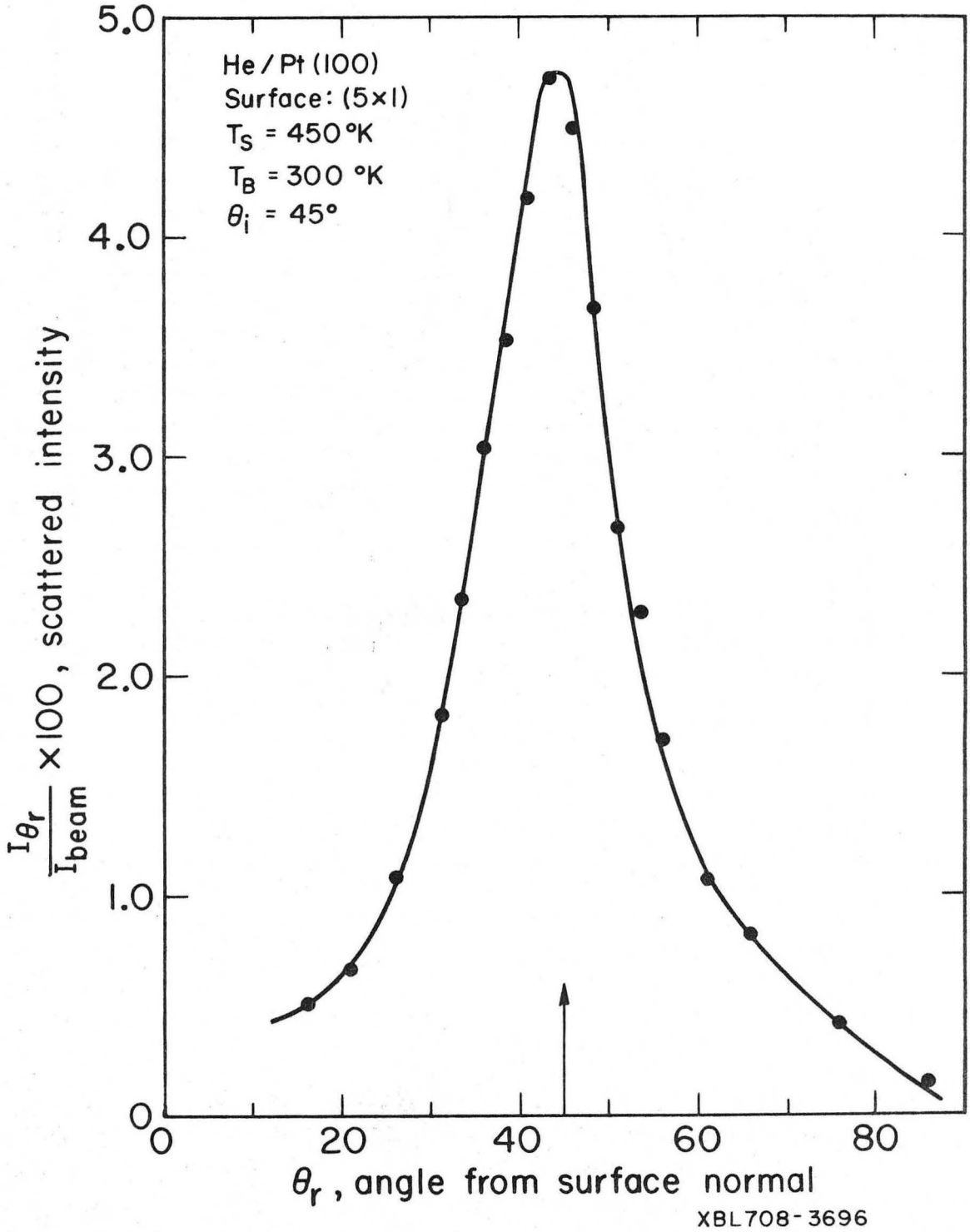

Fig. IV-3b. Helium beam spatial distribution obtained by scattering from a surface showing the (5×1) diffraction pattern. I_{beam} = incident beam intensity.

represents nearly 5% of the total incident beam intensity or an increase of almost an order of magnitude over that observed for an ion bombarded surface. While the angular distribution is sharp, the full-width at half-maximum (FWHM) is rather large (~ 18°) as compared to the width of the incident beam (7°).

Frequently, after treating the platinum crystal with oxygen and then cooling it in the oxygen atmosphere, a previously unreported surface structure could be generated by merely flashing the crystal several times. This structure is characterized by a diffraction pattern with quarter order spots rotated 45° to the axes of the principal platinum features and is designated Pt(100)-($\sqrt{2} \times 2\sqrt{2}$)R-45°.[22] Its distinctive diffraction pattern is shown in Fig. IV-4a when clean and in Fig. IV-4b when CO is present.

Although the exact composition of this structure has not been conclusively identified by AES, it is likely to be the result of either surface reconstruction[18] under the influence of chemisorbed oxygen, or due to coadsorption of oxygen and either carbon or carbon monoxide. Since this surface structure was readily reproducible, it was utilized in several scattering experiments. Pictured in Fig. IV-4c is the helium beam scattering distribution from this surface. A comparison of Figs. IV-3b and IV-4c shows that the two curves have nearly the same half-width and approximately the same intensity at the specular angle. From the high scattering efficiency of this surface compared to those that will be presented in section C of this chapter, and because the scattering dispersion is equal to that observed with

0 0 0 0 3 6 0 3 5 2 3

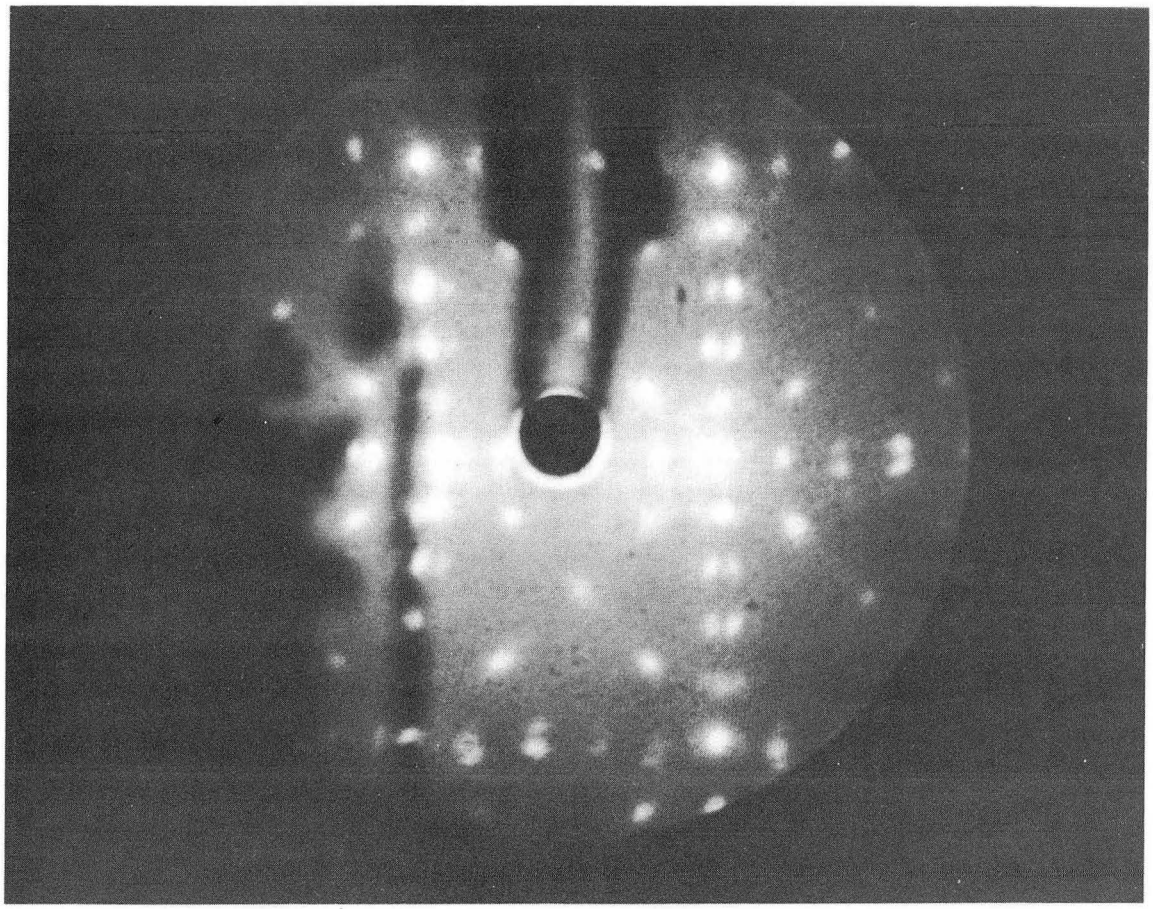

XBB 708-3756

Fig. IV-4a. Diffraction pattern for a Pt(100) sample yielding both the (5×1) and $(\sqrt{2} \times 2\sqrt{2})$R-45° surface structures at V = 63 volts.

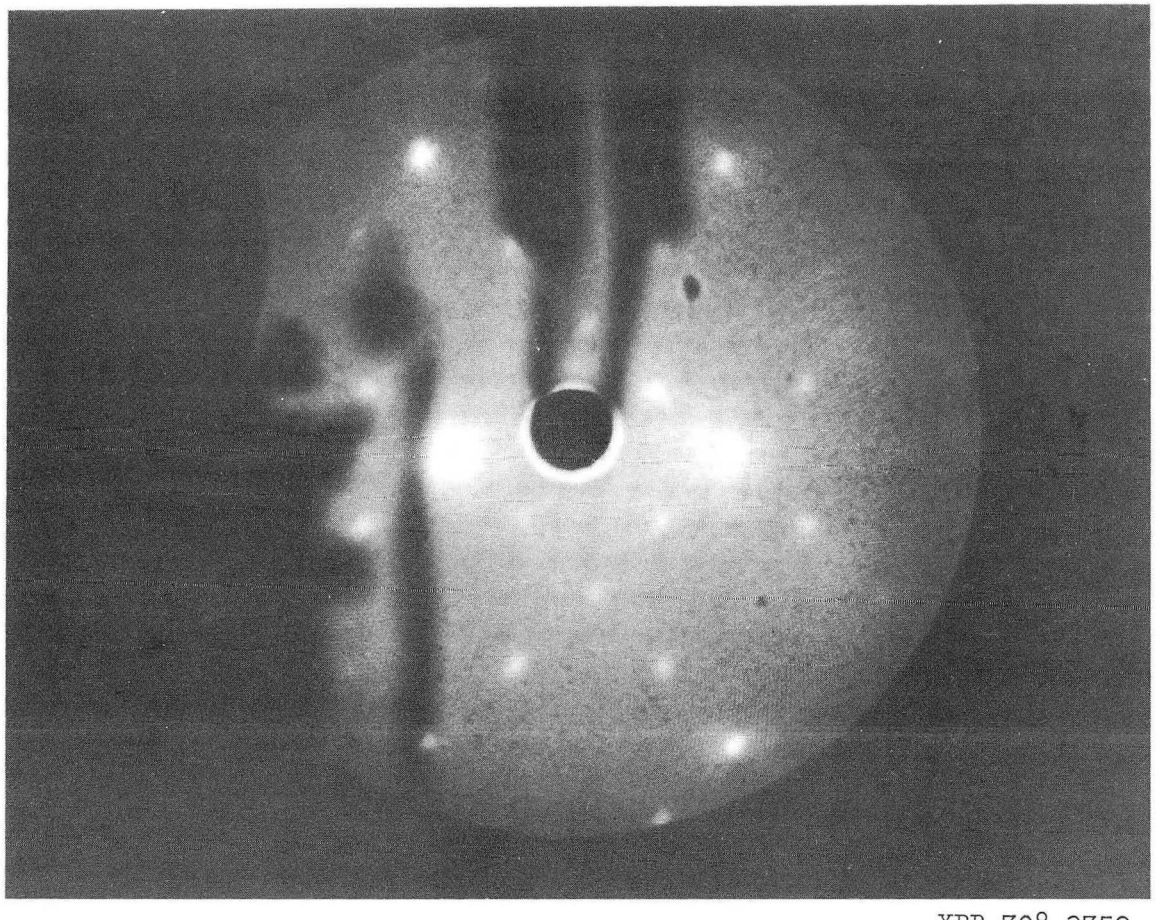

XBB 708-3752

Fig. IV-4b. $(\sqrt{2} \times 2\sqrt{2})$R-45° surface structure with CO adsorbed on the surface, V = 63 volts.

0 0 0 0 3 6 0 3 5 2 4

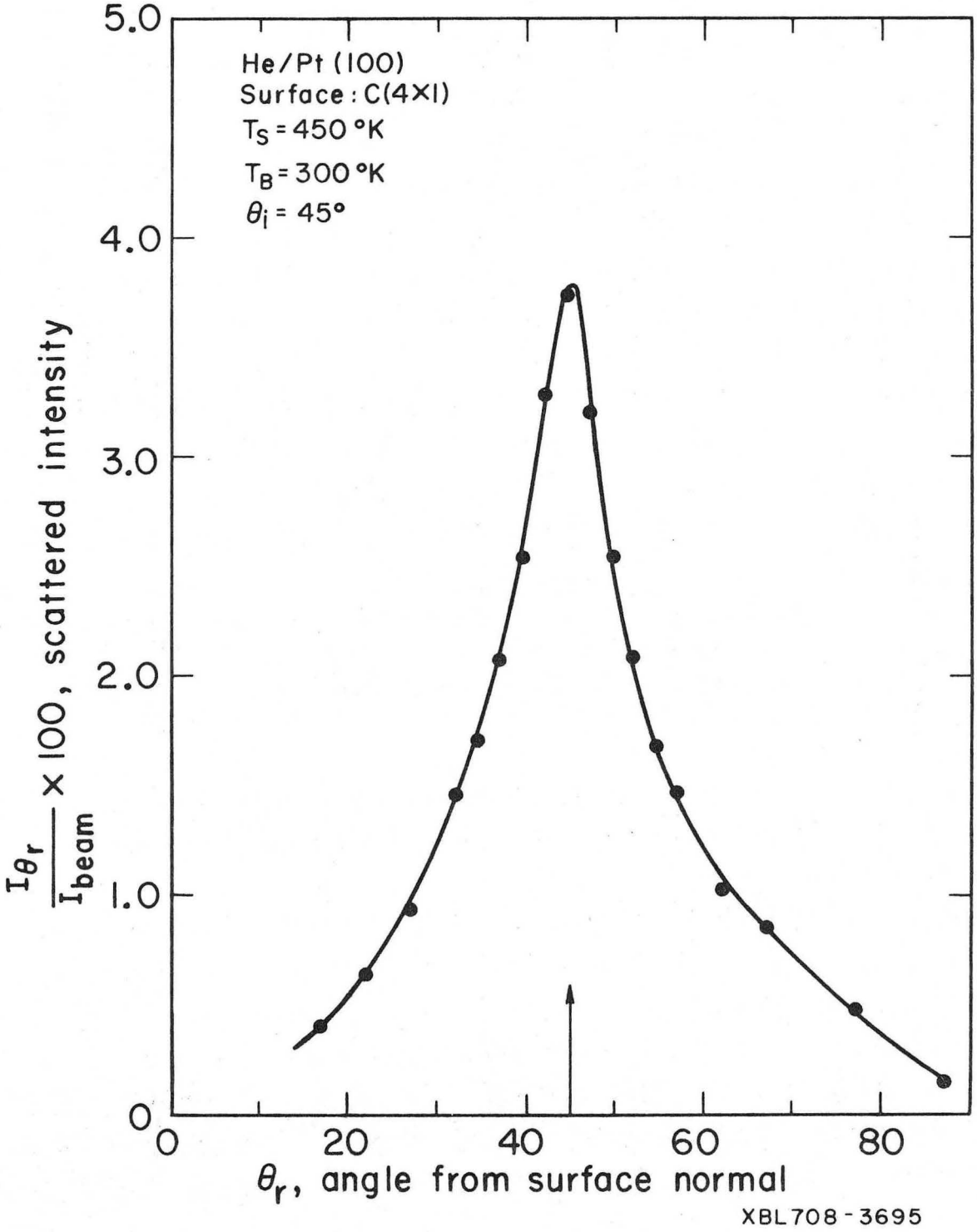

Fig. IV-4c. Helium beam scattering profile from the surface shown in Fig. IV-4a. I_{beam} = incident beam intensity.

the clean surface, surface reconstruction rather than order adsorption of low molecular weight gases may be the cause of the formation of this surface structure.

If the clean surface of Fig. IV-3a is allowed to remain unheated in the vacuum chamber for long periods of time, the (5×1) diffraction pattern gradually disappears and is replaced by a (1×1) pattern as given in Fig. IV-5a. This structure is indicative of the presence of surface carbon (presumably in the form of CO) as shown by the Auger spectrum in Fig. IV-6. In the case of CO on the surface, the (5×1) pattern can be regenerated by flash desorption; however the introduction of a small amount of a small amount of a crackable unsaturated hydrocarbon such as acetylene or ethylene into the ambient permanently removes the (5×1). Figure IV-5b gives the angular distribution for helium scattering from this surface that is characterized by the presence of disordered carbon. Again this distribution is peaked at the specular angle, but the intensity has fallen off sharply to only 1% of the incident beam strength. Not all of this drop can be attributed to the higher surface temperature (900°K) during the run because similar high temperature experiments with clean platinum give intensities greater than 2%.

If this particular surface is now heated to 1200°K for roughly half an hour, the surface carbon aggregates into hexagonal patches representing the basal plane of graphite. Because the patches are randomly oriented with respect to one another, they give rise to the ring-like diffraction pattern shown in Fig. IV-7a. The interesting

0 0 0 0 3 6 0 5 5 2 5

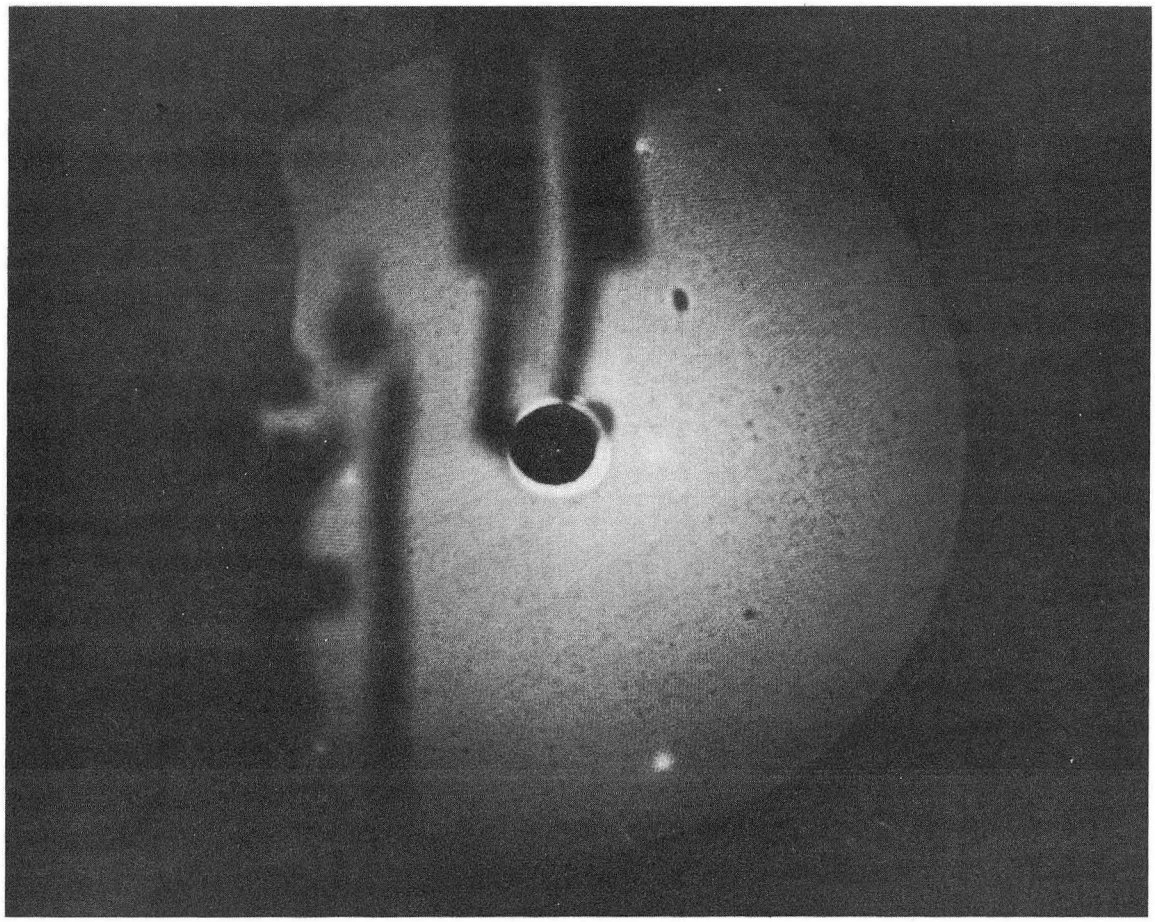

XBB 708-3754

Fig. IV-5a. Pt(100)-(1×1) diffraction pattern at V = 63 volts in the presence of chemisorbed carbon monoxide.

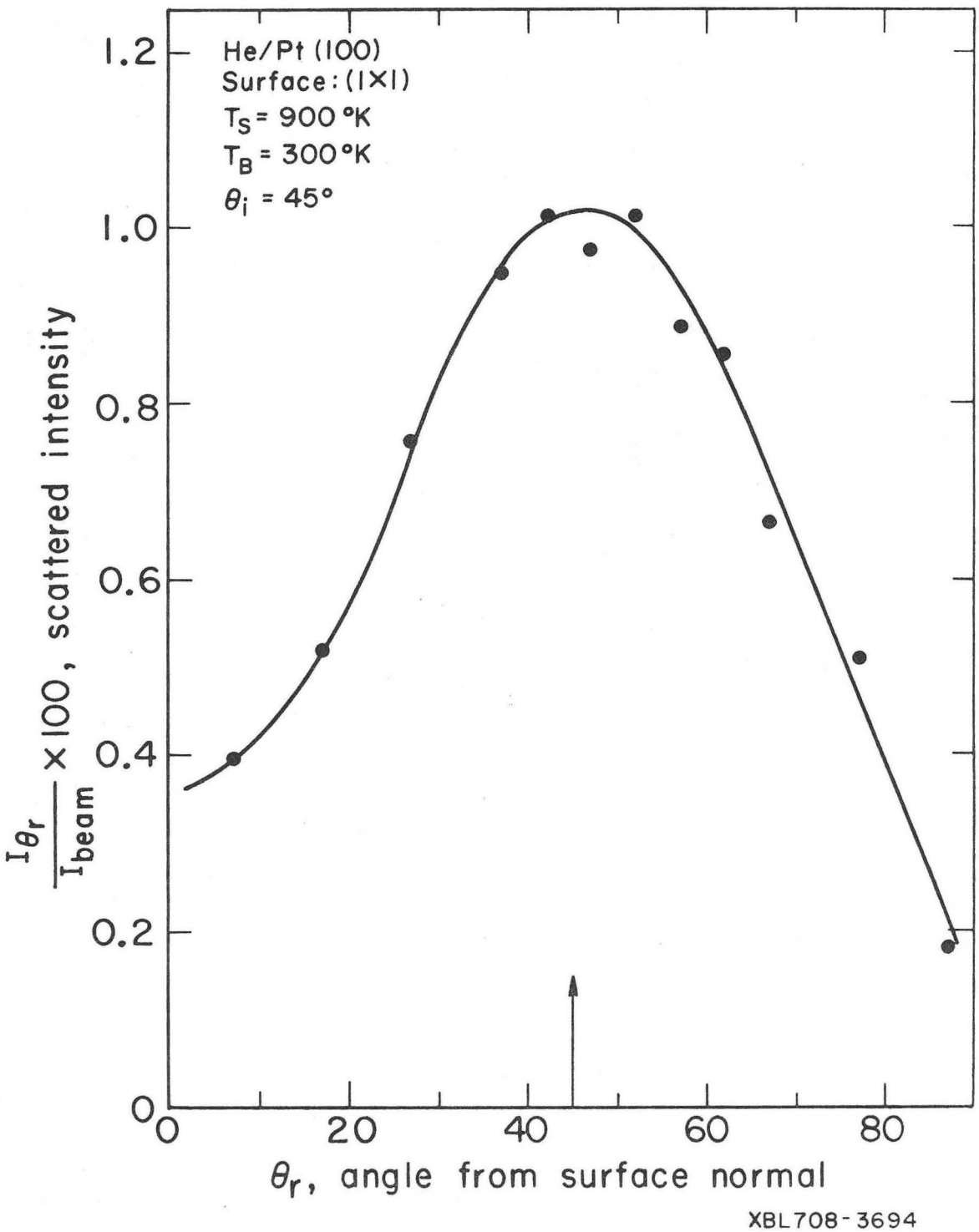

Fig. IV-5b. Angular distribution of helium beam scattered from a carbon contaminated Pt(100) surface. I_{beam} = incident beam intensity.

0 0 0 0 3 6 0 5 5 2 6

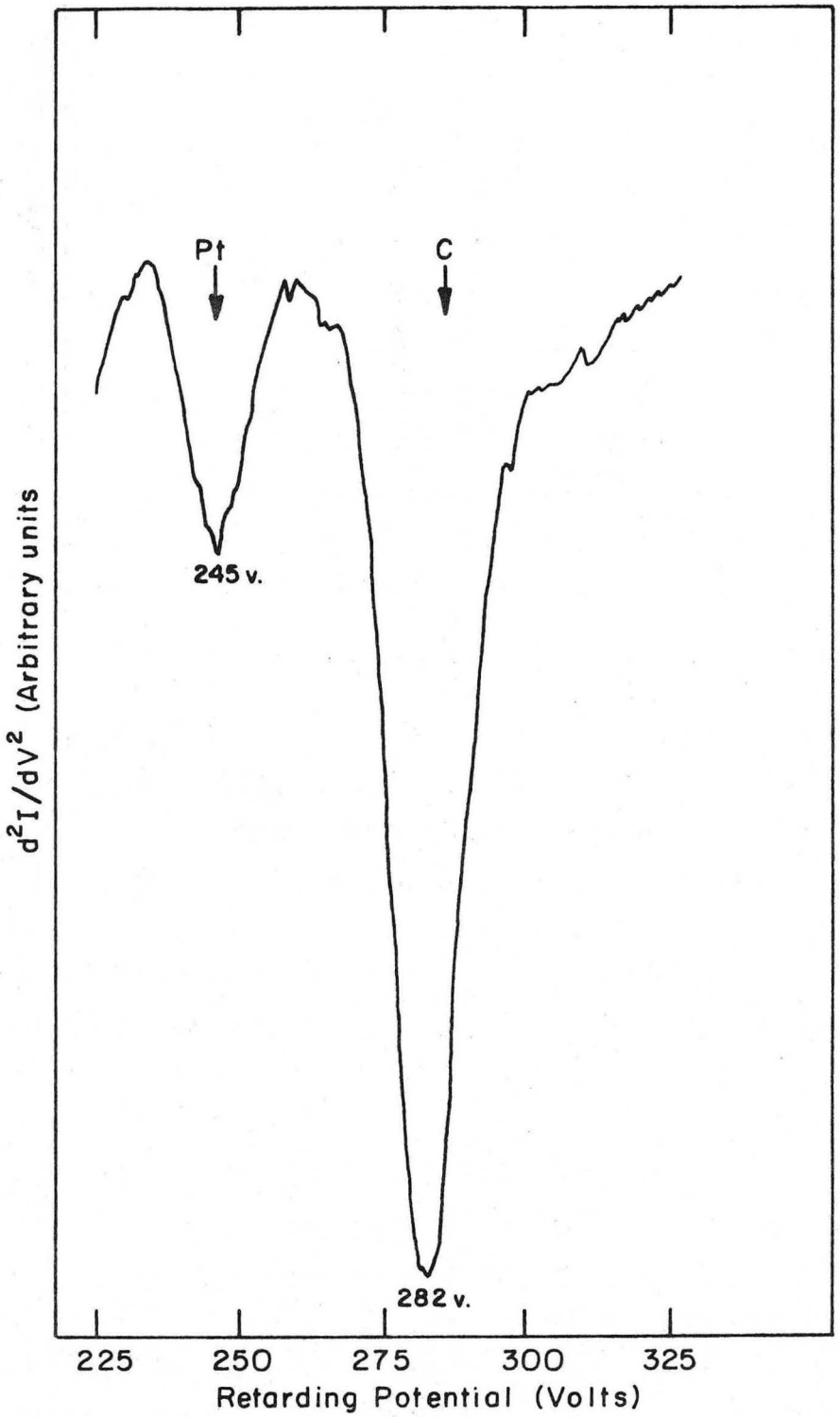

Fig. IV-6. Auger spectrum of the surface yielding the Pt(100)-(1×1) diffraction pattern.

feature to note about Fig. IV-7b is that the helium scattering from this ordered surface is more intense and narrower than that shown in Fig. IV-5b. The peak maximum is greater than 2% of the incident beam, a value approximately half that observed for the clean surface.

C. Effect of Adsorbed Gases on Helium Atomic Beam Scattering

Now that we have explored the effects of the surface disorder and the effects of various ordered surface structures on the scattering of helium, we turn to an investigation of the effect of adsorbed gases on the nature of helium atom scattering. The scattering curve for helium from a layer of carbon monoxide that is adsorbed on the platinum surface is shown by the open circles in Fig. IV-8. As stated earlier CO forms several ordered structures on the (100) face of platinum and at the temperature of this experiment (300°K), CO molecules adsorbed in all three binding states should have been present. The (1×1) diffraction pattern of this surface was quite diffuse and the broad diffraction spots were barely distinguishable from the background. These conditions indicate a highly disordered chemisorbed surface layer and the helium scattering bears out this contention (Fig. IV-8). The intensity about the specular position is quite low (~ 0.3%) and there is a definite cosine contribution near the surface normal as shown in the open circles.

The weakly bound α-CO molecules can be desorbed by heating the crystal to 500°K, leaving only the more strongly bound β-CO.[106] A helium scattering distribution obtained in the presence of this tightly

0 0 0 0 3 6 0 5 5 2 7

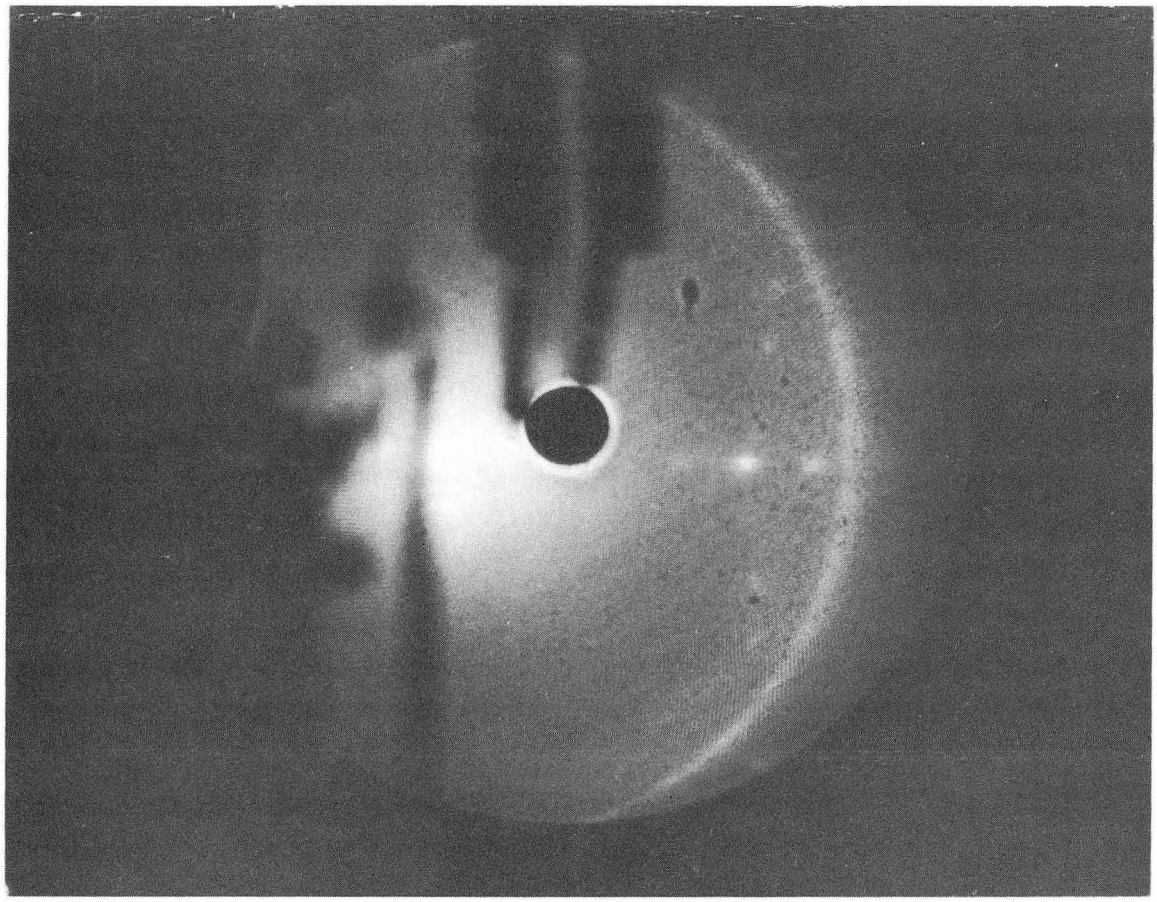

XBB 708-3755

Fig. IV-7a. Ring-like diffraction pattern due to randomly oriented islands of graphite on the Pt(100) surface.

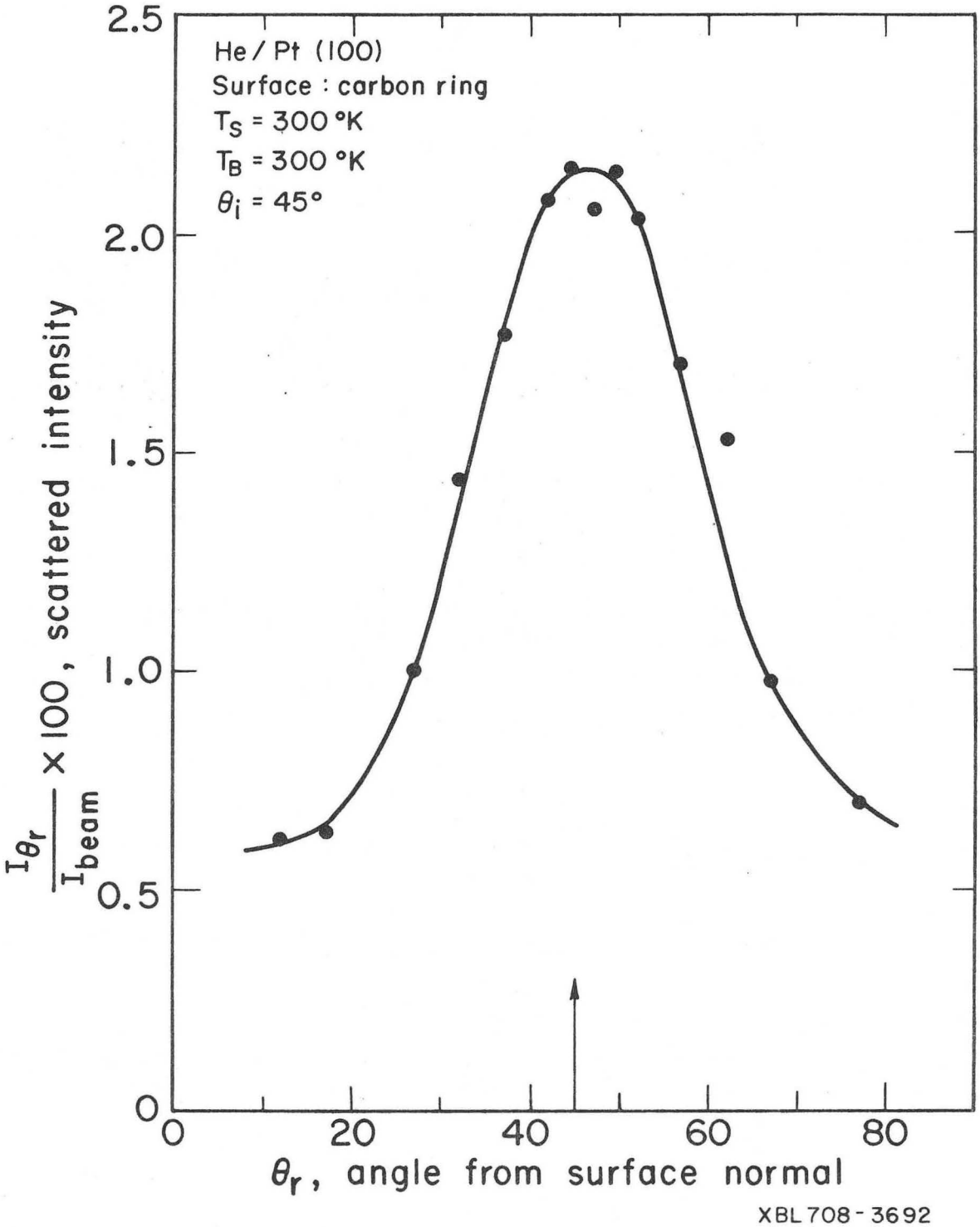

Fig. IV-7b. Helium beam scattering profile from the graphite surface structure shown in Fig. IV-7a. I_{beam} = incident beam intensity.

0 0 0 0 3 6 0 5 5 2 8

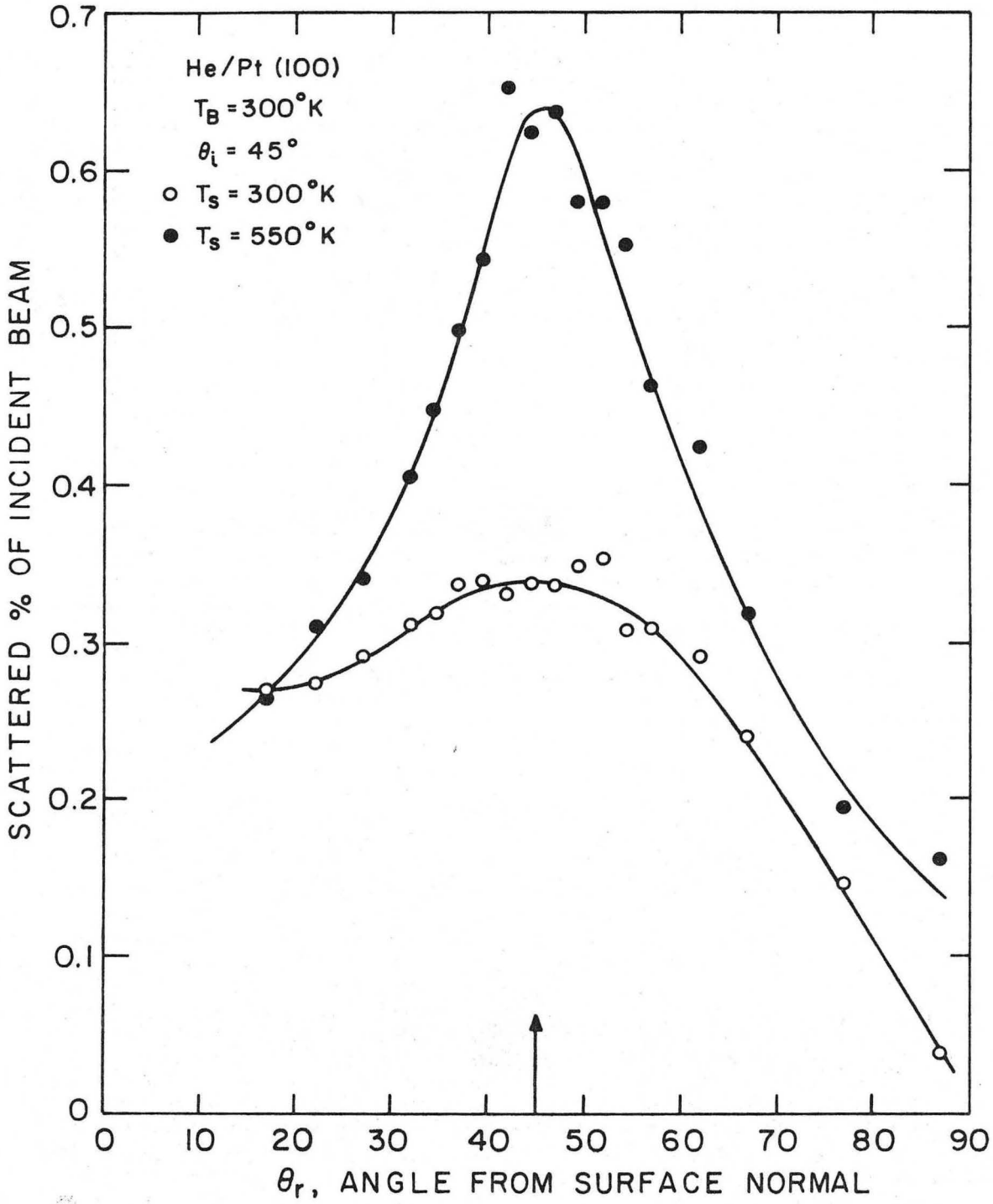

XBL 7010-6786

Fig. IV-8. Helium beam scattering from a CO contaminated Pt(100) surface. The open circles show results in the presence of both α and β CO binding states. The filled circles indicate data taken after desorbing the CO from the α binding state.

bound species is shown by the filled circles in Fig. IV-8. Note the striking increase of nearly a factor of two in the scattering efficiency of the surface and the near symmetry of the peak.

Acetylene, when chemisorbed on the Pt(100) surface gives rise to a c(2×2) diffraction pattern indicative of 50% surface coverage. The diffraction spots are well defined but broad (Fig. IV-9a) and the high background intensity reveals a great deal of surface disorder. In agreement with the work of Smith[154] who studied the adsorption of ethylene on Pt(111), the helium scattering curve is almost cosine in nature. The specularly directed intensity is Fig. IV-9b is low (~ 0.5%) and the intensity peak broad. Such behavior is to be expected as the result of momentum transfer for the scattering of helium from light weight atomic species that are not rigidly bound to the solid.

D. Effect of Surface Temperature on Scattered Helium Intensity

Variation in the surface temperature in order to probe the intensity-temperature relationship has been difficult to achieve in scattering studies employing epitaxial thin films because of the possible changes in surface roughness (sintering) and surface orientation with surface temperature. Similarly, beam scattering experiments in non-UHV systems are restricted to elevated temperatures on account of the contamination problem. Thus it was of interest to measure the surface temperature dependence of the scattered helium intensity and dispersion. The results are tabulated in Table IV.1 for the temperature range 450 to 1300°K. It can be seen that while there is a decrease

0 0 0 0 3 6 0 3 3 2 9

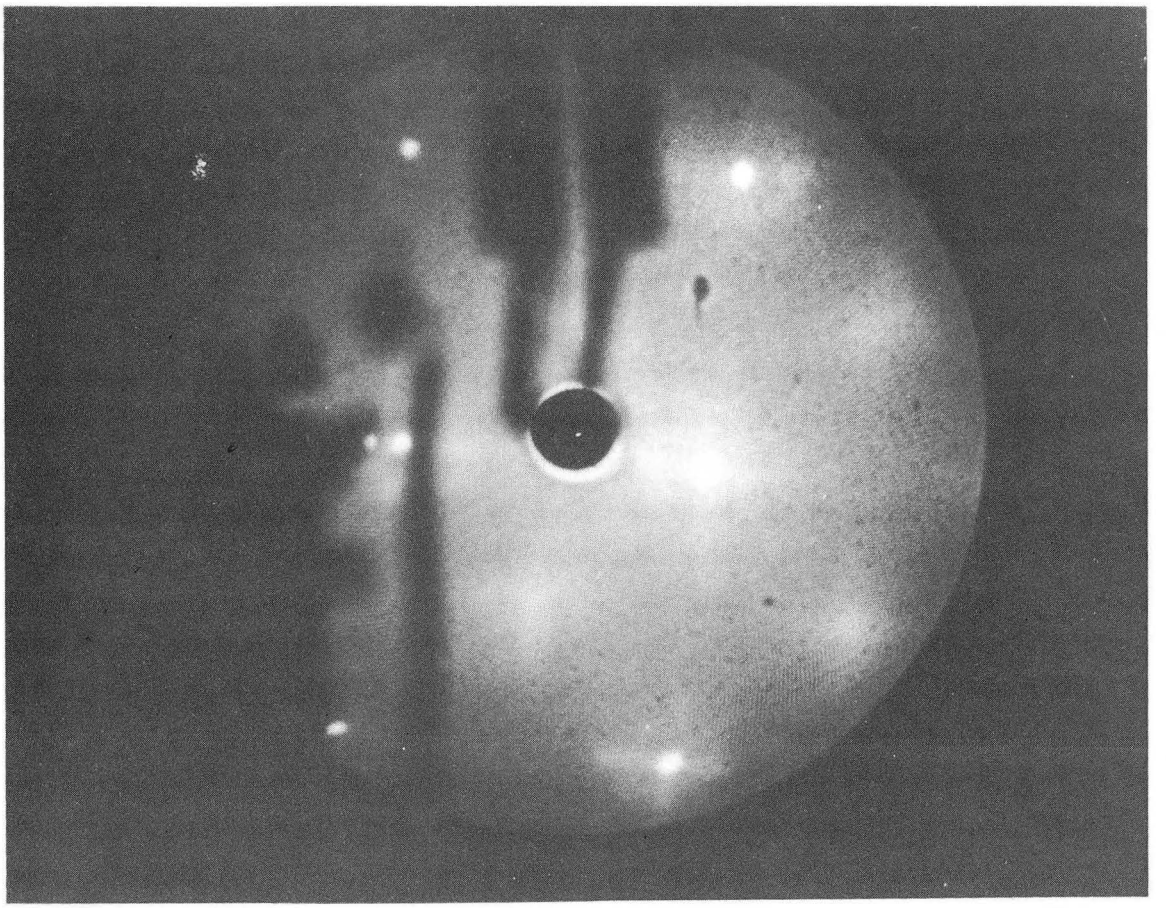

XBB 708-3753

Fig. IV-9a. Pt(100)-c(2×2)-C_2H_2 diffraction pattern, V = 63 volts.

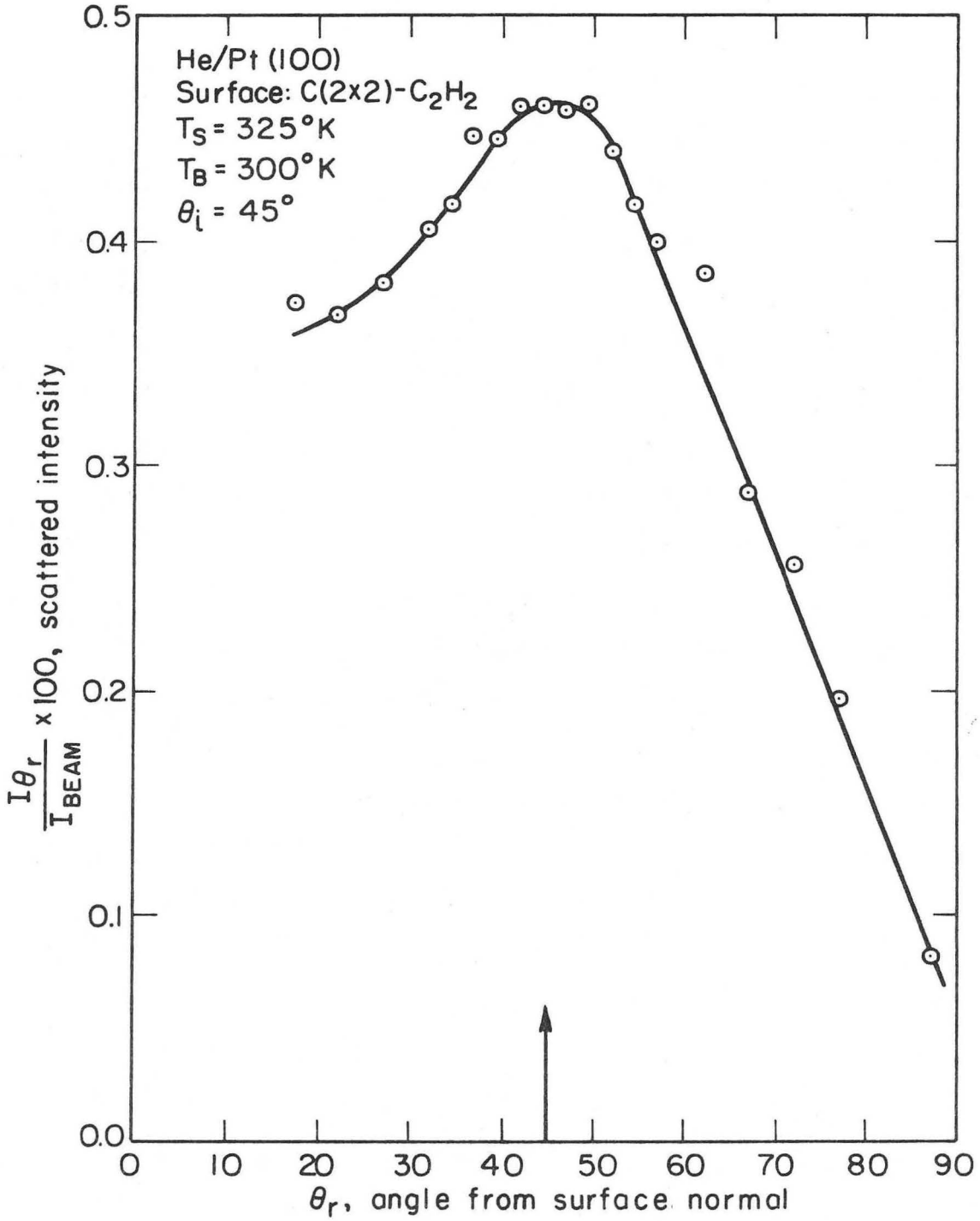

XBL 708-1972

Fig. IV-9b. Helium beam scattering profile from a Pt(100) surface covered with chemisorbed acetylene and yielding the diffraction pattern shown in Fig. IV-9a. I_{beam} = incident beam intensity.

Table IV.1. Temperature variation of intensity and dispersion of a helium beam scattered in the specular direction (θ_i = angle of incidence).

θ_i	Surface Temperature (°K)	Scattering Intensity (%)	Dispersion (FWHM) (degrees)
45°	450	4.72	18
45°	900	2.05	40
45°	1125	2.32	33
45°	1200	2.22	33
45°	1275	2.15	35

in the scattered intensity with increasing surface temperature, this decrease in the scattering efficiency of the surface is not monotonic as one would expect due to thermal vibrations of surface atoms. The minimum observed at 900°K is very reproducible and is probably due to the adsorption of CO into the β binding state on the (100) face of platinum during the course of the experiment.

E. Scattering of Other Monatomic Gases

Only a few experiments were conducted with rare gases other than helium. Some early runs were made with xenon but were discontinued because (1) the high through-put of the beam source made such experiments very costly, and (2) the scattered intensities were very low ($\lesssim$ 0.5%). Figure IV-10 shows the results of an experimental run in which argon was scattered from the clean surface. This curve is more disperse and lower in intensity than those observed under the same circumstances for helium indicating that argon undergoes a stronger interaction with the surface as one might expect from its higher polarizability and larger heat of adsorption. The maximum intensity for this run is identical to that reported by Stoll, Smith and Merrill[124] for Ar scattering from a Pt(111) surface that was concurrently characterized by LEED. This observation, in contrast to the vastly different He scattering results obtained with the two surfaces, indicates that argon is a much less sensitive probe of the surface environment than is helium.

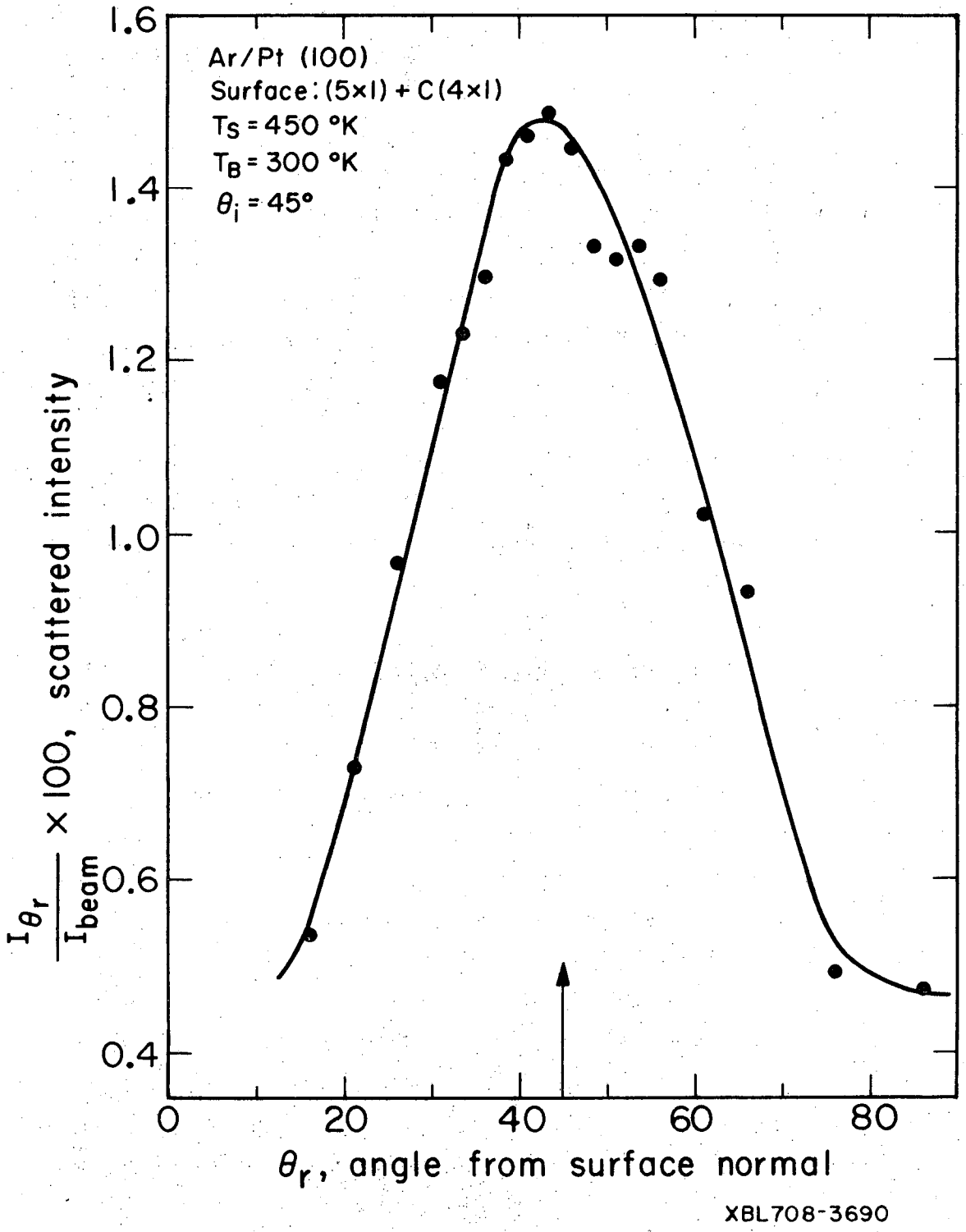

Fig. IV-10. Argon beam scattering from a clean Pt(100) surface. I_{beam} = incident beam intensity.

F. Discussion

We shall first consider the extent of agreement of the observations reported here with previously published work. Then we shall discuss the results of these studies and the conclusions that can be drawn.

From the data shown in Figs. 1, 2, 3b, 4c, 5b, 7b, 8, and 9b of this chapter, it is apparent that although the beam dispersion varies greatly, there is always a maximum in the helium scattering distribution at the specular angle for a (100) platinum single crystal surface in the range of gas and surface temperatures investigated. Similar findings have been reported for helium scattering on epitaxially grown single crystal films of Ag, Ni, and Au[52] and on single crystal surfaces of W[56,125] and Pt.[90,124]

Our results have also confirmed the great sensitivity of helium scattering to surface disorder. It appears that there is a qualitative correlation between the diffraction spot intensities of the LEED patterns and both the beam dispersion and the scattered beam intensity at the specular angle for helium atoms as observed by Smith.[154] The loss of diffraction features and the corresponding increase in background intensity coincide with the decrease in the scattering efficiency of the surface to below 1% of the incident beam.

A comparison of our helium scattering from the (100) face of platinum with the results obtained by Datz, Moore, and Taylor,[53] and those of Hinchen and Foley[54] using polycrystalline platinum targets reveals certain discrepancies. Both studies yielded cosine-like distributions for scattering from surfaces at 300°K. This would

certainly be expected if the platinum surfaces were covered by a disordered layer of low molecular weight gas (viz. Fig. IV-8). The scattered intensity observed by these investigators at higher temperatures (> 500°K) however was predominantly backscattered (i.e., the peaks were located between the specular angle and the surface normal). More recent observations of helium scattering on a variety of clean single crystal surfaces,[13,41, 51, 52, 56, 90, 124-127] as well as our own observations for the (100) face of platinum, indicate that the scattered helium peak does not deviate from the specular position as the surface temperature is raised. As has been shown in this chapter, surface contamination reduces scattered intensity and increases the dispersion of the scattered beam but it does <u>not</u> shift the scattered beam maximum in the case of helium. Consequently, contamination, even by species diffusing from the bulk, cannot account for the observation. One possible reason for this discrepancy lies in the different topography of the single crystal and polycrystalline surfaces. Experiments conducted during the epitaxial growth of a (111) Au film[13] (in order to maintain a clean surface) have shown that helium scattering from polycrystalline surfaces tends to be somewhat backscattered and is much broader than from a monocrystalline surface of the same material. The presence of grain boundaries, differences in step heights, and dislocation and point defect densities may markedly affect the scattered intensity distribution from polycrystalline surfaces. Unfortunately, no temperature-dependence studies of helium scattering from clean

polycrystalline surfaces have yet been reported, so we cannot check our contention that the local microscopic topography of the surface is responsible for the observed angular deviation with temperature.

Our studies indicate that while the scattered helium beam may be useful for monitoring surface disorder, it cannot distinguish well between ordered surface structures of different kinds. No diffraction features were observed in the plane of incidence for incident angles between 45° and 60°, and no exhaustive search of the out of plane region was conducted. If atomically rough surfaces cause diffraction of helium beams as suggested by the work of Tendulkar and Stickney,[48] then a surface yielding the (5×1) diffraction pattern might also be expected to diffract, especially when the beam strikes the crystal within 5° of the ⟨100⟩ direction as in this work (see Fig. IV-3a). Observed diffraction beams, however, are very narrow[47,48] and our detector may simply have integrated out the effects of any sharp, extra features in the scattering distributions. Because the intensity maxima for scattering from the (5×1) and $(\sqrt{2} \times 2\sqrt{2})$R-45° structures were nearly of identical magnitude, the helium beam seems relatively insensitive to the periodicity of the scattering lattice. The clean platinum surface and the graphitic carbon surface, however, yielded scattered maxima that differed in intensity by a factor of two. This is largely due to the different atomic masses of platinum and carbon (a mass ratio effect with the helium), because a calculation of the relative helium scattering intensities from platinum and graphite surfaces using the hard cube model[87,88] gives roughly a factor-of-3

difference, even though the predicted angle of maximum intensity is incorrect. Thus, while the scattered intensity of the helium beam is slightly sensitive to the chemical nature of the scattering surface, it is probably not selective enough to be experimentally useful because the scattered intensities from the (100) surface are too weak. The real test of this contention is to compare in the same apparatus the scattering intensities from (100), (110), and (111) surfaces prepared under identical conditions.

The temperature dependence of the scattered helium distribution shows a decrease in the maximum intensity of more than fifty percent with increasing temperature in the range of 450°K to 1300°K. Due to increasing thermal disorder with increasing surface temperature, one would expect a monotonic decrease in the specular intensity. The deviation at 900°K from the expected fall off is probably due to the adsorption of the β binding state of CO from the ambient atmosphere. As we stated earlier, this species desorbs near 880°K and the small temperature difference is probably not enough to prevent the gradual readsorption of the gas. Above 900°K, the peak shapes and dispersion were remarkably similar.

We have observed a <u>decrease</u> in the scattered helium dispersion upon ordering of surface carbon. On the (100) surface there appears to be a slight decrease (40° → 30°) in the half-width in going to the ordered surface as would be predicted by our earlier arguments concerning dispersion and surface order. Merrill and Smith[128] however have reported a drastic increase in the half width (18° → 40°) in

going from the amorphous to the ordered carbon surface structure on a platinum (111) surface. These differences in the dispersion of the scattered beams from the two platinum surfaces may be due to the inherent differences in the atomic structure of the two crystal planes.

Finally let us consider the differences in the observed half-widths of the helium scattering distributions. On the (111) faces of the face-centered cubic metals studied to date, the observed scattered helium peak half-widths increase in the order Ni[52] > Pt[90] > Ag[52] > Au[52] which parallels the increase in the Debye temperatures of these solids. Smith and Merrill[90] have reported half-widths for helium as small as 8° on the (111) face of platinum. We note that LEED studies of the clean (111) faces of these metals have shown that they do not readily undergo structural rearrangements (reconstruction). The (5×1) surface structure on the (100) face of platinum may, however, represent a rearranged surface with respect to the bulk-like (1×1) unit mesh. There would then be a periodic "buckling" of the surface plane[129] resulting in increased surface roughness which, according to data presented earlier, would yield broadened scattering peaks. A (111) overlayer seems unlikely, though, in view of the intense specularly directed scattering (~ 25%) observed with that surface[90] compared to the ~ 5% maximum intensity measured with a Pt(100)-(5×1) surface.

Yamamoto and Stickney recently reported on rare gas scattering from a W(110) surface and they found surprisingly broad half-widths (~ 30°) for helium scattering. Their crystal was cleaned by oxidizing the carbon impurities in 2×10^{-7} torr of oxygen at 1300°K with

occasional flashes to 2000°K. Germer and May,[130] in studies conducted between 3×10^{-10} and 3×10^{-7} torr of oxygen, have postulated that oxygen atoms are adsorbed into the tungsten lattice by interchange with the W atoms along alternate rows in the surface layer (surface reconstruction). Subsequent heating to temperatures up to 2000°K produces the evaporation of WO_3 and its polymers.[131-133] If this treatment were to leave a rather rough surface that did not have sufficient time to anneal out due to continued reaction with background oxygen ($P_{O2} \sim 5 \times 10^{-10}$ torr), the presence of such a rough surface could possibly account for the observed half-widths. Such a rough surface is even more likely in view of the recent work of Weinberg[125] who reports 10-12° half-widths for helium scattering from a (110) single crystal tungsten surface characterized by LEED.

The only other reported case of scattering from a (100) surface is from an epitaxial thin film of silver grown on a LiF substrate.[134] For this surface, the authors show a scattered peak with a half-width of approximately 15°, a value similar to that we observe with platinum. Using ball models, a comparison of the (100) and (111) planes of a fcc solid shows that the former is somewhat rougher than the latter. Since the helium atom is small and it penetrates deeply into the repulsive part of the interaction potential, the different microscopic surface geometry experienced during its trajectory may induce the broader scattering observed with the (100) surface.

V. SCATTERING OF POLYATOMIC GASES

A. Introduction

While there is still much to be learned about the detailed mechanisms of various gas-solid interactions by scattering rare gas beams from well-characterized surfaces, the molecular beam technique also appears to be an ideal tool to investigate the processes taking place during surface chemical reactions. Experiments with crossed molecular beams have long been used to probe the elementary steps of gas phase reactions[3-5] and a similar approach to the problems of surface chemistry should yield much valuable information. Theoretically, such studies can be used to obtain the angular distribution of the scattered gas particles and reaction products, the partition of interaction energy among translational, vibrational, and rotational modes, the surface residence time, and the reaction probability as a function of surface and gas temperatures. As pointed out in the first chapter, very little work of this type have been carried out to date. The work described in this chapter was undertaken to lay a foundation upon which future investigations might be based.

Before we proceed to discuss the data, however, let us first examine the magnitude of the energy and time scales important to the processes that concern us. In the incident molecular beam, the gas pressure is so low that the particles behave independently. Hence, their internal energy states are determined by the conditions at their point of origin and are subject only to unimolecular relaxation

processes. The internal motions of an individual molecule, though, can be markedly affected by a collision with the surface. By summing the energies associated with translational (T), rotational (R), vibrational (V), and electronic (E) modes of excitation, a good approximation to the total energy E_{tot} of the molecule may be obtained.

$$E_{tot} = E_T + E_R + E_V + E_E \qquad \text{(V-1)}$$

For a particle of mass m contained in a box of side S, the translational energy levels are given by[135]

$$E_T = \frac{h^2(n_1^{\,2} + n_2^{\,2} + n_3^{\,2})}{8m\,S^2} \qquad \text{(V-2a)}$$

where h is Planck's constant and the $n_i = 1,2,3...$ are integers. Taking nitrogen as a representative molecule in a box of macroscopic size (1 cm), we find that the level separation is

$$\Delta E_T = 7.5 \times 10^{-20}\ \text{eV} \qquad \text{(V-2b)}$$

It can be shown[135] that the rotational and vibrational energies for a rigid rotor and a harmonic oscillator are given, respectively, by

$$E_R = J(J+1)\hbar\omega_R \qquad \text{(V-3a)}$$

$$E_V = (n_V + \tfrac{1}{2})\hbar\omega_V \qquad \text{(V-4a)}$$

where $J = 0,1,2,\ldots$ and $n_V = 0,1,2,\ldots$ are the rotational and vibrational quantum numbers, respectively, and ω_R, ω_V are the corresponding angular frequencies. The latter quantities may be obtained from Table V.2 and the relationship

$$\omega_{R,V} = \frac{k\,\theta_{R,V}}{\hbar} \qquad \text{(V-5)}$$

where k is Boltzmann's constant. Substituting the appropriate values for nitrogen yields

$$\Delta E_R = 1.5 \times 10^{-3}\ \text{eV} \qquad \text{(V-3b)}$$

$$\Delta E_V = 0.15\ \text{eV} \qquad \text{(V-4b)}$$

Clearly the rotational and vibrational levels are spaced successively further apart. While many rotational levels are occupied, few molecules are above the lowest vibrational state. The relative population of these different states at equilibrium is simply given by the Boltzmann factor[135]

$$\frac{N_i}{N_j} = \exp -\left(\frac{\Delta E_{i \leftarrow j}}{kT}\right) \qquad \text{(V-6)}$$

Table V.1 shows the number of molecules in the first vibrational state compared to those in the ground state for several diatomic molecules. Even at 1000°K this fraction is small for such gases as H_2, CO, and N_2.

Table V.1. Relative occupation of vibrational energy levels at equilibrium

Gas	Fraction of molecules in first vibrational state compared to ground state	
	T = 300°K	T = 1000°K
H_2	2.16×10^{-9}	2.51×10^{-3}
N_2	1.40×10^{-5}	3.50×10^{-2}
CO	3.43×10^{-5}	4.58×10^{-2}
O_2	5.74×10^{-4}	1.07×10^{-1}
I_2	3.60×10^{-1}	7.36×10^{-1}

In the case of nitrogen the energy difference between the ground and first excited state is

$$\Delta E_E = 8.6 \text{ eV} \qquad \text{(V-7)}$$

and while this is somewhat high, it is still a typical value and demonstrates that essentially all molecules are in their lowest electronic state. Tables V.2 and V.3 list some relevant parameters for the gases of interest to this thesis and compare energy level spacings for rotational and vibrational transitions to the energy of the maximum Debye phonon

$$E_{phonon} = k\,\theta_D^s \qquad \text{(V-8)}$$

where θ_D^s is the surface Debye temperature obtained from LEED experiments. The reason for this comparison is that the optimal coupling (and thus maximum energy transfer) between the gas and the solid occurs when there is a near resonance between the surface modes and a vibrational or rotational mode of the gas.

The reaction of hydrogen and oxygen to form liquid water is a very exothermic, but common, chemical reaction:

Table V.2. Rotational, vibrational, and electronic energy level spacings of selected diatomic molecules*

Gas	θ_R(°K)	θ_V(K°)	ΔE_E(eV)	D_o^o (eV)	$\frac{\Delta E_R}{E_{phonon}}$	$\frac{\Delta E_V}{E_{phonon}}$
H_2	87.46	6322.3	11.431	4.476	4.77 j = 2→0 7.95 j = 3→1	57.48
HD	65.67	5490.7	11.433	4.511	1.19 j = 1→0 2.39 j = 2→1	49.92
D_2	43.77	4485.8	11.432	4.554	2.39 j = 2→0 3.98 j = 3→1	40.78
N_2	2.89	3394.2	8.638	9.756	0.16 j = 2→0 0.37 j = 3→1	30.86
CO	2.78	3121.7	8.113	11.108	0.51 j = 1→0 0.10 j = 2→1	28.38
CN	2.73	2975.7	1.152	7.6	0.50 j = 1→0 0.99 j = 2→1	27.05
NO	2.45	2738.3	0.015	5.296	0.45 j = 1→0 0.89 j = 2→1	24.90
O_2	2.08	2273.8	0.987	5.080	0.11 j = 2→0 0.26 j = 4→2	20.67

* Values listed were obtained from those reported in Ref 136 by multiplying by hc/k to convert cm^{-1} to °K. Note that $E_{phonon} = k\,\theta_D^s$, where θ_D^s = 110°K for platinum.[105] The bulk Debye temperature of platinum is 234°K.

Table V.3. Vibrational and electronic energy level spacings for some polyatomic molecules*

Gas	θ_1(°K)	θ_2(°K)	θ_3(°K)	θ_4(°K)	θ_5(°K)	ΔE_e(eV)	D_o^o (eV)
CO_2	1996.8	960.0	3379.2	-	-	5.735	D(O-CO) = 5.433
N_2O	321.9	846.9	1848.3	-	-	4.068	$D(N_2-O)$ = 1.677 D(N-NO) = 4.930
NO_2	1898.3	1078.6	2327.1	-	-	1.870	D(O-NO) = 3.115 $D(N-O_2)$ = 4.056
NH_3	4799.0	1341.4	4953.4	2339.1	-	5.751	$D(H-NH_2)$ = 4.38
C_2H_2	4851.1	2838.8	4739.5	879.9	1048.9	5.261	$D(H_2C_2-H)$ = 4.9 D(HC-CH) = 9.886
C_2N_2	3351.4	1228.7	3103.9	729.3	335.3	4.150	D(NC-CN) = 6.261
N_2O_4	-	-	-	-	-	-	$D(O_2N-NO_2)$ = 0.594

* Obtained from values listed in Ref. 137 by multiplying by hc/k to convert cm^{-1} to °K.

$$H_2(g) + \frac{1}{2} O_2(g) \rightarrow H_2O(\ell) \quad \Delta H^\circ_{298} = -68.3 \text{ kcal} = -2.97 \text{ eV} \qquad \text{(V-9)}$$

One can see that the release of almost 3 eV provides enough energy to induce transitions in vibrational if not electronic states. Fortunately most chemical reactions are less exothermic than this and thus one can usually disregard possible electronic excitation of the product species except in a few special cases. Thermal energies on the other hand are very much smaller, $\frac{3}{2}$ kT = 0.039 eV at 300°K, so that even vibrational transitions become highly unlikely. Generally speaking, all species except the hydrogenic molecules are fully rotationally excited and consequently energy transfer into rotational modes would be difficult to detect. (We note in passing, however, that Saltsburg and his coworkers[127,138] have observed the effect on the angular scattering distributions of energy transfer into the rotational modes of H_2, HD, and D_2 produced by collisions with the surface.) Because the translational energy levels are extremely close together and for practical purposes continuous, a molecule can easily lose or gain energy through this mode. In principle changes in the mean velocity of the scattered beam (due to partial thermal accommodation and/or phonon interactions with the surface) as small as a few percent of the average speed should be detectable. For ΔV = 1000 cm/sec, this corresponds roughly to $\Delta E \sim 3 \times 10^{-5}$ eV for nitrogen or a small fraction of thermal energies. Whether such fine resolution will be achieved depends upon solving the incumbent experimental difficulties.

So far we have only indicated the energies involved in possible transitions, but what about the associated time scales? While the gas-phase transfer of energy via $E \rightarrow E$, $E \rightarrow V$, $E \rightarrow R$, $E \rightarrow T$, $V \rightarrow V$, $V \rightarrow R$, $V \rightarrow T$, $R \rightarrow R$, $R \rightarrow T$, and $T \rightarrow T$ relaxation modes has been studied,[139] excitation and de-excitation during two phase collisions have received much less attention. Our experiments involve energy exchange of both types.

Once the gas beam is formed, particles in the rarefied stream travel free of external interactions for $\sim 10^{-3}$ seconds before striking the target surface. Following a collision whose duration may vary from one to many surface vibrational periods, the molecule spends an additional $\sim 10^{-4}$ seconds in a collisionless state before reaching the detector. In its flight time on either side of the crystal, the molecule can undergo only pure intramolecular relaxation processes (i.e., spontaneous emission), but, during the collision, energy may be exchanged between the gas and the solid. This latter process is called thermal accommodation and was first treated by Knudsen.[140] The thermal accommodation coefficient is usually defined by

$$\alpha = \frac{E_i - E_r}{E_i - E_s} \qquad \text{(V-10a)}$$

where E_i is the energy of the incident molecules, E_s is the energy the gas molecules would have if they were in equilibrium with the solid, and E_r is the energy of the reflected molecules. For a Boltzmann distribution these energies are given by $E_i = 2kT_iN$ where N is the

number of molecules striking with the surface per second. Thus we obtain

$$\alpha = \frac{T_i - T_r}{T_i - T_s} \qquad \text{(V-10b)}$$

In the case of polyatomic gases, one can define two accommodation coefficients — α_T associated with translational energy exchange and α_I associated with internal energy exchange. Feuer[141] has shown that the translational and rotational accommodation coefficients are not in general equal and that for surface temperatures in excess of incident gas temperatures, "those transitions are favored in which there is a loss of energy from the solid to the gas molecules." Additionally, there are experimental indications that α_I can be considerably smaller than α_T.[142-146] Calculations by Hunter[147] concerning vibrational energy transfer at gas-solid interfaces have demonstrated that the probability of vibrational deactivation during specular reflection, i.e., collision lasting $\sim 10^{-13}$ seconds, is small (less than 2% for CO_2 and N_2O on NaCl) but that the probability is near unity when the molecule is adsorbed for 10^{-9} to 10^{-10} seconds. Since the typical period of a single surface atom vibration is about 10^{-12} seconds, this corresponds to 100-1000 collisions.

Table V.4 lists some representative gas-phase relaxation times. Under STP conditions there are $\sim 10^9$ collisions per second and the number of collisions required to produce a desired relaxation process is normally given by the product of the relaxation time and the number of kinetic collisions per second. For $V \rightarrow V$ transitions this number is

Table V.4. Typical molecular relaxation times[139]

Process	Collisional relaxation (gas phase at STP) (sec)	Spontaneous Relaxation (sec)
E → E	10^{-6} - 10^{-8}	10^{-7}*, 10^{-4}†
V → V	10^{-5} - 10^{-8}	0.1 - .05
V → T	10^{-5} - 10^{-6}	n.c.
R → R	10^{-8} - 10^{-10}	(long)
R → T	10^{-8}	n.c.
T → T	10^{-9}	n.c.

* electric dipole allowed

† electric quadrupole allowed

n.c. not characterized

10-10,000 which is the same value we deduced from Hunter's work. To deduce the rates for relaxation in a collision free state such as exists in the beam, we can use the Einstein A and B coefficients.[148]

$$A = \frac{8\pi h\nu^3}{c^3} \qquad \text{(V-11)}$$

where A is the probability of a spontaneous transition and B is the probability of an induced transition, both per unit time. In the dipole approximation, B is given by

$$B = \frac{2\pi}{3\hbar^2} |D|^2 \qquad \text{(V-12)}$$

where $|D|$ is the dipole matrix element whose magnitude may be approximated by the molecular dipole moment. Dipole moments range typically from 0.1 to 3 Debye units (1×10^{-18} e.s.u.-cm) so that a value of 1 Debye may be chosen as representative. For an electronic transitions of energy 5 eV, the corresponding frequency is $\nu = 1.2 \times 10^{15}$ sec^{-1} so that we can calculate

$$A = 2 \times 10^7 \text{ sec}^{-1} \qquad \text{(V-13)}$$

or the relaxation time is

$$\tau_E = A^{-1} = 5 \times 10^{-8} \text{ sec.} \qquad \text{(V-14)}$$

Other mechanisms such as magnetic dipole or electric quadrupole are operative in spontaneous emission if $|D| = 0$ and the relaxation

times can be much longer. We can use the same approach for estimating vibrational lifetimes. Again setting $|D| = 1$ Debye and using $\Delta E_V = .05$ eV or $\nu = 1.2 \times 10^{13}$ sec^{-1}, the spontaneous emission relaxation time is

$$\tau_V = 0.05 \text{ sec} \tag{V-15}$$

For practical purposes, spontaneous rotational relaxation will not occur because rotational frequencies are larger than vibrational frequencies by one or two orders of magnitude and consequently the relaxation times may be 10^3 to 10^6 times longer. Clearly for molecular beam experiments one does not need to consider internal relaxation of the beam species except in very special cases. Table V.4 can give us some idea about feasible energy exchange experiments.

Species vibrationally excited by their collision with the surface could live long enough to reach the detector, but some way would have to be found to distinguish them from unexcited molecules. From Tables V.2 and V.3 it is apparent that to occur, such an excitation would require either a multiphonon process (highly improbable) or a chemical reaction to provide the energy. It might be somewhat easier to study collisional quenching. A beam of molecules in an excited rotational or vibrational state could be impinged on the surface and then the scattering compared with the same experiment performed with ground state species. Again, however, there is the detector problem with which to contend. Photon detectors could be employed to study surface induced $E \rightarrow E$ transitions, but a molecule with a very long-lived excited

electronic state would need to be found. Probably the most exciting possibility is to measure the translational energy of the reflected particles as a function of angle. In this way one could probe the angular dependence of thermal accommodation, adsorption, and surface chemical reactions.

As with all preliminary investigations, though, one can rarely perform the ultimate experiment and learn everything on the first attempt. A basic apparatus must be assembled and proven before sophisticated changes are made to undertake more idealized studies. Consequently we restricted our attention to measuring the angular distribution of gases we felt were important to specific chemical reactions that were to be attempted. The following sections relate that data.

B. Non-Reactive Scattering Studies

When a polyatomic molecule collides with a surface it may exchange translational, rotational, or vibrational energy with the solid, or it may undergo a chemical reaction. Results descriptive of the former type of interaction are presented below.

1. Nitrogen and its Oxides

Figure V-1 portrays the scattering of nitrogen from the clean (100) surface of platinum. The overall intensity is lower than that for helium (1% vs. 5%) but we would expect this because nitrogen is a diatomic molecule, has a larger mass, and, as its ΔH_{ads} is larger, interacts more strongly with the substrate. In fact, the N_2 scattering

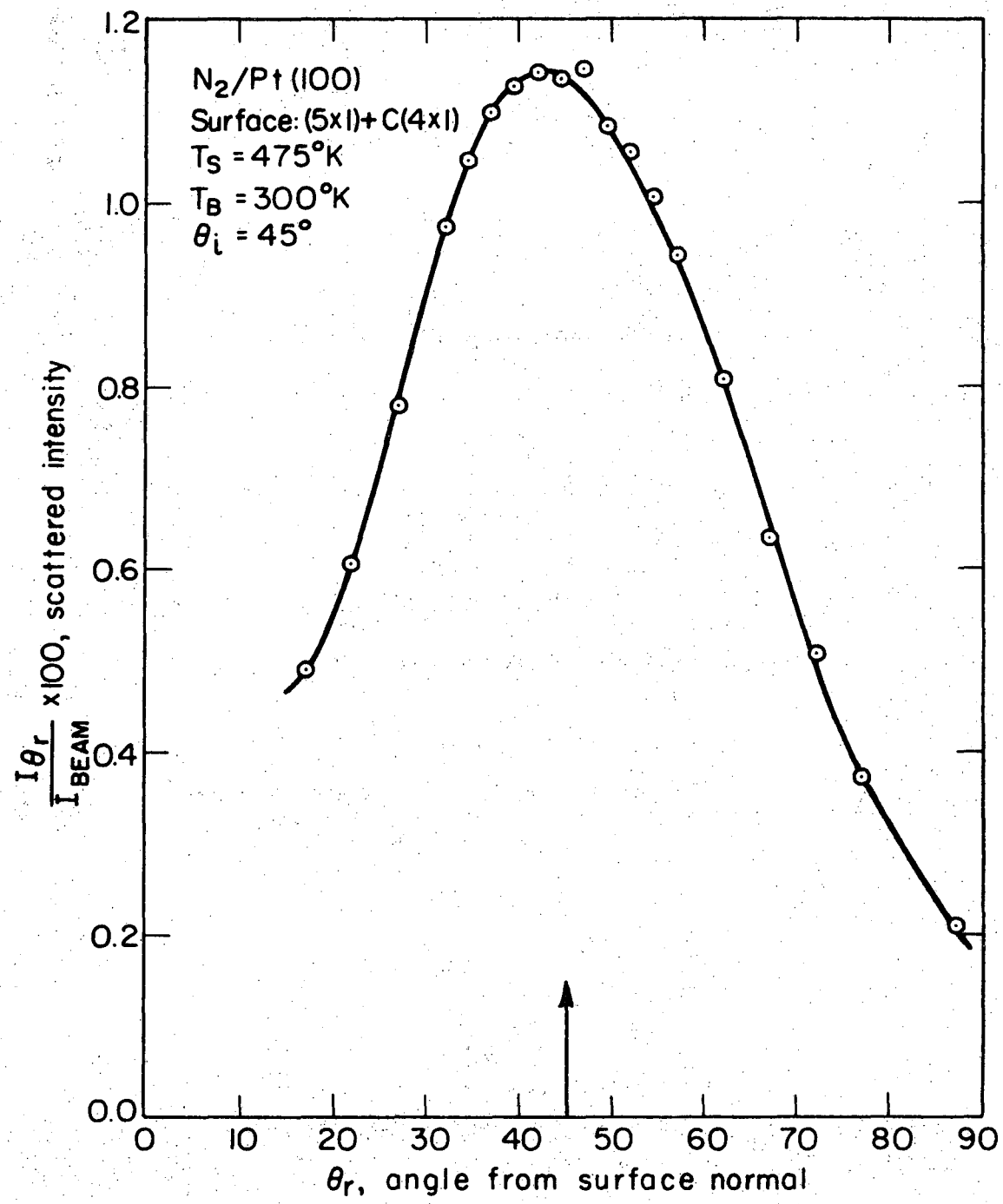

XBL 708-1965

Fig. V-1. Spatial distribution for a nitrogen beam scattered from a clean Pt(100) surface. I_{beam} = incident beam intensity.

compares favorably with that of argon which has a similar atomic mass. Scattering curves for nitric oxide (NO) are shown in Figs. V-2a and V-2b. The angle of incidence was 45° as in the previous experiment, but now the surface was much hotter than the gas and the peak maxima are backscattered, confirming Feuer's[141] hypothesis of energy transfer to a cold gas from a hot surface. Of course, from the hard cube picture and simple arguments concerning momentum transfer, we would also predict such backscattering. The two surfaces employed for the experiments were the clean (100) face (Fig. V-2a) and the carbon ring structure (Fig. V-2b). Evidently nitric oxide sees little difference in these surfaces as the overall peak intensities are similar.

In Figures V-3a and V-3b we show the scattering distributions for the linear triatomic molecule nitrous oxide. Again the peaks are slightly backscattered and the intensities of the two curves are similar, with that from the clean surface being somewhat higher. Finally, Fig. V-4 presents the results from the carbon covered platinum of scattering nitrogen dioxide, a bent triatomic molecule. While the peak intensity of this curve is lower than that for N_2O from a like surface, the maximum in the curve appears to fall in the same location. The paucity of points on this curve is due to the extremely corrosive nature of NO_2 and the strange effects it was having on the beam generating system.

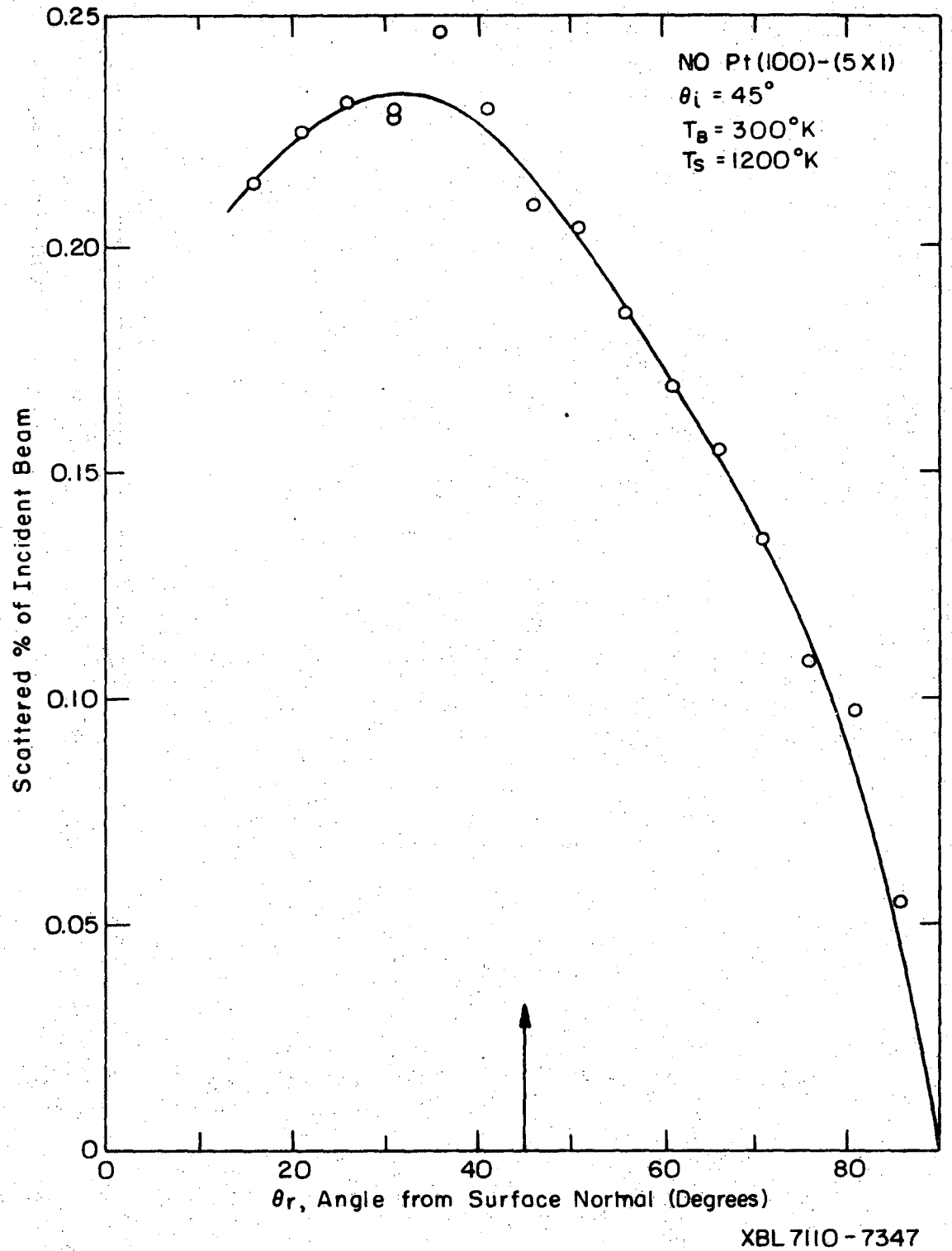

Fig. V-2a. Nitric oxide scattering distribution from a clean (100) platinum surface.

0 0 0 0 3 6 0 5 5 4 3

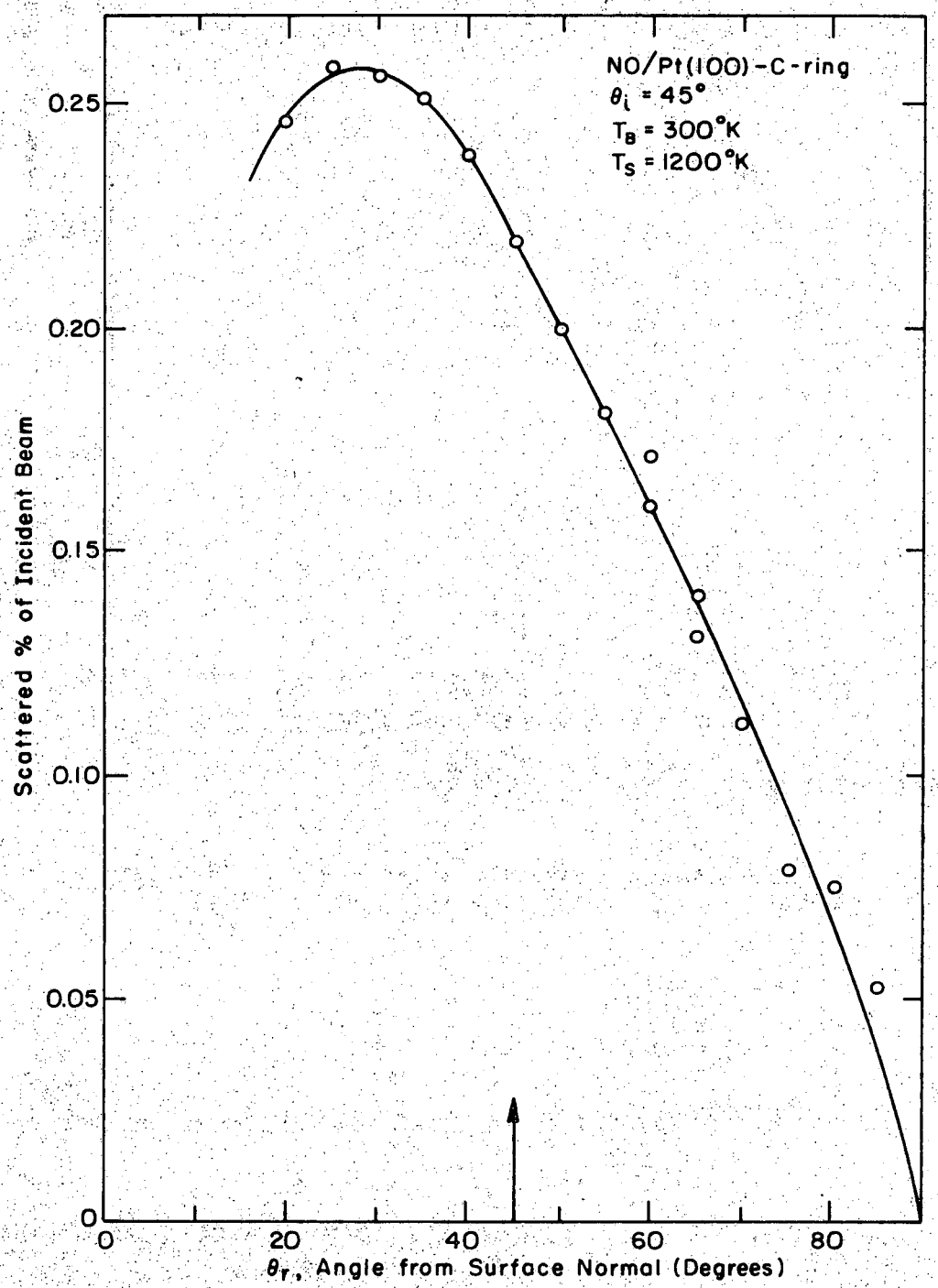

Fig. V-2b. Nitric oxide scattering distribution from a graphite overlayer on a (100) platinum surface.

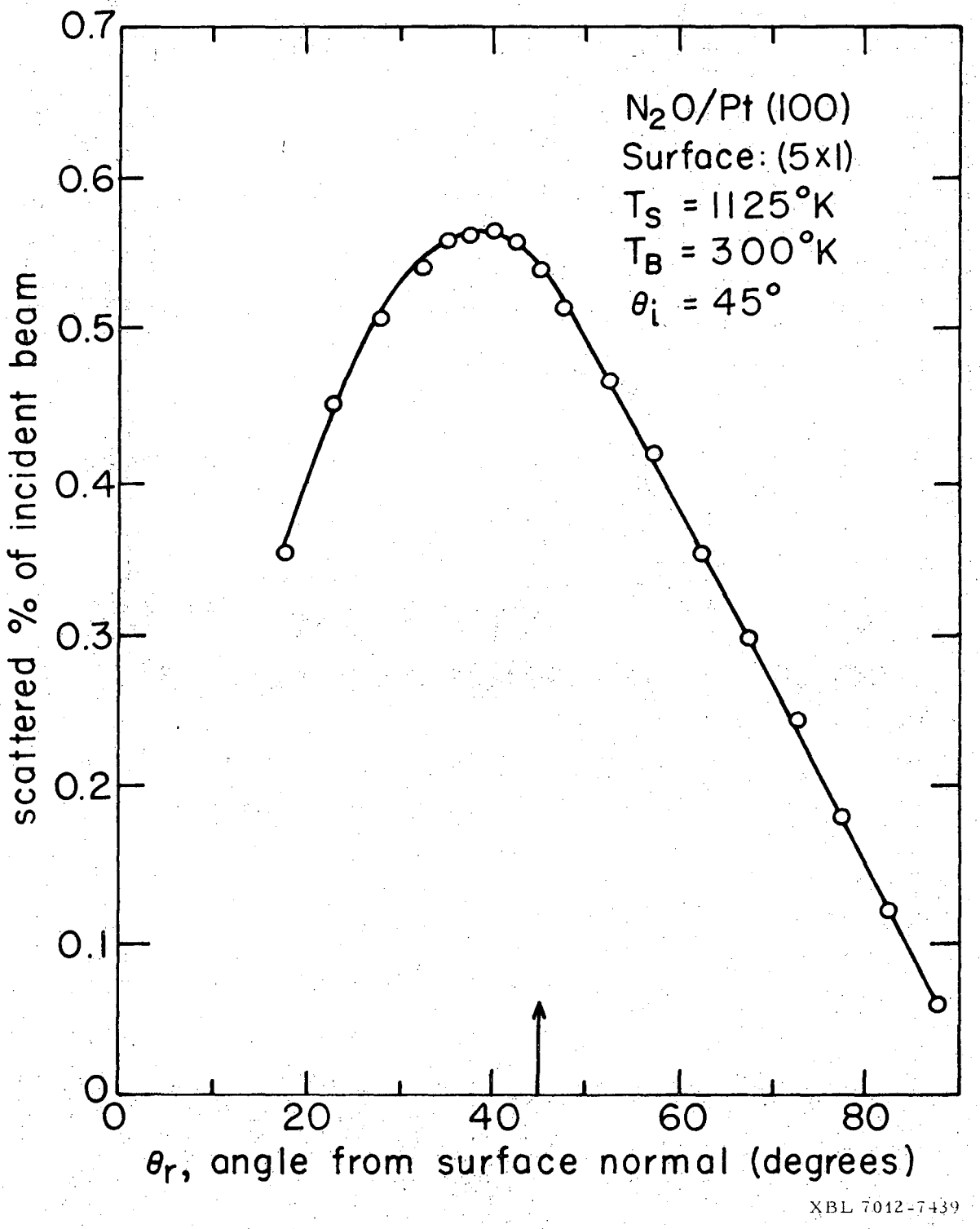

Fig. V-3a. Angular distribution of nitrous oxide scattered from a clean Pt(100) surface.

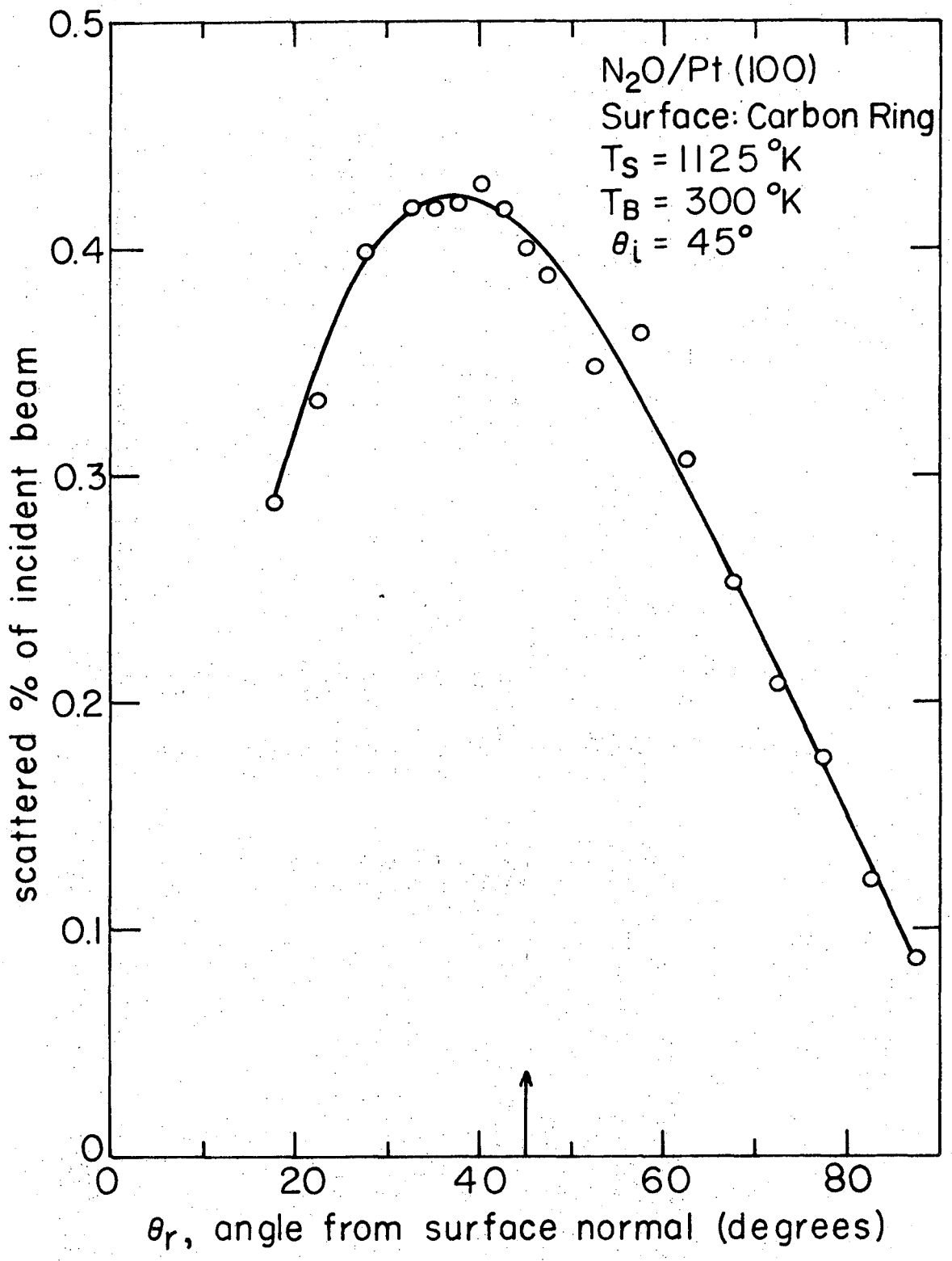

XBL 7012-7437

Fig. V-3b. Angular distribution of nitrous oxide scattered from a graphite overlayer on a Pt(100) surface.

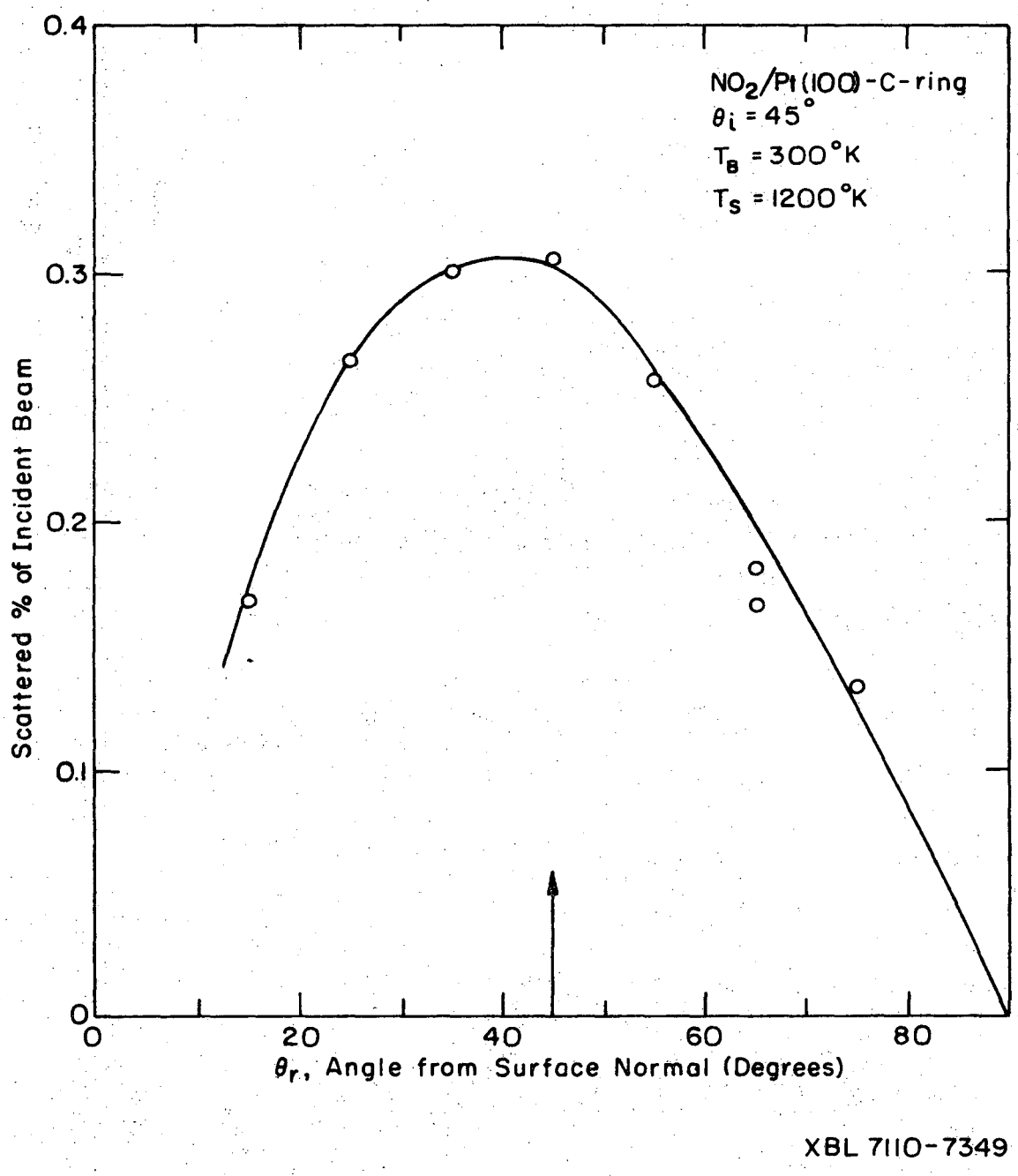

Fig. V-4. Nitrogen dioxide scattering pattern from a Pt(100) graphite surface.

2. Hydrocarbons, Carbon Dioxide, and Carbon Monoxide

Whenever unsaturated hydrocarbons were admitted to the clean Pt(100) surface, carbon deposits eventually formed, especially at elevated surface temperatures. Figures V-5 and V-6 show the scattering distributions for acetylene and methylenecyclobutane. The acetylene run was performed by flashing the crystal between data points to remove adsorbed acetylene. During the course of the run, a ring-like diffraction pattern developed. Note that the peak maximum represents only 0.5% of the incident beam. In the case of methylenecyclobutane, the surface was maintained hot to preclude the possibility of adsorption and, as before, a ring developed from the surface carbon. Error bars are included in this figure to give some idea of the noise level during the measurements.

Results for CO_2 scattering are presented in Fig. V-7. Within the accuracy of the data, the maximum in the angular distribution comes at the specular position. Like acetylene, carbon monoxide interacts strongly with the platinum substrate (See Chapter III-B). Figure V-8 gives the angular distribution for CO scattered from a surface flashed between points as above. The maximum intensity is very weak (~ 0.25%) and falls at the specular angle. This event is somewhat fortuitous as indicated by Fig. V-9 were scattering for an incident angle of 60° is shown. The difference in intensity between the two curves is probably due to the loss of particles in the first instance through absorption onto the clean surface because in the

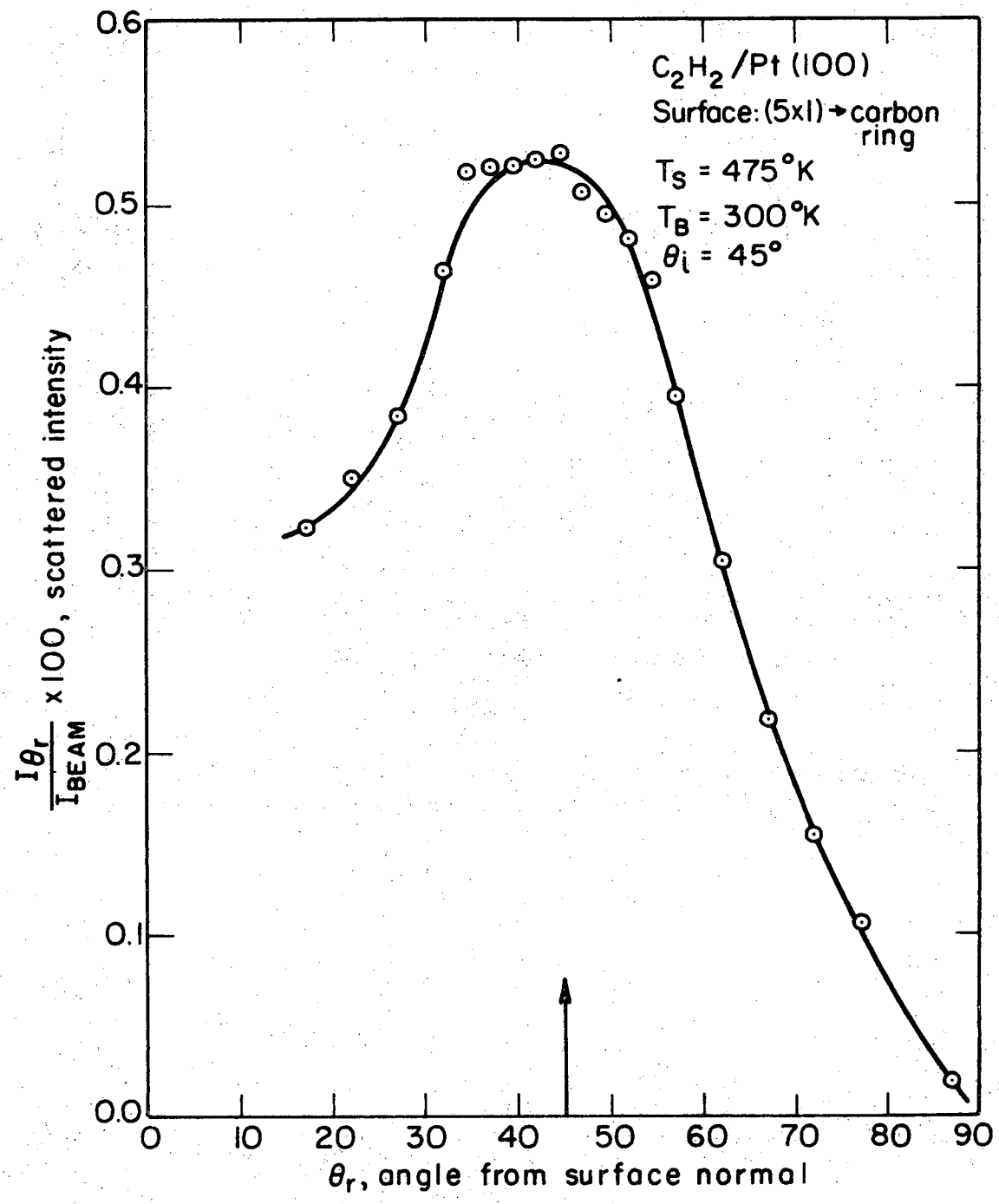

XBL 708-1968

Fig. V-5. Spatial distribution obtained by scattering acetylene from (100) platinum. I_{beam} = incident beam intensity.

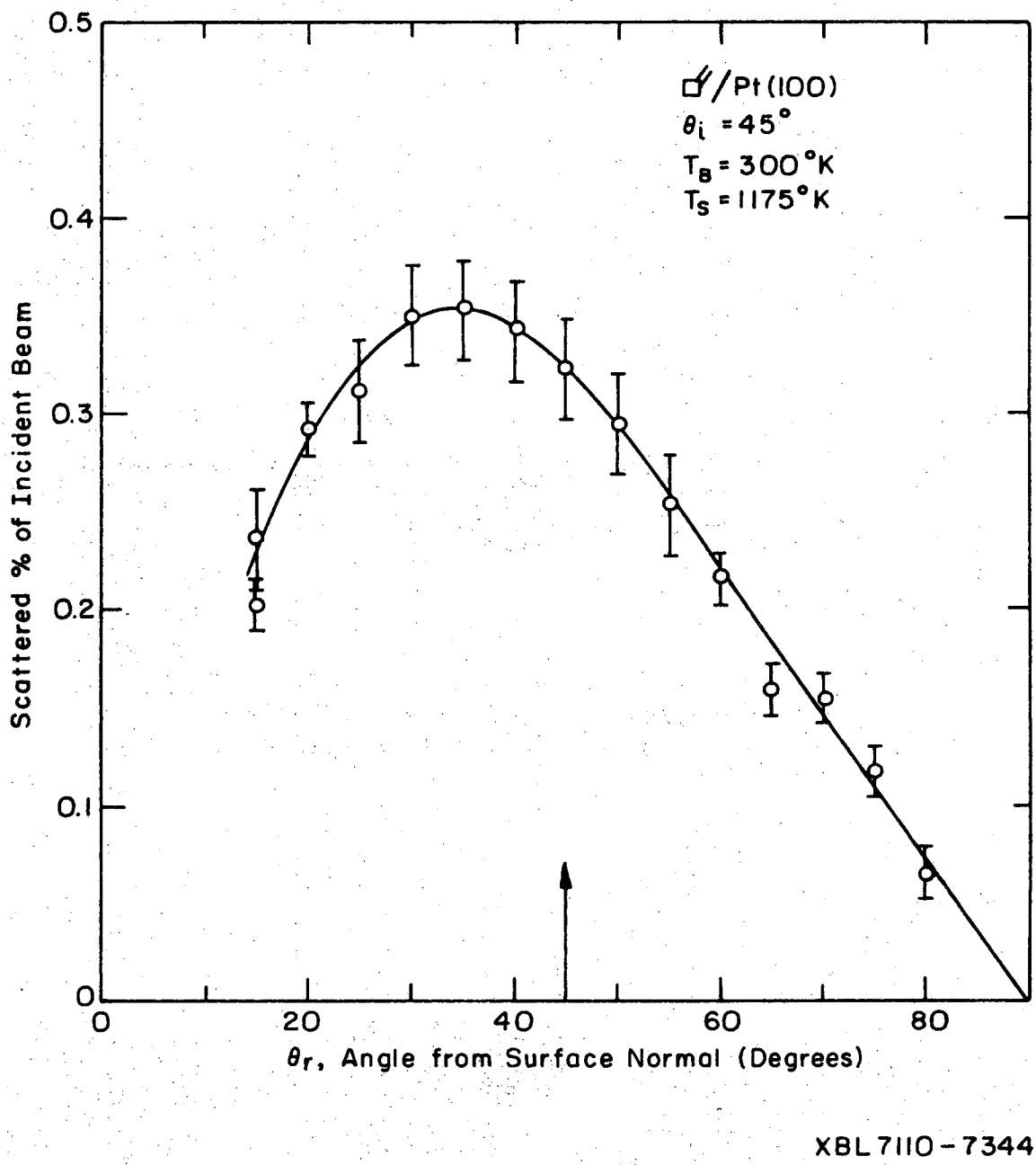

Fig. V-6. Methylene cyclobutane angular distribution for scattering from a Pt(100) surface. The error bars represent the noise level of the observed signal.

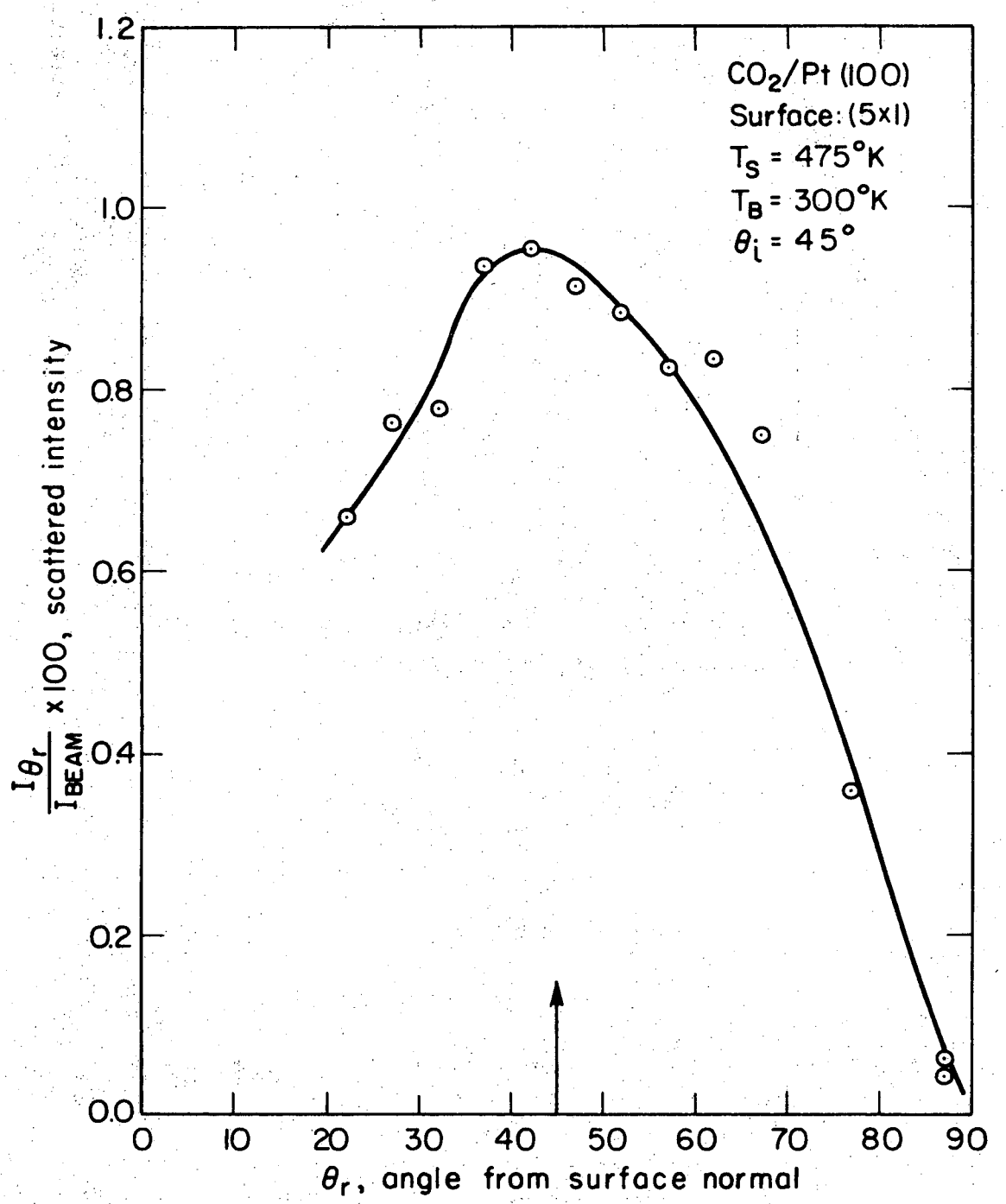

XBL 708-1969

Fig. V-7. Angular distribution of a CO_2 beam scattered from a clean (100) platinum surface. I_{beam} = incident beam intensity.

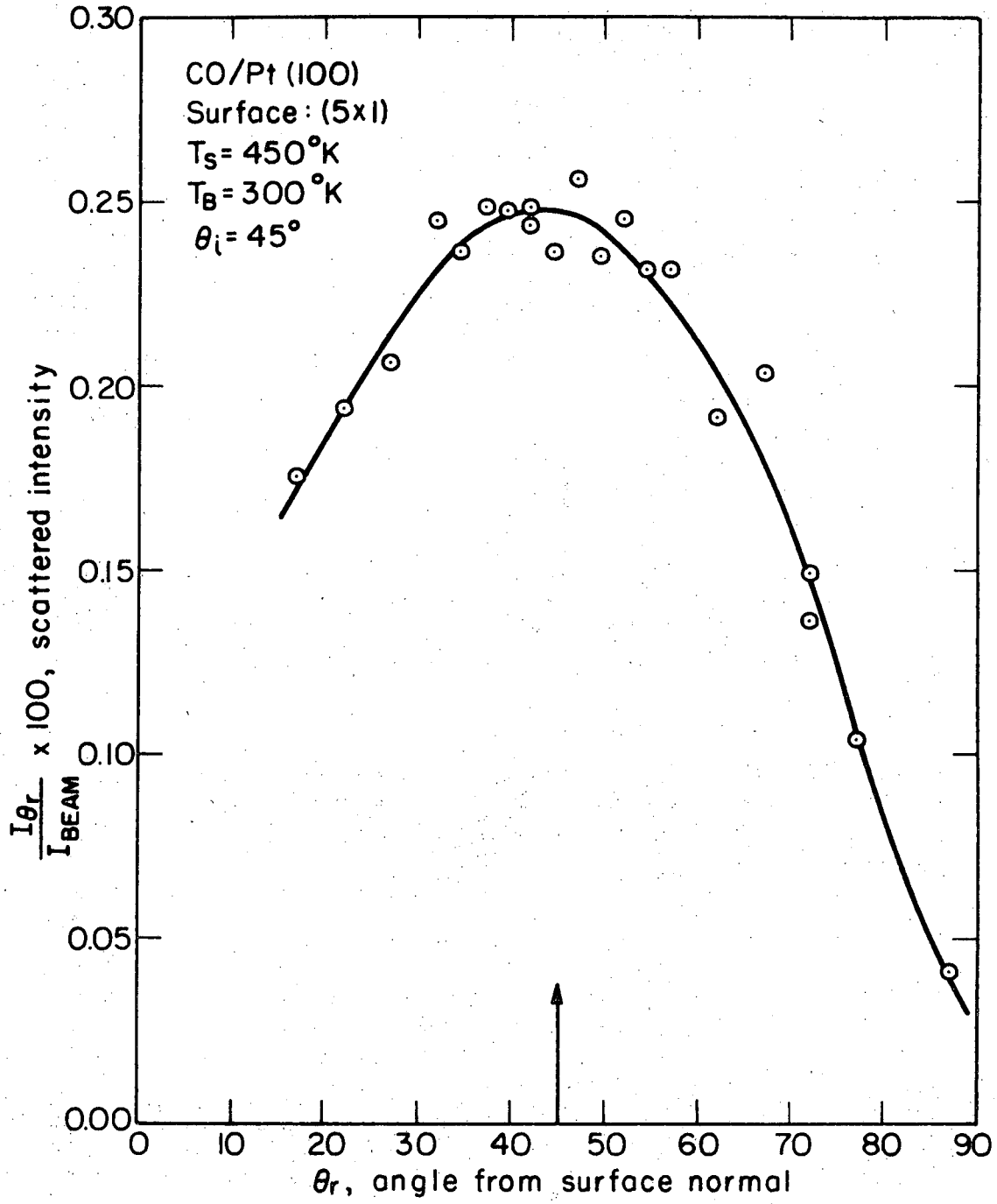

XBL 708-1971

Fig. V-8. Carbon monoxide scattering distribution taken by flashing the Pt(100) sample between data points I_{beam} = incident beam intensity.

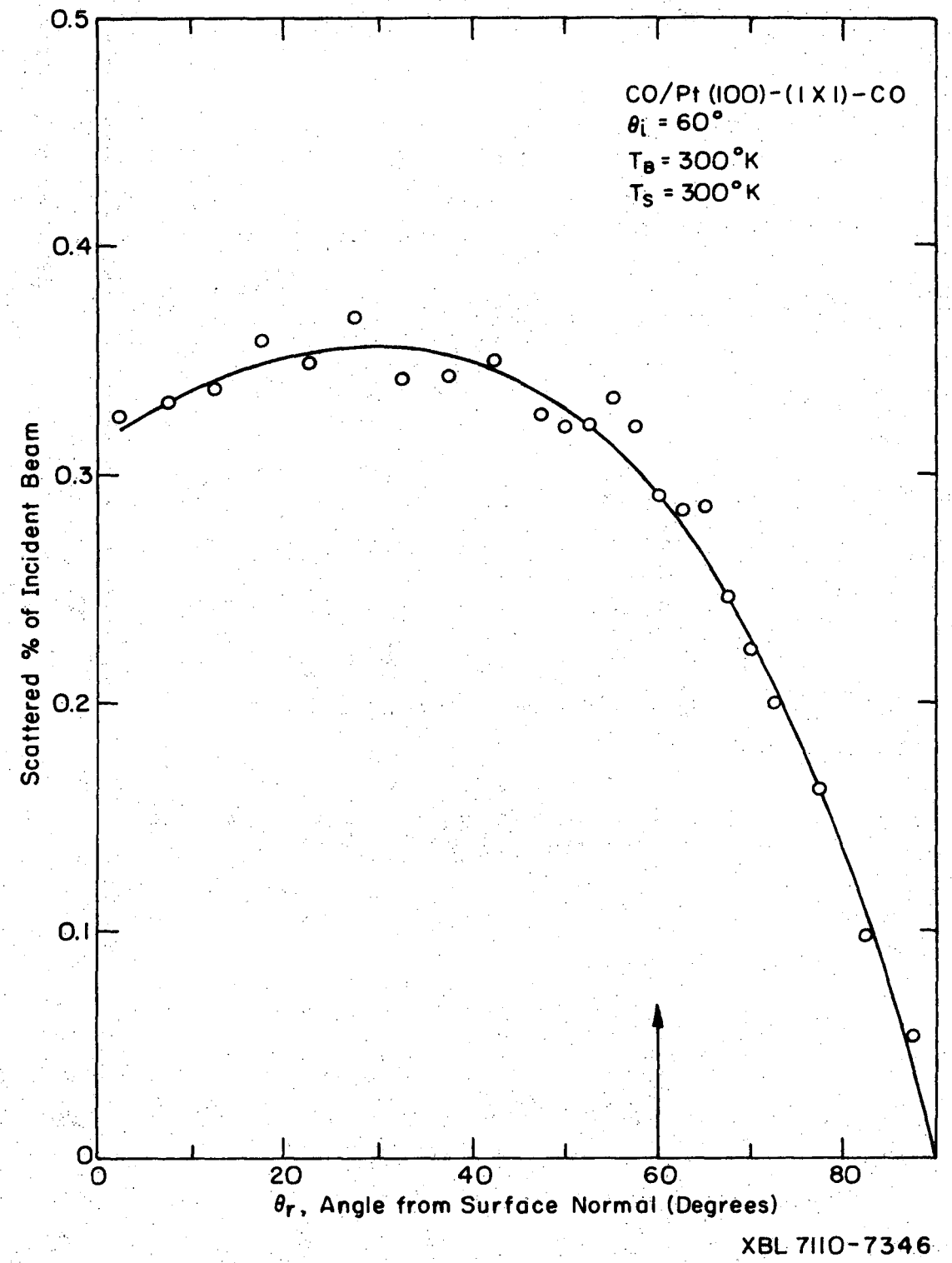

Fig. V-9. Carbon monoxide scattering distribution for scattering from a CO covered Pt(100) surface.

latter experiment the crystal was not flashed or to the slightly higher surface temperature. If the temperature of the solid is raised above the desorption point of the β binding state for CO on platinum, adsorption of the beam can be minimized. In spite of the decidedly asymmetric peak, a striking increase of more than a factor of two in the scattered intensity is observed in Fig. V-10 which shows the results of a run in which the crystal was heated to 925°K. An intensity decrease would be expected if only thermal roughening of the surface were important. Again the curve is backscattered due to energy transfer to the gas.

3. Oxygen and Ammonia

Figures V-11 and V-12 compare the scattering of oxygen from platinum under two entirely different surface conditions. The curve in Fig. V-11 was obtained after flashing the sample to 850°K between data points. Note the backscattering which is probably due to enhanced energy exchange with the solid because of the presence of residual CO. In Fig. V-12 is shown the result on the distribution of flashing the crystal to 1000°K between measurements to free the surface of the tightly bound CO. Although the intensity has not changed, the peak maximum has shifted to the specular position.

The scattering of ammonia is portrayed in Fig. V-13. The angular distribution is very broad and the presence of oxygen in the scattering chamber ambient seems to have no measurable effect on the interaction. Clearly from the weak intensity compared to the preceeding curves the

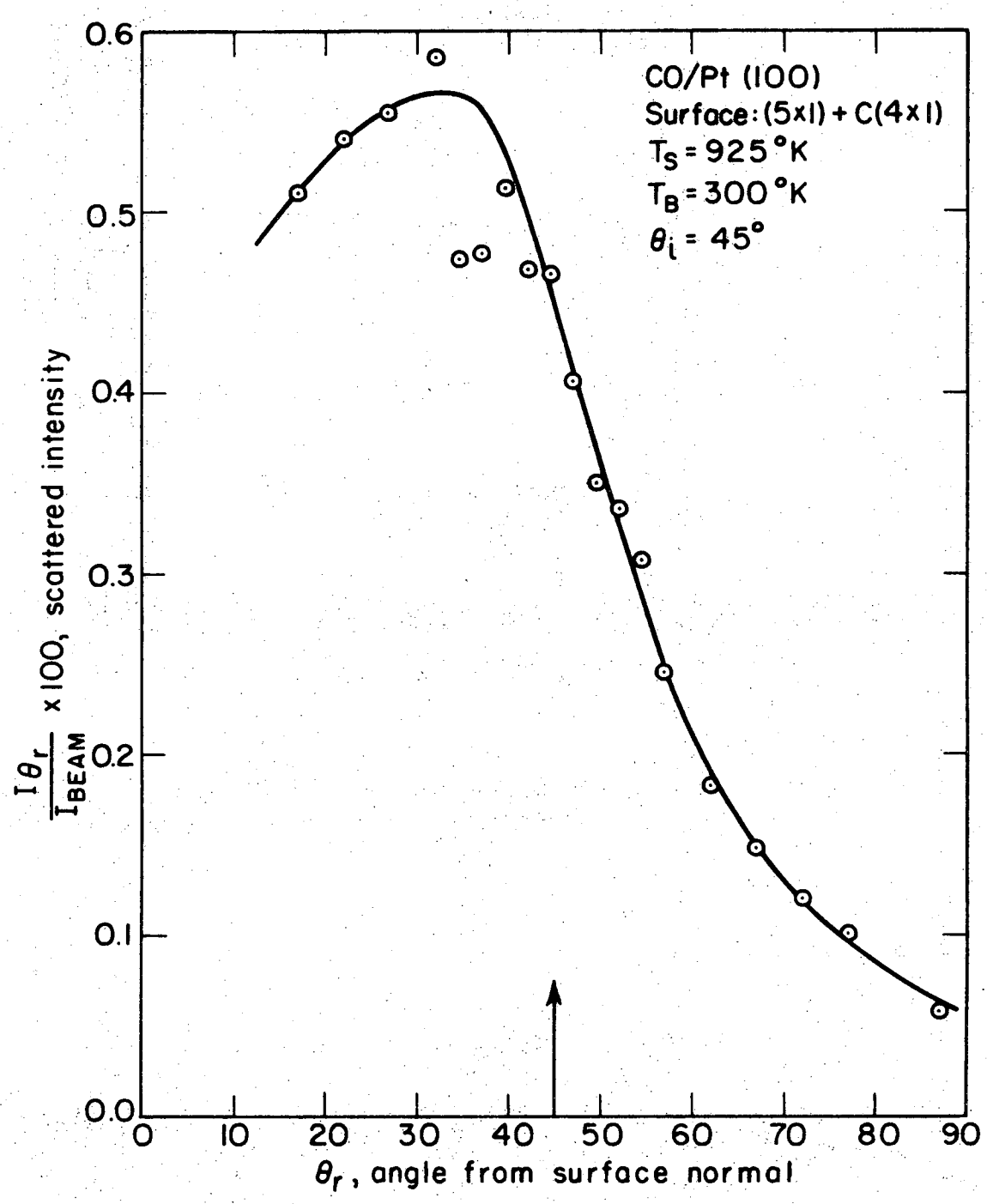

XBL 708-1970

Fig. V-10. Spatial distribution of a CO beam scattered from a hot Pt(100) surface. I_{beam} = incident beam intensity.

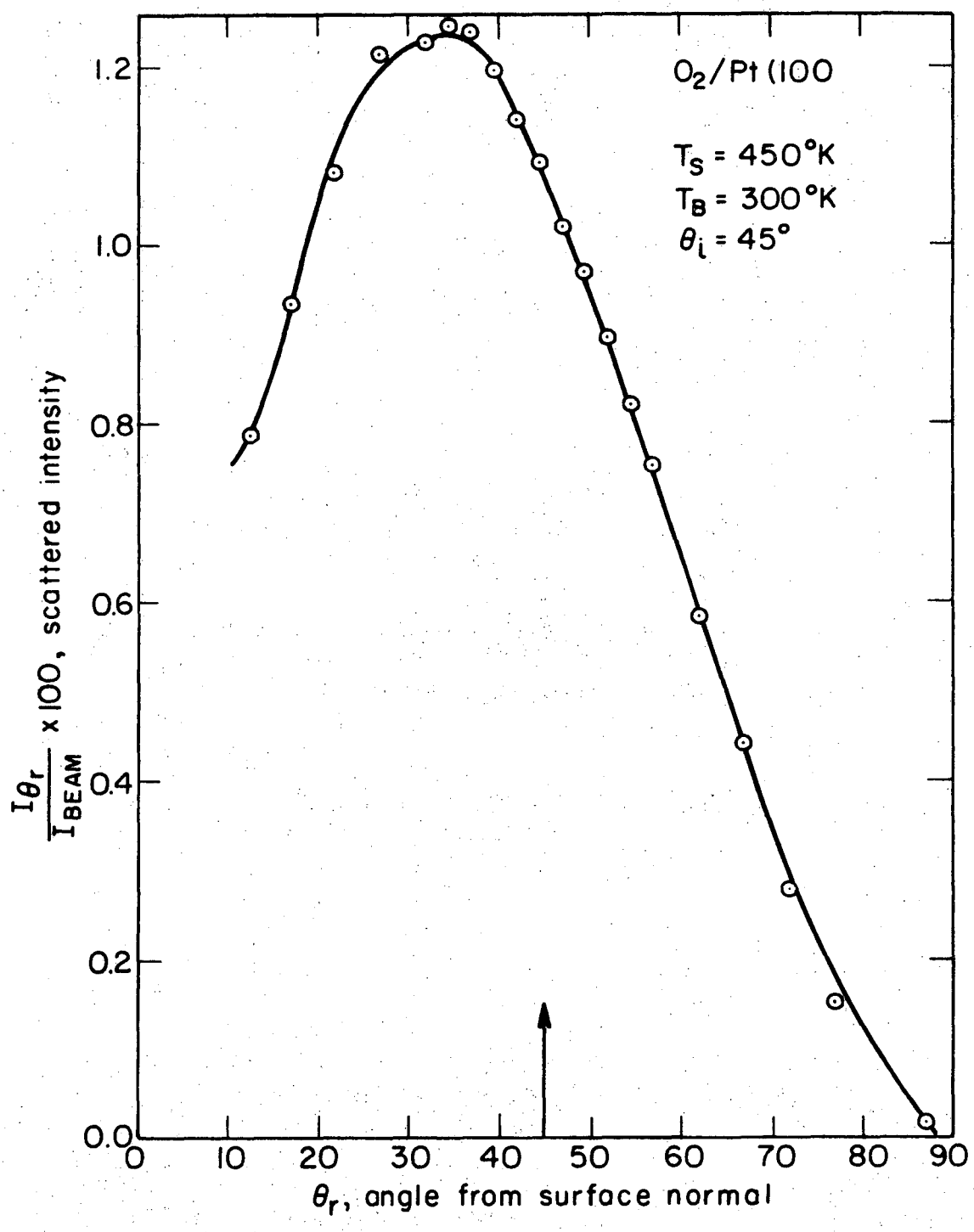

XBL 708-1967

Fig. V-11. Angular distribution of an oxygen beam scattered from a Pt(100) surface with some residual surface CO. I_{beam} = incident beam intensity.

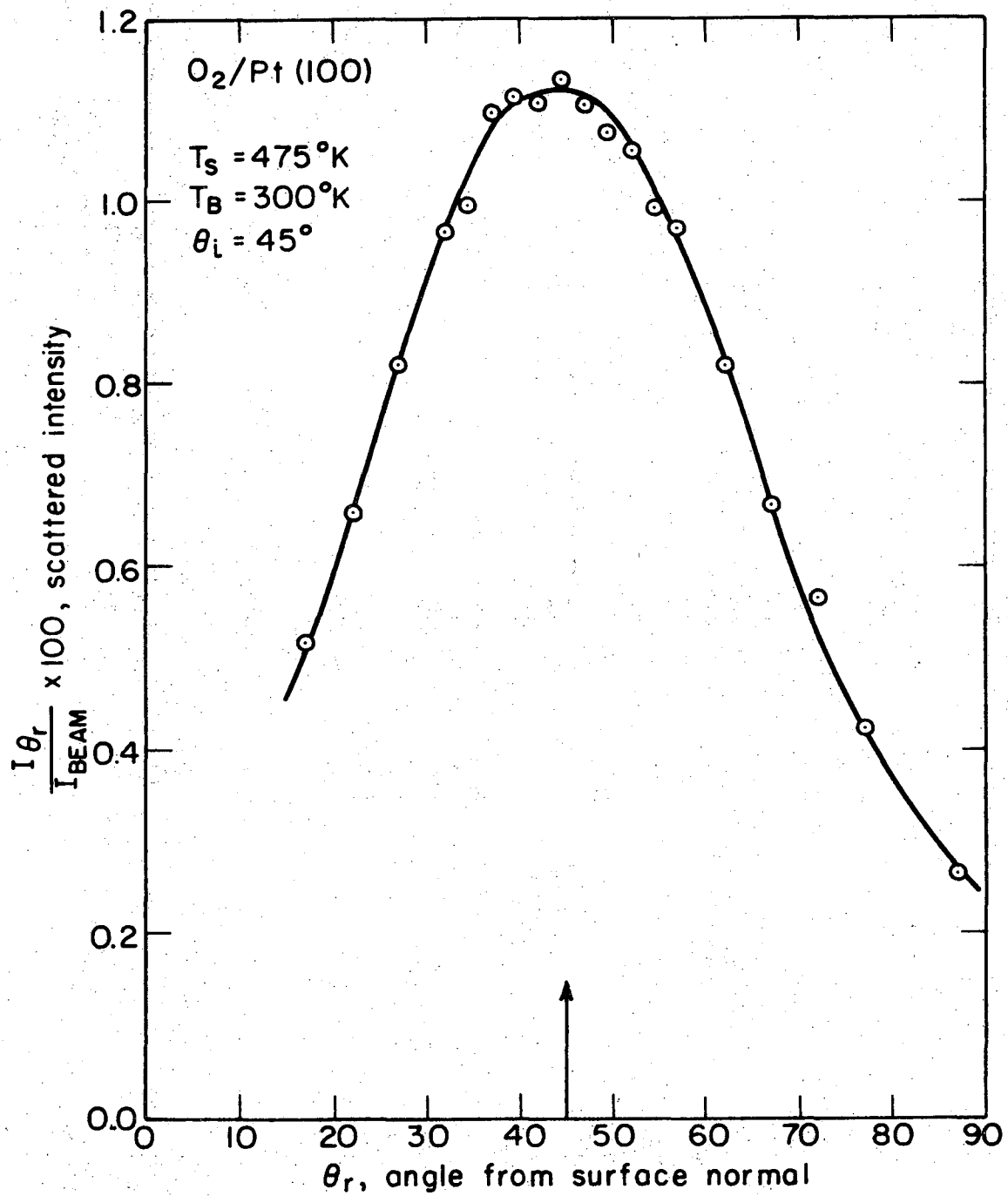

XBL 708-1966

Fig. V-12. Angular distribution of an oxygen beam scattered from a clean Pt(100) surface. I_{beam} = incident beam intensity.

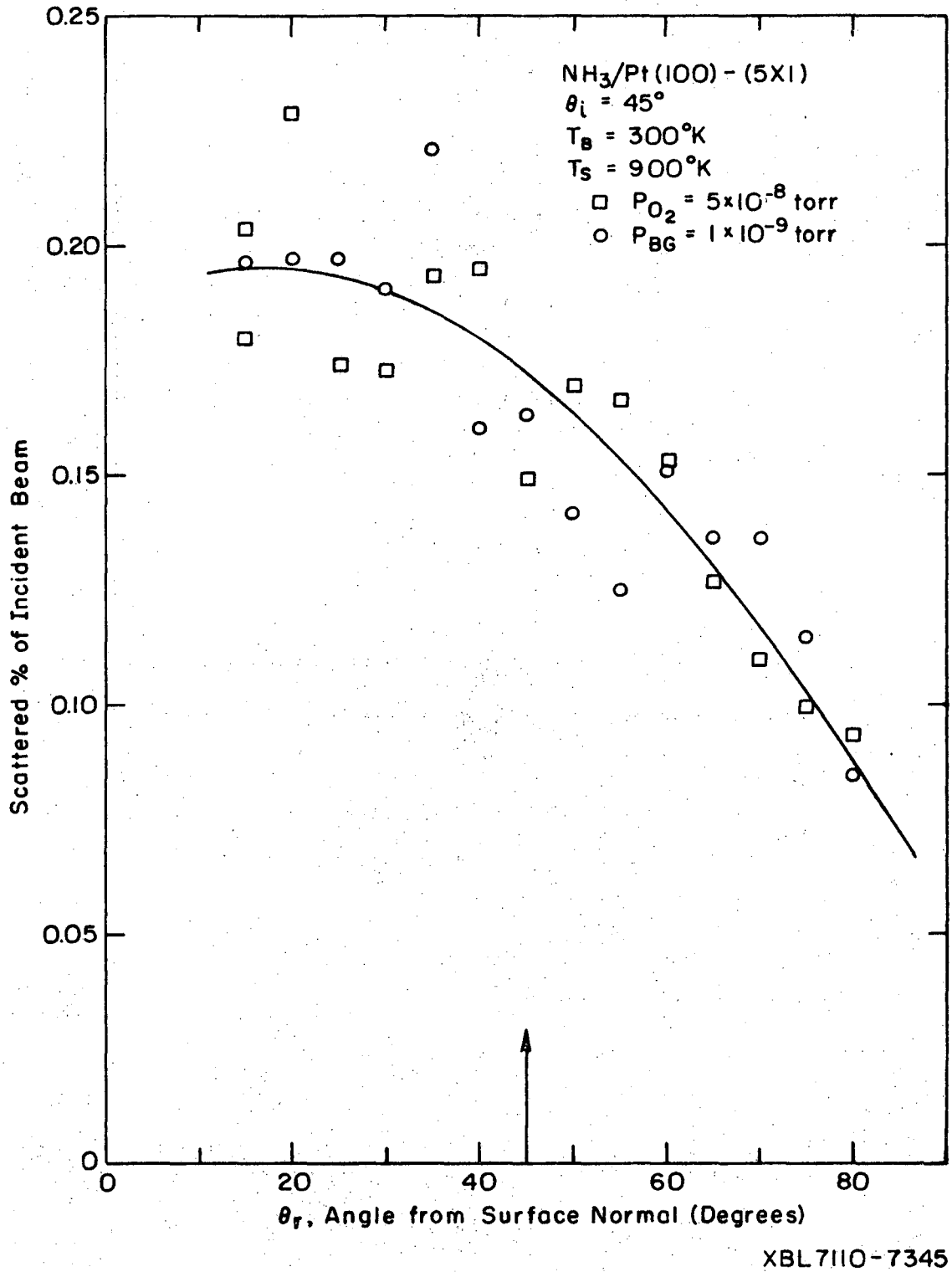

Fig. V-13. Scattering pattern observed when a beam of ammonia was scattered from (100) platinum with and without an oxygen ambient.

ammonia-platinum interaction is very strong (ΔH_{ads} is large) and a long collision with the surface presumably leads to near equilibration of the NH_3 with the surface, and thus a cosine-like distribution. Flash desorption experiments did not reveal the presence of any ammonia on the surface during this work, but AES was not used to check for surface nitrogen and thus the adsorption of ammonia cannot be ruled out completely.

4. Hydrogen and Deuterium

Hydrogen and deuterium scattering were studied because these gases have been investigated previously on a variety of other surfaces[17,35,40,41,53,90,125,127,138] and because they were of interest to reaction studies. Due to the large amount of residual hydrogen in the chamber background, however, it proved impossible to use this gas as the beam species in reactive scattering experiments. In Fig. V-14 we present the scattering results for hydrogen from a clean platinum surface maintained at 1175°K. Compared to other polyatomic gases scattered from hot surfaces, this curve is intense and the maximum falls at the specular position as noted in previous studies,[40,41,90,125,127,138] although the distribution is surprisingly broad. Figure V-15 shows the data for a similar experiment performed with deuterium. This curve appears to be somewhat more narrow than that for hydrogen and the overall intensity may be slightly higher. Neither the presence of oxygen or hydrogen in the ambient (Fig. V-16) seemed to effect the deuterium scattering, but there is a large amount

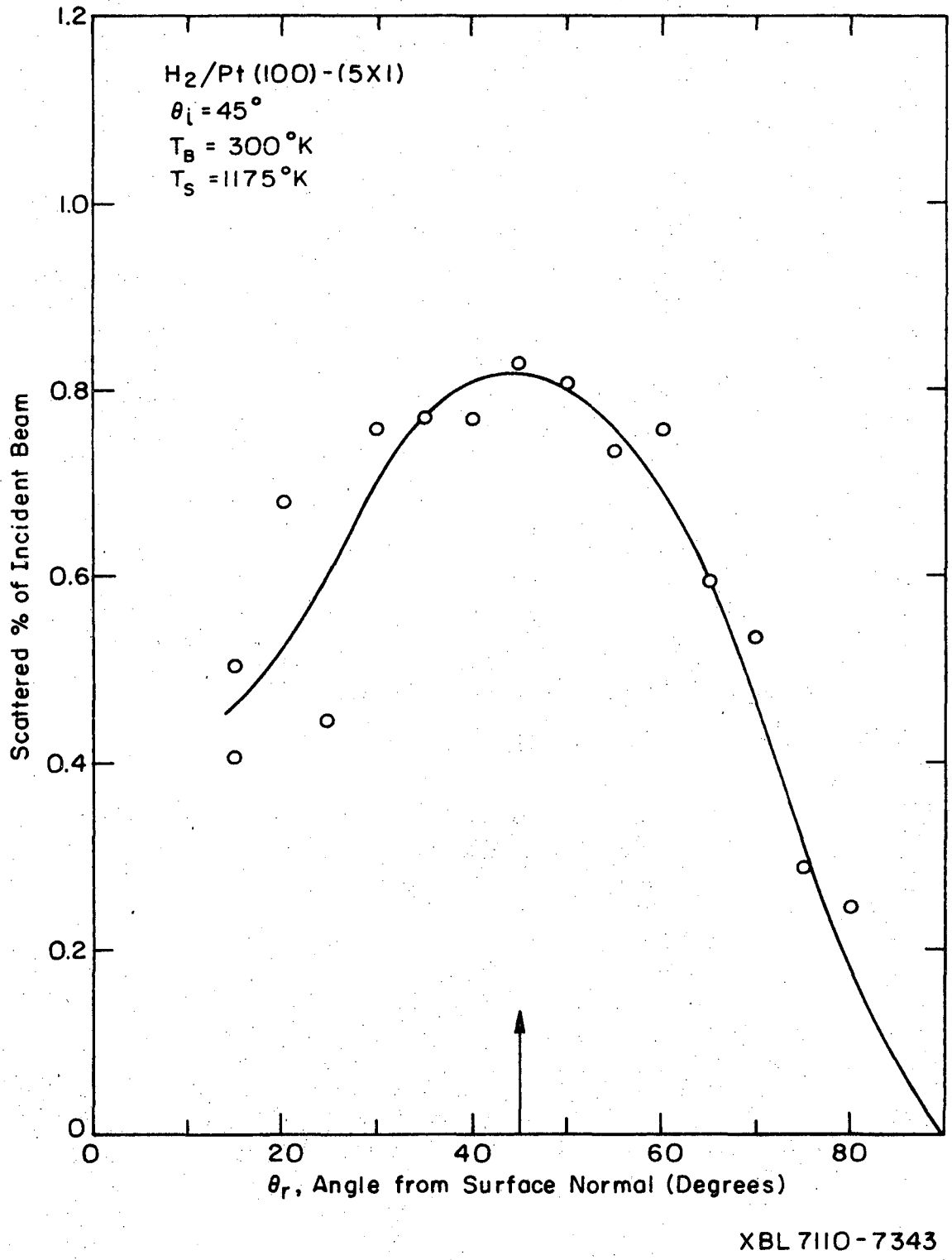

Fig. V-14. Hydrogen beam spatial distribution for scattering from a clean Pt(100) crystal surface.

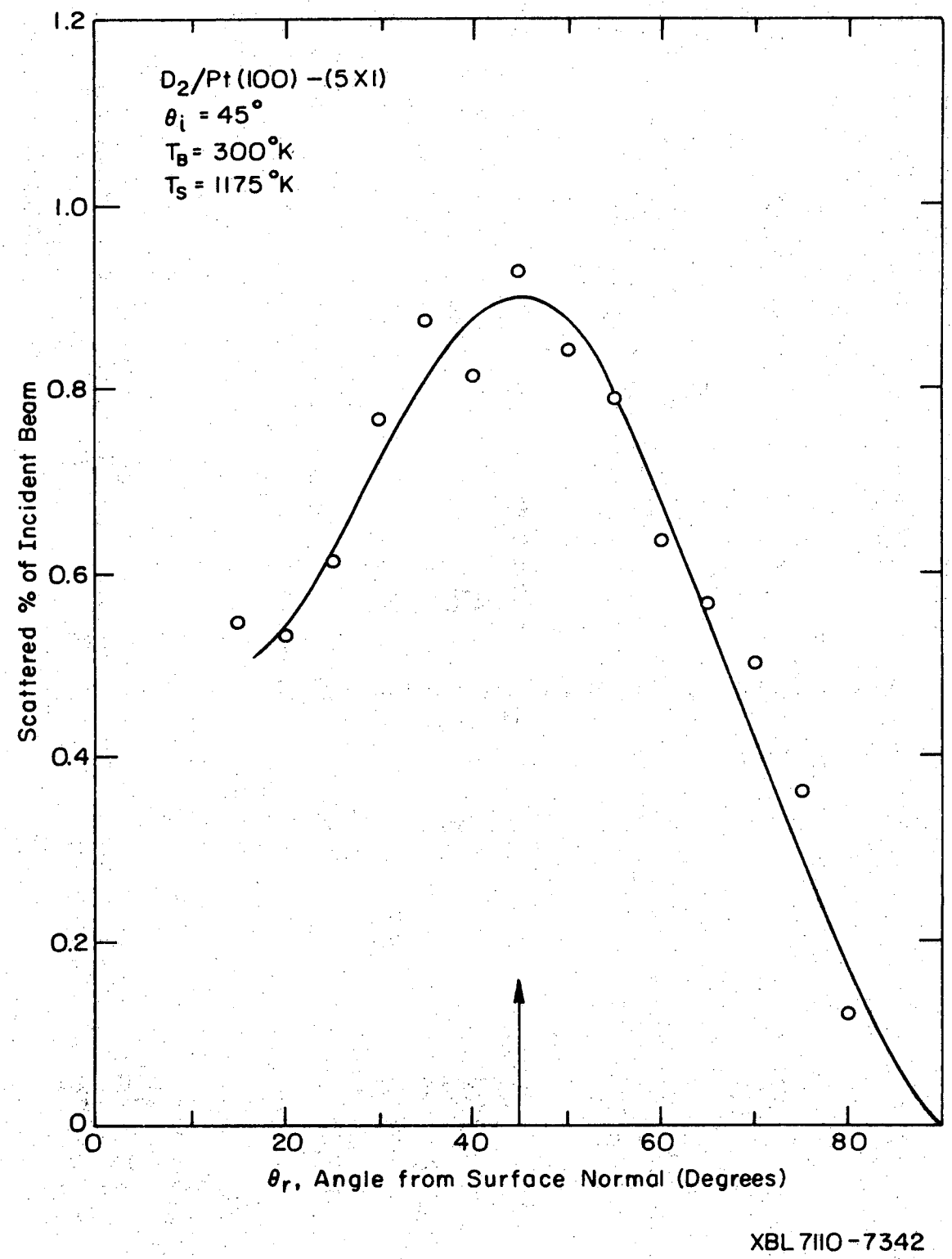

Fig. V-15. Deuterium beam spatial distribution for scattering from a clean Pt(100) crystal surface.

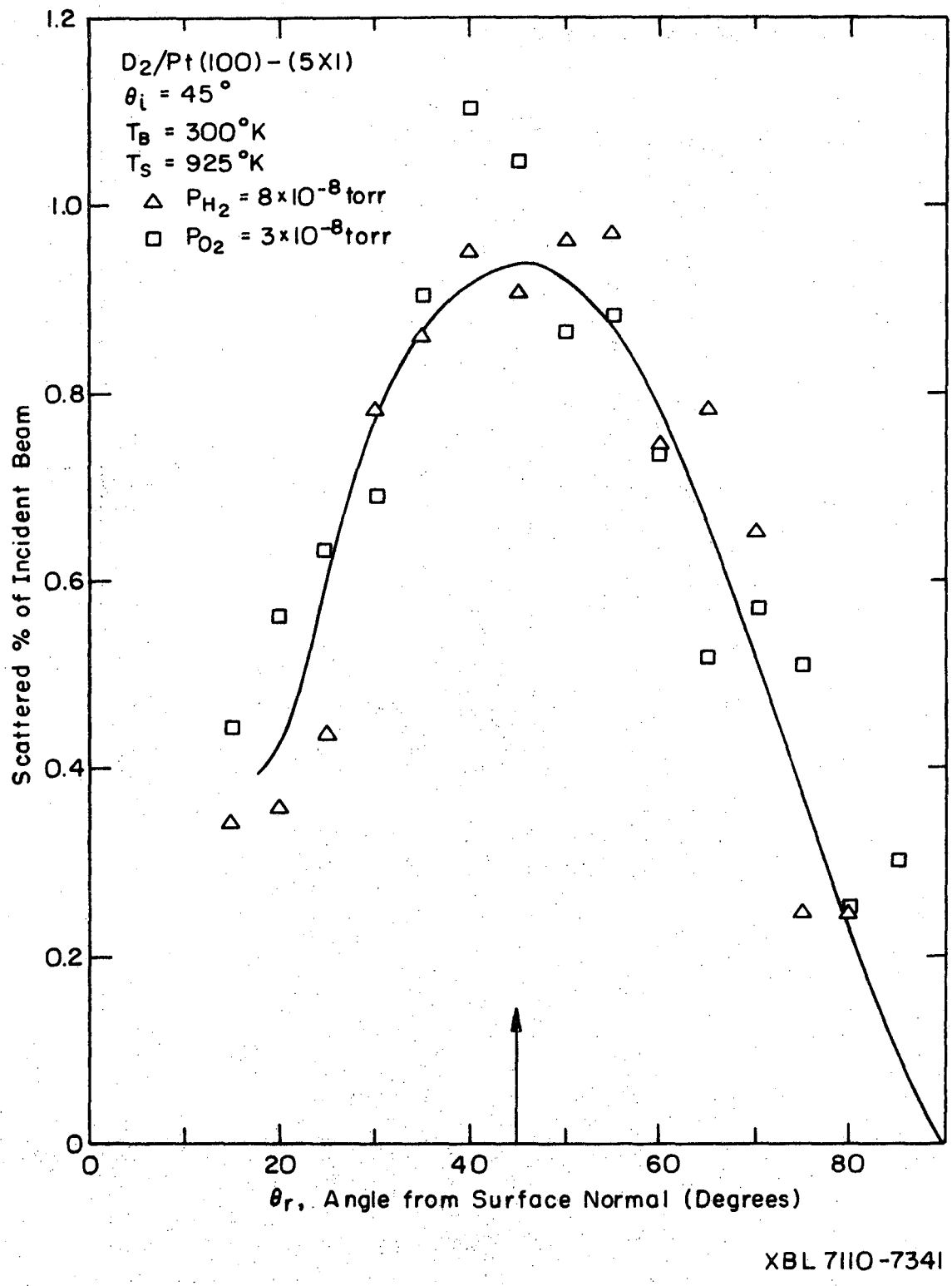

Fig. V-16. Deuterium scattering results with an ambient atmosphere of hydrogen or oxygen surrounding the Pt(100) surface.

of scatter in the data from the high background noise level.

5. Discussion

It is possible to compare the scattering results above with data previously obtained for scattering various diatomic and polyatomic molecules from the (111) surfaces of several other face-centered cubic metals,[40,41,90,127,138,149] the (110) surface of tungsten,[125] and from different polycrystalline solids.[35,53,57,58] Coltharp, Scott, and Muschlitz[57,58] have studied the scattering of nitrous oxide from a tungsten ribbon composed primarily of crystallites having the (112) orientation. At room temperature they detected a cosine angular distribution for the reflected gas. This observation is not too surprising because the ambient pressure in their scattering chamber ($\sim 10^{-6}$ torr) was high enough to insure that the surface was covered by adsorbed gases. We have already demonstrated that the presence of low molecular weight speices on a surface considerably broadens the spatial scattering distribution. They also observed, however, that higher surface temperatures yielded pronounced lobular distributions with broad intensity maxima in the vicinity of the specular position. These same authors report[58] that both nitrogen and nitric oxide are backscattered from a tungsten surface heated to 2500°K. Although our platinum surface temperature was considerably lower, we have also observed that nitric oxide scatters back toward the surface normal from a hot surface in agreement with their observation.

The scattering of nitrogen molecules has been studied by several authors.[9,58,149] Hurlbut[9] found that nitrogen was scattered diffusely

from polished steel, polished aluminum and unpolished glass except at near grazing incident angles ($\theta_i \gtrsim 80°$) where some peaking was observed. In view of the poor residual vacua achieved (c.a. 10^{-6} torr) and the presence in the work chamber of hydrocarbon vapors from the diffusion pump oil,[10] the specimen surfaces were undoubtedly contaminated and we would thus expect them to yield distributions of scattered gas molecules close to the cosine pattern. Stickney and Hurlbut[150] and Stickney[151] have measured the normal momentum transfer between rare gases, N_2, H_2, and CO_2 and the surfaces of tungsten, aluminum, and platinum through the use of a sensitive torsion balance. Angular distributions were not determined, but they observed that for argon and nitrogen the transfer of momentum from the gas to the solid in the direction normal to the surface was similar. Carbon dioxide, on the other hand, was more efficient than these gases at transferring normal momentum to the solid while neon, hydrogen, and helium were less efficient. If the normal momentum transfer can be taken as a measure of the energy lost by the incident gas, then one would expect many molecules to be scattered diffusely and thus perhaps lost to our a.c. detection system. A comparison of Figs. V-7 and V-1 for CO_2 and N_2, respectively, shows a lower CO_2 intensity as predicted. Such a relationship should only hold for gases not adsorbed on the substrate, for that could also account for a particle loss in the a.c. mode of detection.

In the only other systematic investigation of the scattering of polyatomic gases besides the studies reported in this thesis,

Saltsburg, Smith, and Palmer[149] have reported the scattering of several diatomics (H_2, HD, D_2, O_2, N_2, CO) and CO_2 from an epitaxially grown (111) silver single crystal. Their results for nitrogen show a slight backscatter, but the surface was held at 560°K in their experiment as compared to T_S = 475°K in our work where no backscatter was observed. A better comparison between their work and ours may be achieved by looking at the scattering of nitrogen and oxygen. Their data indicate that both curves have maxima at the same location and are similar in intensity and peak shape. From Figs. V-1 and V-12 we can see that the scattering of nitrogen and oxygen from the platinum (100) surface yields the same results. Additionally, CO_2 scattering in their system produces a lower intensity maximum than the scattering of either N_2 or O_2 although all three gases have peak intensities at the same angle. Comparing Figs. V-1, V-7, and V-12 shows that a similar trend exists for the platinum surface.

There are no data in the literature for hydrocarbon scattering except for methane which shows backscatter form a (111) silver surface at T_S = 560°K.[126] Smith and Merrill[152] have studied the irreversible chemisorption of ethylene on a Pt(111) single crystal by combined LEED and helium beam techniques but evidently did not attempt to scatter the gas. Thus, our results for acetylene and methylenecyclobutane must stand alone. Table V.3 shows that the likelihood of either electronic or vibrational excitation for C_2H_2 is small although we already know from our work that this gas readily adsorbs and decomposes on platinum.

Methylenecyclobutane seems to be the largest projectile (13 atoms) used to date in gas-solid scattering experiments. The reason for the choice of this molecule will be made clear in the section concerning reactive scattering.

In their investigation of the scattering behavior of polyatomic gases on (111) silver, Saltsburg et al.[149] found that the CO and CO_2 scattering distributions were quite similar. This is in contrast to our observations of CO and CO_2 scattering from the (100) platinum surface. It should be noted, however, that CO does not adsorb on silver at room temperature and CO_2 adsorbs on neither metal.[106,153] On the other hand, CO adsorbs readily on the platinum surface. While Figs. V-8 and V-10 graphically portray the effect of surface adsorption on the intensity of the scattered beam, the observed backscatter from the hot surface is in agreement with the silver study. The surface of silver was also employed in a study of the angular distribution of scattered ammonia.[126] The pattern was found to be very broad and almost completely diffuse in nature which is similar to the data shown in Fig. V-13 for NH_3 scattering from Pt(100).

Much attention has been directed toward the scattering of hydrogen and deuterium from metal surfaces and data now exist for experiments conducted on nickel,[35,40] gold,[51] silver,[127,138] platinum,[15,41,53,90] and tungsten.[125] For all of these solids, provided the surface is clean, the maximum intensity occurs at the specular position although the dispersion varies somewhat. In fact, in order to explain a broad

peak they observe between the surface normal and the specular angle in the angular distributions of H_2, HD, and D_2, Palmer et al.[40,127,138] invoked energy transfer via surface phonons between the rotational energy states of the incident hydrogenic species and the vibrational modes of the surface atoms in the silver and nickel lattices. There can be no doubt about the markedly different scattering distributions observed by Palmer et al. when hydrogen isotopes were impinged upon the epitaxially grown thin films. Our studies of hydrogen and deuterium scattering from the Pt(100) surface and those of Smith[154] for deuterium from the Pt(111) surface show no peaks other than the specularly directed one. Although the Debye temperatures of platinum and silver are similar (234°K for Pt and 225°K for Ag), rotational-vibrational energy transfer has not been detected for the studied single crystal platinum surfaces. Smith and Merrill,[90] however, have found a spatial distribution reminiscent of those observed by Palmer et al.[40,127,138] when deuterium is scattered from an unetched Pt(111) crystal surface. This result indicates that perhaps surface roughness is important in affecting rotational-vibrational energy transfer between incident diatomic molecules and a solid. It appears that the epitaxial silver and nickel surfaces used in the experiments by Palmer et al. could have been considerably rougher on an atomic scale than the well-characterized platinum single crystals used in the works cited above.

If microscopic disorder enhances rotational coupling to the solid, even a surface disordered through heating could cause significant internal excitation of hydrogenic molecules. We have already pointed

out that the hydrogen and deuterium data presented in Figs. V-14 to V-16 show rather broad peaks. At $T_s = 775°K$, Smith[154] reports a half-width (FWHM) of 29.5° for deuterium scattering from Pt(111) and a maximum intensity of 1.5%, down from 3.6% at $T_s = 375°K$. These values may be compared to those we find at 1175°K for deuterium scattering from Pt(100) ($I/I_o \sim 0.9\%$, FWHM ~ 50°) where one would expect a lower intensity and perhaps wider dispersion due to the higher surface temperature.

Feuer's analysis of the energy exchanged between a rigid-rotor diatomic molecule and a solid surface also helps to explain the observations. The model predicts that when the temperature of the solid exceeds that of the gas, quantum transitions not only allow the transfer of vibrational energy from the lattice into rotational modes of the gas, but also permit the conversion of some of the rotational energy of the gas into translational energy. The net effect of these two processes should be to broaden the angular distribution and to impart a diffuse component to the scattered gases. This is indeed what we see in Fig. V-14.

Clearly, from the data presented, the simple collision models discussed in section C-3 of Chapter I fail to describe the scattering of diatomic and polyatomic molecules. Especially for linear polyatomic gases such as N_2O, CO_2, and C_2H_2 there may be orientation effects that contribute in some yet unknown manner to the scattering process. Then too, the interaction of the particle's internal degrees of freedom with the solid during the collision certainly complicates the

scattering process. Although for most species rotational transitions involve energy changes too small to be resolved in scattering experiments as they are now conducted, these transitions may play an important role in the exchange of energy between the gas and the solid due to the ease with which rotation to translation relaxations can occur during the collision. The large heats of chemisorption for polyatomic gases contribute a strong attractive potential to the gas-solid interaction and, if the incident particle loses any translational energy through scattering, is difficult to overcome after the collision. Consequently interaction times are long and hence energy accommodation higher than for monatomic gases. Taken together, the data in Figs. V-1 through V-16 show, at a constant temperature, a qualitative correlation between the strength of the gas-surface interaction potential and the dispersion and intensity of the measured angular distribution.

C. Verification of a Classical Model for Gas-Solid Scattering

In Chapter I, section C-3 we described briefly several models that have been formulated to describe the spatial and energy distributions of thermal energy noble gas atomic beams scattered from crystal surfaces. In general, those models that do not restrict the solid temperature to zero degrees Kelvin yield the best results.

Recently Busby, Haygood and Link[82] have presented a theoretical analysis of gas-surface interactions based upon classical mechanics and have tested it with experimental data for the scattering of gaseous argon from a solid argon matrix. The model is based upon the collision of hard spheres, and allows scattering from ordered crystal

domains of hexagonal and square arrays that simulate well the surface structure used in most experimental studies of surface scattering. Their formulation also permits the inclusion of an attractive square well potential in addition to the surface temperature. Unlike the hard-cube model which permits a closed form solution to the angular scattering distribution, their analysis requires a Monte-Carlo calculation of the trajectories of the reflected gas atoms. The major conclusions of these calculations are: a) the angle of maximum scattered intensity is independent of the beam's incident angle and energy and of the surface temperature, and b) the capture coefficient or condensation coefficient for the incident beam increases with decreasing angle of incidence (defined with respect to the surface normal where $\theta_r = 0°$). Although the theoretical spatial angular distributions are narrower than those measured experimentally, the computed trajectories compare favorably with the observed data, and if the heat of sublimation is used as the magnitude of the attractive well, so do the capture coefficients.

Since the calculations have been restricted to a consideration of the scattering of atoms from their own crystal lattice (that is, scattering of atoms from surface atoms of identical atomic weight, polarizability, size, etc.), a test of the model with molecular species might reveal whether their assumptions about the hard sphere interaction are also valid for particles having internal structure. We can easily approximate the experimental conditions that formed the basis for the computations of Busby et al. (same molecular weight of colliding

gas and surface atom) by depositing a layer of a strongly chemisorbed gas on our platinum substrate. Carbon monoxide and acetylene both satisfy this criterion and also form ordered surface structures on platinum,[106] but the largest fraction of the chemisorbed molecules is in small square domains that that give rise to broad, low-intensity diffraction spots (again, the structure of the real surface is similar to that assumed in the scattering model by Busby et al.).

We have studied the angular distribution of carbon monoxide molecular beams scattered from a layer of carbon monoxide chemisorbed on the (100) crystal face of platinum and of acetylene molecular beams scattered from a layer of acetylene chemisorbed on the (100) crystal face of platinum as a function of the incident angle. Both gases were adsorbed on the surface at a pressure of approximately 10^{-7} torr and a temperature of 300°K prior to the run. Once the LEED pattern indicated the appearance of the surface structure characteristic of these adsorbed gases, the experiment commenced. Figure V-17 shows the spatial distribution of CO scattered from the CO-covered platinum (100) surface at various angles of incidence and 300°K surface temperature. Figure V-18 shows a similar plot for C_2H_2 scattered from absorbed C_2H_2. For both gas-surface systems, the spatial distribution of the scattered beams appears to be independent of the incident angle within the experimental accuracy. The scattered CO beam shows a broad intensity maximum between 30° and 40°, while the C_2H_2 beam appears to have a plateau in the 10-40° range with respect to the surface normal.

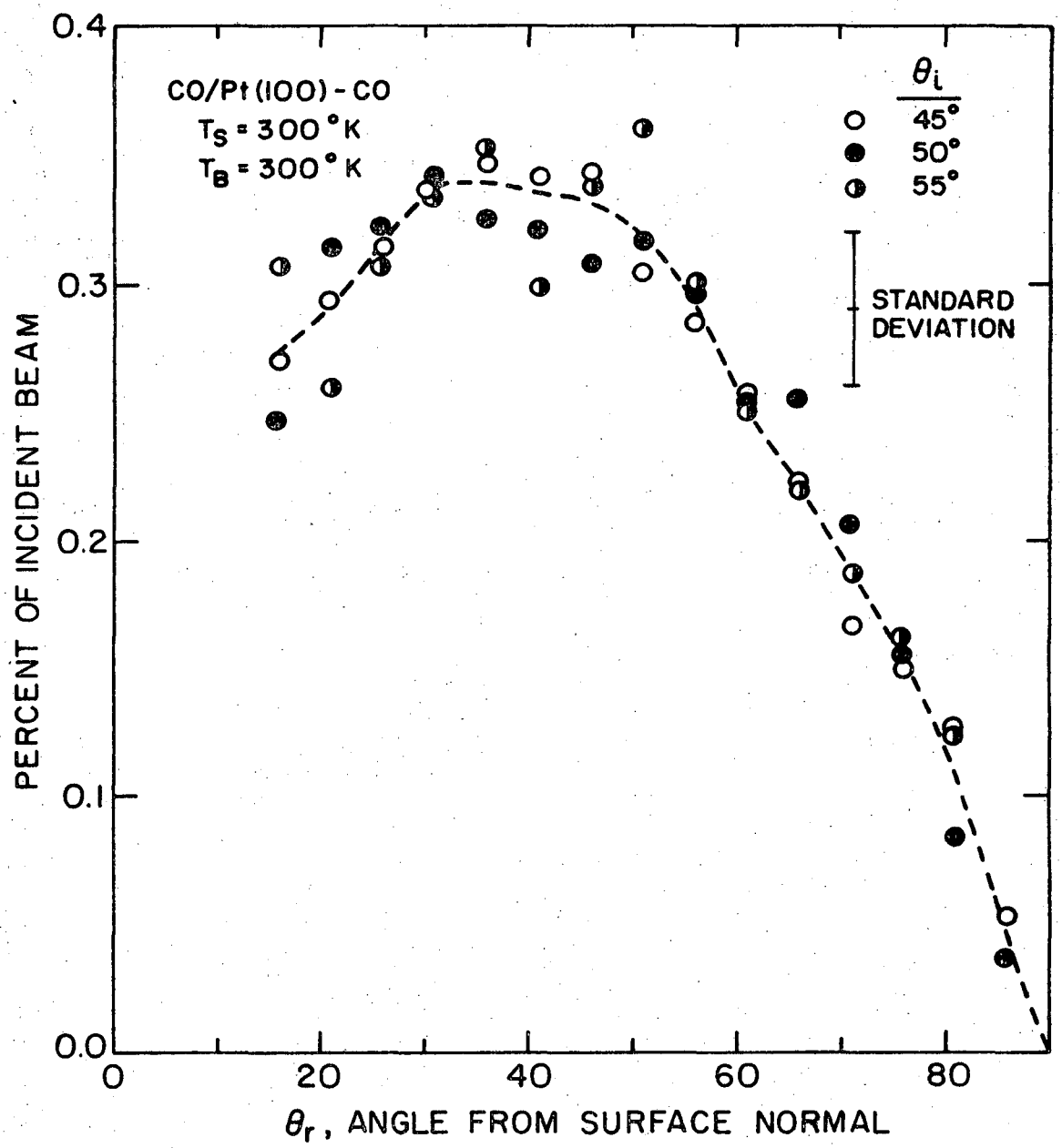

XBL 715-6731

Fig. V-17. Angular scattering patterns for CO obtained from a Pt(100)-CO surface at three angles of incidence.

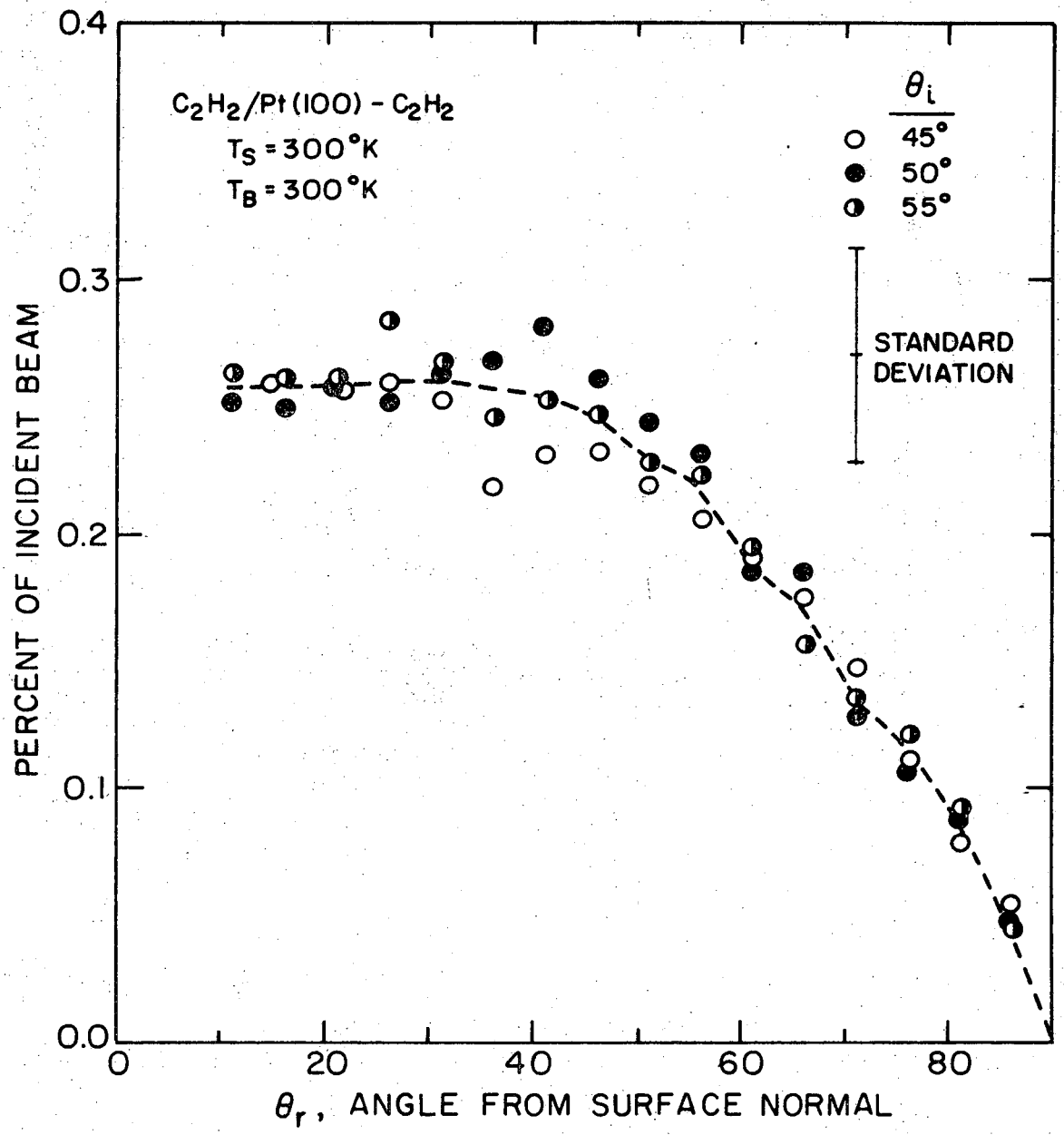

XBL715-6730

Fig. V-18. Angular scattering patterns for C_2H_2 obtained from a Pt(100)-C_2H_2 surface at three angles of incidence.

In Figure V-9, the CO data are extended to a 60° angle of incidence and within the experimental accuracy, that curve can be superimposed on the curve in Fig. V-17 except at the low angles where the points on the $\theta_i = 60°$ plot do not fall off. This discrepancy is felt to be an artifact of the system rather than a true representation of the scattering. Earlier (Ch.II, B-7) we noted that at incident angles near 60°, the projected size of the crystal perpendicular to the beam line was comparable to the width of the beam. Thus a small misalignment could mean that part of the beam is being scattered by the target mounting pieces rather than the target itself. Helium scattering supports this hypothesis as shown in Fig. V-19. Neither diffraction nor phonon losses can account for the shoulder on the low angle side of the specularly directed peak. Subbarao and Miller[155] however, have reported a similar shoulder for helium scattering ($\theta_i = 77°$) from (111) silver and attribute it to inelastic processes.

One additional feature of the trajectories computed by Busby, et al. is that they are independent of the depth of the attractive square well potential assumed operative between the incident gas and the surface. It is encouraging that molecules that are highly polarizable and have heats of sublimation different from that of argon (1.8 kcal for CO and 5.1 kcal/mole for C_2H_2) conform to the spatial distribution characteristics predicted by the classical mechanical model. This agreement between experiment and theory in the angular scattering patterns indicates that the calculation qualitatively describes the

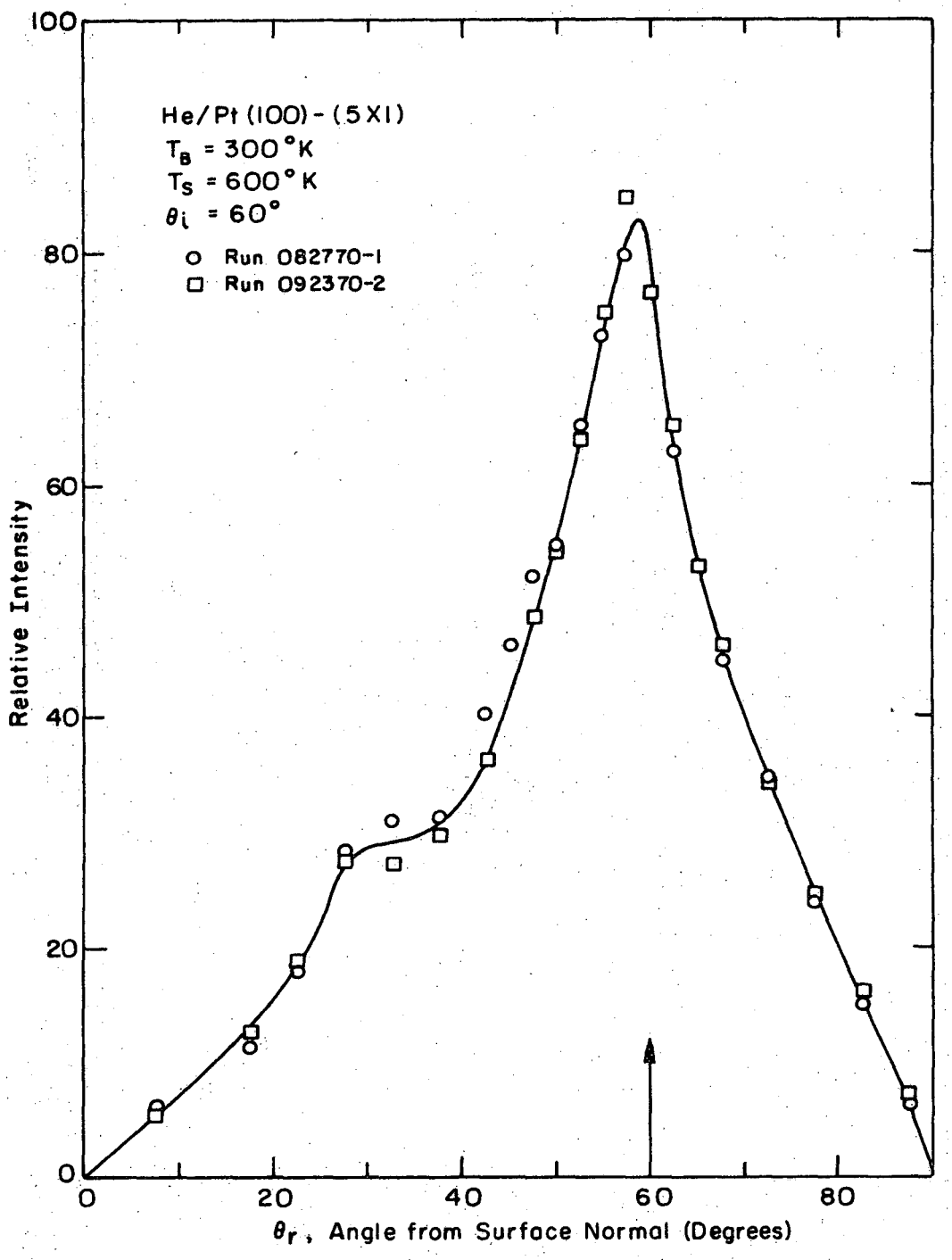

Fig. V-19. Helium beam scattering distributions for $\theta_i = 60°$ showing a barkscattered shoulder.

non-reactive scattering of molecules from their own lattice and that the model may be used to describe the scattering of molecules of various size and chemical properties (polarizability, dipole moment, symmetry) from crystal surfaces. The large scatter in the data and the broad distributions, however, make these conclusions tentative at the present time. More work is being conducted to resolve the issue.

D. Reactive Scattering Studies

The scattering of atomic or molecular beams from surfaces provides information about the dynamics of the interaction between incident particles and the surface atoms. Until recently, however, most investigators in this field have restricted their attention to the scattering of beams of inert gases or hydrogenic molecules from a variety of surfaces as already indicated. From the angular distribution of the scattered gas atoms as a function of the nature of the surface (temperature, orientation, order) and of the incident beam (energy, direction) the dynamics of the gas-surface interaction have been probed. Such experiments have already been described in the previous chapter and the foregoing portions of this chapter.

The scattering of gases that may react during a collision with the solid surface has been studied to a lesser extent. These studies should yield information concerning the dynamics of surface chemical reactions. At least three types of reactive collisions may be postulated. 1) The gas molecule may undergo rearrangement or dissociate through the influence of the surface exerted via the collision.[17,35,57,58]

2) The incident molecule may react with some species previously adsorbed on the surface or continuously bombarding the solid in an isotropic manner from the ambient.[40,41] 3) The gas particle may react with substrate yielding a surface atom among the gaseous products of the interaction.[14,36-39] Several experiments that may be placed in the above categories have been attemped and the results of those undertakings are related in the following pages.

1. Ammonia Oxidation

The oxidation of ammonia on metals of the platinum group is one of the most exothermic catalytic reactions and, although it has been in commercial use for many years, there is still some controversy over the detailed steps of the heterogeneous reaction.[156] It has been estimated[104] that every collision of the gas with the solid results in reaction. While nitrogen and water are the final products of ammonia oxidation, nitric oxide is an intermediate species that can be recovered in high yields under suitable conditions. All of the proposed mechanisms[156] assume that the initial process in the oxidation sequence is the reaction of a gaseous ammonia molecule with an adsorbed oxygen atom to form either hydroxylamine or NH radicals.

$$NH_3(g) + O(ads) \rightarrow NH_2OH(ads) \qquad (V\text{-}16)$$

$$NH_3(g) + O(ads) \rightarrow NH(ads) + H_2O \qquad (V\text{-}17)$$

Since the surface plays an important role in the postulated mechanisms, and since the major reaction products (N_2, H_2O, NO) are gaseous, this

system seemed to be an excellent choice for investigation by combined LEED, AES, and molecular beam techniques.

A previous study of ammonia oxidation on a polycrystalline platinum ribbon by Nutt and Kapur[157] employed a beam system but no provision was made to investigate the angular distribution of the products. Three capillary tubes were used to direct the reactant gases toward the target surface and a fixed mass spectrometer then sampled the evaporating species. Typical experimental impingement rates corresponded to equivalent pressures of 10^{-2} torr in a background $\geqslant 10^{-4}$ torr. A beam shutter located between the target and the detector permitted the authors to distinguish between molecules in the gas phase and those originating on the surface as the result of the catalytic reaction. Nitrogen, water, and nitric oxide were the only observable products between room temperature and 1600°K. The optimum temperature for the formation of NO was found to be 890°K and at that temperature the NO production rate was proportional to the ratio of the partial pressures of oxygen and ammonia up to a value of 3:1 after which it became constant. As a result of their work, Nutt and Kapur conclude that the oxidation of ammonia to produce NO proceeds to completion entirely on the catalytic surface with no contribution from gas-phase reactions.

Taking this study as a point of departure, the Pt(100) crystal was prepared in a manner similar to that used in the above work. It was "activated" by heating in 5×10^{-4} torr of oxygen for two hours at 1300°K and then exposed to the ammonia beam. Since the effective

beam pressure is ca. 10^{-8} torr, the background oxygen pressure was reduced to 5×10^{-8} torr. The crystal temperature was then allowed to stabilize at 900°K and the angular distribution of the scattered NH_3 recorded. At no angle was there any trace of a signal at m/e = 30 corresponding to the formation of NO. Due to the large residual backgrounds at m/e = 18 and 28, no attempt was made to search for either H_2O or N_2. Unfortunately during this sequence of experiments the AES system was inoperative and consequently there was no way to check for the presence of surface nitrogen. The LEED pattern showed the (5×1) surface structure before and after the run, indicating at least that NH_3 does not form an ordered structure at 900°K on (100) platinum.

There are several possible conclusions to be drawn from this abortive experiment. First, assuming that the reaction did not take place, we must conclude that the (100) surface of platinum is inactive as an oxidation catalyst for ammonia. Morgan and Somorjai[106] have reported that oxygen does not chemisorb on the Pt(100)-(5×1) surface at either room or elevated temperatures, an observation which seems to contradict the strong chemisorption of oxygen noted during typical catalytic studies.[104] If the reaction of ammonia with an adsorbed oxygen atom is the rate controlling step in the ammonia oxidation as postulated,[158] then clearly no reaction can occur unless the oxygen chemisorbs. More recent work by Lang, Joyner, and Somorjai[159] has shown that oxygen will absorb on a stepped crystal surface (i.e., one containing ledges and terraces) in a manner not encountered on an

atomically flat, low index plane. Apparently the adsorption is atomic and occurs at the steps even at pressures as low as 3×10^{-8} torr and at room temperature. Heating the stepped crystals in oxygen led to surface disorder and then to reconstruction with a platinum oxide surface structure in one instance. Compared to the well-defined low index single crystal target used in the scattering work reported in this thesis, a polyscrystalline sample has large numbers of dislocation and point defects, grain boundaries, and steps--all of which could be effective in promoting oxygen adsorption. Hence it might be expected that a low index single crystal would be inactive in catalyzing the oxidation of ammonia unless its surface had been intentionally stepped by cutting the crystal at a small angle to the low index plane. Second, assuming that the reaction took place, our inability to find any reaction product implies either that the a.c. detection method failed because the surface residence time of the NO is long compared to the 150 Hz. beam modulation frequency, or that the sensitivity of the mass spectrometer was inadequate to detect the NO accumulated in the background. This latter instance might hold if the quantum yield is small, for in that case, the fact that we are operating in a pressure regime six orders of magnitude below that of Nutt and Kapur[157] would mean that the amount of NO produced would be undetectable.

2. Deuterium Oxidation and Hydrogen-Deuterium Exchange on (100) Platinum

a. Oxidation of Deuterium. Surprisingly few fundamental investigations of the oxidation of hydrogen (deuterium) have been made despite its simplicity and neither the mechanism nor the kinetics of the

surface catalyzed reaction has been sufficiently well resolved to preclude further study. The literature contains conflicting results concerning the rate of the reaction on a platinum catalyst. Donnelly and Hinshelwood[160] found that the rate is independent of the hydrogen pressure but depends upon the oxygen pressure in a complex manner. Others[161-163] have reported that the rate is either inhibited by or independent of the oxygen pressure but is proportional to the hydrogen pressure. Clearly an examination of this system by the current combination of techniques might yield a deeper insight into the mechanistic details of the reaction than has heretofore been available.

A very recent study by Smith and Palmer[41] utilizing modulated molecular beams has studied the oxidation of deuterium on an epitaxially grown (111) platinum single crystal film. The usual experimental arrangement was to impinge the D_2 beam onto the target which was maintained in an isotropic oxygen environment. Their data are consistent with a reaction mechanism involving the angularly dependent, activated adsorption of deuterium and the overall rate corresponds to the surface recombination of adsorbed deuterium atoms with an adsorbed oxygen molecule.

In spite of the previous failure to observe any products during oxidation of ammonia with our platinum single crystal surfaces, we have attempted to investigate the interaction of D_2 and O_2 because the apparatus employed by Smith and Palmer is similar to that used in this work, and a direct comparison of the reaction on the (100) single

crystal surface and the (111) orientation epitaxial platinum film would then be possible. From the data of Smith and Palmer the optimal surface temperature for the formation of D_2O appeared to be 825°K while small angles of incidence yielded higher $D_2 \rightarrow D_2O$ conversions rates than large angles. As previously discussed, the adsorption of CO is possible below 900°K on the Pt(100) surface and consequently it was decided to conduct the run at 925°K. An incident angle of 45° was chosen as the best compromise between decreasing conversion efficiency and the loss of data about the surface normal due to the size of the detector. Experimental measurements at $P_{O_2} \sim 3 \times 10^{-8}$ torr and $P_{O_2} \sim 3.5 \times 10^{-6}$ torr yielded no detectable modulated signal at m/e = 20 (D_2O), even at an angle of 15° from the surface normal. For a cosine product angular distribution such as that observed with the Pt(111) surface, the signal at $\theta_i = 15°$ should be roughly 97% of the $\theta_i = 0°$ value and hence observable if D_2O was formed in detectable quantities. The LEED pattern during this work showed the presence of the (5×1) surface structure.

Earlier we stated that the equivalent pressure of the incident molecular beam was about 10^{-8} torr. With a flux rate corresponding to a D_2 pressure at the target of approximately 10^{-8} torr, Smith and Palmer[41] found, depending upon the oxygen pressure, a D_2O signal of from two to six percent of the maximum value they observed with a flux rate greater by a factor of ten. Thus, the fact that we did not observe any D_2O may mean that it was below the sensitivity limit of the mass

spectrometer. It was noted, however, that the d.c. peak at m/e = 20 decreased sharply when the O_2 flow was terminated but this peak may have resulted from the presence of argon in the scattering chamber due to ion pump outgassing under high load conditions. Then again, the scattered D_2 signal was observed to be much weaker in the presence of $\sim 10^{-6}$ torr oxygen background than in a 10^{-8} torr oxygen ambient although part of the loss can be attributed to gas phase collisional scattering as well as to chemical reaction.

With the helium scattering data reported by Smith and Palmer[41] it becomes possible for the first time to compare scattering from epitaxial thin films and well-characterized single crystals of the same material. At comparable surface temperatures, Smith and Merrill[90] report slightly more intense and slightly narrower scattering patterns than those observed by Smith and Palmer.[41] Provided these differences are real, the lower maximum intensity implies that the thin film is somewhat rougher than the single crystal. Such microscopic roughness could easily facilitate the adsorption of oxygen due to the higher density of atomic steps on the surface as discussed in the previous section. For this reason, it would definitely be of interest to repeat the $D_2 + O_2$ experiments using a stepped surface to see whether or not a reaction is discernable.

b. Exchange of Hydrogen with Deuterium. Because the theoretical treatment is relatively simple and because the products and reactants are chemically identical, hydrogen exchange reactions have been widely studied in the past, primarily by classical techniques[104] although

molecular beam experiments have been attempted.[17,35] Generally speaking, the observed kinetics are uncomplicated. A standard technique for investigating the reaction mechanism has been to react adsorbed atoms of one isotope with a second isotope intially present only in the gas phase. The first successful molecular beam study of the HD exchange was reported by Palmer, Smith, Saltsburg, and O'Keefe.[40] They adapted the above approach by employing a steady-state hydrogen background and a modulated deuterium beam to probe the catalytic reaction of H_2 and D_2 to yield HD on the surface of a (111) epitaxial nickel film. Hydrogen, deuterium, and hydrogen-deuteride in the beam were all found to be scattered in an inelastic lobe directed at the specular angle. Surprisingly enough, however, the HD produced by the recombination of the incident D_2 from the beam with adsorbed hydrogen was distributed as $\cos^3 \theta_r$ rather than as $\cos \theta_r$ as one might have expected. Such results can be rationalized[46] if one assumes that the reaction product is formed by the simultaneous evaporation of proximate H and D atoms. Provided individual atoms on the surface conform to the cosine evaporation law, the HD product should be distributed at least as $\cos^2 \theta_r$. Further, if the probability of escape from the surface depends upon the normal component of the escape trajectory, then the angular distribution would indeed be $\cos^3 \theta_r$ as observed. Smith and Palmer[41] have conducted similar experiments on the (111) platinum surface described above. Again they have observed the $\cos^3 \theta_r$ dependence for the HD product.

In order to test the activity of the (100) surface toward exchange, the crystal was cleaned in oxygen as reported in Chapter II and then 8×10^{-8} torr of H_2 was admitted and the surface temperature allowed to stabilize at 925°K. The deuterium beam was next directed toward the target and the angular distribution of the unreacted D_2 was measured. Only near the surface normal could any trace of an a.c. signal at m/e = 3 be detected, thus confirming at least qualitatively the sharp peaking about $\theta_r = 0°$ observed by others.[40,41] Signal-to-noise limitations prevents a reliable quantitative measure of the scattered fraction, but the HD product did have a definite phase lag with respect to the main beam, which is what one would expect for a surface reaction. Further evidence to support the belief that HD was being produced at the crystal surface is provided by the observations that 1) when the incident D_2 beam was blocked by the Whittaker gate valve the d.c. m/e = 3 signal decreased somewhat, and 2) when the H_2 ambient was pumped away, the m/e = 3 signal degraded rapidly to zero. These latter two observations could also be attributed to the production of HD in the ion pump, but such an argument does not apply to the a.c. measurement. To study this system further requires an improvement in the signal-to-noise ratio of the detector. Such a change is now being made to allow pulse counting.

3. Thermal Dissociation of Hydrocarbons on (100) Platinum

Probably the most frequently studied surface reaction via molecular beams is the dissociation of molecules. Tungsten[35] and tantalum[17] ribbons have been used to investigate hydrogen dissociation and tungsten

surfaces have been employed to decompose nitrous oxide[57,58] and to form free radicals from methyl iodide, nitromethane, diethyl ether, and azomethane.[164]

Because of the peculiar ability of platinum to decompose unsaturated hydrocarbons at relatively low temperatures, it was felt that a study of the angular dependence of the scattered hydrocarbon decomposition products would make a useful contribution to the platinum literature and might shed some light on the poisoning of platinum catalysts by carbon (i.e., coking). It soon became apparent that the primary gas phase decomposition product (hydrogen) of the acetylene molecules was buried in the large residual hydrogen background of the scattering chamber. There could be little doubt that the gas was decomposing because definite changes were evident in the LEED pattern (ring formation - see Fig. IV-7a) and in the Auger spectrum. AES clearly showed the build-up of a carbon Auger peak shortly after exposure to the beam. A typical Auger trace has already been shown in Fig. IV-6. While one could plot the intensity of the Auger carbon transitions against beam exposure, such a calibration curve was not made because the ratio of the molecules reflected to those decomposed was not constant with time but decreased as the carbon deposit grew. Obviously carbon surfaces are not as efficient as platinum in promoting the dissociation.

Due to the difficulty of detecting the gas-phase dissociation product from the acetylene reaction, another molecule with a dissociation product at a useful mass number was sought. Eventually

methylenecyclobutane was chosen as the reactant. This molecule has a ring structure with an external unsaturated linkage and in the gas phase is known to decompose to ethylene and allene at moderate temperatures via a free radical intermediate. The heavier allene fragment (C_3H_4) produces a peak at m/e = 40 where there is only a small residual background in the scattering chamber. Figures V-20 and V-21 show the angular distribution of the allene product at two surface temperatures. Within the accuracy of the data, which is obtained by measuring the ratios of peak intensities, the decomposition product has a cosine angular distribution. Such a curve indicates that the evaporating species is in thermal equilibrium with the solid although we have no way at present to actually monitor the velocity distribution of the scattered molecules. No attempt was made to measure the angular distribution of the ethylene formed during the dissociation because of the large background at m/e = 28.

4. Dissociation of Nitrous Oxide on (100) Platinum

Once the technique for studying the dissociation products was shown to be satisfactory by investigating the dissociation of methylenecyclobutane, attention was focused on the molecular dissociation of nitrous oxide, N_2O. Coltharp, Scott, and Muschlitz had previously surveyed this reaction using a polycrystalline tungsten ribbon at surface temperatures between 1800 and 2500°K.[57,58] They found both N_2 and NO in the scattered beam and reported that at 2500°K the ratio of the two species (N_2/NO) was approximately 12 to 1. The emitted products were observed to have cosine angular distributions and the

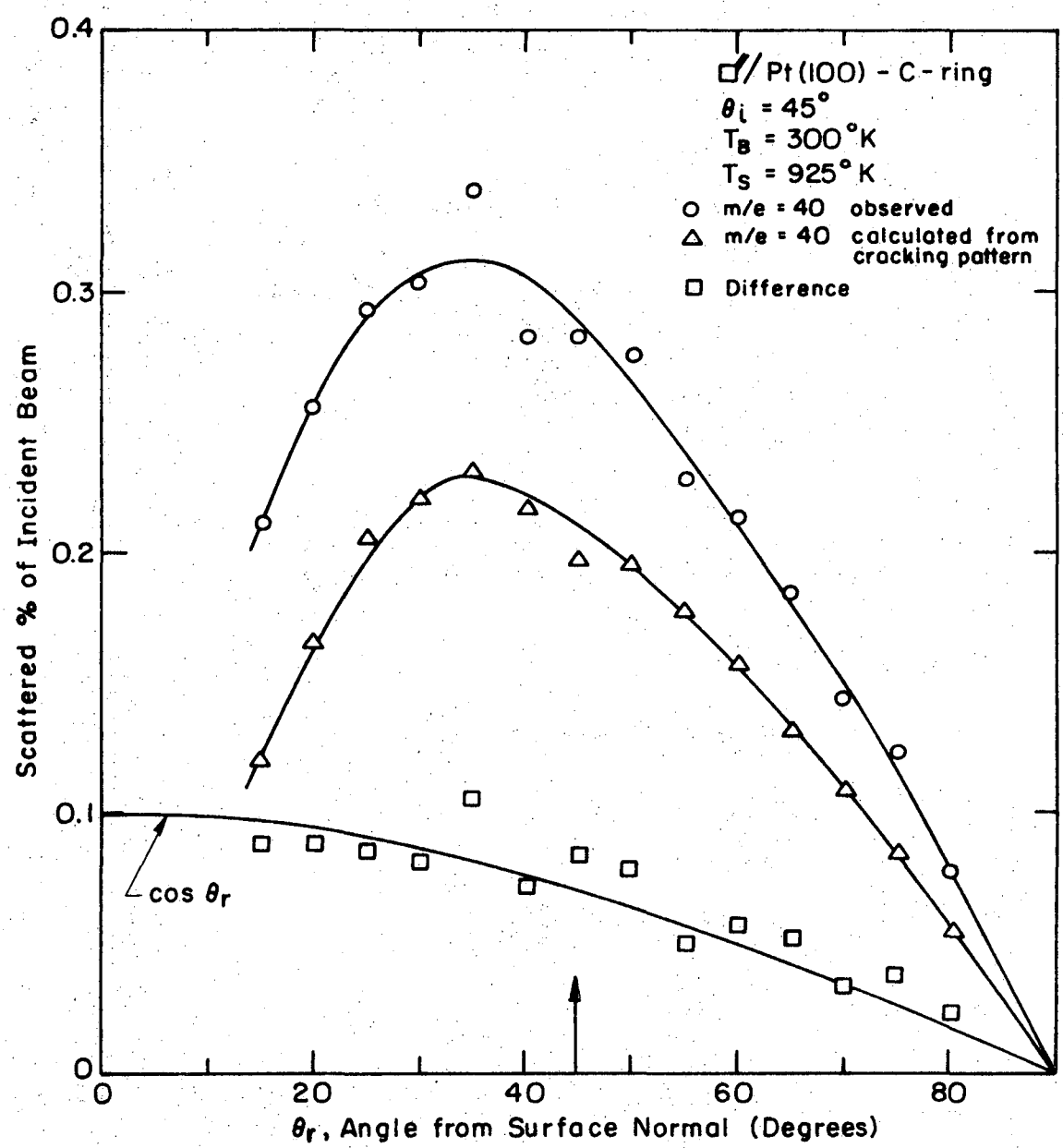

XBL 7110-7339

Fig. V-20. Dissociation of methylenecyclobutane to produce allene (and ethylene) at T_s = 925°K. The ordinate represents the scattered allene signal expressed as a percent of the incident C_5H_8 beam strength.

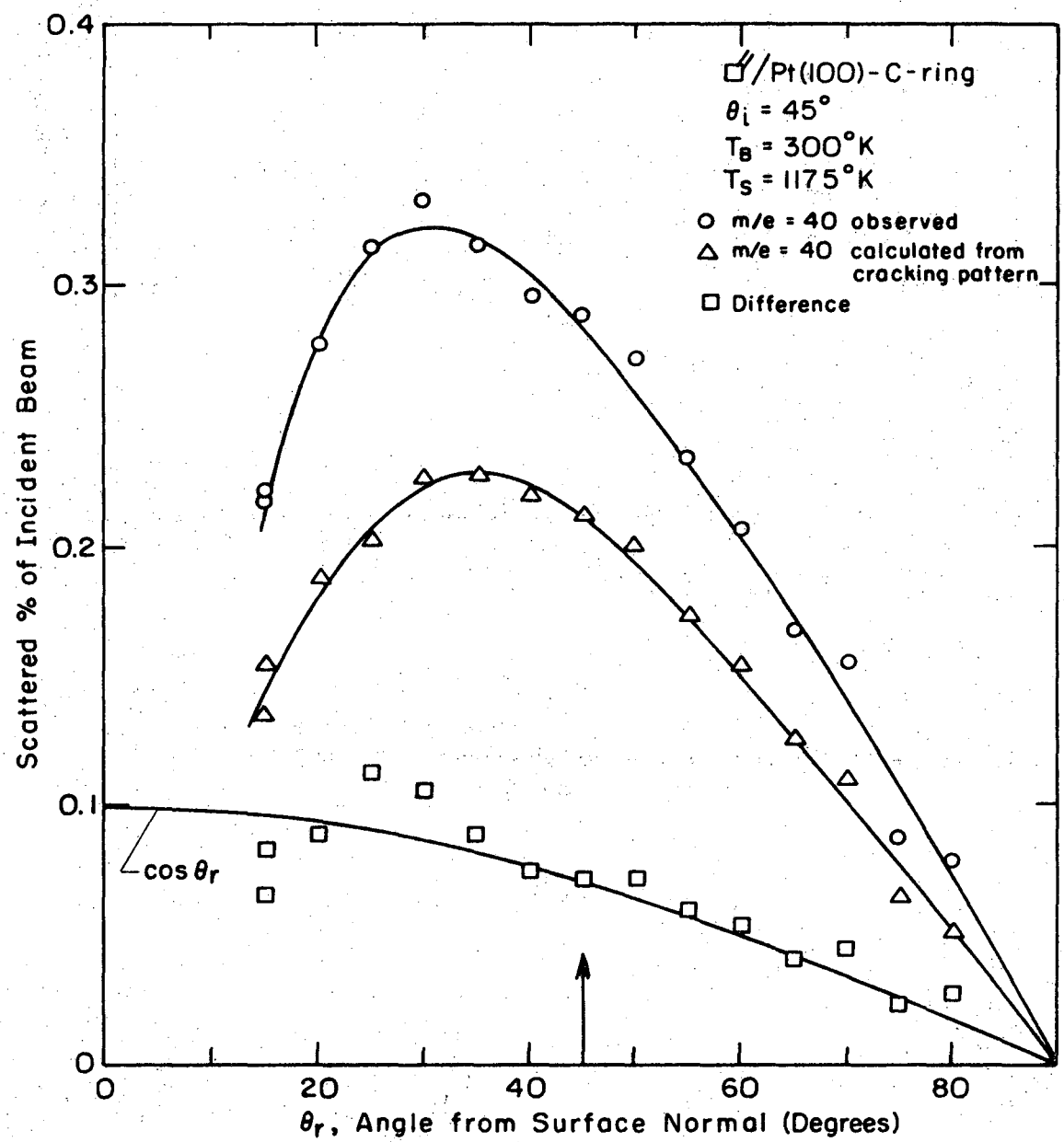

Fig. V-21. Dissociation of methylenecyclobutane to produce allene (and ethylene) at T_s = 1175. The ordinate represents the scattered allene signal expressed as a percent of the incident C_5H_8 beam strength.

N_2O decomposition probability was found to approach unity at high temperatures. Unfortunately, there can be some doubt whether these observations represent a true catalytic reaction because energy accommodation between the gas and the hot solid could induce thermal decomposition.

N_2O is a linear molecule ($\bar{N} = \overset{+}{N} = O$).[137] Spectroscopic studies indicate that the energy of the NN bond is 113.7 kcal/mole while the energy of the NO bond is 38.7 kcal/mole. Photochemical dissociation of gaseous N_2O yields primarily N_2 with atomic oxygen subsequently undergoing further chemical reactions with other N_2O molecules to form NO and O_2.

$$N_2O \xrightarrow[(a)]{} N_2 + O \begin{cases} \xrightarrow[(b)]{+N_2O} NO + NO \\ \xrightarrow[(c)]{+N_2O} N_2 + O_2 \end{cases} \qquad \text{(V-18)}$$

Scattering experiments were carried out from both clean and carbon covered (100) platinum surfaces at temperatures between 900 and 1500°K to investigate the role of the substrate in the dissociation of nitrous oxide. Although the background pressure in the scattering chamber can be as low as 5×10^{-10} torr, during the higher temperature experiments the ambient pressure sometimes rose to as high as 10^{-8} torr due to outgassing of the system walls by radiant heating. Hydrogen, carbon monoxide, carbon dioxide, and water vapor are the dominant species in the background gas. Carbon was deposited on the platinum surface by cracking acetylene as described in section B-1 of this

chapter. To clean the surface, the crystal was heated at an elevated temperature in the presence of 10^{-6} to 10^{-5} torr of oxygen for half an hour.

Electron impact ionization of N_2O in the mass spectrometer detector yields predominantly the molecular ions N_2O^+ and NO^+ with a smaller amount of N_2^+. The observed cracking, pattern, which was found to be very sensitive to the ionizer potentials, is listed in Table V.5 along with values reported in the API tables for a magnetic instrument. While the quadrupole sampled the gas phase species, the crystal surface structure was monitored <u>in situ</u> by LEED and the chemical composition of the surface was ascertained by AES when desirable. The latter technique yielded a valuable piece of information concerning the surface reaction.

Since the scattering of N_2O and other nitrogen oxides from both clean and carbon covered platinum surfaces has been studied, it is worth while to consider the various possible reactions that may occur as the result of the collision at the gas-solid interface. These are listed in Table V.6 along with the corresponding enthalpy changes. The change in free energy for reactions V-20, 22 and 23 are negative at the temperatures of this work, indicating that all are thermodynamically feasible. However, because the scattering experiments are carried out far from thermodynamic equilibrium, it is likely that kinetic factors (i.e., the relative magnitude of reaction rates at a given temperature) will predominate. This is apparent from the fact that Coltharp et al. observe both NO and N_2 in the scattered beam in the case of tungsten.

0 0 0 0 3 6 0 5 5 6 7

Table V.5. N_2O Cracking Pattern

m/e	Relative Intensity	
	Quadrupole	API*
28	.223	.108
30	.436	.311
44	1.000	1.000

* Serial No. 96, Mass Spectral Data, American Petrolium Institute Research Project 44.

Table V.6. Thermodynamics of Nitrogen Oxides for the Carbon-Platinum System[165]

Reaction	ΔH^{o}_{298}(kcal/mole)	Equation
$N_2O(g) \xrightarrow{Pt} N(g) + NO(g)$	+ 115.1[a,b]	(V-19)
$N_2O(g) \xrightarrow{Pt} O(ads) + N_2(g)$	- 40.7[c]	(V-20)
$N_2O(g) + C(s) \xrightarrow{Pt} N_2(g) + CN(g)$	+ 111.8[a,d]	(V-21)
$N_2O(g) + C(s) \xrightarrow{Pt} N_2(g) + CO(g)$	- 46.1	(V-22)
$2N_2O(g) + C(s) \xrightarrow{Pt} 2N_2(g) + CO_2(g)$	- 135.4	(V-23)
$NO(g) + C(s) \xrightarrow{Pt} N(g) + CO(g)$	+ 65.0[a,b]	(V-24)

[a] The free radical was considered to be produced in the gas phase for the enthalpy calculation. Depending upon the heat of adsorption of this species, the reaction may or may not be endothermic as written.

[b] Mimeault and Hansen[166] have reported that the heat of adsorption of atomic nitrogen on filaments of rhodium and irridium is 58 kcal/mole. The value for platinum should not be too much different from this.

[c] The heat of adsorption of O on Pt calculated from the data of Cassel and Glückauf[167-170] = -80.8 kcal/mole.

[d] Because CN is in the gas phase, this enthalpy contains the heat of sublimation of carbon (170.9 kcal/mole). Atomic nitrogen would probably react with solid carbon to form a C - N chemical bond. Consequently, subtracting 170.9 from the above value of ΔH yields $\Delta H \sim -59$ kcal/mole. In the gas phase, the strength of the CN bond is 175 kcal/mole (from Table V.2) which we can use to approximate the enthalpy for the reaction

$$C(s) + N(g) \rightarrow CN(ads) \quad \Delta H \sim -175 \text{ kcal/mole}$$

Adding this equation to Eq. (V-19) would give Eq. (V-21) with a $\Delta H \sim -60$ kcal/mole which agrees with our earlier value as it should.

While the free energy change for reaction V-21 can only be estimated, it also appears to be a likely reaction since the overall enthalpy change is probably negative due to the strength of the CN bond (175 kcal in the gas phase). If the heat of adsorption of atomic nitrogen on platinum is similar to that for oxygen, then reaction V-24 also has a negative enthalpy. Of course when the adsorbed nitrogen atoms combine to yield gaseous N_2, reactions V-19 and V-24 are both very exothermic. Even though experiments have shown that N_2O does not adsorb on (100) platinum in the temperature range of this study, Auger electron spectroscopy indicates the presence of nitrogen on the carbon covered surfaces (see Fig. V-22). Low energy electron diffraction studies demonstrate that N_2O does not form an ordered surface structure at 300°K.

a. Results. From equations V-19 through V-24 in Table V.6, it is apparent that all the potential gaseous reaction products have atomic masses of 28, 30, or 44. These species can result from either the catalytic dissociation of N_2O on platinum, or from the surface reaction of N_2O with carbon [NO(m/e = 30), N_2(m/e = 28), CO_2(m/e = 44)], or from the electron impact ionization of unreacted N_2O in the mass spectrometer ionizer [N_2O (m/e = 44), N_2 (m/e =38), NO(m/e = 30)]. Due to the presence of carbon monoxide in the ambient, the peak at m/e = 28 cannot reliably be monitored during the experiment because random noise from the high d.c. background saturates the detection electronics. Thus we have monitored the ion ratio NO^+/N_2O^+ throughout the experiment

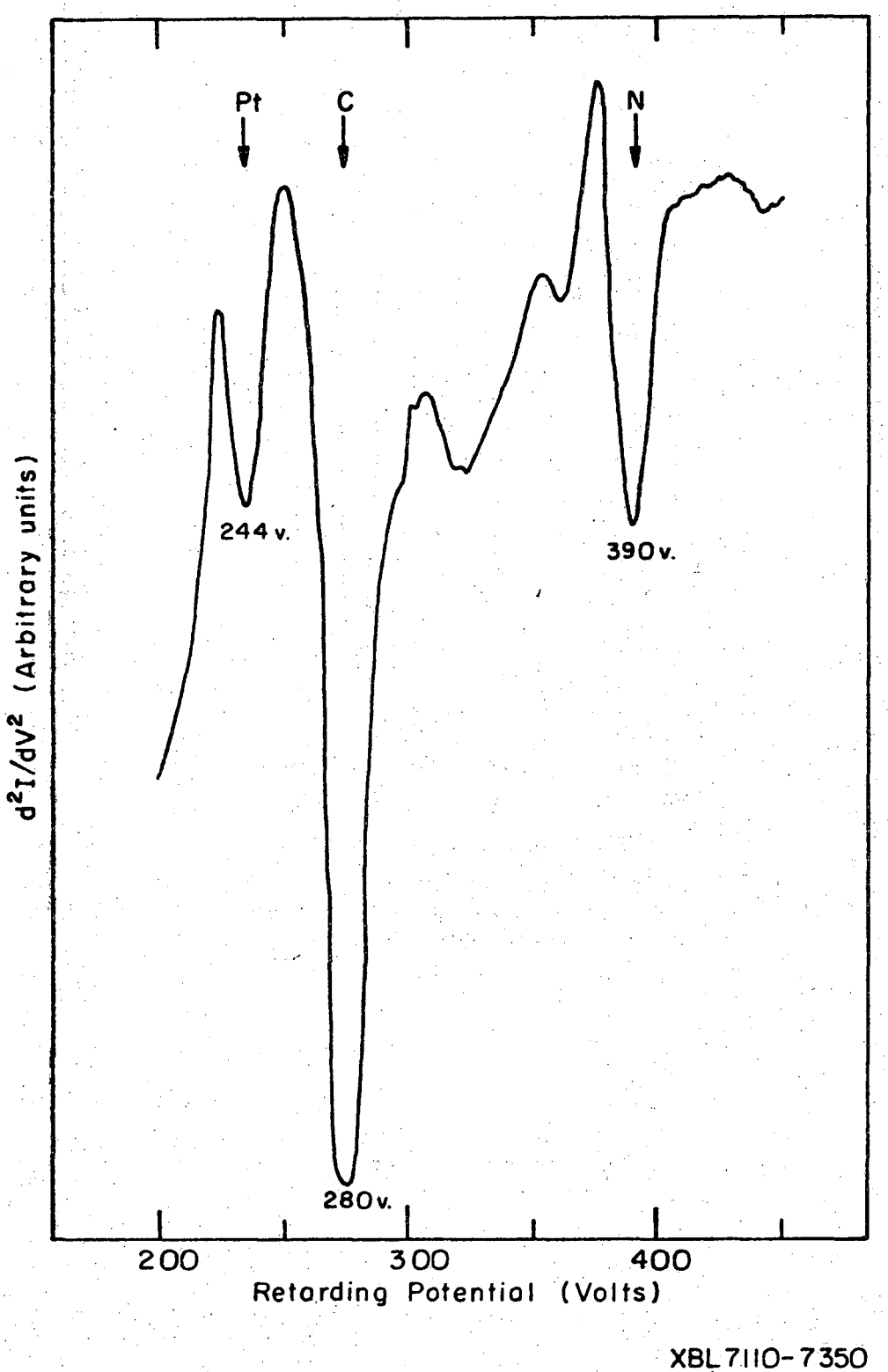

Fig. V-22. Auger spectrum of carbon covered platinum surface after a N_2O decomposition run.

as a function of scattering angle and surface temperature, comparing the observed ratio in the scattered beam with that in the incident beam. We have assumed that the NO^+/N_2O^+ ratio from the ionization of N_2O is independent of the vibrational energy of the molecule. In view of the small number of vibrational modes, their relatively large energy spacing compared to kT (See Table V.3), and the fact that vibrational transitions are optically allowed (thus permitting energy release via radiation) this assumption should be justified in the case of N_2O. If the NO^+/N_2O^+ ratio (henceforth we shall refer to this ratio as $\mathcal{R}$) increases with respect to that of the incident beam after surface scattering, NO molecules have been formed by the dissociation of N_2O at the platinum surface. If $\mathcal{R}$ remains unchanged, presumably the reactive scattering produced N_2 and O as this process would not change the ratio. Of course, a ratio that remains unchanged may also indicate that the reaction did not take place at a detectable rate on the surface. If $\mathcal{R}$ decreases, it can only be due to a chemical reaction that produces CO_2(m/e = 44) since within our mass resolution, the ion signals from N_2O^+ and CO_2^+ are indistinguishable. The smaller value of $\mathcal{R}$ arises because the CO_2^+ intensity increases the denominator of the NO^+/N_2O^+ ratio.

We have found indications that all of the reactions that can affect the NO^+/N_2O^+ ratio can take place in the temperature range of this study (900-1500°K) using clean and carbon covered (100) platinum surfaces. Figures V-23 and V-24 show the angular distributions of

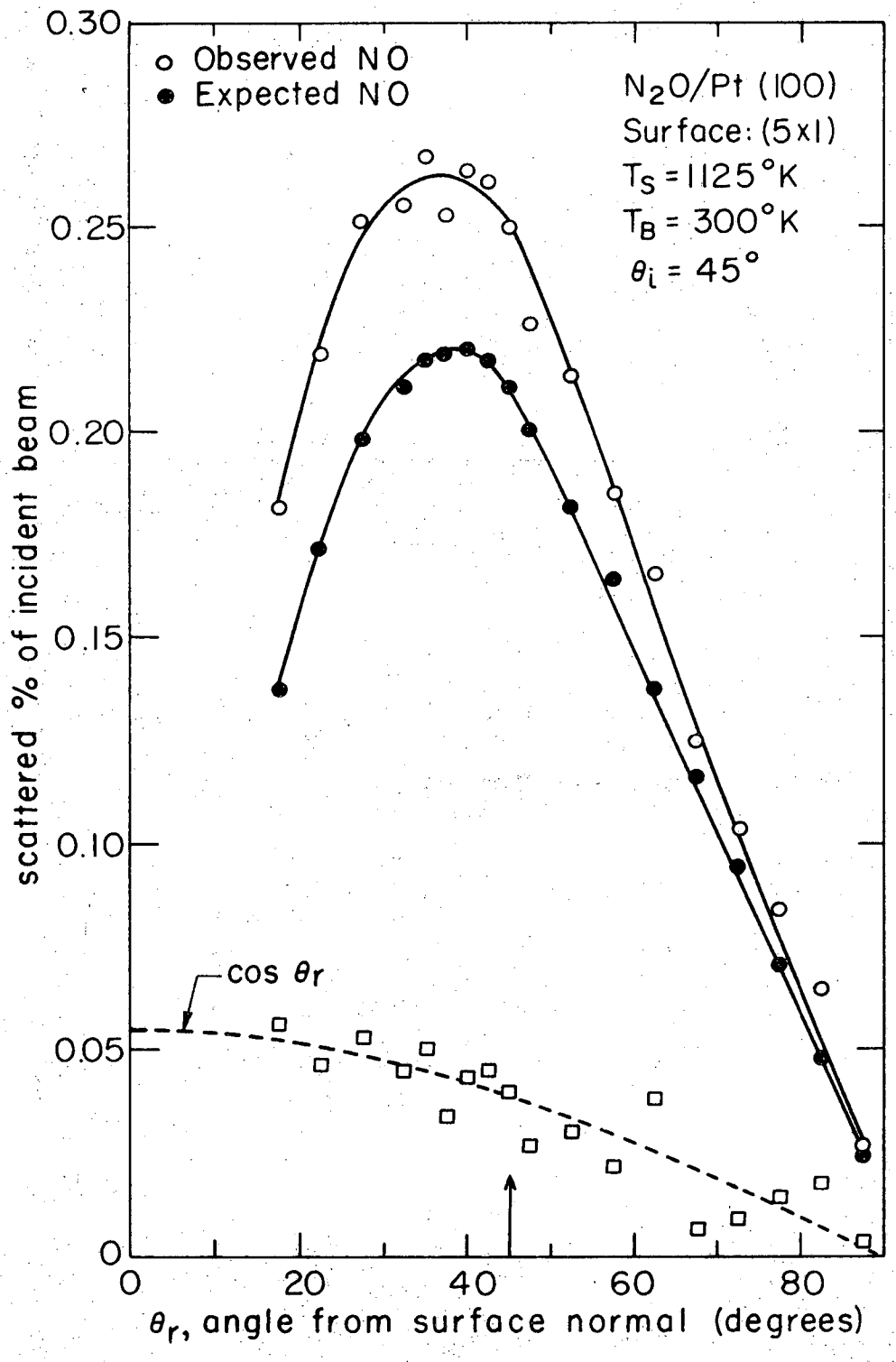

XBL 7012-7440

Fig. V-23. Dissociation of nitrous oxide on cleam platinum to yield nitric oxide. The ordinate represents the scattered NO signal expressed as a percent of the incident N_2O beam strength and the expected NO results from multiplying the measured N_2O scattering distribution by the cracking pattern.

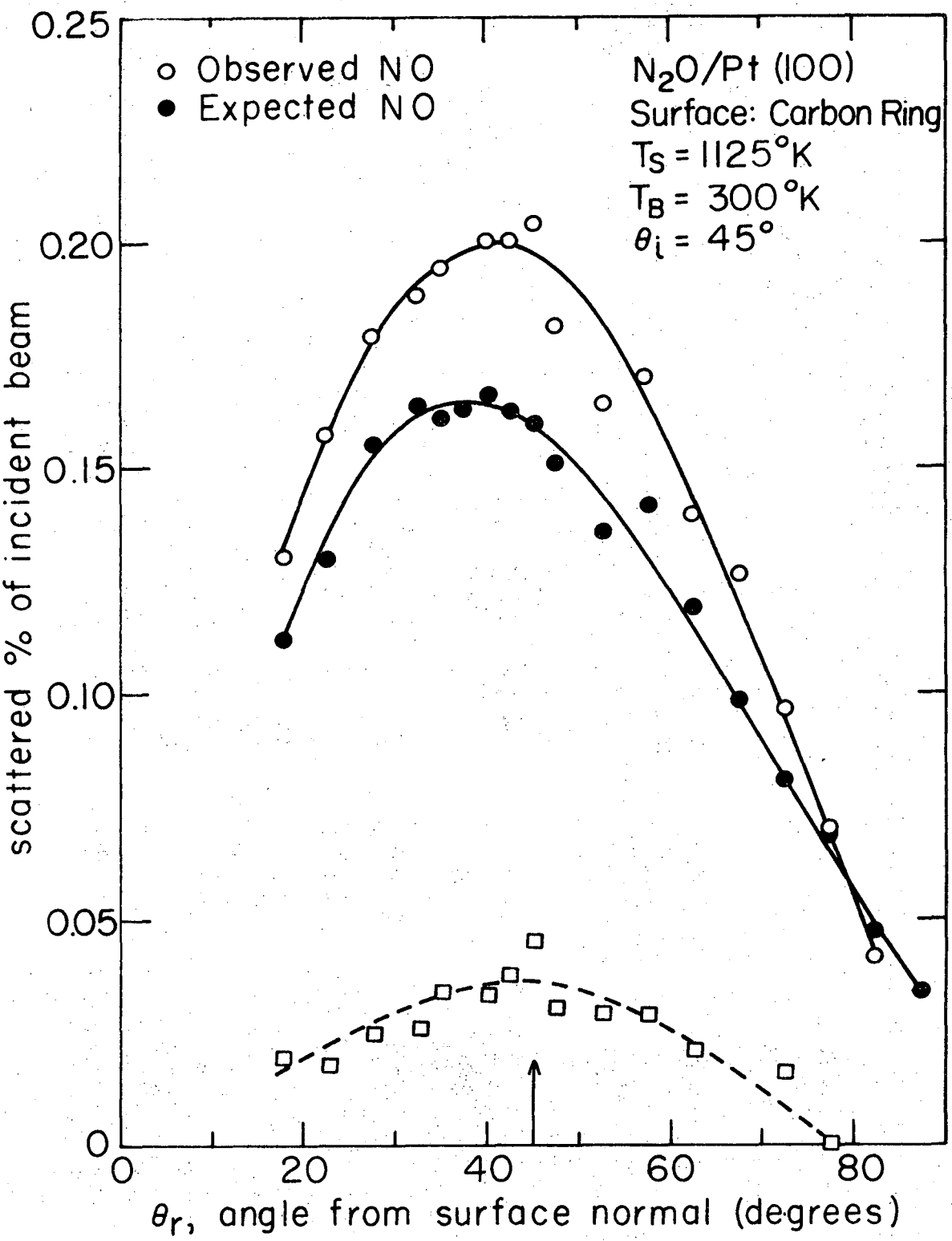

XBL 7012-7438

Fig. V-24. Dissociation of nitrous oxide on graphite covered platinum to yield nitric oxide. The ordinate represents the scattered NO signal expressed as percent of the incident N_2O beam strength.

the scattered ratio $\mathcal{R}$ at T_s = 1125°K from a clean and a carbon covered surface, respectively. The intensities have been normalized to the strength of the incident beam, and the arrow indicates the angle of incidence. The solid circles show the ratio obtained from the fragmentation pattern while the open circles indicate the observed ratio; by subtraction one obtains the angular distribution of that portion of the NO that is the result of the dissociation at the platinum surface. It appears that the angular distribution of the product NO molecules formed by dissociation at the clean platinum surface is of the cosine type, indicating complete thermal accommodation of the NO molecule on the surface prior to reemission. The angular distribution is quite different, however, for the NO product molecules that are scattered from carbon covered platinum surfaces at 1125°K. As is shown in Fig. V-24, the dissociation product does not peak at the surface normal and the angular distribution is not cosine. Such a peaked angular distribution reflects a lack of energy accommodation during the surface dissociation reaction of N_2O on the carbon-covered platinum surface and suggests a direct reactive scattering mechanism. To put it in other terms, the non-cosine spatial distribution implies that the incident particles "remember" their initial direction of approach. In order for this to be possible, the reaction must proceed in a time short compared to the length of the collision and this places an upper limit of 10^{-12} seconds on the reaction time.

The angular distribution and the ratio $\mathcal{R}$ are sensitive functions of the surface carbon concentration. Frequently, especially at higher temperatures, N_2O beam scattering from the platinum (100) surface yielded an $\mathcal{R}$ that was smaller than in the incident beam. Such negative deviations from the fragmentation ratio reflect the formation of CO_2 as a result of the chemical reaction between the incident N_2O and surface carbon. In fact, it has been found that during long periods of N_2O exposure at about 1300°K the surface carbon could be completely removed unless acetylene was added to the ambient background to replenish the carbon deposit on the platinum surface. A similar phenomenon was noted with nitric oxide. After a five hour exposure to the NO beam, it was found that the surface carbon had been removed. This latter observation lends credibility to our contention that the heat of adsorption of atomic nitrogen is a least 65 kcal/mole as Eq. (V-24) would require. It also has significance to antipollution studies in which people are striving to reduce or eliminate nitric oxide emissions associated with the operation of the internal combustion engine.

In a few instances, using either clean or carbon coated platinum surfaces, the value of $\mathcal{R}$ remained unchanged, indicating that in some manner the surface had been passivated, or that the reaction products had changed to predominantly N_2 and O. Unfortunately this latter possibility could not be investigated in either the a.c. or d.c. detection modes due to the relatively large concentration of CO in the background.

b. Discussion. N_2O may undergo a variety of different chemical surface reactions upon scattering from platinum surfaces. It appears that most of the reactions that have been considered in Eq. (V-19) through (V-24) can and do take place in the temperature range of this study. A clean platinum surface seems to dissociate N_2O only poorly; at the surface temperatures employed in this work only a few percent of the incident molecules undergo bond breaking. This reaction appears to be endothermic and shows only a small temperature dependence. The incident molecules that dissociate are fully accommodated at the surface before reemission as indicated by the cosine angular distribution of the scattered beam. On the carbon covered platinum (100) surface, the scattering process appears to be entirely different. Due to the interaction between N_2O and surface carbon, the surface reaction can be strongly exothermic. As a result, it appears that evidence for a direct reactive scattering mechanism has been detected. Such scattering has not previously been observed on surfaces although it is common in the gas phase.[3,4] The NO molecules are reflected without energy accommodation between the incident beam and the surface as indicated by the non-cosine angular distribution of the scattered product in Fig. V-21. Direct scattering is commonly observed in crossed molecular beam studies of chemical reactions that are exothermic and exoergic [for example, $K + CH_3I \rightarrow KI + CH_3$[171]].

The evidence for direct scattering of N_2O on the carbon covered platinum surfaces is not quite conclusive, however, since the NO^+/N_2O^+ ratio depends upon both the carbon concentration at the surface and the

surface temperature. Other surface reactions between N_2O and carbon can compete with the reaction mechanism yielding the direct interaction. In addition, the possibility that the scattered N_2O molecules may be vibrationally excited and thus give rise to a different NO^+/N_2O^+ ratio cannot be ruled out. Clearly more studies are needed to verify the results that suggest direct scattering of NO product molecules. It is hoped that more conclusive evidence will be accumulated in the near future by continued work in this laboratory.

VI. CONCLUSIONS AND RECOMMENDATIONS

This thesis clearly demonstrates that non-reactive and reactive scattering of molecular beams can provide detailed information about the dynamics of gas-surface interactions and can be studied by present techniques. An ultra high vacuum system has been built and, through the use of differential pumping techniques, it has been demonstrated that molecular beam scattering studies of clean, well-characterized single crystals are feasible. Precise control of the gas composition, temperature, angle of incidence, and intensity are possible with a beam. From the angular distribution of the scattered particles, and knowing the angle of incidence and initial energy of the beam, one can investigate the elementary energy transfer processes that occur during the collision of a gas with a solid surface. Without such techniques the direct reactive scattering of N_2O from carbon covered platinum crystal surfaces could not have been observed.

Low energy electron diffraction has been employed to monitor the structure of the Pt(100) surface and the surface structure of adsorbed molecules throughout these studies. Auger electron spectroscopy has been used to monitor the chemical composition of the surface before, during, and after the scattering experiments and to detect changes in the surface composition as the result of reactive scattering. Together these two techniques provide an understanding of the surface structure and composition that is invaluable to the analysis of the scattering data.

It has been shown how combined LEED and helium atomic beam scattering can be used to probe the surface topography and to investigate the adsorption of gases. Low energy electron diffraction is inherently sensitive only to ordered surface coverage but the intensity of the scattered helium beam provides a measure of total surface order. We have measured the scattering of helium from disordered platinum surfaces, carbon covered platinum surfaces, and ordered Pt(100) surfaces exhibiting the (5×1) surface structure. In all cases the maximum reflected intensity occurred at the specular angle and its magnitude proved to be a sensitive function of the atomic order in the surface. The scattering of helium from surface structures of adsorbed acetylene and carbon monoxide was also carried out. While our measurements have not resolved the question of whether or not the (5×1) surface structure observed on the Pt(100) crystal face is impurity stabilized, the helium scattering results do prove that no light molecular weight species such as oxygen can be present on the surface in a weakly bound state. This and the Auger spectra of platinum surfaces exhibiting the (5×1) surface structure lends strong support to the arguments in favor of a clean surface.

The non-reactive scattering of several diatomic and polyatomic molecules (N_2, NO, CO, O_2, H_2, D_2, N_2O, NO_2, CO_2, C_2H_2, NH_3, and C_5H_8) has been studied. It was found that the spatial distributions of the scattered species were non-cosine under most of the experimental conditions, thus indicating the lack of rapid energy accommodation between the clean single crystal surface and the incident molecules. There is

evidence, however, that increased surface roughness on an atomic scale enhances the probability of energy accommodation between the surface and the incident polyatomic molecules.

At a constant surface temperature, the scattering of polyatomic species seems to show a qualitative correlation between the observed scattered intensity maxima and dispersion and the known strength of the gas-solid interaction potential as measured by the heat of adsorption. Calculations have been presented to show what type of experiments might be conducted in the future to probe the nature of the energy transfer between polyatomic gases and well-defined surfaces. Vibrational de-excitation of incident molecules by the solid surface might be investigated by comparing the scattering of molecules in an excited vibrational state to those in the ground state.

The reactive scattering of N_2O, C_2H_2, and C_5H_8 has been studied. Long residence times accompanied by complete energy accommodation during thermal dissociation is indicated by the spatial scattering distribution in the case of methylenecyclobutane on the Pt(100) surface. There is evidence, however, that N_2O molecules can undergo a faster type of reaction resulting in a non-cosine angular distribution if there is carbon on the platinum surface.

The surface reaction between D_2 beams and O_2 or H_2 in the ambient has been attempted. Contrary to the observations of others, we were not able to detect evidence for significant chemical reaction. Most probably the absence of atomic steps and other lattice defects that

facilitate the chemisorption of O_2 and H_2 is responsible for this failure to obtain reaction.

Currently the study of chemical reactions, while possible, is hampered by signal-to-noise limitations. This was evident from our inability to quantitatively follow the scattered HD signal in the hydrogen-deuterium experiment. Before further systems are investigated it would be advisable to improve the sensitivity of the apparatus. There are at least three ways in which this might be done: (1) increase the strength of the incident beam by the use of a supersonic nozzle or by shortening the beam flight path; (2) decrease the scattering chamber background still further by the addition of cryopumping, and (3) convert the detection system to a pulse counting mode so that effectively longer time constants can be used in the meaurements. If the pulse counting method is chosen, time-of-flight capabilities could later be added to yield the energy distribution of the scattered particles. This is the one piece of information most necessary to gaining a fuller understanding of the gas-solid interaction.

Once the system sensitivity has been increased, the ammonia oxidation reaction should be reinvestigated, both on the clean and carbon covered surfaces. AES should be employed to test for the presence of surface nitrogen during the reaction. Should the reaction again fail, a stepped surface could be substituted for the smooth, low index (100) plane to see whether our hypothesis concerning the higher reactivity of epitaxial films is born out.

Rather than attempting further dissociation reactions that usually yield products at some mass number with a non-zero background, addition reactions may prove easier to study. One such reaction might occur between an adsorbed hydrocarbon (say acetylene) and a beam of hydrogen atoms to produce a gas-phase product (ethylene or ethane). Alternatively, a hydrocarbon beam could be scattered from a surface containing atomic hydrogen (e.g., a palladium crystal saturated with hydrogen). One dissociation reaction worth study, however, would appear to be the H_2S-platinum system. Sulfur is a common catalyst poison in many industrial processes and we have already seen that our platinum samples are free of detectable sulfur. Thus it would be interesting to use AES, LEED, and molecular beam scattering to see whether H_2S will decompose at a platinum surface. Along this same line, vanadium has a strong affinity for sulfur and a study of the H_2S decomposition at this surface might provide an interesting comparison to platinum. The dissociation of azomethane might also be investigated.

In the realm of non-reactive scattering, once a method to obtain the velocity distribution of the scattered gases is achieved, surface lattice dynamics could be studied in a manner similar to neutron scattering.[172] A determination of the surface phonon distribution for a series of metals could provide the impetus for more theoretical studies of surface modes and could eventually help lead to an understanding of the adsorption and desorption processes.

VII. APPENDIX

A. Computer Programs

The following pages contain print-outs of computer codes used in the processing of data collected in this work. Program DATACON was used in the analysis of molecular beam scattering results as described in section B-7 of Chapter II. A typical set of input and output information follows the listing to acquaint the reader with the use of the program. Subroutines PLOTIT and PLOTTER are plotting routines that employ the output printers to display results on an x-y grid while subroutine LINEUP merely scales the numbers to be plotted. The analysis of LEED photographs sometimes requires the evaluation of lattice parameters from the separation of diffraction spots and, while the calculation is straight forward, a table of spot spacing versus gun voltage was found to be invaluable for this purpose. Program SPACING requires only the focal lenght of the lens and the picture magnification to produce a table such as that following the program listing. The value of Y is the distance between the (00) spot, which must be placed at the center of the screen, and the spot of interest, and YMAX is the radius of the screen in the photograph.

Occasionally, the Vidar Data Acquisition System was employed to record signal levels during an experiment. To extract the information from the punched paper tape output of the Vidar, it was necessary to write a computer program. This routine, called FRAMCON, is listed along with extensive documentation on its use to assist future operators of the DAS in retrieving their data.

```
      PROGRAM DATACON (INPUT,OUTPUT,TAPE1=INPUT,TAPE3=OUTPUT)
C
C     THIS PROGRAM CONVERTS RAW DATA FROM MBA-ECHO SCATTERING
C     EXPERIMENTS TO THE PERCENT OF THE INCIDENT BEAM
C     INPUT DATA - 1 CARD WITH NUMBER OF DATA PTS, REF SCALE,
C     SIG SCALE, CORRECTION FACTOR, INCIDENT ANGLE, IN FORMAT
C     (I2,5X,2(F7.3,5X),F6.2,5X,F5.1), N CARDS WITH LAB ANGLE,
C     REF IN PHASE, REF OUT OF PHASE, SIG IN PHASE, SIG OUT OF
C     PHASE IN FORMAT((5(F5.1,5X)), AND 1 CARD WITH A 1 IN COL
C     ONE IF MORE DATA DECKS FOLLOW AND A 0 OTHERWISE
C     THE CORRECTION FACTOR CONVERTS THE REF SIGNAL FROM THE
C     VALUE MEASURED AT 180 DEG. TO THAT AT 0 DEG.
C
      DIMENSION ANG(50),RIN(50),ROUT(50),SIN(50),SOUT(50),
     1  RPHI(50),SPHI(50),PERCNT(50)
      EQUIVALENCE (ROUT,RPHI),(SOUT,SPHI)
      RADANG=180./3.1415927
      BMLINE=180.
7     READ(1,1) N,REF,SIG,COR,ANGINC
      DO 2 I=1,N
      READ(1,3) ANG(I),RIN(I),ROUT(I),SIN(I),SOUT(I)
      ANG(I)=BMLINE-ANGINC-ANG(I)
      RPHI(I)=ATAN(ROUT(I)/RIN(I))
      SPHI(I)=ATAN(SOUT(I)/SIN(I))
      RIN(I)=0.01*REF*RIN(I)/COS(RPHI(I))
      SIN(I)=0.01*SIG*SIN(I)/COS(SPHI(I))
      PERCNT(I)=100.*COR*SIN(I)/RIN(I)
      RPHI(I)=RPHI(I)*RADANG
      SPHI(I)=SPHI(I)*RADANG
2     CONTINUE
      WRITE(3,4)
      WRITE(3,5) (ANG(I),RIN(I),RPHI(I),SIN(I),SPHI(I),
     1  PERCNT(I),I=1,N)
      READ(1,6) MORE
6     FORMAT(I1)
      IF(MORE.EQ.1) GO TO 7
      STOP
C
1     FORMAT(I2,5X,2(F7.3,5X),F6.2,5X,F5.1)
3     FORMAT(5(F5.1,5X))
4     FORMAT(1H1,5X,5HANGLE,6X,9HREFERANCE,6X,5HPHASE,6X,
     1  6HSIGNAL,6X,5HPHASE,6X,7HPERCENT,/,6X,5H(DEG),8X,
     2  4H(MV),9X,5H(DEG),7X,4H(MV),7X,5H(DEG),///)
5     FORMAT(6X,F5.1,7X,2(F8.3,5X,F6.2,4X),F7.3)
      END
```

```
C       TYPICAL SET OF DATA

09      500.        5.          1.1221      45.
120.        78.2        11.0        29.4        0
115.        78.6        10.6        39.0        0
110.        81.0        10.7        42.5        0
105.        81.6        10.8        48.0        0
100.        80.1        10.9        47.0        0
95.         79.7        10.8        49.0        0
90.         79.0        10.0        43.0        0
85.         78.9        09.8        40.0        0
80.         78.2        10.3        33.0        0
1-MORE
05      500.        2.          1.1221      45.
80.         78.1        10.5        86.5        0
75.         77.6        10.3        78.0        0
70.         76.5        09.2        63.0        0
65.         76.0        09.0        55.0        0
60.         75.4        09.0        38.0        0
1-MORE
02      500.        1.          1.1221      45.
60.         75.2        09.0        81.0        0
55.         75.7        09.0        55.0        0
0-MORE
```

C TYPICAL PROGRAM OUTPUT

ANGLE (DEG)	REFERANCE (MV)	PHASE (DEG)	SIGNAL (MV)	PHASE (DEG)	PERCENT
15.0	394.849	8.01	1.470	0.	.418
20.0	396.558	7.68	1.950	0.	.552
25.0	408.518	7.53	2.125	0.	.584
30.0	411.558	7.54	2.400	0.	.654
35.0	404.191	7.75	2.350	0.	.652
40.0	402.142	7.72	2.450	0.	.684
45.0	398.152	7.21	2.150	0.	.606
50.0	397.531	7.08	2.000	0.	.565
55.0	394.377	7.50	1.650	0.	.469

ANGLE (DEG)	REFERANCE (MV)	PHASE (DEG)	SIGNAL (MV)	PHASE (DEG)	PERCENT
55.0	394.013	7.66	1.730	0.	.493
60.0	391.403	7.56	1.560	0.	.447
65.0	385.256	6.86	1.260	0.	.367
70.0	382.655	6.75	1.100	0.	.323
75.0	379.676	6.81	.760	0.	.225

(DEG) ANGLE	(MV) REFERANCE	(DEG) PHASE	(MV) SIGNAL	(DEG) PHASE	PERCENT
75.0	378.683	6.82	.810	0.	.240
80.0	381.166	6.78	.550	0.	.162

```
      SUBROUTINE PLOTIT (X,Y,NUM)
C
C     THIS SUBROUTINE, GIVEN A SET OF N X-Y COORDINATES, WILL
C     PLOT THEM ON A 51 BY 101 XY GRID.  OUT OF RANGE POINTS
C     ARE IGNORED.  THE X AND Y ARRAYS ARE UNAFFECTED.
C
      DIMENSION X(1), Y(1), XGRID(11), YGRID(11), GRID(101)
      DIMENSION BLA(37)
      DIMENSION ROUND(4)
      DATA (BLA(I),I=1,37)/1H ,1H*,1H2,1H3,1H4,1H5,1H6,1H7,1H8,
     * 1H9,1HA,1HB,1HC,1HD,1HE,1HF,1HG,1HH,1HI,1HJ,1HK,1HL,
     * 1HM,1HN,1HO,1HP,1HQ,1HR,1HS,1HT,1HU,1HV,1HW,1HX,1HY,
     * 1HZ,1H$/
      DATA NROUND,(ROUND(I),I=1,4)/4,1.0,2.0,2.5,5.0/
      INTEGER BLA,GRID
      CALL LINEUP (X,NUM,ROUND,NROUND,10.0,XMIN,XMAX)
      CALL LINEUP (Y,NUM,ROUND,NROUND,10.0,YMIN,YMAX)
   20 T1 = (XMAX - XMIN) / 10.
      T2 = (YMAX - YMIN) / 10.
      XGRID(1) = XMIN
      YGRID(1) = YMAX
      DO 25 I = 2, 11
      XGRID(I) = XGRID(I - 1) + T1
   25 YGRID(I) = YGRID(I - 1) - T2
      WRITE (3, 35)
   40 WRITE (3, 45)
      WRITE(3,100)
      L = 1
      M = 1
      DO 65 K = 1, 10
      DO 50 I = 1, 101
   50 GRID(I)=1
      A=M
      Q = (YMAX * (51. - A) + YMIN * (A - 1.))/ 50.
      DO 53 IL = 1, NUM
      IF (ABS(Q - Y(IL)) - (YMAX - YMIN) / 100.) 41, 53, 53
   41 IXP = 100. * (X(IL) - XMIN) / (XMAX - XMIN) + 1.5
   51 IF(IXP.GE.1 .AND. IXP.LE.101) GRID(IXP)=GRID(IXP)+1
   53 CONTINUE
   52 DO 54 J1=1,101
      J2=MIN0(GRID(J1),37)
   54 GRID(J1)=BLA(J2)
      WRITE (3,75) YGRID(L),(GRID(I), I = 1, 101)
      N = M + 1
      M = N + 3
      DO 60 J = N, M
      DO 55 I = 1, 101
   55 GRID(I)=1
      A=J
      Q = (YMAX * (51. - A) + YMIN * (A - 1.))/ 50.
      DO 57 IL = 1, NUM
```

```
      IF (ABS(Q - Y(IL)) - (YMAX - YMIN) / 100.) 46, 57, 57
   46 IXP = 100. * (X(IL) - XMIN) / (XMAX - XMIN) + 1.5
   56 IF(IXP.GE.1 .AND. IXP.LE.101) GRID(IXP)=GRID(IXP)+1
   57 CONTINUE
      DO 59 J1=1,101
      J2=MIN0(GRID(J1),37)
   59 GRID(J1)=BLA(J2)
   60 WRITE (3,76) GRID
      M = M + 1
   65 L = L + 1
      DO 66 I = 1, 101
   66 GRID(I)=1
      DO 72 IL = 1, NUM
      IF (ABS(YMIN - Y(IL)) - (YMAX - YMIN) / 100.) 69, 72, 72
   69 IXP = 100. * (X(IL) - XMIN) / (XMAX - XMIN) + 1.5
   70 IF(IXP.GE.1 .AND. IXP.LE.101) GRID(IXP)=GRID(IXP)+1
   72 CONTINUE
   71 DO 73 J1=1,101
      J2=MIN0(GRID(J1),37)
   73 GRID(J1)=BLA(J2)
      WRITE (3,75) YGRID(11),(GRID(I), I = 1, 101)
      WRITE(3,100)
   80 WRITE (3, 45)
      WRITE (3,85) (XGRID(I), I = 1, 11)
   35 FORMAT (1H1)
   45 FORMAT (20X, 1HI, 10(9X, 1HI))
   75 FORMAT (8X,1PE9.1,1X,2H-.,101A1,2H.-)
   76 FORMAT (19X,1H.,101A1,1H.)
   85 FORMAT (16X, 11(1PE9.1, 1X))
  100 FORMAT (19X,103(1H.))
      RETURN
      END
```

```
      SUBROUTINE PLOTTER (NUM,X,Y)
C
C     PROGRAM PLOTS DATA ON A 51 BY 101 XY GRID.
      DIMENSION M(101,51),N(101),X(1),Y(1)
      DIMENSION ROUND(4)
      DATA NROUND,(ROUND(I),I=1,4)/4,1.0,2.0,2.5,5.0/
      INTEGER DOT,BLANK,STAR,PLUS
      DATA BLANK/1H /,STAR/1H*/,DOT/1H./,PLUS/1H+/
C
      CALL LINEUP (X,NUM,ROUND,NROUND,10.0,XMIN,XMAX)
      CALL LINEUP (Y,NUM,ROUND,NROUND,10.0,YMIN,YMAX)
1     DO 70 I=1,101
      N(I)=DOT
      DO 70 J=1,51
70    M(I,J)=BLANK
C
      XUNIT=(XMAX-XMIN)/100.
      YUNIT=(YMAX-YMIN)/50.
C
      DO 10 I=1,NUM
      IX=(X(I)-XMIN)/XUNIT+1
      IY=(Y(I)-YMIN)/YUNIT+1
      IF(M(IX,IY)-BLANK) 11,12,11
12    M(IX,IY)=STAR
      GO TO 10
C
11    IF(M(IX,IY)-STAR) 53,54,53
54    M(IX,IY)=M(IX,IY)-1300000000000000000B
53    M(IX,IY)=M(IX,IY)+0100000000000000000B
      IF(4455555555555555555B-M(IX,IY)) 55,10,10
55    M(IX,IY)=PLUS
C
10    CONTINUE
C
      WRITE(3,101)
      WRITE(3,100) N
      DO 41 J=1,51
      K=52-J
      WRITE(3,100) (M(I,K),I=1,101)
41    CONTINUE
      WRITE(3,100) N
      WRITE(3,120) XUNIT,XMIN,XMAX,YUNIT,YMIN,YMAX
C
100   FORMAT(5X,1H.,101A1,1H.)
101   FORMAT(1H1)
120   FORMAT(1H0,4X,22HCOORDINATE INFORMATION,/,10X,
     1 10HHORIZONTAL,10X,13H1 DIVISION = ,E15.7,5X,7HXMIN = ,
     2 E15.7,5X,7HXMAX = ,E15.7,/,10X,8HVERTICAL,12X,
     3 13H1 DIVISION = ,E15.7,5X,7HYMIN = ,E15.7,5X,7HYMAX = ,
     4 E15.7)
      RETURN
      END
```

```
      SUBROUTINE LINEUP(A,NA,ROUND,NROUND,ASPACE,AMINS,AMAXS)
C
C     THIS PROGRAM ASSUMES A FLOATING TO FIXED CONVERSION
C     AND TRUNCATES BOTH POSITIVE AND NEGATIVE NUMBERS.
C     NOTE THAT ANY POWER OF 10 TIMES ASPACE IS EQUIVALENT
C     TO ASPACE.
C
      DIMENSION A(1),ROUND(1)
      DATA ALMOST1/1720 3777 7777 7777 7777B/
      SPACE=ASPACE
      IF(ASPACE.LE.10./9.)SPACE=10.
      AMIN=A(1)
      AMAX=A(1)
      DO 1 I=1,NA
      IF(A(I).LT.AMIN)AMIN=A(I)
      IF(A(I).GT.AMAX)AMAX=A(I)
1     CONTINUE
      IF(AMAX.NE.AMIN)GO TO 2          $IF(AMAX)12,10,11
10    AMAX=1.      $AMIN=-1. $GO TO 2
11    AMAX=AMAX+AMAX          $AMIN=0.  $GO TO 2
12    AMAX=0.      $AMIN=AMIN+AMIN
2     R=AMAX-AMIN
      RE=ALOG10(R/SPACE)
      IF(RE.LT.0.)RE=RE-ALMOST1
      IT=RE
      K=IT
      IF((R/SPACE)/10.**IT.GT.ROUND(NROUND))K=IT+1
      DO 5 I=1,NROUND
      L=I
      IF(ROUND(I).GE.(R/SPACE)/10.**K)GO TO 6
5     CONTINUE
6     S=ROUND(L)*10.**K
      RE=((AMAX+AMIN-SPACE*S)*.5)/S
      IF(RE.LT.0.)RE=RE-ALMOST1
      IT=RE
      AMINS=FLOAT(IT)*S
7     AMAXS=AMINS+S*SPACE
      IF(AMAX.LE.AMAXS)RETURN
      AMINS=AMINS+S
      IF(AMINS.LE.AMIN)GO TO 7
      L=L+1
      IF(L.LE.NROUND)GO TO 6
      K=K+1
      L=1
      GO TO 6
      END
```

```
C     PROGRAM CALCULATES LATTICE SPACING FROM GUN VOLTAGE AND PHOTO SPACING
C     INPUT DATA ONE CARD WITH MAGNIFICATION AND FOCAL LENGTH (F10.5,F5.0)
C
      PROGRAM SPACING (INPUT,OUTPUT,TAPE1=INPUT,TAPE3=OUTPUT)
      DIMENSION IND(20),D(20)
      REAL MAG
      R=70.0
      PI=3.1415927
      CONS=SQRT(150.4)
      ANG=0.0
      ANGMAX=48.*PI/180.
      ZERO=.0001
      WRITE(3,102)
102   FORMAT(1H1,63X*GUN VOLTAGE*//)
      DO 60 I=1,20
60    IND(I)=5*I
      WRITE(3,100) IND
100   FORMAT(*Y/YMAX*20I6,///)
      READ(1,1) MAG,F
1     FORMAT(F10.5,F5.0)
      B=(MAG+1.)*F
      A=B/MAG
      YMAX=B*R*SIN(ANGMAX)/(A-R+R*COS(ANGMAX))
      RATIO=0.02
      DO 7 K=1,49
      RATIO=RATIO+0.02
      DO 2 J=1,100
      ANG=ANG+0.01
      RT=(B*R*SIN(ANG)/(A-R+R*COS(ANG)))/YMAX
      S3=ANG
      IF(ABS(1.-RT/RATIO) .LE. ZERO) GO TO 3
      IF(RT .LT. RATIO) GO TO 2
      S1=ANG
      S2=ANG-0.01
5     S3=0.5*(S1+S2)
      RT3=(B*R*SIN(S3)/(A-R+R*COS(S3)))/YMAX
      IF(ABS(1.-RT3/RATIO) .LE. ZERO) GO TO 3
      IF(RT3 .LT. RATIO) GO TO 4
      S1=S3
      GO TO 5
4     S2=S3
      GO TO 5
2     CONTINUE
3     CONST=CONS/SIN(S3)
      DO 6 I=1,20
      V=5*I
6     D(I)=CONST/SQRT(V)
      WRITE(3,101) RATIO,D
101   FORMAT(1H ,F4.2,3X,20F6.2)
7     CONTINUE
      WRITE(3,103) R,A,F,MAG
103   FORMAT(1H0,56X,*IMAGE  DISTANCE =*F6.0* MM*/
     1          57X,*OBJECT DISTANCE =*F6.0* MM*//
     2          57X,*FOCAL  LENGTH   =*F6.0* MM*/
     3          57X,*MAGNIFICATION   =*F6.4)
      STOP
      END
```

XBL 7011-6919

GUN VOLTAGE

Y/YMAX	5	10	15	20	25	30	35	40	45	50	55	60	65	70	75	80	85	90	95	100
.04	171.80	121.48	99.19	85.90	76.83	70.14	64.94	60.74	57.27	54.33	51.80	49.60	47.65	45.92	44.36	42.95	41.67	40.49	39.41	38.42
.06	114.54	80.99	66.13	57.27	51.22	46.76	43.29	40.50	38.18	36.22	34.54	33.07	31.77	30.61	29.57	28.64	27.78	27.00	26.28	25.61
.08	85.93	60.76	49.61	42.97	38.43	35.08	32.48	30.38	28.64	27.17	25.91	24.81	23.83	22.97	22.19	21.48	20.84	20.25	19.71	19.22
.10	68.76	48.62	39.70	34.38	30.75	28.07	25.99	24.31	22.92	21.75	20.73	19.85	19.07	18.38	17.75	17.19	16.68	16.21	15.78	15.38
.12	57.31	40.53	33.09	28.66	25.63	23.40	21.66	20.26	19.10	18.12	17.28	16.55	15.90	15.32	14.80	14.33	13.90	13.51	13.15	12.82
.14	49.14	34.75	28.37	24.57	21.98	20.06	18.57	17.37	16.38	15.54	14.82	14.19	13.63	13.13	12.69	12.29	11.92	11.58	11.27	10.99
.16	43.01	30.42	24.83	21.51	19.24	17.56	16.26	15.21	14.34	13.60	12.97	12.42	11.93	11.50	11.11	10.75	10.43	10.14	9.87	9.62
.18	38.25	27.05	22.09	19.13	17.11	15.62	14.46	13.52	12.75	12.10	11.53	11.04	10.61	10.22	9.88	9.56	9.28	9.02	8.78	8.55
.20	34.45	24.36	19.89	17.22	15.41	14.06	13.02	12.18	11.48	10.89	10.39	9.94	9.55	9.21	8.89	8.61	8.36	8.12	7.90	7.70
.22	31.33	22.16	18.09	15.67	14.01	12.79	11.84	11.08	10.44	9.91	9.45	9.05	8.69	8.37	8.09	7.83	7.60	7.39	7.19	7.01
.24	28.74	20.32	16.59	14.37	12.85	11.73	10.86	10.16	9.58	9.09	8.67	8.30	7.97	7.68	7.42	7.19	6.97	6.77	6.59	6.43
.26	26.55	18.77	15.33	13.27	11.87	10.84	10.03	9.39	8.85	8.40	8.00	7.66	7.36	7.10	6.85	6.64	6.44	6.26	6.09	5.94
.28	24.67	17.44	14.24	12.33	11.03	10.07	9.32	8.72	8.22	7.80	7.44	7.12	6.84	6.59	6.37	6.17	5.98	5.81	5.66	5.52
.30	23.04	16.29	13.30	11.52	10.31	9.41	8.71	8.15	7.68	7.29	6.95	6.65	6.39	6.16	5.95	5.76	5.59	5.43	5.29	5.15
.32	21.62	15.29	12.48	10.81	9.67	8.83	8.17	7.64	7.21	6.84	6.52	6.24	6.00	5.78	5.58	5.40	5.24	5.10	4.96	4.83
.34	20.37	14.40	11.76	10.18	9.11	8.31	7.70	7.20	6.79	6.44	6.14	5.88	5.65	5.44	5.26	5.09	4.94	4.80	4.67	4.55
.36	19.25	13.61	11.12	9.63	8.61	7.86	7.28	6.81	6.42	6.09	5.80	5.56	5.34	5.15	4.97	4.81	4.67	4.54	4.42	4.31
.38	18.26	12.91	10.54	9.13	8.17	7.45	6.90	6.46	6.09	5.77	5.51	5.27	5.06	4.88	4.71	4.56	4.43	4.30	4.19	4.08
.40	17.36	12.28	10.02	8.68	7.77	7.09	6.56	6.14	5.79	5.49	5.24	5.01	4.82	4.64	4.48	4.34	4.21	4.09	3.98	3.88
.42	16.56	11.71	9.56	8.28	7.40	6.76	6.26	5.85	5.52	5.24	4.99	4.78	4.59	4.42	4.27	4.14	4.02	3.90	3.80	3.70
.44	15.82	11.19	9.13	7.91	7.08	6.46	5.98	5.59	5.27	5.00	4.77	4.57	4.39	4.23	4.09	3.96	3.84	3.73	3.63	3.54
.46	15.15	10.71	8.75	7.58	6.78	6.19	5.73	5.36	5.05	4.79	4.57	4.37	4.20	4.05	3.91	3.79	3.67	3.57	3.48	3.39
.48	14.54	10.28	8.39	7.27	6.50	5.94	5.50	5.14	4.85	4.60	4.38	4.20	4.03	3.89	3.75	3.63	3.53	3.43	3.34	3.25
.50	13.98	9.88	8.07	6.99	6.25	5.71	5.28	4.94	4.66	4.42	4.21	4.03	3.88	3.74	3.61	3.49	3.39	3.29	3.21	3.13
.52	13.46	9.52	7.77	6.73	6.02	5.49	5.09	4.76	4.49	4.26	4.06	3.88	3.73	3.60	3.47	3.36	3.26	3.17	3.09	3.01
.54	12.98	9.18	7.49	6.49	5.80	5.30	4.91	4.59	4.33	4.10	3.91	3.75	3.60	3.47	3.35	3.24	3.15	3.06	2.98	2.90
.56	12.53	8.86	7.24	6.27	5.61	5.12	4.74	4.43	4.18	3.96	3.78	3.62	3.48	3.35	3.24	3.13	3.04	2.95	2.88	2.80
.58	12.12	8.57	7.00	6.06	5.42	4.95	4.58	4.29	4.04	3.83	3.65	3.50	3.36	3.24	3.13	3.03	2.94	2.86	2.78	2.71
.60	11.74	8.30	6.78	5.87	5.25	4.79	4.44	4.15	3.91	3.71	3.54	3.39	3.26	3.14	3.03	2.93	2.85	2.77	2.69	2.62
.62	11.38	8.04	6.57	5.69	5.09	4.64	4.30	4.02	3.79	3.60	3.43	3.28	3.16	3.04	2.94	2.84	2.76	2.68	2.61	2.54
.64	11.04	7.81	6.37	5.52	4.94	4.51	4.17	3.90	3.68	3.49	3.33	3.19	3.06	2.95	2.85	2.76	2.68	2.60	2.53	2.47
.66	10.73	7.58	6.19	5.36	4.80	4.38	4.05	3.79	3.58	3.39	3.23	3.10	2.97	2.87	2.77	2.68	2.60	2.53	2.46	2.40
.68	10.43	7.37	6.02	5.21	4.66	4.26	3.94	3.69	3.48	3.30	3.14	3.01	2.89	2.79	2.69	2.61	2.53	2.46	2.39	2.33
.70	10.15	7.18	5.86	5.08	4.54	4.14	3.84	3.59	3.38	3.21	3.06	2.93	2.82	2.71	2.62	2.54	2.46	2.39	2.33	2.27
.72	9.89	6.99	5.71	4.95	4.42	4.04	3.74	3.50	3.30	3.13	2.98	2.86	2.74	2.64	2.55	2.47	2.40	2.33	2.27	2.21
.74	9.64	6.82	5.57	4.82	4.31	3.94	3.64	3.41	3.21	3.05	2.91	2.78	2.67	2.58	2.49	2.41	2.34	2.27	2.21	2.16
.76	9.41	6.65	5.43	4.70	4.21	3.84	3.56	3.33	3.14	2.98	2.84	2.72	2.61	2.51	2.43	2.35	2.28	2.22	2.16	2.10
.78	9.19	6.50	5.30	4.59	4.11	3.75	3.47	3.25	3.06	2.91	2.77	2.65	2.55	2.46	2.37	2.30	2.23	2.17	2.11	2.05
.80	8.98	6.35	5.18	4.49	4.02	3.67	3.39	3.17	2.99	2.84	2.71	2.59	2.49	2.40	2.32	2.24	2.18	2.12	2.06	2.01
.82	8.78	6.21	5.07	4.39	3.93	3.58	3.32	3.10	2.93	2.78	2.65	2.53	2.44	2.35	2.27	2.20	2.13	2.07	2.01	1.96
.84	8.59	6.08	4.96	4.30	3.84	3.51	3.25	3.04	2.86	2.72	2.59	2.48	2.38	2.30	2.22	2.15	2.08	2.03	1.97	1.92
.86	8.41	5.95	4.86	4.21	3.76	3.43	3.18	2.97	2.80	2.66	2.54	2.43	2.33	2.25	2.17	2.10	2.04	1.98	1.93	1.88
.88	8.24	5.83	4.76	4.12	3.69	3.37	3.12	2.91	2.75	2.61	2.49	2.38	2.29	2.20	2.13	2.06	2.00	1.94	1.89	1.84
.90	8.08	5.71	4.67	4.04	3.61	3.30	3.05	2.86	2.69	2.56	2.44	2.33	2.24	2.16	2.09	2.02	1.96	1.90	1.85	1.81
.92	7.93	5.61	4.58	3.96	3.55	3.24	3.00	2.80	2.64	2.51	2.39	2.29	2.20	2.12	2.05	1.98	1.92	1.87	1.82	1.77
.94	7.78	5.50	4.49	3.89	3.48	3.18	2.94	2.75	2.59	2.46	2.35	2.25	2.16	2.08	2.01	1.95	1.89	1.83	1.79	1.74
.96	7.64	5.40	4.41	3.82	3.42	3.12	2.89	2.70	2.55	2.42	2.30	2.21	2.12	2.04	1.97	1.91	1.85	1.80	1.75	1.71
.98	7.51	5.31	4.33	3.75	3.36	3.07	2.84	2.65	2.50	2.37	2.26	2.17	2.08	2.01	1.94	1.88	1.82	1.77	1.72	1.68
1.00	7.38	5.22	4.26	3.69	3.30	3.01	2.79	2.61	2.46	2.33	2.23	2.13	2.05	1.97	1.91	1.84	1.79	1.74	1.69	1.65

IMAGE DISTANCE = 226 MM
OBJECT DISTANCE = 336 MM

FOCAL LENGTH = 135 MM
MAGNIFICATION = .6719

XBL 7011-6920

USE OF PAPER TAPES PRODUCED BY THE VIDAR

To convert the paper tape output of the Vidar into useful information, a Fortran subroutine, FRAMCON, has been written. This routine makes use of the LRL 6600 library subroutine PTGET which reads the tape record by record, a Vidar record consisting of a sequence of punched frames, twelve per Vidar channel scanned, terminated by a punch in column eight of the tape. These records are edited by FRAMCON and, if acceptable, are returned to the calling program. The procedure for deleting records is described in Section A of Miscellaneous Information. An option permits the user to specify whether or not the rejected records are to be printed at the job's conclusion. These two subroutines occupy approximately 14,200 octal words in core.

It is suggested that users monitor the returned data to eliminate any spurious information acceptable to FRAMCON (e.g. the polarity could have the opposite sign).

USAGE

CALL FRAMCON (NAME, NCHAN, D, IDENT, NGOOD, OUT)

NAME — name of the COMMON FILE* into which the paper tape was read. NAME must be no longer than six characters and these characters must be left adjusted in the word, e.g. NAME = 5LVIDAR

NCHAN — total number of channels per record on the tape, i.e. the number of channels used per scan. This number is assumed constant for the entire tape.

---

* The recommended operating procedure for reading paper tape on the LRL 6600 is to use the job name, e.g., the above hypothetical job was called VIDAR, as the paper tape file name. Before the computer begins execution of the job, an operator copies the tape onto a disk COMMON FILE and sets the COMMON FILE name to the job name as it appears on the job card. This is done because reading from the paper tape reader is considerably slower than from the disk file, and would thus waste PP time.

D — a two dimensional real matrix of minimum size (NCHAN, NGOOD) that returns the paper tape data. The first entry contains the sequential number of the channel and the second contains the recorded e.m.f. in volts. In the calling program, the second dimension of D must be equal to or greater than the total number of records on the tape.

IDENT — a one dimensional integer vector of length NCHAN that returns in order of use the true channel numbers.

NGOOD — returns the actual number of entries in each column of the D matrix. Clearly NGOOD $\leq$ the total number of records on the tape.

OUT — specifies a printout option. If set equal to 1, a frame by frame decimal copy of the deleted records is appended to the program output. Any other number produces no results. In any case, the reason for exit from FRAMCON, and the total number of records read and rejected are written onto TAPE2 and added to the output file at the job's conclusion.

RESTRICTIONS AND REQUIREMENTS

A. Subroutines Required But Not Included

1. System Subroutines

B. Subroutines Supplied

1. PTGET — an LBL library routine that reads the paper tape one record at a time. A Vidar record consists of a complete scan of from 1 to 10 channels by the Vidar Master Scanner terminated by a punch in column eight on the paper tape. The end of the file mark is assumed to be two consecutive end of record marks. PTGET has been modified to include the statement

```
IF(FRAME .EQ. 377B) GO TO 40
```

immediately following statement number 35 of that program.

2. NIGHT — machine subroutine called by PTGET

3. NARITY — machine subroutine called by PTGET

C. Common Usage

1. FRAMCON uses a labelled common block COMMON/PTCOM/ to communicate with PTGET. No other commons are required.

D. Tape Usage

1. FRAMCON requires TAPE2 (actually assigned to a disk) for output. This tape must be specified in the program card, as indicated in the example, or an error will result.

USE OF THE SUBROUTINE

In order to simplify the use of subroutine FRAMCON, the following example is provided. The job name is assumed to be VIDAR and the program to be executed is called PTTEST. Explanations of the control cards are provided in parenthesis. Also assumed are 3 channels and 500 or fewer records. (Each record consists of one entry per channel so there may be up to 500 entries per channel.) Paper tape jobs should only be submitted to the A machine.

```
VIDAR, 7, 100, 50000.  400001, ALBERT EINSTEIN              (normal job card)

*A.                              (6411 control card sending the job to 6600-A)
.PAPER TAPE FILE VIDAR.          (alerts operator that a paper tape is expected)
COMMON VIDAR.                    (creates appropriate COMMON FILE)
RUNF(S)                          (compile and list source program)
LODE (I=LGO, M=MAPFILE)          (load program into memory)
XEQ.                             (execute source program)
EXIT.                            (control point for error exit from program)
DMP.                             (dump option)
WBR(11, 350000)                  (saves core image)
DMPS.                            (dump option)
FIN.                             (control point for normal exit from program)
RELEASE VIDAR.                   (omit if further use to be made of file)
COPY(TAPE2/RBU,1F,MAPFILE/RB,1F, OUTPUT)     (transfers TAPE2 and MAPFILE to
                                              OUTPUT file)
7-8-9                            (end of record)
```

```
PROGRAM PTTEST (INPUT, OUTPUT, TAPE2, . . .)
DIMENSION VOLTS (3,500), ID (3), . . .
MYTAPE = 5LVIDAR
CALL FRAMCON (MYTAPE, 3, VOLTS, ID, NUMOUT, 1)
.
.          (rest of source program PTTEST requiring
.           data from Vidar)
END
```

```
      SUBROUTINE FRAMCON (NAME, NCHAN, D, IDENT, NGOOD, OUT)
        .
        .            (more subroutines)
        .
7-8-9                (end of record)
        .
        .            (any other data cards)
        .
6-7-8-9              (end of file)
```

MISCELLANEOUS INFORMATION

A: Use of the Delete Option

The delete option may be used in either the manual or single scan mode of operation to eliminate known erroneous records, but cannot be used in the recycle mode. In this last case, it is necessary to find the bad record on the tape and hand punch a delete mark somewhere in the record by using the manual punch available at the computer center. To delete the preceding record when operating the Vidar in the 1 cycle (i.e. single scan) mode, push the delete button once and then the EOR/EOF button once. Omission of the EOR punch causes the record following the delete to be dumped. Finally, in the manual advance mode of operation, the delete button may be pressed anywhere within the record. The record may then be terminated by an EOR punch, or the scan maybe completed. Note that the action of the delete frame is to eliminate one entire record and not just one objectionable channel.

B: Notes on Paper Tape

Paper tapes submitted to be read on the 6600 should be wound clockwise with channel one next to the front flange on a reel with 3" hub (LBL Stock No. 7520-44100). The reel should be identified by a TAPE NAME sticker available from the I/O desk. The beginning of the tape must be on the outside of the coil preceded by approximately six feet of leader. Tapes may be rewound at the Computer Center Ready Room. Black paper tape (LBL stock No. 7530-90219) produces better results with the CDC 3691 optical readers than does either pink or yellow tape. Splicing material is available in the Ready Room to repair damaged tapes.

Job tapes should be submitted to the I/O desk with a properly filled out COS card heading the program deck containing subroutine FRAMCON.

C: Vidar - Tally Tape Code

The tape code supplied by the Vidar to the Tally punch and the tape format are shown on the following page.

← punch level →

Tape Direction ↑	8	7	6	5	4	(SPROCKET)	3	2	1	
										End of file/End of Record
										Odd parity
										B
										A
										2^3
										2^2
										2^1
										2^0
		0				o				0
						o			0	1
						o		0		2
		0				o		0	0	3
						o	0			4
		0				o	0		0	5
		0				o	0	0		6
						o	0	0	0	7
					0	o				8
		0			0	o			0	9
						o			0	+
						o		0		-
	0					o				EOR/EOF
	0	0	0	0	0	o	0	0	0	Delete

Tape Code

Tape Direction ↑	8	7	6	5	4	(SPROCKET)	3	2	1	
		0				o				CH ID
		0				o				CH ID
						o	0			CH ID
						o		0		Polarity
						o	0	0	0	Decimal Loc.
		0				o				Zero
						o		0		X-Data
		0				o		0	0	X-Data
						o	0			X-Data
		0				o	0		0	X-Data
		0				o	0	0		X-Data
		0			0	o			0	X-Data
	0					o				EOR

Tape Format

(shown above is -23.4569 mv in channel 4)

D: Trouble Shooting

Should the computer reject a large number of records from a tape, the actual contents of that tape may be checked by listing it on the teletype (TT) located in the main shop office of Building 77. Since the character set differs from that used by the Vidar, a conversion table is supplied below.

Vidar	TT	Vidar	TT
0	-	5	n
1	1	6	o
2	2	7	7
3	ℓ	8	8
4	4	9	r

Experience has shown that the most common reason for record rejection by the computer is incorrect record length, e.g. one or more frames have beed dropped. This may be easily checked by the above approach. Usually one finds that the tape is correct. If so, show it to the CDC engineers, have them check the spacing and explain what happened. Tell them that this has happened in the past and ask them if there is a problem with the reader. This approach usually results in a reader tune up and the problem disappears. Then resubmit the job and hope for the best. Real problems with the Tally-Vidar should be reported to Paul Saltz, Building 25A, Extension 5244.

```
      SUBROUTINE FRAMCON (NAME,NCHAN,D,IDENT,NGOOD,OUT)
C
C     THIS SUBROUTINE MAY BE USED TO CONVERT PAPER TAPE DATA
C     FROM THE VIDAR DATA ACQUISITION UNIT. IT CALLS SUBROUTINE
C     PTGET, EDITS THE RETURNED RECORDS, AND CONVERTS THE
C     INFORMATION IN EACH CHANNEL TO VOLTAGES THAT ARE RETURNED
C     TO THE CALLING PROGRAM IN A TWO DIMENSIONAL MATRIX D.
C     THE CHANNEL IDENTIFICATION NUMBERS ARE RETURNED IN A
C     VECTOR IDENT.
C
      COMMON/PTCOM/LOOK,ER,EF,PECHO,UWCHO,EBCHO,ROCHO,PECHAR,
     1     UWCHAR,EBCHAR,NC,LEADER,VAL(15),CHAR(15)
      INTEGER ER,EF,PECHO,UWCHO,EBCHO,ROCHO,PECHAR,UWCHAR,
     1     EBCHAR,VAL,CHAR,FRAME(132),OUT
      DIMENSION D(NCHAN,1),IDENT(NCHAN)
      DATA PECHO,UWCHO,EBCHO,ROCHO,PECHAR,UWCHAR,EBCHAR,L5,L4,
     1     L3,L2,L1,(VAL(I),CHAR(I),I=1,11)/
     2     3,3,2,2,3333,4444,3777,100000,10000,1000,100,10,
     3     100B,0,1B,1,2B,2,103B,3,4B,4,105B,5,106B,6,7B,7,10B,8,
     4     10B,8,111B,9,377B,377B/
      WRITE(2,108)
      IF(OUT.NE.1) GO TO 9
      WRITE(2,103)
9     LOOK=377B
      ER=200B
      EF=200B
      NC=11
      LEADER=0000B
      NF=12*NCHAN
      NGOOD=0
      NBAD=0
      ME=1
      LIM=NF+12
      ICOUNT=0
      ISIT=0
11    CALL PTGET(NAME,FRAME,NFRAME,ME,LIM)
      IF(ME.EQ.2.AND.NFRAME.EQ.0) GO TO 11
      IF(ME.EQ.3.AND.NFRAME.EQ.0) GO TO 11
      ICOUNT=ICOUNT+1
      DO 12 I=1,NFRAME
      MYFRAM=FRAME(I)
      IF(MYFRAM.EQ.377B) GO TO 17
      IF(MYFRAM.GT.9) GO TO 2
12    CONTINUE
      IF(NFRAME.NE.NF) GO TO 1
      NGOOD=NGOOD+1
      DO 6 J=1,NCHAN
      LOC=12*J-12
      IF(FRAME(LOC+1).NE.0) GO TO 3
      IF(FRAME(LOC+2).NE.0) GO TO 3
      ID=FRAME(LOC+3)
```

```
      IF(FRAME(LOC+4).EQ.1) GO TO 21
      IF(FRAME(LOC+4).NE.2) GO TO 4
21    IF(FRAME(LOC+6).NE.0) GO TO 5
      VALU=FRAME(LOC+7)*L5+FRAME(LOC+8)*L4+FRAME(LOC+9)*L3
      VALU=VALU+FRAME(LOC+10)*L2+FRAME(LOC+11)*L1+FRAME(LOC+12)
      IEXP=FRAME(LOC+5)
      VALU=VALU/10.**IEXP
      IF(FRAME(LOC+4).EQ.2) VALU=-VALU
      ISIT=1
      IDENT(J)=ID
6     D(J,NGOOD)=VALU
      GO TO (11,11,11,7,8) ME
1     MD=1
      GO TO 14
2     MD=2
      GO TO 14
3     MD=3
      GO TO 15
4     MD=4
      GO TO 15
5     MD=5
      GO TO 15
17    IF(NFRAME.EQ.1) 20,2
20    IF(ISIT.EQ.0) 22,23
22    NGOOD=NGOOD+1
      NBAD=NBAD-1
23    NFRAME=NF
      MD=2
      ICOUNT=ICOUNT-1
15    NGOOD=NGOOD-1
14    NBAD=NBAD+1
      ISIT=0
      IF(OUT.NE.1) GO TO 16
      WRITE(2,101) ICOUNT,MD
      WRITE(2,102) (FRAME(I),I=1,NFRAME)
16    GO TO (11,11,11,7,18) ME
18    IF(NGOOD.EQ.0.AND.NFRAME.EQ.0.AND.(FRAME(1).AND.777777B)
     1      .EQ.LOCF(FRAME(1))) 19,8
19    WRITE(2,109)
      NBAD=0
      GO TO 13
7     WRITE(2,104)
      GO TO 13
8     WRITE(2,105)
13    NTOT=NGOOD+NBAD
      WRITE(2,106) NTOT,NBAD
      IF(OUT.NE.1) GO TO 10
      WRITE(2,107)
10    END FILE 2
      RETURN
C
```

```
101   FORMAT(1H0,4X,*RECORD NUMBER *I4* REJECTED FOR REASON *I1)
102   FORMAT(4X,12(1X,I4))
103   FORMAT(1H ,*BELOW IS A DECIMAL COPY OF THE FRAME *
     1      *CONTENTS OF THE DELETED RECORDS*)
104   FORMAT(1H0,*EXIT FROM FRAMCON DUE TO ENDFILE MARK ON *
     1      *PAPER TAPE*)
105   FORMAT(1H0,*EXIT FROM FRAMCON DUE TO END OF PAPER TAPE*
     1      * COMMON FILE -- ENDFILE MARK MISSING ON TAPE*)
106   FORMAT(1H0,*TOTAL NUMBER OF RECORDS READ = *,I6,/,1X,
     1      *NUMBER OF RECORDS REJECTED = *,I6,//)
107   FORMAT(1H0,9X,*REASONS FOR REJECTION*,27X,*EXPLANATION*
     1      * OF FRAME CONTENTS*,///,
     2      10X,*1 -- INCORRECT RECORD LENGTH*,20X,
     3                * 0-9 -- VALID CHARACTERS*,/
     4      10X,*2 -- ILLEGAL CHARACTER IN RECORD*,16X,
     5                *3333 -- EVEN PARITY FRAME*,/
     6      10X,*3 -- IMPROPER CHANNEL I.D. NUMBER*,15X,
     7                *3777 -- ERROR SIGNAL FROM OPERATOR*,/
     8      10X,*4 -- UNRECOGNIZED POLARITY SYMBOL*,15X,
     9                *4444 -- UNWANTED CHARACTER IN FRAME*,/
     1      10X,*5 -- SIXTH FRAME NOT BLANK*,22X,*   9 -- *
     2                *SIGNALS VOLTAGE OVERLOAD IF IN FRAME 4*,/
     3      58X,* 255 -- RECORD ELIMINATED BY DELETE BUTTON*)
108   FORMAT(1H1)
109   FORMAT(1H0,*PAPER TAPE COMMON FILE WAS NOT DEFINED *
     1      *BEFORE PROGRAM EXECUTION -- EXIT FROM FRAMCON*)
C
      END
```

```
      SUBROUTINE PTGET (NAME,REC,NREC,ME,NLIM)
      INTEGER PECHO,PECHAR,EBCHO,EBCHAR,ROCHAR,VAL,CHAR
      INTEGER REC,BUF,SHIFT,FRAME,EF ,ER ,UWCHO,UWCHAR,ROCHO
      DIMENSION   REC(1),BUF( 513),IBUF(5)
      COMMON /PTCOM/ LOOK,ER,EF
     1,PECHO, UWCHO, EBCHO, ROCHO
     2,PECHAR,UWCHAR,EBCHAR,NC,LEADER,VAL(15),CHAR(15)
      IF(ME.NE.1) GO TO 3
      ROCHAR=LOOK.AND.377B
C     INITIALIZE BUFFER
      IBUF(1)=NAME.AND.7777 7777 7777 0000 0000 B
      IBUF(2)=LOCF(BUF)
      IBUF(3)=IBUF(2)    $IBUF(4)=IBUF(2)
      IBUF(5)=IBUF(2)+513
      IBUF(1)=IBUF(1).OR. 56B
      CALL XEQCIO(IBUF)
      CALL IOWAIT(IBUF)
      SHIFT=60
      NREC=0
      ISAME=0
      IF(ER.EQ.EF) ISAME=1
11    ME=2
      RETURN
3     NREC=0
      NR=0
1     IF(NREC.EQ.NLIM) GO TO 11
      SHIFT=SHIFT-12
      IF(SHIFT.GE.0) GO TO 2
      SHIFT=48
      IBUF(4)=IBUF(4)+1
      IF(IBUF(4).EQ.IBUF(5)) IBUF(4)=IBUF(2)
2     IF(IBUF(4).NE.IBUF(3))GO TO 6
      IF((IBUF(1).AND.30B).EQ.30B) GO TO 60
      IBUF(1)=IBUF(1).AND.7777 7777 7777 0000 0000B.OR.12B
      CALL XEQCIO(IBUF)
      CALL IOWAIT(IBUF)
      GO TO 2
6     IWORD=IBUF(4)-IBUF(2)+1
      FRAME=NIGHT(BUF(IWORD),SHIFT).AND.7777B
      IF(FRAME.EQ.7777B) GO TO 1
      IF(FRAME.NE.3777B) GO TO 35
      IF(EBCHO.EQ.1) GO TO 1
      NREC=NREC+1
      REC(NREC)=EBCHAR
      GO TO 1
35    FRAME=FRAME.AND.LOOK
      IF(FRAME.EQ.377B) GO TO 40
      IF(FRAME.EQ.LEADER) GO TO 1
      IF(FRAME.EQ.ROCHAR.AND.ROCHO.EQ.1) GO TO 1
      IF(PECHO.EQ.1) GO TO 40
```

```
      NBITS=NARITY(FRAME)
      IF(MOD(NBITS,2) .EQ.1) GO TO 40
      IF(RECHO.EQ.2) GO TO 1
      NREC=NREC+1
      REC(NREC)=RECHAR
      GO TO 1
40    CONTINUE
      IF(NC.EQ.0) GO TO 120
      DO 100 I=1,NC
      IF(FRAME.EQ.VAL(I)) GO TO 101
100   CONTINUE
120   IF(FRAME.EQ.ER) GO TO 130
      IF(FRAME.EQ.EF) GO TO 125
      GO TO(175,165,170),UWCHO
165   NREC=NREC+1
      REC(NREC)=FRAME
      GO TO 1
170   NREC=NREC+1
      REC(NREC)=UWCHAR
175   GO TO 1
125   ME=4
      RETURN
130   IF(NR.EQ.1) GO TO 125
      IF(ISAME.EQ.1) GO TO 140
135   ME=3
      RETURN
140   NR=1
      GO TO 1
101   IF(NR.EQ.1) GO TO 110
105   NREC=NREC+1
      REC(NREC)=CHAR(I)
      GO TO 1
110   ME=3
      SHIFT=SHIFT+12
      IF(SHIFT.NE.60) RETURN
      SHIFT=0
      IBUF(4)=IBUF(4)-1
      RETURN
60    ME=5
      RETURN
      END
          IDENT PARITY
          ENTRY NARITY
          VFD 42/0HNARITY,18/1
NARITY    DATA 0
          SA1 B1
          CX6 X1
          JP NARITY
          END
```

```
        IDENT     NIGHT
        ENTRY     NIGHT
        VFD       42/5HNIGHT,18/2
NIGHT   DATA      0
        SA1 B1
        SA2 B2
        SB3 X2
        AX6 B3,X1
        JP        NIGHT
    END
```

B. Etchants and Cleaning Solutions

During the course of this work, it was necessary to clean and prepare surfaces for use under UHV conditions. For a more extensive list of etchants than that below, the reader is referred to Table III-III in the thesis of Richard M. Goodman.[93]

1. Chemical Polish for 304 Stainless Steel

50 ml	conc.	H_2O_2
15 ml	conc.	HCl
20 ml	conc.	HF
15 ml	distilled water.	

Note: Use solution only at ice temperature as the reaction is very violent.

2. Chemical Polish for Tantalum

20 ml	conc.	HF
20 ml	conc.	HNO_3
50 ml	conc.	H_2SO_4

Note: Sulfuric acid must be added last! Use solution only at ice temperature with running water nearby to quench the reaction if it gets too violent.

3. Glass and Ceramic Cleaner

30 ml	conc.	H_2O_2
6 ml	conc.	NH_4OH
970 ml	distilled water	

Note: Boil object in solution for ten minutes. In a pinch, H_2O_2 and NH_4OH alone can be used at ice temperature.

C. Photographic Data and Slide Preparation

Many pictures were printed on photographic paper during this work. The following seven steps were found to result in reproducible picture quality.

1. Develop paper 2.0 min. with constant agitation
2. Stop 10 sec.
3. Fix 5-10 min. with agitation during first minute and then periodically
4. Rinse print in water
5. Hypoclear 2.5 min.
6. Wash print in water for 30 min.
7. Dry.

Color slides proved to be an effective means of communication during seminars. With the assistance of Doug Kreitz from the IMRD Photography group, two techniques were evolved for the preparation of these slides.

Color Slide Film Method

1. Have Graphic Arts make a 8 × 10 negative of the drawing.
2. Take this negative to the Building 90 Print Room and have a "Blue Line" copy made via the blue print machine.
3. Photgraph the "Blue Line" using High Speed Ektachrome (Type B) in the group Nikon.
4. Send the film to Kodak for processing.
5. This procedure produces permanent slides of excellent quality.

Diazo Method

1. Photograph the original line drawing at a size appropriate for 35 mm slides with the MP-3 camera using Kodalith film.
2. Process the negative
3. Expose a piece of Diazo (clear base) to UV light (or sunlight) through the negative for 1-5 minutes depending upon the light intensity.
4. Develop the Diazo in 2 molar NH_4OH until uniformly colored
5. Dry the Diazo on a soft cotton pad to avoid scratching it
6. Cut the print to seize and place it in a 35 mm glass slide mount
7. This procedure produces high quality slides in a short period of time.

D. New Ionizer

As noted in Chapter II, the ionizer used in this work has certain inherent difficulties. One solution to this problem is to use an electron bombardment source similar to that described by Brink[173] or by Davis.[174] Brink's design, however, is more suitable for use in a LEED system because it relies on electrostatic rather than magnetic fields to contain the electrons. Such a device could have several advantages over the ionizer currently in use. First, because the ionizing region is cylindrically symmetric about the axis of the quadrupole array, the scattered beam would encounter a more uniform electron flux than it now does after it passes through the collimation aperture. Second, the viewing factor bias could be decreased by making

the size of the ionizing region more comparable to the radius of the collimation aperture (i.e. in Fig. II-12, perhaps R could be reduced to 5D rather than 14D as in the present configuration). Third, by making both the grid and the shield out of wire mesh, the electron source would definitely respond to the beam density. The current design of the ionizer may be sensitive to a mixture of flux and density due to the beam exit aperture. Fourth, the high electron density in the ionizing region means that it will probably convert a larger fraction of the scattered beam into detectable ions than the present ionizer. Provided the background pressure of the beam species can be kept very low in the scattering region, this should result in an increase in the signal-to-noise ratio. For these reasons, a new ionizer is now being designed.

One of the goals of future research is to determine the energy of the scattered species. This might be achieved as suggested by Smith and Fite[35] by determining both the flux and density of the scattered beam with the same detector. The average velocity of the detected molecules could then be obtained from the ratio of the flux to the density:

$$\bar{v} = (\text{Flux Signal})/(\text{Density Signal})$$

For the detector to be truly flux sensitive, the molecules to be ionized must be in thermal equilibrium with their surroundings (i.e. the measuring device). In practice, this criterion might be approximated by taking advantage of the thermal accommodation coefficient to reduce the temperature of the scattered beam toward that of the measuring

system. Recall that in Chapter V we had

$$\alpha = \frac{T_i - T_r}{T_i - T_s} \qquad \text{(V-106)}$$

where T_i, T_r are the "temperatures" of the incident and reflected particles, and T_s is the surface temperature. This equation may be rearranged to yield the temperature of the reflected particle as the result of a single collision:

$$T_r^{(1)} = \alpha T_s + (1 - \alpha) T_i \qquad \text{(VII-1)}$$

For multiple collisions we may write

$$T_r^{(2)} = \alpha T_s + (1 - \alpha) T_r^{(1)}$$

$$= \alpha T_s \, [1 + (1 - \alpha)] + (1 - \alpha)^2 \, T_i \qquad \text{(VII-2)}$$

$$T_r^{(3)} = \alpha T_s + (1 - \alpha) \, T_r^{(2)}$$

$$= \alpha T_s \, [1 + (1 - \alpha) + (1 - \alpha)^2] + (1 - \alpha)^3 \, T_i \qquad \text{(VII-3)}$$

$$\vdots$$

$$T_r^{(n)} = \alpha T_s \sum_{k=1}^{n} (1 - \alpha)^{k-1} + (1 - \alpha)^n \, T_i \qquad \text{(VII-4)}$$

The sum of the power series is given by

$$\sum_{j=0}^{n-1} x^j = \frac{1 - x^n}{1 - x} \qquad \text{(VII-5)}$$

so that Eq. (VI-2) may be rewritten as

$$T_r^{(n)} = T_s[1 - (1 - \alpha)^n] + (1 - \alpha)^n T_i$$

or

$$T_r^{(n)} = T_s + (1 - \alpha)^n (T_i - T_s) \qquad \text{(VII-6)}$$

This equation gives the temperature of a molecule after it has undergone n collisions with a solid, suffering partial thermal accommodation with each collision. Clearly if $T_i > T_s$, the temperature of the reflected beam will decrease from T_i toward T_s while if $T_s > T_i$, the temperature of the reflected beam will increase from T_i toward T_s. Table VII.1 shows the number of collisions necessary as a function of the thermal accommodation coefficient to reduce the temperature of a 1500°K incident particle to within 10% of 300°K, a typical surface temperature. Only for very low values of α is a prohibitively large number of collisions required. Thus, if one were to attach a snorkel-like sampling divice to a stagnation chamber atop a Brink ionizer, both the density and flux of the scattered beam could be determined <u>in situ</u> by raising or lowering the quadrupole. For rare gases, the residence times in a properly designed chamber might be short enough compared to

0 0 0 0 3 6 0 3 5 8 9

Table VII.1. Number of collisions needed to reduce the temperature of a 1500°K molecule to 330°K via termal accommodation.

α	n
0.010	365
0.025	146
0.050	72
0.100	35

150 Hz. so that the captured particles would maintain their phase information. In this way, knowledge of the energy of the scattered beam could be obtained.

SYMBOLS

λ = particle wavelength, cm or Å

h = Planck's Constant = 6.625×10^{-27} erg-sec

P = particle momentum, g-cm/sec

m = particle mass, g/atom

E = particle energy, ergs or electron volts

V = accelerating potential, volts

v = particle velocity, cm/sec

θ_r = scattering angle measured from surface normal, degrees

θ_i = incident angle, measured from surface normal, degrees

B = impact parameter, cm or Å

θ_m = angle of maximum scattering intensity, degrees

I = beam intensity, molecules/sec

Q = molecular flow rate, molecules/sec

Q_i = leak rate for chember i, molecules/sec

A_d = detector area, cm^2

A_s = source area, cm^2

L = length of beam path, cm

M = molecular weight of gas, grams/mole

T = absolute temperature of gas or solid

n = number density, atoms/cm^3

$\bar{v}$ = average particle velocity, cm/sec

p_i = pressure in chamber i, dynes/cm^2 or torr

$\lambda(p)$ = pressure dependent mean free path in a gas, cm

ℓ = length of gas particle flight path at pressure p, cm

σ = collision diameter of molecule, cm^2 or $Å^2$

R = gas constant = 8.32×10^7 ergs/mole-deg = 1.987 cal/mole-deg

N_o = Avogadros number = 6.025×10^{23} atoms/mole

S = pumping speed, liters/sec.

ξ = constant = 3.51×10^{22} atoms-$g^{1/2}$ - $deg^{1/2}$/torr-cm^2-sec

K = constant = 3.21×10^{19} atoms/torr-liter

a = distance between source and source collimator, cm

b = distance between source collimator and selector collimator, cm

w = half-width of incident beam, inches or cm

D = half-width of detector aperture, inches or cm

r = distance from crystal to ionizer collimator, inches or cm

R = distance from ionizer collimator to extractor aperture, inches or cm

ℓ_1, ℓ_2 = projected scattered beam widths in the ionizer, inches or cm

δ = angle mass spectrometer must be rotated about its axis, degrees

$\mathcal{E}$ = lock-in amplifier output voltage, volts

S_o = amplitude of modulated signal, volts

ω = modulation frequency of incident beam, sec^{-1}

τ = time period of modulation, sec.

ϕ = phase lead or lag of modulated beam compared to an arbitrary referance, degrees.

$v_{m.p.}$ = most probable particle velocity, cm/sec.

ϕ_r = out of plane scattering, degrees ($\phi_r \equiv 0°$)

S = length of side of box for translational energy level spacing calculation, cm

n_i = translational quantum number, 1, 2, 3,. . .

n_v = vibrational quantum number, 0, 1, 2, . . .

$\theta_{R,V}$ = rotational and vibrational temperatures, °K

N_i = number of atoms in molecular state i

θ_D^s = surface Debye temperature = 110°K for platinum.

α = thermal accommodation coefficient

A = Einstein coefficient for spontaneous emission

B = Einstein coefficient for induced absorption

c = speed of light = 3×10^{-10} cm/sec

$\omega_{R,V}$ = rotational and vibrational angular frequencies

ν = transition frequency in Einstein coefficient, sec^{-1}

$\tau_{E,V,R}$ = electronic, vibrational, or rotational relaxation times, sec

ΔH_{ads} = heat of adsorption, kcal.

REFERENCES

1. L. Dunoyer, Comptes Rendus 152, 594 (1911).
2. Norman F. Ramsey, Molecular Beams (Oxford University Press, London, 1956).
3. D. R. Hershbach in Advances Chem. Phys. 10, I. Prigogine and S. A. Rice, eds. (John Wiley and Sons, New York, 1966).
4. J. P. Toennies, Ber. Bunsenges. Physik. Chem. 72, 927 (1968).
5. E. F. Greene and J. Ross, Science 159, 587 (1968).
6. O. Stern, Naturwiss. 17, 391 (1929).
7. R. E. Stickney, in Advances Atomic and Mol. Phys. 3, D. R. Bates and I. Estermann, eds. (Academic Press, New York, 1967).
8. M. Knudsen, Ann. Physik 48, 1113 (1915).
9. F. C. Hurlbut, J. Appl. Phys. 28, 844 (1957).
10. F. C. Hurlbut and D. E. Beck, Univ. of Calif. Eng. Proj. Rept. HE-150-166 (1959).
11. G. S. Hollister, R. T. Brackmann, and W. L. Fite, in Physical Chemistry in Aerodynamics and Space Flight (Pergamon Press, 1960).
12. D. R. O'Keefe, Joe N. Smith, Jr., R. L. Palmer, and Howard Saltsburg, J. Chem. Phys. 52, 4447 (1970).
13. Joe N. Smith, Jr., and H. Saltsburg, J. Chem. Phys. 40, 3585 (1964).
14. R. J. Madix, G. Melin, and A. Susu, Entropie n°30, 70 (Nov.-Dec. 1969).
15. D. L. Smith and R. P. Merrill, in Rarefied Gas Dynamics, Supplement 5, Vol. II, L. Trilling and H. Y. Wachman, eds. (Academic Press, New York, 1969).

16. L. A. West, E. I. Kozak, and G. A. Somorjai, J. Vac. Sci. Technol. 8, 430 (1971).

17. R. A. Krakowski and D. R. Olander, J. Chem. Phys. 49, 5027 (1968).

18. G. A. Somorjai and H. H. Farrell, in Advances Chem. Phys. 20, I. Prigogine and S. A. Rice, eds. (John Wiley and Sons, New York, 1971).

19. P. Auger, J. Phys. Radium 6, 205 (1925).

20. C. Davisson and L. H. Germer, Nature 119, 558 (1927).

21. C. Davisson and L. H. Germer, Phys. Rev. 30, 705 (1927).

22. E. A. Wood, J. Appl. Phys. 35, 1306 (1964).

23. J. J. Lander, in Progress in Solid State Chemistry, Vol. II, H. Reiss, ed. (Pergamon Press, Oxford, 1965).

24. D. S. Boudreaux and V. Heine, Surface Sci. 8, 426 (1967).

25. E. G. Macrae, J. Chem. Phys. 45, 3258 (1968).

26. E. G. Macrae, Surface Sci. 8, 14 (1967).

27. E. G. Macrae, in Fundamentals of Gas Surface Interactions H. Saltsburg, J. N. Smith, Jr., and M. Rogers, eds. (Academic Press, New York, 1967).

28. J. L. Beeby, J. Phys., C. (Proc. Phys. Soc.) 1 [2], 82 (1968).

29. C. B. Duke and C. W. Tucker, Jr., Surface Sci. 15, 231 (1969).

30. J. J. Lander, Phys. Rev. 91, 1382 (1953).

31. L. A. Harris, J. Appl. Phys. 39, 1428 (1968).

32. E. H. Burhop, The Auger Effect and Other Radiationless Transitions (The University Press, Cambridge, 1952).

33. C. C. Chang, Surface Sci. 25, 53 (1971).

34. R. E. Weber and A. L. Johnson, J. Appl. Phys. 40, 314 (1969).

35. Joe N. Smith, Jr., and Wade L. Fite, in Rarefied Gas Dynamics, Supplement 2, Vol. I, J. A. Laurman, ed. (Academic Press, New York, 1963).

36. Robert J. Madix and James A. Schwarz, Surface Sci. 24, 264 (1971).

37. Robert J. Madix, Ray Parks, Alfred A. Susu, and James A. Schwarz, Surface Sci. 24, 288 (1971).

38. J. D. McKinley, J. Chem. Phys. 40, 120 (1964).

39. J. D. McKinley, J. Chem. Phys. 40, 576 (1964).

40. R. L. Palmer, Joe N. Smith, Jr., Howard Saltsburg, and D. R. O'Keefe, J. Chem. Phys. 53, 1666 (1970).

41. Joe N. Smith, Jr., and R. L. Palmer, J. Chem. Phys. (to be published 15 Dec. 1971).

42. B. J. Wood, J. S. Mills, and H. J. Wise, J. Phys. Chem. 67, 1462 (1963).

43. Henry Wise and Bernard J. Wood, in Rarefied Gas Dynamics, Supplement 2, Vol. I, J. A. Laurman, ed. (Academic Press, New York, 1963).

44. Joe N. Smith, Jr., and Howard Saltsburg, in Fundamentals of Gas Solid Interactions, H. S. Saltsburg, J. N. Smith, Jr., and M. Rogers, eds. (Academic Press, New York, 1967).

45. F. C. Hurlbut, Univ. of Calif. Eng. Rept. HE-150-208 (1962).

46. Robert P. Merrill, Catalysis Rev. 4, 115 (1970).

47. W. H. Weinberg and R. P. Merrill, Phys. Rev. Lett. 25, 1198 (1970).

48. D. V. Tendulkar and R. E. Stickney, Surface Sci. (to be published).

49. F. London, Z. Physik 63, 245 (1930).

50. F. London, Trans. Faraday Soc. 33, 8 (1937).

51. Joe N. Smith, Jr., and H. Saltsburg, in Rarefied Gas Dynamics, Supplement 3, Vol. II, J. H. de Leeuw, ed. (Academic Press, New York, 1966).

52. Joe N. Smith, Jr., Howard Saltsburg, and R. L. Palmer, in Rarefied Gas Dynamics, Supplement 5, Vol. II, L. Trilling and H. Y. Wachman, eds. (Academic Press, New York, 1969).

53. Sheldon Datz, George E. Moore, and Ellison H. Taylor, in Rarefied Gas Dynamics, Supplement 2, Vol. I, J. A. Laurman, ed. (Academic Press, New York, 1963).

54. John J. Hinchen and William M. Foley, in Rarefied Gas Dynamics, Supplement 3, Vol. II, J. H. de Leeuw, ed. (Academic Press, New York, 1966).

55. L. A. West and G. A. Somorjai, J. Chem. Phys. 54, 2864 (1971).

56. S. Yamamoto and R. E. Stickney, J. Chem. Phys. 53, 1594 (1971).

57. R. N. Coltharp, J. T. Scott, and E. E. Muschlitz, Jr., in The Structure and Chemistry of Solid Surfaces, G. A. Somorjai, ed. (John Wiley and Sons, New York, 1969).

58. R. N. Coltharp, J. T. Scott, and E. E. Muschlitz, Jr., J. Chem. Phys. 51, 5180 (1969).

59. W. van Willigen, Phys. Letters 28A, 80 (1968).

60. N. Cabrera, V. Celli, F. O. Goodman, and R. Manson, Surface Sci. 19, 67 (1970).

61. Frank O. Goodman, Surface Sci. 19, 93 (1970).

62. F. O. Goodman, J. Phys. Chem. Solids 23, 1269 (1962).

63. F. O. Goodman, J. Phys. Chem. Solids 23, 1491 (1962).

64. F. O. Goodman, J. Phys. Chem. Solids. 24, 1451 (1963).

65. F. O. Goodman, J. Phys. Chem. Solids 26, 85 (1965).

66. F. O. Goodman, in Rarefied Gas Dynamics, Supplement 3, Vol. II, J. H. de Leeuw, ed. (Academic Press, New York, 1966).

67. F. O. Goodman, in Rarefied Gas Dynamics, Supplement 4, Vol. I, C. L. Brundin, ed. (Academic Press, New York, 1967).

68. F. O. Goodman, Surface Sci. 7, 391 (1967).

69. F. O. Goodman, in The Structure and Chemistry of Solid Surfaces, G. A. Somorjai, ed. (John Wiley and Sons, New York, 1969).

70. F. O. Goodman, in Rarefied Gas Dynamics, Supplement 5, Vol. II, L. Trilling and H. Y. Wachman, eds. (Academic Press, New York, 1969).

71. R. A. Oman, A. Bogan, and C. H. Li, in Rarefied Gas Dynamics, Supplement 3, Vol. II, J. H. de Leeuw, ed. (Academic Press, New York, 1966).

72. R. A. Oman, J. Chem. Phys. 48, 3919 (1968).

73. R. A. Oman, in Rarefied Gas Dynamics, Supplement 4, Vol. I, C. L. Brundin, ed. (Academic Press, New York, 1967).

74. R. A. Oman, in Rarefied Gas Dynamics, Supplement 5, Vol. II, L. Trilling and H. Y. Wachman, eds. (Academic Press, New York, 1969).

75. V. S. Calia and R. A. Oman, J. Chem. Phys. 52, 6184 (1970).

76. J. D. McClure and Y. Wu, in Rarefied Gas Dynamics, Supplement 5, Vol. II, L. Trilling and H. Y. Wachman, eds., (Academic Press, New York, 1969).

77. J. D. McClure, J. Chem. Phys. 51, 1687 (1969).

78. J. D. McClure, J. Chem. Phys. 52, 2712 (1970).

79. L. M. Raff, J. Lorenzen, and B. C. McCoy, J. Chem. Phys. 46, 4265 (1967).

80. J. Lorenzen and L. M. Raff, J. Chem. Phys. 49, 1165 (1968).

81. J. Lorenzen and L. M. Raff, J. Chem. Phys. 52, 6134 (1970).

82. M. R. Busby, J. D. Haygood, and C. H. Link, Jr., J. Chem. Phys. 54, 4642 (1971).

83. J. E. Lennard-Jones and A. F. Devonshire, Nature 137, 1069 (1936).

84. See review by Frank O. Goodman, Surface Sci. 26, 327 (1971).

85. Joe N. Smith, D. R. O'Keefe, Howard Saltsburg, and R. L. Palmer, J. Chem. Phys. 50, 4667 (1969).

86. Joe N. Smith, Jr., D. R. O'Keefe, and R. L. Palmer, J. Chem. Phys. 52, 315 (1970).

87. R. M. Logan and R. E. Stickney, J. Chem. Phys. 44, 195 (1966).

88. R. M. Logan, J. C. Keck, and R. E. Stickney, in Rarefied Gas Dynamics, Supplement 4, Vol. I, C. L. Brundin, ed., (Academic Press, New York, 1967).

89. R. M. Logan and J. C. Keck, J. Chem. Phys. 49, 860 (1968).

90. D. L. Smith and R. P. Merrill, J. Chem. Phys. 53, 3588 (1970).

91. F. Keywell, Phys. Rev. 97, 611 (1955).

92. F. Jona, Surface Sci. 8, 57 (1967).

93. Richard M. Goodman, Ph.D. Dissertation, Univ. of Calif., Berkeley (1969); UCRL-19008 (1969).

94. E. L. Knuth, Appl. Mech. Review 17, 751 (1964).

95. R. H. Jones, D. R. Olander, and V. R. Kruger, J. Appl. Phys. 40, 4641 (1969).

96. Donald R. Olander, J. Appl. Phys. 40, 4650 (1969).

97. D. R. Olander and R. H. Jones, Entropie n°30, 42 (Nov-Dec. 1969).

98. Donald R. Olander and Vallerie Kruger, J. Appl. Phys. 41, 2769 (1970).

99. D. R. Olander, R. H. Jones, and W. J. Siekhaus, J. Appl. Phys. 41, 4388 (1970).

100. W. J. Siekhaus, R. H. Jones, and D. R. Olander, J. Appl. Phys. 41, 3492 (1970).

101. J. M. Morabito, R. Steiger, R. Muller, and G. A. Somorjai, in The Structure and Chemistry of Solid Surfaces, G. A. Somorjai, ed., (John Wiley and Sons, New York, 1969).

102. E. I. Kozak and J. M. Morabito, UCRL-18038 (1968).

103. H. V. Hostettler and R. B. Bernstein, Rev. Sci. Inst. 31, 872 (1960).

104. J. C. Bond, Catalysis by Metals (Academic Press, New York, 1962).

105. H. B. Lyon and G. A. Somorjai, J. Chem. Phys. 46, 2539 (1967).

106. A. E. Morgan and G. A. Somorjai, Surface Sci. 12, 405 (1968).

107. D. G. Fedak and N. A. Gjostein, Acta Met. 15, 827 (1967).

108. D. G. Fedak and N. A. Gjostein, Surface Sci. 8, 77 (1967).

109. P. W. Palmberg and T. N. Rhodin, Phys. Rev. 161, 586 (1967).

110. J. T. Grant, Surface Sci. 18, 228 (1969).

111. J. T. Grant and T. W. Haas, Surface Sci. 18, 457 (1969).

112. P. W. Palmberg, in The Structure and Chemistry of Solid Surfaces, G. A. Somorjai, ed., (John Wiley and Sons, New York, 1969).

113. H. B. Lyon, Ph.D. Dissertation, Univ. of Calif., Berkeley (1967); UCRL-17549 (1967).

114. J. J. Burton and G. Jura, in The Structure and Chemistry of Solid Surfaces, G. A. Somorjai, ed. (John Wiley and Sons, N.Y., 1969).

115. T. N. Rhodin, P. W. Palmberg, and E. W. Plummer, in The Structure and Chemistry of Solid Surfaces, G. A. Somorjai, ed., (John Wiley and Sons, New York, 1969).

116. L. Fiermans and J. Vennik, Surface Sci. 24, 541 (1971).

117. R. W. Joyner, C. S. McKee and M. W. Roberts, Surface Sci. 26, 303 (1971).

118. R. W. Joyner, J. L. Gland, and G. A. Somorjai, Surface Sci. (to be published).

119. R. H. Siller, W. A. Oates, and R. B. McLellan, J. Less Common Metals 16, 71 (1968).

120. G. L. Selman, P. J. Ellison, and A. S. Darling, J. Materials Sci. 4, 14 (1969).

121. B. J. Wood, N. Endow, and H. Wise, J. Catalysis 18, 70 (1970).

122. S. E. Fink and R. P. Merrill, paper delivered at the Eighth Conference on Microbalance Techniques (1969).

123. A. E. Morgan and G. A. Somorjai, Trans. Amer. Crystl. Assoc. 4, 59 (1968).

124. A. George Stoll, Donald L. Smith, and Robert P. Merrill, J. Chem. Phys. 54, 163 (1971).

125. William Henry Weinberg, Ph.D. Dissertation, Univ. of Calif., Berkeley (1971).

126. Howard Saltsburg and Joe N. Smith, Jr., J. Chem. Phys. 45, 2175 (1966).

127. Robert L. Palmer, Howard Saltsburg, and Joe N. Smith, Jr., J. Chem. Phys. 50, 4661 (1969).

128. R. P. Merrill and D. L. Smith, Surface Sci. 21, 203 (1970).

129. J. J. Burton and G. Jura, J. Phys. Chem. 71, 1937 (1967).

130. L. H. Germer and G. W. May, Surface Sci. 4, 452 (1966).

131. J. A. Becker, E. J. Becker, and R. G. Brandes, J. Appl. Phys. 32, 411 (1961).

132. J. B. Berkowitz-Mattuck, A. Buchler, J. L. Engelke, and S. N. Goldstein, J. Chem. Phys. 39, 2722 (1963).

133. P. O. Schissel and O.C. Trulson, J. Chem. Phys. 43, 737 (1965).

134. R. L. Palmer, D. R. O'Keefe, H. Saltsburg, and J. N. Smith, Jr., J. Vac. Sci. Technol. 7, 91 (1970).

135. Terrell L. Hill, Introduction to Statistical Thermodynamics (Addison-Wesley, Reading, Mass., 1960).

136. G. Herzberg, Molecular Spectra and Molecular Structure, I. Diatomic Molecules, (D. van Nostrand, New York, 1950).

137. G. Herzberg, Molecular Spectra and Molecular Structure, III. Electronic Spectra and Electronic Structure of Polyatomic Molecules (D. van Nostrand, Princeton, 1966).

138. H. Saltsburg, J. N. Smith, Jr., and R. L. Palmer, in Rarefied Gas Dynamics, Supplement 4, Vol. I, C. L. Brundin, ed., (Academic Press, New York, 1967).

139. W. H. Flygare, Accounts of Chem. Research 1, 121 (1968).

140. M. Knudsen, Ann. Physik 6, 129 (1930).

141. P. Feuer, J. Chem. Phys. 39, 1311 (1963).

142. H. H. Rowley and K. F. Bonhoeffer, Z. Phys. Chem. 21, 84 (1933).

143. K. Schäfer, W. Rating, and A. Eucken, Ann. Physik 42, 176 (1942).

144. K. Schäfer and K. H. Riggert, Z. Elektrochem. 57, 751 (1953).

145. P. Welander, Arkiv Fysik 7, 507 (1954).

146. H. von Ubisch, Arkiv Fysik 10, 157 (1956).

147. T. F. Hunter, J. Chem. Phys. 51, 2641 (1969).

148. John L. Powell and Bernd Craseman, Quantum Mechanics (Addison-Wesley, Reading, Mass., 1961).

149. Howard Saltsburg, Joe N. Smith, Jr., and Robert L. Palmer, in The Structure and Chemistry of Solid Surfaces, G. A. Somorjai, ed., (John Wiley and Sons, New York, 1969).

150. R. E. Stickney and F. C. Hurlbut, in Rarefied Gas Dynamics, Supplement 2, Vol. I, J. A. Laurman, ed., (Academic Press, New York, 1963).

151. Robert E. Stickney, Phys. Fluids 5, 1617 (1962).

152. Donald L. Smith and Robert P. Merrill, J. Chem. Phys. 52, 5861 (1970).

153. D. O. Hayward and B. M. W. Trapnell, Chemisorption (Butterworths, London, 1964).

154. Donald L. Smith, Ph.D. Dissertation, Univ. of Calif., Berkeley (1969).

155. R. Bhaskara Subbarao and David R. Miller, J. Chem. Phys. 51, 4679 (1969).

156. J. Zawadzki, Disc. Faraday Soc. 8, 140 (1950).

157. C. W. Nutt and S. Kapur, Nature 220, 697 (1968).

158. E. Molinari, F. Cramarossa, A. Pullo, and L. Triolo, J. Catalysis 4, 341 (1965).

159. B. Lang, R. W. Joyner, and G. A. Somorjai, Surface Sci. (to be published).

160. R. P. Donnelly and C. N. Hinshelwood, J. Chem. Soc. 132, 1727 (1929).

161. W. A. Bone and R. V. Wheeler, Phil. Trans. A206, 1 (1906).

162. I. Langumir, Trans. Faraday Soc. 17, 621 (1922).

163. H. G. Tanner and G. B. Taylor, J. Amer. Chem. Soc. 53, 1289 (1931).

164. C. W. Nutt and A. G. Carter, Trans. Faraday Soc. 64, 771 (1968).

165. G. N. Lewis and M. Randall, rev. by K. S. Pitzer and L. Brewer, Thermodynamics (McGraw-Hill, New York, 1961).

166. V. J. Mimeault and R. S. Hansen, J. Phys. Chem. 70, 3001 (1966).

167. H. Cassel and E. Glückauf, Z. Physik Chem. ABT.B 9, 427 (1930).

168. H. Cassel and E. Glückauf, Z. Physik Chem. ABT.B 17, 380 (1932).

169. H. Cassel and E. Glückauf, Z. Physik Chem. ABT. B 18, 347 (1932).

170. H. Cassel and E. Glückauf, Z. Physik Chem. ABT. B 19, 47 (1932).

171. G. H. Kwei, J. A. Norris, and D. R. Hershbach, J. Chem. Phys. 52, 1317 (1970).

172. Brian R. Williams, J. Chem. Phys. 55, 3220 (1971).

173. Gilbert O. Brink, Rev. Sci. Instr. 37, 857 (1966).

174. W. D. Davis, J. Vac. Sci. Technol. 6, 85 (1969).

ACKNOWLEDGMENTS

The foundation upon which this thesis rests is the product of contributions by many people over a long period of years. For showing me the fascinating and varied aspects of mathematics, physics and chemistry, I am indebted to my former teachers. Among them, two men in particular have been instrumental in the development of my scientific career. To Professor Donald F. Swinehart, who took an inquisitive freshman into his laboratory and introduced him to the fundamentals of research, my sincere thanks seems inadequate recompense. To Professor Gabor A. Somorjai, under whose guidance this work was performed, I wish to express my appreciation for his encouragement and inspiration. Never have I met an individual with such boundless drive and enthusiasm, or such an intense interest in the progress of his students.

Numerous members of the Somorjai research group, past and present, should be acknowledged for their companionship, advice, suggestions, and criticisms. In this respect, the early guidance of Dr. A. E. Morgan was most helpful. I am grateful to Whalun Szeto for his assistance in overcoming electronic problems and for teaching me the basics of photography. Thanks are also due to Helen H. Farrell and Richard M. Goodman for their guidance in the theory and practice of LEED and to Fredrick J. Szalkowski for his help in the design and initial operation of my Auger Spectometer. Discussion of the technical aspects of surface research with J. Gordon Davy or John Gland with his amazing

diversity of interests usually resulted in mutual enlightenment. Albert Wong deserves special commendation for his aid in processing data and in conducting some late night experimental runs; and for a year of stimulating conversation and noon-hour Bridge sessions, I wish to thank Dr. Richard W. Joyner.

Without the services of the blue ribbon support staff of IMRD, life would have been many times more difficult. My special gratitude goes to the members of the neighboring Technical Typing Group: Shirley Ashley, Alice Ramirez, Jean Wolslegel, and before them Pat Shand and Jane Ball, for their cheery greeting each morning and for their assistance in the preparation of publications including this thesis. Additionally I would like to thank Glen Baum for helping to keep my vacuum system in operation, Doug Kreitz for answering a multitude of questions regarding photography, Pat Patenaude for instructing me in the use of the student shop, and Dan Curtis and Del Peterson, respectively, for engineering and constructing the electrical components that control MBA-Echo.

To Emergy Kozak, I can only say that words alone cannot express my appreciation for his contribution to this work. His skill and genius in the design and fabrication of vacuum equipment converted an idea into reality. I shall never forget the lessons he taught me or the many discussions we had. Duane Newhart, another master craftsman, provided numerous suggestions and sorely needed assistance on several occasions.

The drafting of Gloria Pelatowski and the typing of the rough draft of this tome by Claudia Redwood are sincerely appreciated.

Many others have added significantly to my life and work in Berkeley during these past four years. In particular I wish to single out Bob and Jane McCloud for treating me as a member of their family.

This research was supported by the United States Atomic Energy Commission. A Graduate Fellowship from the National Science Foundation during the years 1967-1971 is also gratefully acknowledged.

LEGAL NOTICE

This report was prepared as an account of work sponsored by the United States Government. Neither the United States nor the United States Atomic Energy Commission, nor any of their employees, nor any of their contractors, subcontractors, or their employees, makes any warranty, express or implied, or assumes any legal liability or responsibility for the accuracy, completeness or usefulness of any information, apparatus, product or process disclosed, or represents that its use would not infringe privately owned rights.

TECHNICAL INFORMATION DIVISION
LAWRENCE BERKELEY LABORATORY
UNIVERSITY OF CALIFORNIA
BERKELEY, CALIFORNIA 94720